Cytoskeletal and integrin-mediated mechanobiology of the alveolar epithelium

A thesis submitted for the degree of Doctor of Philosophy, Imperial College London

By

David Salman

2017

Inflammation, Repair and Development

National Heart and Lung Institute

Imperial College London

London SW3 6LY

Declaration of originality

This thesis is the result of my own work. Work assessing the effect of CD98hc knockdown on stretch-induced and IL-1β-induced IL-8 generation (panels B and D of Figure 4-1) was performed in collaboration with Professor Tariq Sethi and Dr. Wei Wang from the department of Asthma, Allergy and Lung Biology, Kings College London. This thesis was composed on the basis of work carried out under the supervision of Professor Mark Griffiths and Dr. Charlotte Dean (Department of Inflammation, Repair and Development, Imperial College, London) and Professor Mark Johnson (Faculty of Medicine, Department of Surgery & Cancer, Imperial College London). Work using FLIM and FRET was performed under the supervision of Dr. Leo Carlin (Faculty of Medicine, National Heart & Lung Institute).

David Salman

July 2017, London

Copyright Declaration

The copyright of this thesis rests with the author and is made available under a Creative Commons Attribution Non-Commercial No Derivatives licence. Researchers are free to copy, distribute or transmit the thesis on the condition that they attribute it, that they do not use it for commercial purposes and that they do not alter, transform or build upon it. For any reuse or redistribution, researchers must make clear to others the licence terms of this work.

Abstract

Ventilator-associated lung injury (VALI) describes the process by which mechanical ventilation of the lungs causes systemic injury. Cyclic Mechanical Strain (CMS) of alveolar epithelial cells induces cytokine release, suggesting that mechanotransduction of force into injurious biological signaling occurs in the alveolar epithelium. The work in this thesis investigated the role of integrin and cytoskeletal signalling in CMS-induced cytokine release in these cells. Specifically, the roles of RhoA-Rho associated protein kinase (ROCK) signaling and the integrin-associated protein, CD98hc, were assessed.

Inhibition of ROCK and non-muscle myosin II (NMII), and knockdown of CD98hc abrogated CMS-induced IL-8 release. Preliminary data obtained using FRET probes indicated that CD98hc knockdown reduced baseline RhoA activity. To investigate these pathways upon CMS-induced injury in intact human lung, and to generate translational data, we established a model of CMS using precision-cut lung slices (PCLS). CMS induced cytokine release in both murine and human PCLS and there was also an indication that cells spatially correlating with ATII proliferated in response to CMS.

These data suggest a key role for the RhoA-ROCK-NMII axis in the mechanotransduction of CMS in the alveolar epithelium. CD98hc may modulate baseline RhoA expression and CMS-induced injurious signalling by affecting baseline cellular pre-stress. PCLS respond to CMS thereby enabling mechanotransduction studies in human tissue with near physiological conditions. This will potentially facilitate future translational research in VALI.

Acknowledgements

I am grateful to Thanu Poobalasingham and John-Poul Ng-Blichfeldt for their advice, friendship and introduction to laboratory science, techniques and good practice. I am also grateful to my lab colleagues, including Henry Li, Joana Alçada, Richard Toshner, Cecilia Andersson, Sarah Allden, Dhiren Patel, Ashton Barnett-Vanes, John Mackey and all those others who helped make the last three years an absolute pleasure. Gill Martin and Mandy Hipwell, the senior support technicians, were a great source of help and support throughout my time here.

I am indebted to the microscopy support provided by the FILM facility at Imperial, starting what I think will be a lifelong interest in biological imaging. I am also grateful to Dr. Natasha Madge and Professor Louise Donnelly for their help and advice with setting up the lung slice model.

I cannot thank my supervisors, Professor Mark Griffiths and Dr. Charlotte Dean enough, for their endless patience, gentle encouragement and friendship. Dr. Leo Carlin was a great source of advice, supervision, support, mentorship, coffee and music, and I am grateful to Professor Mark Johnson and Dr. Matthew Hind for their kind and encouraging words.

Finally, I am indebted to my family. My parents have provided unwavering support despite an occasionally vexing son, and my wife and daughter have had nothing but patience and affection despite my frequent evening and weekend absences.

Table of Contents

1 CHAPTER 1: INTRODUCTION 24

1.1 MECHANOBIOLOGY OF THE LUNG 25

1.1.1 VENTILATOR-ASSOCIATED LUNG INJURY (VALI) 25

1.1.2 DISTENDING FORCES IN THE LUNG IN HEALTH AND DISEASE 29

1.2 MECHANOBIOLOGY OF THE ALVEOLAR EPITHELIUM 30

1.2.1 THE ALVEOLAR EPITHELIUM 30

1.2.2 ALVEOLAR EPITHELIAL RESPONSES TO STRETCH 33

1.2.2.1 Force-induced lung maturation and cell differentiation 33

1.2.2.2 Force-induced cell proliferation in the lung 35

1.2.2.3 Force-induced injury in the lung 36

1.2.2.3.1 Physical disruption 36

1.2.2.3.2 Mechanotransduction 38

1.3 STUDYING MECHANOTRANSDUCTION IN THE ALVEOLAR EPITHELIUM 40

1.3.1 *IN VIVO* MODELS 40

1.3.2 *IN VITRO* MODELS 41

1.3.2.1 Application of CMS 41

1.3.2.2 Towards physiologically-relevant systems of *in vitro* stretch 43

1.3.3 MEASURING FORCES IN MECHANOTRANSDUCTION 45

1.4 CELLULAR MECHANOTRANSDUCTION: HOW CELLS TRANSDUCE FORCES INTO BIOLOGICAL SIGNALLING 47

1.4.1 THE INTEGRIN-FOCAL ADHESION COMPLEX 48

1.4.2 INTEGRIN-MEDIATED MECHANOTRANSDUCTION 48

1.4.2.1 Inside-out signalling 51

1.4.2.2 Outside-in signalling 52

1.4.3 FOCAL ADHESION MATURATION 53

1.4.4 MECHANICAL FORCE PROMOTES INTEGRIN-DEPENDENT FOCAL ADHESION MATURATION AND REINFORCEMENT 53

1.4.5 INTEGRIN-DEPENDENT RESPONSES TO MECHANICAL FORCE ARE DYNAMIC AND DEPEND ON THE DEGREE OF FORCE APPLIED 54

1.4.6 RESPONSES TO EXTERNALLY-APPLIED MECHANICAL FORCE 58

1.5 INTEGRIN-ASSOCIATED PROTEINS 59

1.5.1 CD98HC 59

1.6 ACTIN CYTOSKELETAL MECHANOTRANSDUCTION 62

1.6.1 RHOGTPASES 66

1.6.2 MECHANICAL PROPERTIES OF THE CYTOSKELETON 68

1.7 EPITHELIAL REPAIR 69

1.7.1 INTEGRIN AND RHOGTPASE SIGNALLING IN EPITHELIAL REPAIR 69

1.7.2 THE EFFECT OF CMS ON EPITHELIAL REPAIR 70

1.8 HYPOTHESIS AND AIMS 71

2 CHAPTER 2: MATERIALS AND METHODS 75

2.1 REAGENTS AND MATERIALS 76

2.1.1 GENERAL REAGENTS 76

2.1.2 CELLS AND CULTURE REAGENTS 77

2.1.3 CYTOSKELETAL REAGENTS 77

2.1.4 CYTOKINES, INHIBITORS AND OTHER DRUGS 78

2.1.5 MOLECULAR BIOLOGY REAGENTS 78

2.1.5.1 RNA extraction and processing 78

2.1.5.1.1 Taqman primers 79

2.1.5.2 siRNA reagents 80

2.1.5.2.1 siRNA sequences 80

2.1.6 ANTIBODIES 81

2.1.6.1 Primary antibodies 81

2.1.6.2 Secondary antibodies 82
2.1.7 PRECISION CUT LUNG SLICES (PCLS) 83
2.1.7.1 Murine PCLS culture 83
2.1.7.2 Human PCLS culture 84
2.1.8 IMAGING REAGENTS 84
2.1.9 ELISA AND MSD KITS 84
2.1.10 WESTERN BLOT REAGENTS 85
2.1.11 EQUIPMENT 85
2.1.12 SOFTWARE 86
2.1.13 COMPANY LOCATIONS 87
2.2 GENERAL METHODS 91
2.2.1 A549 CELL LINE CULTURE 91
2.2.1.1 Cell counting 91
2.2.1.2 MTT determination of cell viability 92
2.2.2 GENERATION AND CULTURE OF PRECISION CUT LUNG SLICES (PCLS) 92
2.2.2.1 Murine lung slices 92
2.2.2.2 Human lung slices 93
2.2.2.3 PCLS viability studies 96
2.2.3 MOLECULAR BIOLOGY 97
2.2.3.1 Ribose nucleic acid (RNA) extraction 97
2.2.3.2 Reverse transcription (RT) protocol 99
2.2.3.3 Polymerase chain reaction (PCR) 99
2.2.3.3.1 Working principle 99
2.2.3.3.2 Quantitative real time PCR (qPCR) 101
2.2.3.3.3 SYBR Green 1 102
2.2.3.3.4 Taqman 103
2.2.3.3.5 Taqman primers 104

2.2.3.4 Quantification of gene expression 104
2.2.3.5 RNA interference 105
2.2.3.5.1 Working principle 105
2.2.3.5.2 Transfection of siRNA into cells 106
2.2.4 *IN VITRO* CELLULAR ASSAYS 106
2.2.4.1 Application of Cyclic Mechanical Strain (CMS) 106
2.2.4.1.1 Flexercell system and working principle 106
2.2.4.1.2 Application of CMS to cells using the Flexercell system 109
2.2.4.1.3 Preparation of A549 cells for application of cyclic mechanical strain 110
2.2.4.2 'Scratch assay' epithelial migration model 111
2.2.4.3 Electrical impedance assay 112
2.2.4.4 Cell adhesion assay 114
2.2.5 IMAGING TECHNIQUES 114
2.2.5.1 Confocal laser scanning microscopy 114
2.2.5.1.1 Working Principle 114
2.2.5.1.2 Fluorescence 115
2.2.5.1.3 Preparation of cell samples for confocal immunofluorescence 116
2.2.5.1.4 Preparation of tissue samples for confocal immunofluorescence 117
2.2.5.2 Fluorescence Lifetime Imaging 118
2.2.5.2.1 Förster Resonance Energy Transfer (FRET) 118
2.2.5.2.2 Fluorescence Lifetime Imaging Microscopy (FLIM) 120
2.2.5.2.3 Vinculin tension sensor (VinTS) FRET probes 121
2.2.5.2.4 Raichu RhoA GFP probes 123
2.2.5.2.5 Transfection of A549 cells with plasmid DNA 126
2.2.5.2.6 FLIM setup for Raichu and VinTS probes 127
2.2.5.2.7 FLIM analysis 127
2.2.6 OTHER ANTIBODY-BASED ASSAYS 129

2.2.6.1 Enzyme-linked Immunosorbent Assay (ELISA) 129

2.2.6.1.1 Working Principle 129

2.2.6.1.2 Duoset ELISA 131

2.2.6.2 Electrochemiluminescence (MSD) 132

2.2.6.2.1 Working Principle 132

2.2.6.2.2 MSD protocol 133

2.2.6.3 Western Blotting 134

2.2.6.3.1 Working Principle 134

2.2.6.3.2 Western Blot protocol 135

2.2.7 STATISTICAL ANALYSIS 137

2.2.7.1 Data processing 137

2.2.7.2 Data presentation and analysis 138

3 CHAPTER 3: CYCLIC MECHANICAL STRAIN (CMS)-INDUCED CYTOSKELETAL REMODELLING, RHOGTPASE SIGNALLING AND FORCE TRANSDUCTION IN ALVEOLAR EPITHELIAL CELLS 139

3.1 INTRODUCTION 140

3.2 SPECIFIC METHODS 143

3.2.1 CYTOSKELETAL GENE REGULATION FOLLOWING CMS 143

3.2.2 ROCK AND MYOSIN II INHIBITION, AND ANALYSIS OF CMS-INDUCED CYTOKINE GENERATION 143

3.2.3 IMMUNOFLUORESCENCE FOR CYTOSKELETAL AND FOCAL ADHESION REMODELLING AFTER CMS 144

3.2.4 ANALYSIS OF CMS-INDUCED FAK PHOSPHORYLATION 144

3.2.5 MEASUREMENT OF CMS-INDUCED CELL TRACTION FORCES AND RHOA ACTIVITY 145

3.3 RESULTS 146

3.3.1 CMS-INDUCED CYTOSKELETAL REMODELLING 146

3.3.2 CMS-INDUCED FOCAL ADHESION REMODELLING 147

3.3.3 THE EFFECT OF ROCK INHIBITION ON CMS-INDUCED CYTOSKELETAL AND FOCAL ADHESION REMODELLING 148

3.3.4 THE EFFECT OF ROCK INHIBITION ON CMS-INDUCED IL-8 RELEASE 149

3.3.5 THE EFFECT OF LPA AND CYTOCHALASIN D ON CMS-INDUCED IL-8 RELEASE 152

3.3.6 THE EFFECT OF CMS AND ROCK INHIBITION ON FAK PHOSPHORYLATION 153

3.3.7 THE EFFECT OF MYOSIN II INHIBITION ON CMS-INDUCED CYTOKINE RELEASE 155

3.3.8 THE EFFECT OF MYOSIN II INHIBITION ON CMS-INDUCED CYTOSKELETAL AND FOCAL ADHESION REMODELLING 157

3.3.9 THE EFFECT OF CMS ON CELLULAR TRACTION FORCE 158

3.3.10 THE EFFECT OF CMS ON RHOA ACTIVITY 160

3.4 DISCUSSION 162

3.4.1 SUMMARY OF IMPORTANT FINDINGS 162

3.4.2 CMS-INDUCED CYTOSKELETAL AND FOCAL ADHESION REMODELLING 162

3.4.3 RHO-ROCK-MYOSIN II SIGNALLING IS REQUIRED FOR CMS-INDUCED CYTOKINE GENERATION 166

3.4.4 CELLULAR TENSION DURING CMS-INDUCED MECHANOTRANSDUCTION 170

3.4.5 CMS-INDUCED REGULATION OF RHOA ACTIVITY 174

3.4.6 LIMITATIONS 176

3.4.7 CONCLUSIONS 177

3.4.8 FUTURE DIRECTIONS 178

4 CHAPTER 4: THE ROLE OF CD98HC IN RESPONSES OF THE LUNG ALVEOLAR EPITHELIUM TO CYCLIC MECHANICAL STRAIN (CMS) 180

4.1 INTRODUCTION 181

4.2 SPECIFIC METHODS 183

4.2.1 EFFECT OF CD98HC KNOCKDOWN (KD) ON CMS-INDUCED IL-8 PROTEIN, GENE EXPRESSION AND CELL VIABILITY 183

4.2.2 B1-INTEGRIN-MEDIATED SIGNALLING AND MECHANOTRANSDUCTION IN CMS 184

4.2.3 Assessment of the effect of CD98hc kd on cellular tension and RhoA activity 185
4.2.4 Assessment of epithelial cell migration in CD98hc kd cells 185
4.2.5 Assessment of epithelial monolayer integrity in CD98hc kd cells 185
4.2.6 The effect of CD98hc kd on cell-matrix adhesion after CMS 186
4.3 Results 187
4.3.1 The effect of CD98hc knockdown on CMS-induced IL-8 protein and gene expression 187
4.3.2 The effect of CD98hc knockdown on CMS-induced b1-integrin and MAPK p42/44 (ERK 1/2) activity 189
4.3.3 The effect of CD98hc knockdown on CMS-induced FAK and ERK activity, and on actin cytoskeletal integrity 192
4.3.4 The effect of CD98hc knockdown on baseline and CMS-induced cellular tension 194
4.3.5 The effect of CD98hc knockdown on RhoA activity 198
4.3.6 The effect of CD98hc knockdown on epithelial cell migration in a wound healing model 201
4.3.7 The effect of CD98hc knockdown on epithelial monolayer integrity 204
4.3.8 The effect of CD98hc knockdown on cell-matrix adhesion 205
4.4 Discussion 208
4.4.1 Summary of results 208
4.4.2 Mechanotransduction, integrin and focal adhesion signalling 209
4.4.3 CD98hc–regulated tension at focal adhesions and RhoA activity 214
4.4.4 Migration and adhesion 219
4.4.5 Summary and limitations 223
4.4.6 Future directions 225

5 CHAPTER 5: APPLICATION OF CYCLIC MECHANICAL STRAIN (CMS) TO PRECISION CUT LUNG SLICES (PCLS) 228

5.1 INTRODUCTION 229

5.2 SPECIFIC METHODS 231

5.2.1 PCLS ARCHITECTURE FOLLOWING CMS 231

5.2.2 CMS-INDUCED CYTOKINE RELEASE 232

5.2.3 ASSESSMENT OF PCLS VIABILITY 232

5.2.4 CELL PROLIFERATION IN PCLS 232

5.2.5 VISUALISATION OF CYTOKINE RELEASE IN PCLS 233

5.2.6 CYTOKINE GENE REGULATION IN PCLS 233

5.2.7 ASSESSMENT OF ERK PHOSPHORYLATION DOWNSTREAM OF CMS 233

5.3 RESULTS 235

5.3.1 PCLS ARCHITECTURE FOLLOWING CMS 235

5.3.2 CMS-INDUCED CYTOKINE RELEASE IN MURINE PCLS 237

5.3.3 CMS-INDUCED CYTOKINE RELEASE IN HUMAN PCLS 239

5.3.4 VIABILITY OF PCLS 240

5.3.5 CELL PROLIFERATION IN MURINE PCLS EXPOSED TO CMS 242

5.3.6 CELL PROLIFERATION IN HUMAN PCLS EXPOSED TO CMS 243

5.3.7 CHARACTERISATION OF PROLIFERATING CELLS 244

5.3.8 VISUALISATION OF CYTOKINE RELEASE IN PCLS 247

5.3.9 CYTOKINE GENE REGULATION IN PCLS 249

5.3.10 CMS-INDUCED DOWNSTREAM SIGNALLING IN PCLS 251

5.4 DISCUSSION 253

5.4.1 SUMMARY OF RESULTS 253

5.4.2 APPLICATION OF CMS TO PCLS 254

5.4.3 CMS-INDUCED CYTOKINE RELEASE 256

5.4.4 VIABILITY OF PCLS 259

5.4.5 CMS-INDUCED PROLIFERATION 262

5.4.6 SUMMARY AND LIMITATIONS 266

5.4.7 FUTURE DIRECTIONS 267

6 CHAPTER 6: DISCUSSION AND FURTHER WORK 269

6.1 SUMMARY OF IMPORTANT RESULTS FROM THIS THESIS 270

6.2 THE ROLE OF THE CD98HC-RHOA-NMII AXIS IN ALVEOLAR EPITHELIAL MECHANOBIOLOGY 271

6.2.1 CELLULAR TENSION AND PRE-STRESS 271

6.2.2 MITOCHONDRIAL ROS AND ERK SIGNALLING 273

6.2.3 CD98HC SIGNALLING 274

6.3 TARGETTING CD98HC-RHOA-NMII SIGNALLING IN CLINICAL PRACTICE 276

6.4 FUTURE WORK 277

6.5 OVERALL CONCLUSIONS 279

7 REFERENCES 281

8 APPENDIX 1: COPYRIGHT AND PERMISSIONS 308

List of Figures

Figure 1-1 Ventilator-associated lung injury (VALI) 28

Figure 1-2 The alveolar epithelium 32

Figure 1-3 Proposed mechanotransduction pathways in VALI 40

Figure 1-4 Flexcell mechanism of equibiaxial cell strain 42

Figure 1-5 Focal adhesions in 3-dimensions do not resemble those seen in culture on flat surfaces 45

Figure 1-6 Conformation of integrins 50

Figure 1-7 The molecular clutch hypothesis of integrin-matrix adhesion 57

Figure 1-8 Structure of CD98 62

Figure 1-9 Putative mechanism by which integrin and RhoA GPTase signalling may mediate CMS-induced injury in alveolar epithelial cells .. 74

Figure 2-1 Generation and culture of Precision Cut Lung Slices (PCLS) 95

Figure 2-2 Optimisation of Calcein and Ethidium staining in murine Precision Cut Lung Slices (PCLS) 97

Figure 2-3 Principle of the Polymerase Chain Reaction 101

Figure 2-4 The Flexcell FX-5000™ system 108

Figure 2-5 Optimising cell seeding density for CMS-induced IL-8 release .. 110

Figure 2-6 Outline of 'scratch assay' epithelial migration model 112

Figure 2-7 Electrical impedance assay 113

Figure 2-8 Line diagram representation of confocal microscopy process ... 115

Figure 2-9 Jablonski diagram 116

Figure 2-10 Vinculin tension sensor (VinTS) constructs and plasmid map . 123

Figure 2-11 pRaichu RhoA probe 125

Figure 2-12 Enzyme-linked immunosorbent assay (ELISA) working principle 130

Figure 2-13 Mesoscale Discovery (MSD) electrochemiluminescence 133

Figure 2-14 Western Blot general principle 135

Figure 3-2 Cyclic Mechanical Strain (CMS)-induced focal adhesion remodelling 148

Figure 3-3 Effect of Rho-associated protein kinase (ROCK) inhibition on CMS-induced cytoskeletal and focal adhesion remodelling 149

Figure 3-6 The effect of CMS and ROCK inhibition on FAK phosphorylation 154

Figure 3-8 The effect of myosin II inhibition on CMS-induced cytoskeletal and focal adhesion remodelling 157

Figure 3-9 The effect of CMS on cellular traction force 160

Figure 3-10 The effect of CMS on RhoA activity 161

Figure 4-2 The effect of CD98hc knockdown on CMS-induced β1-integrin activity 192

Figure 4-3 The effect of CD98hc knockdown on CMS-induced FAK and ERK activation, and on actin cytoskeletal integrity 193

Figure 4-4 Dual transfection of A549 cells with CD98hc knockdown siRNA and RhoGFP FRET probe 196

Figure 4-5 The effect of CD98hc knockdown on cellular traction forces 197

Figure 4-6 The effect of CD98hc knockdown on RhoA activity 200

Figure 4-7 The effect of CD98hc knockdown on epithelial cell migration in a wound healing model 203

Figure 4-8 The effect of CD98hc knockdown on epithelial monolayer permeability as measured by trans-epithelial resistance 205

Figure 4-9 The effect of CD98hc kd on cell-matrix adhesion following CMS207

Figure 4-10 The HUTS4 antibody detects β1-integrin activation at the exposed hybrid domain in the high-affinity state 213

Figure 4-11 Putative mechanism for the effect of CD98hc kd on reducing CMS-induced injurious signalling 224

Figure 5-1 Proposed workflow for investigating CMS-induced signalling using PCLS 234

Figure 5-2 PCLS architecture following CMS 236

Figure 5-3 CMS-induced cytokine release in murine PCLS 238

Figure 5-4 CMS-induced cytokine release in human PCLS 240

Figure 5-5 Viability of PCLS 241

Figure 5-6 Cell proliferation in murine PCLS exposed to CMS..... 243

Figure 5-7 Cell proliferation in human PCLS exposed to CMS..... 244

Figure 5-8 Characterisation of proliferating cells 247

Figure 5-9 Visualisation of cytokine release in murine PCLS 248

Figure 5-10 Cytokine gene regulation in PCLS 250

Figure 5-11 CMS-induced ERK phosphorylation in murine PCLS..... 252

Figure 6-1 Proposed CMS-induced mechanotransduction pathway in alveolar epithelial cells 276

List of tables

Table 1-1 Major classes of integrin-ligand partners 49

Table 2-1 Taqman Primers 79

Table 2-2 siRNA sequences used 80

Table 2-3 Table of primary antibodies 82

Table 2-4 Table of secondary antibodies 83

Table 2-5 siRNA transfection protocol 106

Table 2-6 Protocol for lipofectamine-induced transfection of plasmid DNA into A549 cells 126

Table 2-7 Duoset ELISA reagents 131

Table 2-8 Western blot reagents 137

List of equations

Equation 1 Comparative CT method 105

Equation 2 FRET efficiency 119

Equation 3 Förster radius 119

Equation 4 Marquardt mono-exponential decay model 128

Equation 5 FRET efficiency 128

Abbreviations

ACE	Angiotensin-Converting Enzyme
AFM	Atomic Force Microscopy
AQP5	Aquaporin-5
ARDS	Acute Respiratory Distress Syndrome
ATI	Alveolar epithelial cell Type I
ATII	Alveolar epithelial cell Type II
AURKC	Aurora Kinase C
BALF	Bronchoalveolar Lavage Fluid
BAIAP2	Brain-specific Angiogenesis Inhibitor 1-Associated Protein 2
BASC	Bronchoalveolar Stem Cell
BSA	Bovine Serum Albumin
CD98	Cluster of Differentiation 98
CMS	Cyclic Mechanical Strain
CPAP	Continuous Positive Airways Pressure
DASC	Distal Airway Stem Cell
DMEM	Dulbecco's Modified Eagle Medium
DMSO	Dimethyl Sulphoxide
DTT	Dithiothreitol

ECM	Extracellular Matrix
EDTA	Ethylenediaminetetraacetic acid
EGF	Epidermal Growth Factor
ELISA	Enzyme-Linked Immunosorbent Assay
ENA	*Drosophila* enabled
ERK	Extracellular signal Related Kinase
EPCAM	Epithelial Cell Adhesion Molecule
ESC	Embryonic Stem Cell
EVLP	*Ex Vivo* Lung Perfusion
FA	Focal Adhesion
FasL	Fas ligand
FAK	Focal Adhesion Kinase
FITC	Fluorescein isothiocyanate
FLIM	Fluorescence Lifetime Imaging Microscopy
FRET	Förster Resonance Energy Transfer
FRC	Functional Residual Capacity
GAP	GTP-ase Activating Protein
GDI	Rho GDP-Dissociation Inhibitor
GDP	Guanosine Diphosphate
GEF	Guanine nucleotide Exchange Factor

GFP	Green Fluorescent Protein
GROα	Growth Related Protein alpha
GTP	Guanosine Triphosphate
HBSS	Hank's Buffered Saline Solution
HOPX	Homeodomain-only protein
HPAEC	Human Pulmonary Artery Endothelial Cells
HRP	Horseradish Peroxidase
HTERT	Human Telomerase Reverse Transcriptase
ICAM	Intercellular Adhesion Molecule
IF	Immunofluorescence
IKK	IκB Kinase
IL	Interleukin
IQR	Interquartile range
KC	Keratinocyte Chemoattractant
KGF	Keratinocyte Growth Factor
LARG	Leukaemia-Associated Rho GEF
LNEP	Lineage-Negative Epithelial Progenitor
LPA	Lypophosphatidic Acid
MAPK	Mitogen-Activated Protein Kinase
MIP	Macrophage Inflammatory Protein

MLC	Myosin Light Chain
MSC	Mesenchymal Stem Cell
MSD	Mesoscale Discovery
mTFP	monomeric Teal Fluorescent Protein
MTT	Methylthiazolitetrazolium
MLE	Murine Lung Epithelial cells
NF-κB	Nuclear Factor Kappa-light-chain-enhancer of activated B cells
NOS	Nitric Oxide Synthase
NMII	Non-muscle Myosin II
NMR	Nuclear Magnetic Resonance
NND	Nearest Neighbour Distance
OMTC	Optical Magnetic Twisting Cytometry
PBS	Phosphate Buffered Saline
PCLS	Precision Cut Lung Slice
PCNA	Proliferating Cell Nuclear Antigen
PCR	Polymerase Chain Reaction
PH3	Phospho-histone H3
PI3k	Phosphoinositide 3-kinase
PJAR	Perijunctional Actin Ring
PECAM	Platelet Endothelial Cell Adhesion Molecule

PMSF	Phenylmethanesulphonyl fluoride
PKN	Protein Kinase-N
PVDF	Polyvinylidene Fluoride
Rac1	Ras-related C3 botulinum toxin substrate 1
RIN	RNA integrity number
ROCK	Rho-associated protein kinase
RFP	Red Fluorescent Protein
RGD	Arginylglycylaspartic acid
RISC	RNA-Induced Silencing Complex
RNA	Ribonucleic Acid
mRNA	messenger RNA
RTCA	Real-Time Cell Analysis
ROS	Reactive Oxygen Species
Src	Proto-oncogene tyrosine-protein kinase sarcoma
α-SMA	alpha smooth muscle actin
Pro-SPC	Surfactant Protein C
SSH2	Slingshot protein phosphatase 2
TAZ	Transcriptional co-activator with PDZ-binding motif
TNF	Tumour Necrosis Factor

TLC	Total Lung Capacity
TRIM72	Tripartite Motif-containing protein 72
TUNEL	Terminal deoxynucleotidyl transferase dUTP Nick End Labelling
UTR	Untranslated Region
VALI	Ventilator-Associated Lung Injury
VASP	Vasodilator-Stimulated Phosphoprotein
VinTS	Vinculin Tension Sensor
WB	Western Blot
YAP	Yes-Associated Protein

1 Chapter 1: Introduction

1.1 Mechanobiology of the lung

The lung is subjected to distending mechanical forces which regulate its development, maturation and repair, but can also promote disease and lead to injury. Mechanical ventilation of critically ill patients is life-saving, but can also induce pulmonary and systemic injury. Mechanical distension of the alveolar epithelium, particularly in the context of lung injury, can lead to injurious biological signalling that promotes multi-organ failure, long-term morbidity and death. Understanding the molecular signalling processes that underlie mechanotransduction in the lung is critical not only to improve outcomes for mechanically ventilated patients, but also to advance research in lung development, regeneration and repair.

1.1.1 Ventilator-associated lung injury (VALI)

Ventilator-associated lung injury (VALI) describes the process by which mechanical ventilation of the lung exacerbates pulmonary and systemic injury (Salman et al. 2013). The pathological appearances of VALI and the Acute Respiratory Distress Syndrome (ARDS) (The ARDS Definition Task Force 2012), are indistinguishable. VALI is a key component of ARDS and the vast majority of patients with the latter require mechanical ventilation (Pinhu et al. 2003). Whilst it was known that mechanical ventilation can cause ARDS in animal models (Dreyfuss & Saumon 1998), the concept that mechanical ventilation strategy is a key determinant of survival in ARDS was confirmed by the landmark ARMA ARDS Network trial in 2000 (ARDS Network 2000).

Patients with ARDS were randomised to either ventilation with the traditional tidal volumes used at the time of the study (12ml/kg predicted body weight) or with lower volumes of 6ml/kg. The latter group not only had reduced concentrations of circulating inflammatory mediators and indices of extra-pulmonary organ failure, but crucially had a 9% absolute survival benefit. Therefore, modulation of mechanical force in the lung is not only critical for reducing lung injury, but also affects the ability of the lung to mediate extra-pulmonary organ damage.

Importantly, high tidal volume ventilation can induce injury in previously 'healthy' lungs, suggesting that mechanical force can have a direct, rather than additive, effect (Guay & Ochroch 2015; Guo et al. 2016; Sutherasan et al. 2014; Serpa Neto et al. 2012; Pinheiro de Oliveira et al. 2010) and reduced tidal volume ventilation can improve clinical outcomes for patients undergoing abdominal surgery (Futier et al. 2013; Futier & Jaber 2014).

Moreover, injury sustained from injurious mechanical ventilation can impact mortality and morbidity in the long term (Needham et al. 2012). ARDS affects approximately 190,000 patients each year in the Unites States alone with a mortality of around 40% (Rubenfeld & Herridge 2007), and reducing VALI is predicted to not only save 10 lives a day, but also to be cost effective even if $10,000 were spent to reduce tidal volumes per patient with ARDS (Cooke et al. 2009). Despite this, implementation of lower tidal volume ventilation into widespread clinical practice has been difficult (Young et al. 2004), and no disease modifying agent has yet been developed to reduce the injury induced by mechanical ventilation.

Distension of the lung, as opposed to high pressures, is thought to mediate injury (de Prost et al. 2011). Rodents ventilated with high pulmonary pressures developed less pulmonary oedema where thoraco-abdominal strapping was used to reduce chest expansion (Hernandez et al. 1989). Over-distension, such as in VALI, is associated with increased pulmonary (Wilson et al. 2003) and systemic cytokine release (Chiumello et al. 1999), such as interleukin (IL)-8, IL-6 and Tumour Necrosis Factor (TNF)-α (Ranieri et al. 1999) in a process whereby the lung becomes an 'engine' of inflammation (Figure 1-1). Conversely, decreasing tidal volumes abrogates this effect (Slutsky 2005). Because high tidal volume ventilation increases expression of IL-6 and TNF-α messenger RNA (mRNA) by the alveolar epithelium (Tremblay et al. 2002), investigations into VALI have focussed here but many cells isolated from human lung parenchyma produce inflammatory mediators in response to mechanical strain (Pinhu et al. 2003).

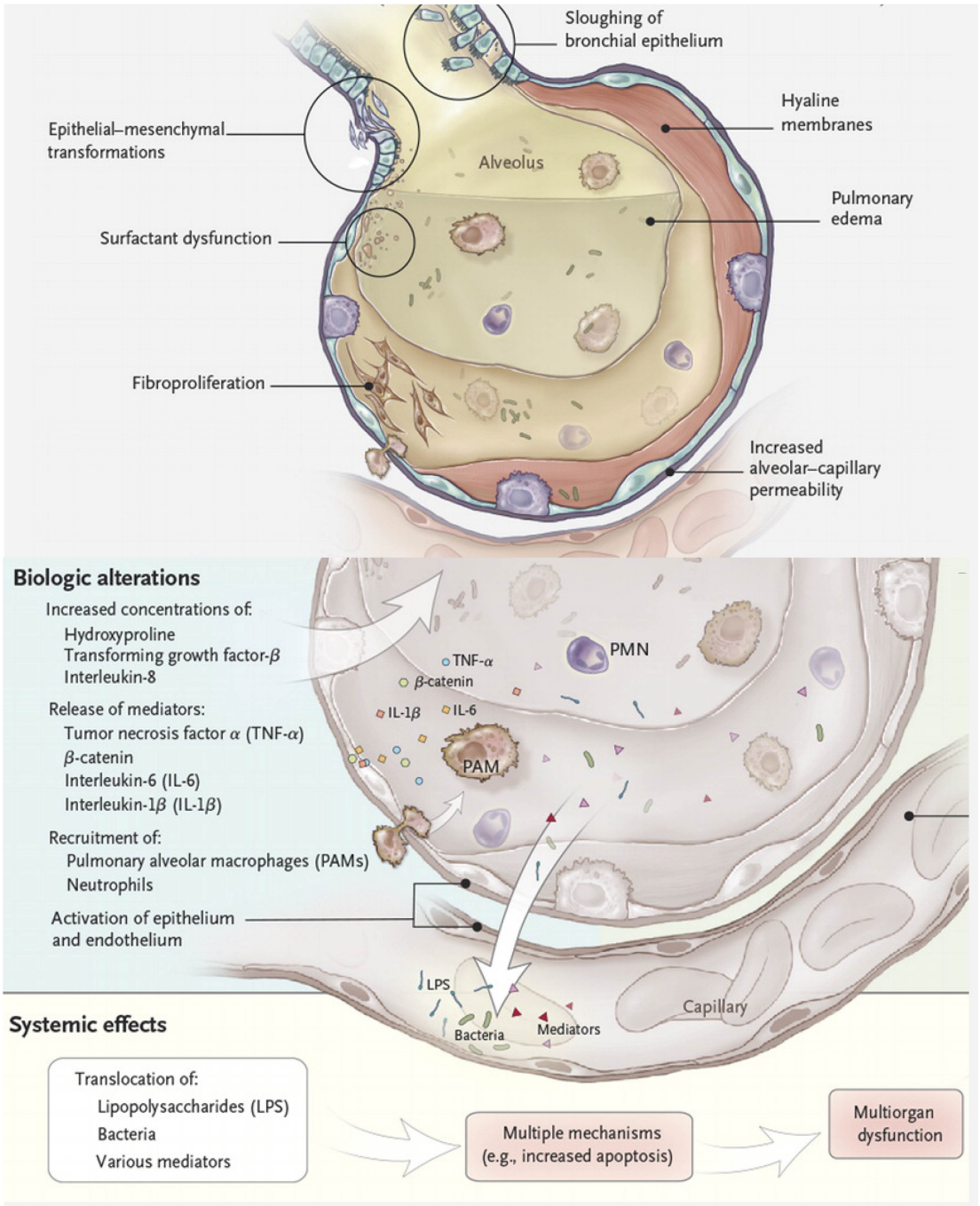


Figure 1-1 Ventilator-associated lung injury (VALI)

Image adapted and reproduced with permission from (Slutsky & Ranieri 2013), copyright Massachusetts Medical Society. Overdistention of the lung can lead to increases in alveolar–capillary permeability and subsequent pulmonary oedema. The injured lung releases mediators that recruit neutrophils to the lung and propagate further injury. Translocation of inflammatory mediators and bacteria into the systemic circulation can occur, leading to multi-organ dysfunction (biotrauma).

IL – interleukin, PMN – polymorphonuclear leukocyte, TGF β - transforming growth factor-β, TNF - tumour necrosis factor

1.1.2 Distending forces in the lung in health and disease

The alveoli form a three dimensional, interconnected network, where neighbouring alveoli share structural walls and are interdependent (Mead et al. 1970). Therefore, this complex structure expands non-uniformly, with external stresses transmitted throughout the structure and the lung parenchyma in particular (Waters et al. 2012). During normal tidal breathing, an increase in the transpulmonary pressure (the difference between the pressure in the pleural space (P_{PL}) and the alveolus (P_{ALV})) causes the lungs to expand. Air flows into the lungs providing that P_{ALV} is less than atmospheric pressure (P_{ATM}). Load is applied to the alveoli from the surface tension of air-fluid interfaces, elastic recoil of tissue, interdependence between neighbouring alveolar units, and P_{ALV} (Roan & Waters 2011). Forces acting on the pleura from the respiratory muscle and chest wall are also transmitted throughout the lung parenchyma (Macklem et al. 1983).

The physiological changes experienced by alveoli during distension are not completely understood (Roan & Waters 2011). Alveoli from isolated rat lungs appear to distend at low pressures by unfolding and re-folding of alveolar septa (pleating), but at higher distending volumes, there is stretching of septal tissue (Tschumperlin & Margulies 1999). During normal tidal breathing, the alveolar basement membrane, composed of load-bearing collagen, elastin and proteoglycans (Suki et al. 2005), is estimated to distend linearly by 4% (Forrest 1970; Roan & Waters 2011) whereas higher tidal volume ventilation may distend the epithelial basement membrane surface

area to approximately 40% (Tschumperlin & Margulies 1999). As a consequence, the distending stresses required increase in a non-linear fashion from very low at residual volume, to approximately 5 cmH_2O at functional residual capacity (FRC), and 30 cmH_2O at total lung capacity (Waters et al. 2012).

The heterogeneous nature of the injured lung tends to spread the load of mechanical strain unevenly. The presence of oedema-filled alveoli both decreases the volume of compliant lung subjected to distending forces (the baby lung) (Gattinoni et al. 1993), and examination of the mechanics of a single alveoli suggested that collapsed or fluid-filled lung units increase the interfacial stresses experienced by neighbouring lung units (Perlman et al. 2011). This over-distension of air-filled lung units (volutrauma) is compounded by the injurious effects of repetitive opening and closing of lung units (atelectrauma) (Dreyfuss et al. 1988), associated with surfactant dysfunction. Although not comprehensively characterised (Hubmayr 2002), atelectrauma may not contribute significantly to lung (Güldner et al. 2016) or systemic (Wakabayashi et al. 2014) injury, but is still taken into consideration when considering mechanical ventilation strategies for patients.

1.2 Mechanobiology of the alveolar epithelium

1.2.1 The alveolar epithelium

The alveolar epithelium comprises a diverse array of cell types working as a unit both to establish a barrier to the external environment, and to enable gas exchange (Zemans et al. 2015). This epithelial barrier is composed of two

key cell types. Flat and broad alveolar type I cells (ATI), which cover the majority of the luminal surface of the alveolar structure, are more sensitive to injury, possibly due to their size and subsequent exposure to insults, and an inability to self-repair (Herzog et al. 2008; Mason 2006). Cuboidal alveolar type II cells (ATII), although more numerous than ATI, cover the remaining 5% of the epithelial surface (Mason 2006). Morphologically, ATII can be characterised by apical microvilli and lamellar bodies (Fujino et al. 2010) (Figure 1-2). Functionally, there are three primary roles of the ATII.

First, they are responsible for the production of pulmonary surfactant to decrease alveolar surface tension (Andreeva et al. 2007). Second, they act as progenitor cells of the alveolar epithelium (Barkauskas et al. 2013). Indeed, following damage to ATI early in the course of lung injury, ATII de-differentiate to ATI-like cells to restore the epithelium (Evans et al. 1975; Desai et al. 2014). Finally, ATII are responsible for the majority of fluid transport across the epithelium, actively transporting sodium from the apical to basolateral surface and clearing fluid from the alveolar space (Mason et al. 1982; Matthay 2005). For these reasons, along with the capacity of the ATII to regulate innate immunity in the lung (Chignalia et al. 2015), ATII have been described as the ‘defender’ of the alveolus (Mason et al. 1982; Mason 2006).

However, this picture may be incomplete. Whereas both ATI and ATII are thought to derive from a bipotent progenitor lineage (Desai et al. 2014), the concept that ATI represent a terminally differentiated cell that can be repopulated by differentiation of ATII is challenged by recent observations that suggest differentiated ATI expressing the homeodomain-containing protein

Hopx can both self-renew and generate ATII in the post-pneumonectomy lung (Jain et al. 2015), suggesting a bidirectional relationship and plasticity between the two cell types in lung regeneration and repair (Figure 1-2).

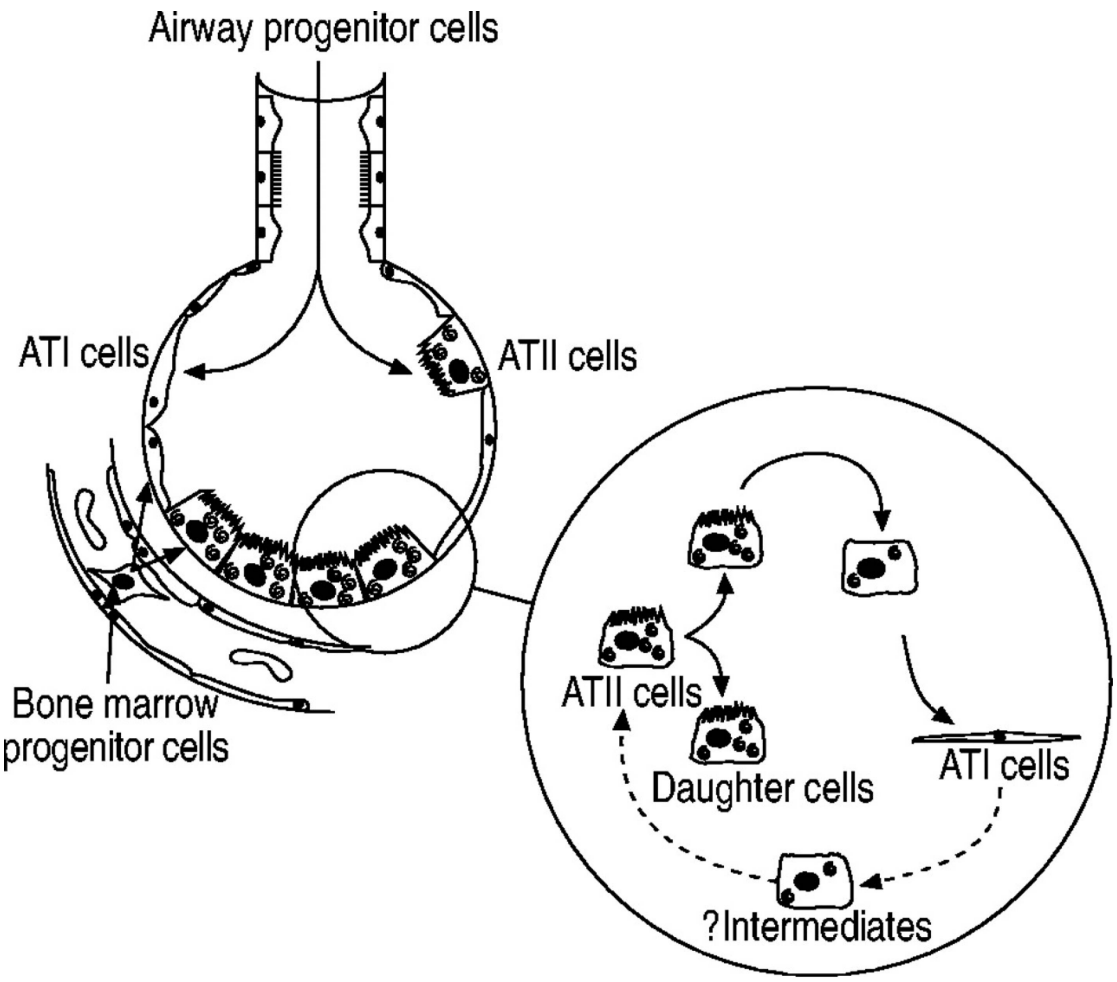


Figure 1-2 The alveolar epithelium

Image reproduced and adapted (McElroy & Kasper 2004) with permission of the © ERS 2004. European Respiratory Journal Oct 2004, 24(4)664-673;DOI: 10.1183/09031936.04.00096003. The alveolar epithelium is populated by thin and numerous ATI, and cuboidal ATII cells containing lamellar bodies and apical microvilli. Following injury, ATII proliferate and transdifferentiate to ATI via intermediate cells, although the relationship may be bi-directional.

ATI- alveolar epithelial type I cell, ATII – alveolar epithelial type II cell

1.2.2 Alveolar epithelial responses to stretch

1.2.2.1 Force-induced lung maturation and cell differentiation

The vast surface area of the alveolar epithelium is exposed to cyclic stretching forces from as early as *in utero*, when foetal breath movements influence its development (Wigglesworth & Desai 1979). Transection of the spinal cord of foetal rabbits above the level of the phrenic nerve, which ablates diaphragmatic-derived foetal breath movements, decreased lung growth by 70% when compared to controls. Indeed, distension of the foetal lung through tracheal obstruction demonstrably increased lung growth (Moessinger et al. 1990), and cellularity (Nardo et al. 2000). Similarly, foetal alveolar epithelial distension also promoted ATII to ATI cell differentiation (Flecknoe et al. 2000; Flecknoe et al. 2002). Cyclic strain of foetal ATII *in vitro* promoted surfactant-protein (SP) B and C gene expression and surfactant protein production, indicating that alveolar epithelial cell maturation and function is directly related to mechanical stimulation (Sanchez-Esteban et al. 2001). In fact, previous studies demonstrated that a single stretch of cultured primary ATII was enough to increase intracellular calcium and surfactant secretion (Wirtz & Dobbs 1990).

However, the relationship between strain and cell differentiation or surfactant release is not linear. Decreases in alveolar distension following birth, due to clearing of alveolar fluid, alter the relative proportions of ATI and ATII further, promoting decreases in ATI and increasing the ATII population (Flecknoe et al. 2003). Therefore, there is a relationship between mechanical force and alveolar epithelial cell differentiation and function, but the precise

nature of this interaction is yet to be determined (Waters et al. 2012). Furthermore, the mechanosensitive component of foetal alveolar epithelial cells has recently been localised to the integrin-cell matrix interface, where depletion of epithelial-specific β1 integrin in embryonic mice was associated with impaired alveolarisation and epithelial cell differentiation, and altered lung branching morphogenesis (Plosa et al. 2014).

Examples of mechanical force-induced cellular differentiation have been demonstrated in other cell types, such as in mesenchymal stem cells (MSC), in which shear stresses induced osteogenesis (Sonam et al. 2016). Crucially, different degrees of force and cell contractility direct cell fate. MSCs cultured on soft matrices undergo neurogenesis, whereas those cultured on stiff matrices adopt myogenic fates, and those on rigid matrices, osteogenic fates (Engler et al. 2006). These force-induced differentiation cues are dependent on myosin II-mediated cell contractility, and abrogated by the non-muscle myosin II (NMII) inhibitor, blebbistatin. Furthermore, only cells with higher contractility responded to force by altering fate (Sonam et al. 2016), and when actomyosin contractility was inhibited, force-induced differentiation did not occur, confirming previous observations that RhoA-mediated cell contractility directs force–induced differentiation (McBeath et al. 2004). Therefore, there are precedents in other cell types that mechanotransduction drives cellular differentiation in a RhoA-myosin II-dependent manner, and that these may be relevant to the alveolar epithelium.

1.2.2.2 Force-induced cell proliferation in the lung

Following birth, the lung, and the alveolar epithelium in particular, continue to show responses to mechanical forces. For example, the capacity of the lung to grow following partial pneumonectomy has been demonstrated (Rannels 1989) in dogs (Hsia et al. 1994), guinea pigs (Hsia 2004), rabbits (Thurlbeck & Langston 1989), rats (Buhain & Brody 1973) and mice (Liu et al. 2014) and is attributed to the increase in distension force in the remaining lung, as prevention of such over-distension by the insertion of prosthetic material to fill vacant area inhibits re-growth (Hsia et al. 2001; Hoffman et al. 2010). This effect has been demonstrated in humans, with evidence of increased lung mass and new alveolar units following pneumonectomy (Butler et al. 2012). Furthermore, alveolar epithelial regrowth comprises a major component of compensatory growth of the lung (Hsia et al. 2001), and there is evidence that proliferation of ATII is implicated (Brody et al. 1978) although the mechanism for this is unclear.

Early observations suggested that Cyclic Mechanical Strain (CMS) increased proliferation of foetal ATII *in vitro* via mechanisms involving platelet derived growth factor (Liu et al. 1995) or stretch activated calcium channels (Liu et al. 1994). Alveolar epithelial cells in culture proliferate in response to low degree CMS for periods greater than 24 hours (Chaturvedi et al. 2006) and recent evidence indicated that mechanical ventilation induced cell cycle entry in murine ATII (Chess et al. 2010). Furthermore, evidence of CMS-induced proliferation has been demonstrated in other cell types, such as airway epithelial cells (Savla et al. 2004), vascular smooth muscle cells

(Mantella et al. 2015), fibroblasts (Cui et al. 2015) and MSCs (Ghazanfari et al. 2009).

Two mechanistic pathways of stretch-induced proliferation have recently gained traction. First, in fibroblasts (Cui et al. 2015) and epithelial cells (Aragona et al. 2013), Yes-associated protein (YAP) and transcriptional co-activator with PDZ-binding motif (TAZ) were activated in response to stretch which promoted entry to S-phase. Furthermore, in epithelial cells, this was dependent on expression of β-catenin and E-cadherin extracellular engagement (Benham-Pyle et al. 2015). Second, CMS activated the transmembrane protein Piezo1 to drive cell cycle entry from G2 (Gudipaty et al. 2017) via calcium-dependent activation of extracellular signal related kinase (ERK) signalling. Finally, the small GTPase Rho is implicated in matrix-rigidity driven cell proliferation (Provenzano & Keely 2011), such as in the breast cancer microenvironment (Provenzano et al. 2009). That YAP and TAZ activation in response to mechanical force require Rho GTPase activity and actomyosin contractility (Dupont et al. 2011) provides exciting evidence of an emerging pathway of mechanotransduction and proliferation that may be applicable to the alveolar epithelium.

1.2.2.3 Force-induced injury in the lung

1.2.2.3.1 Physical disruption

Although ventilation at high tidal volumes induces macroscopic lung injury (Ricard et al. 2003; de Prost et al. 2011) and alveolar damage, how this is mediated at the level of the alveolar epithelium is not clear. One

hypothesised method of CMS-induced alveolar epithelial cell injury is via direct rupture of the plasma membrane. Electron microscopy of rabbit lungs exposed to high tidal volume ventilation demonstrated plasma membrane disruption (Costello et al. 1992) and the suggested method of damage is through excessive unfolding of the membrane followed by stretching of plasma membrane lipids and further lipid trafficking (Vlahakis & Hubmayr 2000; Vlahakis & Hubmayr 2005; Vlahakis et al. 2002). A rat model of VALI suggested that the majority of plasma membrane wounds in alveolar epithelial cells are sealed following injury, (Gajic et al. 2003), possibly through tripartite motif-containing protein (TRIM)72-mediated endocytosis and rapid lipid trafficking (Nagre et al. 2016) followed by re-polymerisation of the actin cytoskeleton (Godin et al. 2011). However, plasma wounding in itself may contribute to CMS-induced inflammatory signalling, for example through c-Fos signalling (Grembowicz et al. 1999).

Either due to plasma membrane failure, or independently, CMS may induce alveolar epithelial cell apoptosis or necrosis. Mechanical ventilation of pre-term infants induced alveolar epithelial cell apoptosis (Lukkarinen et al. 2003), and this effect was seen experimentally following mechanical ventilation of pre-term mice (Mokres et al. 2010). High magnitude CMS at 17% elongation induced apoptosis of foetal ATII via increased expression of Fas ligand (FasL) and cleaved caspases (extrinsic pathway) (Kroon et al. 2013). Similar effects have also been seen in mature ATII, where CMS increased the number of dead cells in a magnitude-dependent manner (Tschumperlin & Margulies 1998; Arold et al. 2009). High amplitude stretch also significantly increased the apoptotic index of rat ATII (Crosby et al.

2011), in a mechanism thought to occur via impairment of bradykinin-mediated stimulation of phosphoinositide 3-kinase (PI3K)-B-cell lymphoma (BCL) signalling (Hammerschmidt et al. 2007), and more recent evidence has indicated a role for the intrinsic (mitochondrial) apoptosis pathway (Kuhn et al. 2017).

1.2.2.3.2 Mechanotransduction

VALI is a systemic disease, and CMS-induced injury of alveolar epithelial cells is thought to propagate diffuse injury through transduction of force into injurious biological signalling, such as cytokine release (Belperio et al. 2006). CMS of alveolar epithelial cells induced inflammatory cytokine signalling *in vitro* (Vlahakis et al. 1999) and, several possible upstream signalling pathways have been investigated.

First, CMS induced activation of extracellular signal related kinase (ERK) within 5 minutes in primary rat alveolar epithelial cells via G-protein signalling, and independent of stretch-activated ion channels (Correa-Meyer et al. 2002). Furthermore, CMS of foetal ATII induced ERK and Nuclear Factor Kappa-light-chain-enhancer of activated B cells (NF-κB) mediated IL-6 and macrophage inflammatory protein (MIP)-2 (chemokine (C-X-C motif) ligand 2 CXCL2) (Copland & Post 2007), but these responses were downstream of, and dependent on, calcium mobilisation. Previous results from our group suggested that CMS-induced IL-8 release in A549 cells was inhibited by blockade of ERK signalling with U0126, and that CMS-induced ERK activation was independent of stretch-activated cation channels (Pinhu 2008).

Another putative mechanism of CMS-induced cytokine generation is via redox and NF-κB signalling. CMS induced reactive oxygen species (ROS) generation in ATII at low and high magnitudes of stretch (Chapman et al. 2005), and CMS-induced IL-8 release was abrogated by augmentation of intracellular glutathione, an oxidant scavenger (Jafari et al. 2004). Furthermore, CMS of rat ATI induced superoxide and nitric oxide generation in an NF-κB-dependent manner, and was associated with increased epithelial permeability which was abrogated by the superoxide scavenger, Tiron (Nurit Davidovich et al. 2013). Similarly, high magnitude CMS applied to precision cut lung slices (PCLS) induced superoxide generation associated with tight junction dissociation, and these effects were abrogated by the use of Tiron (Song et al. 2016). Indeed, pre-treatment with an antioxidant improved parameters of oxidative stress, inflammation and pulmonary epithelial integrity in a mouse model of VALI (Fu et al. 2011), but use in a clinical trial in patients undergoing one-lung ventilation failed to show any positive effect in clinical outcomes (Bastin et al. 2016).

Pharmacological inhibition of mitochondrial electron transport chain function by rotenone abrogated CMS-induced oxidative stress in A549 cells, and mitochondrial-free A549 cells did not generate IL-8 or show activation of NF-κB in response to CMS, although IL-8 generation was intact following chemical stimulation (Pinhu 2008). Although no overlap could be found between the ERK and mitochondrial ROS signalling pathways in CMS-induced injury in these studies, mitochondrial ROS generation is clearly part of a multifaceted cellular response to CMS (Figure 1-3).

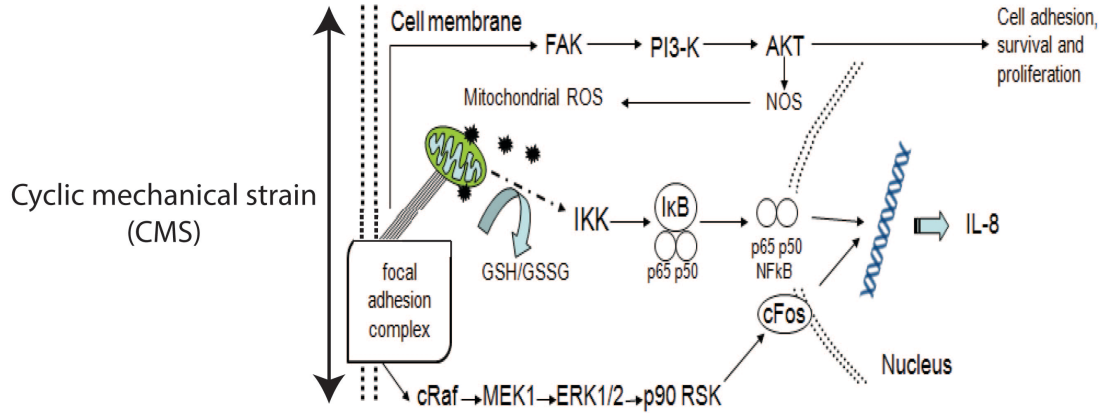


Figure 1-3 Proposed mechanotransduction pathways in VALI

CMS is proposed to induce injurious signalling via mitochondrial reactive oxygen species (ROS) and nuclear factor kappa-light-chain-enhancer of activated B cells (NF-κB). Alternatively, extracellular related kinase (ERK) signalling is activated, but no overlap between the two pathways has yet been found.

AKT - protein kinase B, FAK – focal adhesion kinase, IKK - inhibitor of kappa B kinase, NOS-nitric oxide synthase, PI3-K –phosphoinsitide 3-kinase

1.3 Studying mechanotransduction in the alveolar epithelium

1.3.1 *in vivo* models

Animal models have been invaluable in the research of lung injury, However, translation of observations from these models into human disease are limited by fundamental differences in anatomy (Shapiro 2006), alveolar epithelial biology (Sakuma et al. 1997) and proteomics. Only 21 homologous proteins were identified in a comparative analysis of broncho-alveolar lavage fluid (BALF) from a murine model and a patient with lung injury (Gharib et al. 2010). Although *in vivo* models of human lung injury exist, such as the inflammation induced during one lung ventilation (Bastin et al. 2016), *ex vivo* models offer the prospect of progress in VALI research (Proudfoot et al. 2011). These are comprised of the ventilation and perfusion of consented

donor lungs unsuitable for transplant. The *ex vivo* lung perfusion (EVLP) method is used to re-condition such organs to increase their suitability for transplant (Cypel et al. 2011), and VALI associated with cytokine release can be induced in these lungs (Terragni et al. 2016). This method therefore provides a novel and exciting platform in which to investigate VALI and targeted therapies in human lungs (Tane et al. 2017).

1.3.2 *in vitro* models

1.3.2.1 Application of CMS

The application of strain to alveolar epithelial cells *in vitro* facilitates investigation of mechanistic responses. Stretching devices developed for this purpose can apply uniaxial (pulling at opposite ends) (Moretti et al. 2004) and biaxial (pulling in all directions) (Banes et al. 1985) stretch forces on a flexible cell culture surface. Biaxial stretch has been applied by generating a vacuum beneath a clamped cell culture surface, but this method is limited by heterogeneity of the strain field (Williams et al. 1992), with true equibiaxial strain present at the centre of the well only (Waters et al. 2012). These issues are partially overcome by the use of thinner cell culture membranes (Winston et al. 1989), using an indenter to push into the centre of a well (Hung & Williams 1994), or pulling on the four sides of a cruciform membrane (Waters et al. 2001).

The commercially available Flexcell system uses a vacuum to deform membranes down: either across a loading post, leading to validated homogenous equibiaxial strain fields in the central area covering the post; or

without a post (Figure 1-4). However, evidence that substrate strain does not necessarily correlate with cellular strain (Wall et al. 2007) and that the mechanical properties of the membrane material change over time present on-going issues with these techniques (Bieler et al. 2009). Therefore, studies of cellular mechanotransduction will be limited until methodical improvements can be made.

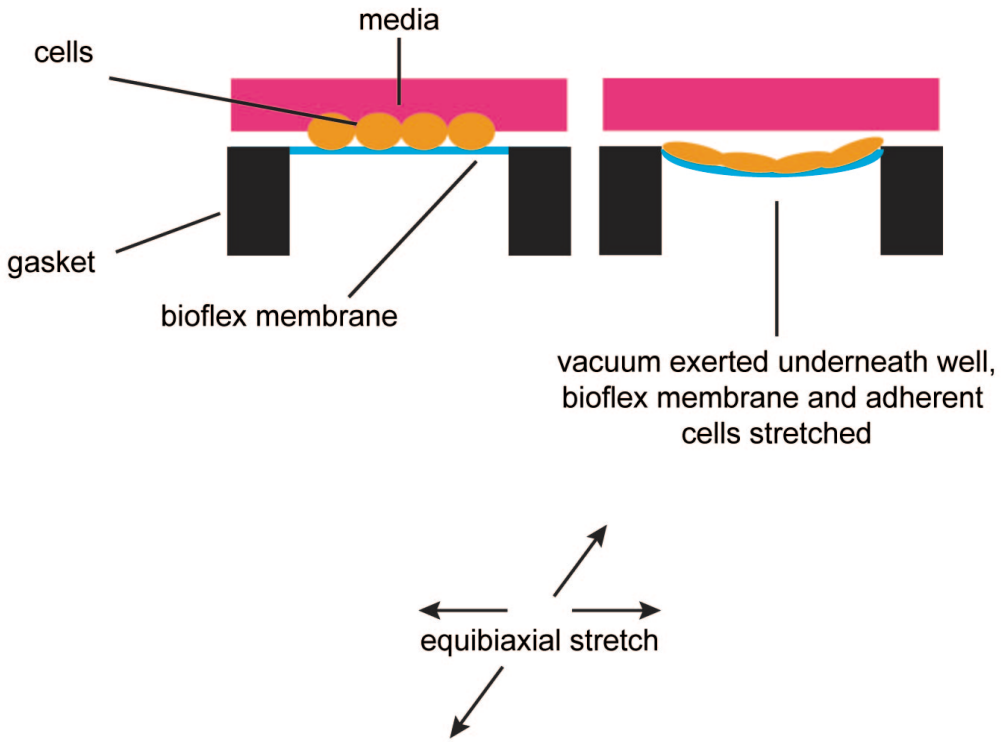


Figure 1-4 Flexcell mechanism of equibiaxial cell strain

Cells are plated on deformable silicone (Bioflex™) membranes. A vacuum exerted beneath the well distorts the membrane, causing equibiaxial strain of the cells.

1.3.2.2 Towards physiologically-relevant systems of *in vitro* stretch

Such *in vitro* systems are further limited by their physiological relevance. Although technically challenging and limited by availability of human tissue, isolation and culture of human ATII cells is feasible (Witherden & Tetley 2001; Mao et al. 2015) although they trans-differentiate to an ATI phenotype after 8-10 days (Fuchs et al. 2003). The human lung adenocarcinoma cell line, A549, was established in 1972 from explant culture of tissue from a 48 year-old Caucasian male (Giard et al. 1973). They contain cytoplasmic inclusion bodies typical of ATII, and synthesise phospholipids in a pattern concordant with surfactant production (Lieber et al. 1976). Recent micro-array analysis suggests that this cell line may further develop ATII characteristics, including multi-lamellar body (MLB) development, in long term culture (Cooper et al. 2016). The recent development of a stable cattle ATII cell line by over-expression of human telomerase reverse transcriptase (HTERT) may facilitate *in vitro* alveolar epithelial cell work further (Su et al. 2013).

However, *in vitro* mechanotransduction studies of a monolayer of alveolar epithelial cells are limited given that the cellular repertoire, polarity, cell-cell and cell-matrix adhesions and composition of extracellular matrix *in vivo* are fundamentally different. Focal adhesions of fibroblasts in three dimensional tissue environments did not resemble those seen in culture on flat surfaces, showing the absence of distinct focal and fibrillar adhesions,

with different rates of migration and proliferation (Cukierman et al. 2001) (Figure 1-5).

A better method of replicating the *in vivo* physiological environment in mechanotransduction studies of the alveolar epithelium is to use 'micro-stretchers' to apply CMS to air lung interface (ALI) cultures of cells on 'lung on a chip' systems (Huh et al. 2010). In this case, epithelial and endothelial cells are seeded on opposite sides of a porous membrane, where the epithelial surface is exposed to air, and the endothelial surface is perfused. A vacuum produced around the membrane induces uniaxial strain.

Another approach is through the use of PCLS. Human or animal lung tissue that has been agarose-inflated and sliced to under 500 μm thickness can survive for several days in culture and retains alveolar epithelial cellular characteristics (Alçada et al. 2014; Uhl et al. 2015). Furthermore, the *in vivo* cellular microenvironment is retained (Sanderson 2011). By stitching (N Davidovich et al. 2013; Song et al. 2016) or clamping the slice (Dassow et al. 2010) to a flexible substrate, equibiaxial CMS can be applied. Transient expression of focal adhesion markers allows for the real-time investigation of cell-matrix and cell-cell interactions in living human tissue (Burgstaller et al. 2015), and coupled with progress in live cell imaging during CMS (Rápalo et al. 2015), this method presents exciting opportunities for cellular mechanobiology research.

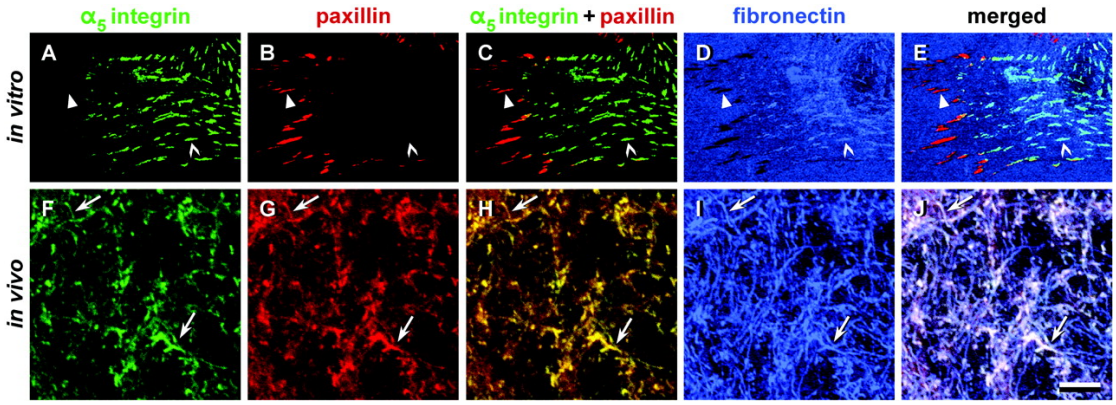


Figure 1-5 Focal adhesions in 3-dimensions do not resemble those seen in culture on flat surfaces

Adapted from (Cukierman et al. 2001) Reprinted with permission from the American Society for the Advancement of Science (AAAS). Panels A-E represent confocal microscopic images of murine fibroblast *in vitro* on a fibronectin-coated cover slip whereas panels F-J represent transverse cryostat craniofacial mesenchyme sections of an E13.5 mouse embryo. α_5 integrin (green) and paxillin (red) colocalize in a fibrillar structure in the mesenchymal tissue [(H), but not in the plated cells *in vitro* (C). Similarly, fibronectin (blue] localises to the *in vivo* fibrillar structures (J)

1.3.3 Measuring forces in mechanotransduction

The repertoire of methods used to study cell adhesion forces, such as atomic force microscopy (AFM) (Charras & Horton 2002), traction force microscopy (TFM) (Sabass et al. 2008) and magnetic twisting cytometry (Mijailovich et al. 2002), have traditionally either required a force to be applied to proteins, or measure micrometre-scale deformation of extra-cellular matrix (ECM) *in vitro* (Jurchenko & Salaita 2015). However, investigation of mechanotransduction events *in vivo* has been facilitated by the advent of fluorescence molecular tension-sensing probes which can measure deformation on a nanometre scale. Förster Resonance Energy Transfer (FRET) describes the non-radiative transfer of energy from a donor fluorophore to an acceptor, depending on the proximity between the two (Jurchenko & Salaita 2015). The Förster distance, at which energy transfer

between a spectrally overlapping donor and acceptor pair is approximately 50%, is generally between 4 to 7 nm. Therefore, this technology has been used to investigate conformational dynamics of single molecules, such as measuring activation of RhoA using a FRET probe (Pertz et al. 2006; Heasman et al. 2010). In respect to measuring forces between cells, and cells and their environment, two main classes of FRET tension probes have emerged.

One group consists of an immobilised fluorophore anchored to a substrate, whereby its fluorophore pair bound to a biological cell-ligand extends a flexible linker between the two (Jurchenko & Salaita 2015). The second consists of genetically engineered fluorophore pairs, split by a flexible linker, encoded within proteins and expressed in the living cell. In both cases, FRET between fluorophores is at its greatest when there is minimal tension between the two, but there is generally some degree of donor-acceptor separation even at this stage (Jurchenko & Salaita 2015). The 2010 tension sensor module (TSMod) consists of an mTFP1 and Venus FRET pair, joined by a 40 amino-acid flexible linker derived from spider silk protein (Grashoff et al. 2010). Calibrated using optical tweezers, when incorporated into vinculin the sensor revealed an average tension across vinculin of 2.5pN and an increase in tension at the protruding edges of the cell. This sensor has been used more recently to investigate the tension applied across E-cadherin (Borghi et al. 2012) and platelet endothelial cell adhesion molecule (PECAM) (Conway et al. 2013) in cell-cell adhesion studies.

AFM and traction force measurements of alveolar epithelial cells have been used to indicate their tensile forces (Alcaraz et al. 2003; Waters et al. 2012) and pre-stress values (Sunyer et al. 2009) in comparison to those from fibroblasts and airway smooth muscle cells. The fact that these values were generally low, in the context of the *in vitro* environment, has lent credence to the theory that the ECM and air-liquid interfaces are responsible for bearing the majority of the load applied to the lung (Waters et al. 2012).

1.4 Cellular mechanotransduction: how cells transduce forces into biological signalling

Alveolar epithelial cells have specialised and flexible basement membrane consisting of laminin and collagen, and the cells are bound to this ECM via cell-matrix interactions (Roan & Waters 2011). The response of cells to mechanical forces acting through cell-matrix attachments is regulated by discrete cellular signalling, depending on the nature, magnitude and duration of applied force. Tension applied to integrins using magnetic microbeads induced either early visco-elastic responses or adaptive strengthening, or late cellular stiffening and increased countering traction forces to sustained force application (Matthews et al. 2006). The early and late responses were dependent on Rho-associated protein kinase (ROCK) signalling, but also on functioning mechanosensitive ion channels, indicating that cell-matrix forces activate specific and conserved cell signalling pathways.

1.4.1 The integrin-focal adhesion complex

The cellular machinery of mechanotransduction can be thought of as comprising a load bearing structure, the cytoskeleton, which acts through and in response to the mechanosensory apparatus of the integrin-focal adhesion-ECM complex. The latter acts as the hub through which cells sense the rigidity or stiffness of their external environment (Discher et al. 2005), and in response, determine cytoskeletal force to exert traction forces on the ECM (Plotnikov et al. 2012). This finely tuned and dynamic force-feedback loop determines cell adhesion and motility (Hoffman et al. 2011; Sun et al. 2016; Li, Lee, et al. 2016) and also determines key cellular behaviours, such as migration (Lo et al. 2000) (Plotnikov et al. 2012), proliferation and differentiation (Engler et al. 2006; Dupont et al. 2011).

1.4.2 Integrin-mediated mechanotransduction

Integrins, the heterodimeric transmembrane receptors that link the cellular cytoskeleton to the ECM (Tamkun et al. 1986), are the primary cellular mechanosensitive machinery (Puklin-Faucher & Sheetz 2009). The heterodimers are composed of one of 18 α subunits non-covalently bound to one of 8 β subunits (Hynes 2002). Thus, 24 different mammalian integrins can be formed, each one specified for a particular ECM ligand (Hynes 2002; Sun et al. 2016; Campbell & Humphries 2011) (Table 1-1). Integrins are bi-directional signal transducers: they can mediate the transmission of force from the cytoskeleton onto the ECM (inside-out signalling), or from the ECM to the cell (outside-in signalling) (Springer & Dustin 2012).

ECM ligand	Integrin
Laminin	α3β1, α6β1, α1β1, α2β1, α10β1, α7β1, α6β4
Collagen	α10β1, α2β1, α1β1, α11β1
Fibronectin	αVβ1, α5β1, α8β1, αVβ6, αVβ3, α11bβ3
ICAM	αXβ2, αMβ2, αLβ2, αDβ2
E-cadherin	αEβ7

Table 1-1 Major classes of integrin-ligand partners

Based on (Humphries et al. 2006). Throughout the normal lung, integrin subunits α1, α2 and α3 are found in epithelial and endothelial alveolar layers, and α6 is present at the basolateral alveolar surface. Normal adult alveolar epithelium shows strong expression of β1 integrins (Koukoulis et al. 1997). The alveolar epithelial basement membrane is composed of laminin, types IV and V collagen, entactin, chondroitin sulphate and heparin sulphate proteoglycans (Dunsmore & Rannels 1996).

ICAM – Intercellular Adhesion Molecule

Both directions of signalling transduction mediate a change in conformation of the integrin heterodimer from a bent structure with low affinity for ECM ligand, to structures with intermediate or high ligand affinity (Luo & Springer 2006). The bent conformation consists of a closed ectodomain headpiece (Takagi et al. 2002; Springer & Dustin 2012), whereas the intermediate or high affinity states consist of either extension of the ectodomain alone in the former (Luo et al. 2007), or extension together with swinging open of the headpiece in the latter (Takagi et al. 2002) (Figure 1-6).

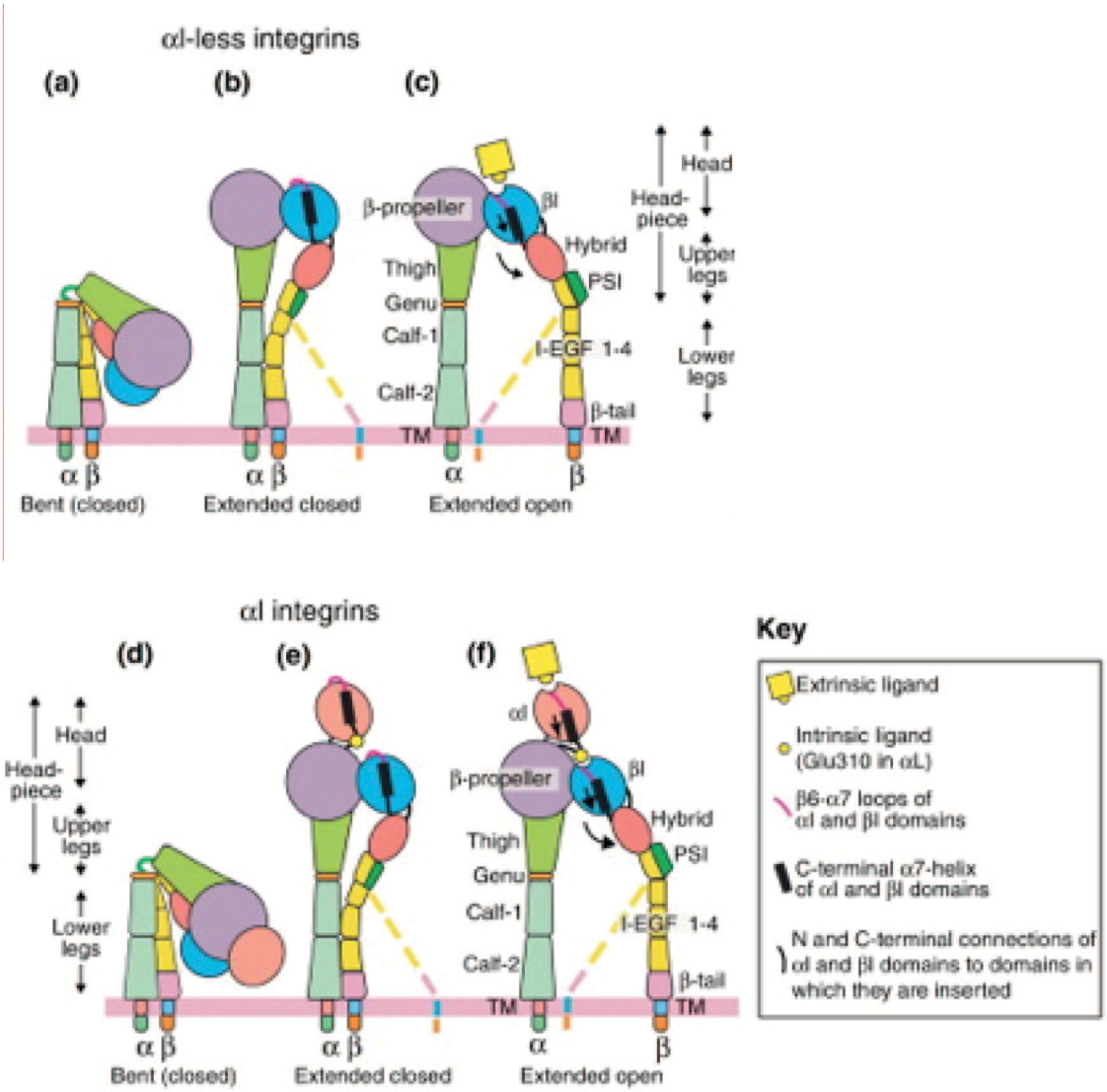


Figure 1-6 Conformation of integrins

Adapted from (Springer & Dustin 2012) (Current opinion in cell biology, vol:24, T.Springer, M.Dustin, Integrin inside-out signalling and the immunological synapse, pgs: 107-15 Copyright (2012), with permission from Elsevier. In the low affinity, bent conformation, the integrin has a closed headpiece. Extension at α- and β-knees leads to an extended-closed conformation but with low affinity. The hybrid domain swings out at the interface with the βI domain and the βI interface connects with the β-propeller domain that increases affinity for ligand in the extended-open conformation. In αI integrins, activation of a binding site for the internal ligand Glu310 in αL, pulls down the αI domain to activate an increase in affinity of the αL I domain for the ligand ICAM-1. The lower β-legs are also highly flexible, as shown by the dashed lower β-leg. Therefore, only large separations between α and β transmembrane (TM) domains such as from lateral motion of β when its cytoplasmic domain is in association with the actin cytoskeleton, can be transmitted through the floppy β-leg to stabilize the high-affinity conformation with open headpiece

1.4.2.1 Inside-out signalling

Forces generated from by the cytoskeleton can be transmitted through the integrin-focal adhesion complex onto the ECM. However, the cytoplasmic domains of integrins do not contain actin binding sites, therefore linkages with the actin cytoskeleton are co-ordinated via adaptor proteins such as talin and kindlin (Calderwood et al. 2013). Although in an auto-inhibited conformation when in the cytoplasm (Yang et al. 2014), talin consists of an N-terminal head domain which interacts with β1-integrin cytoplasmic tails. Actin binding sites in the head and rod complete the linkage with the F-actin cytoskeleton (Calderwood et al. 2013; Ye et al. 2014). For example, binding to F-actin initiates contact, with subsequent force stretching the talin rod to expose cryptic binding sites for the critical focal adhesion protein, vinculin (del Rio et al. 2009; Sun et al. 2016).

Vinculin binding reinforces talin-actin engagement, exposing more vinculin binding sites, promoting further linkage with actin (Atherton et al. 2015; Yao et al. 2016). Nuclear magnetic resonance (NMR) spectroscopy studies revealed that talin-integrin association promotes integrin activation by unclasping association between the α and β cytoplasmic tails (Vinogradova et al. 2002). Therefore, inside-out force transmission from actin, and in particular, lateral force as provided by moving actin filaments, induces integrin affinity for ECM ligand (Zhu et al. 2008), and regulates force across the integrin complex (Nordenfelt et al. 2016).

The integrin co-activator, kindlin, also directly binds β-integrin tails, but much less is known about kindlin interactions in the actin-talin-integrin

complex (Calderwood et al. 2013), although it is possible that the talin head forms a complex together with kindlin and β-integrin tails. Recently, it has been shown that kindlin directly binds actin to mediate force transmission (Bledzka et al. 2016), and pull-down experiments in fibroblasts have demonstrated that kindlin binds and recruits a further focal adhesion protein, paxillin, which recruits the tyrosine kinase, focal adhesion kinase (FAK), to the signalling complex (Theodosiou et al. 2016).

1.4.2.2 Outside-in signalling

Whereas inside-out force transmission from the actin cytoskeleton regulates integrin-ECM binding affinity, ligand binding also drives and stabilises integrin headpiece opening (Du et al. 1991; Takagi et al. 2002), and increases integrin clustering (Welf et al. 2012), to promote outside-in force transmission. The precise steps leading from changes in ECM-induced integrin affinity to activation of talin are not completely understood (Ginsberg et al. 2005), but it is thought that both conformational change and integrin clustering drive the recruitment of effector proteins, such as focal adhesion kinase (FAK) and Proto-oncogene tyrosine-protein kinase sarcoma (Src kinase) (Arias-Salgado et al. 2003; Hu & Luo 2013), to the integrin tail, triggering further downstream signalling. It is likely that the bi-directional signalling processes are not mutually exclusive, and are closely linked to each other (Shattil et al. 2010) to regulate cell sensing and response (Puklin-Faucher & Sheetz 2009).

1.4.3 Focal adhesion maturation

Talin-mediated integrin activation and integrin clustering promote the formation of protein complexes at the integrin cytoplasmic tail, through which mechanotransduction is finely tuned. These complexes show dynamic variation in their size, mechanical properties, and role in mechanotransduction (Schiller & Fässler 2013; Sun et al. 2016). The initial 'nascent' adhesion, or focal complex, is constructed at the cell leading edge, following integrin, talin, actin, vinculin and paxillin assembly (Zaidel-Bar et al. 2003). The maturation of these nascent complexes to larger adhesions depends on actin flow (Alexandrova et al. 2008), the recruitment of other proteins such as zyxin (Zaidel-Bar et al. 2003), tyrosine phosphorylation of paxillin and FAK (Zaidel-Bar et al. 2006; Ballestrem et al. 2006) and integrin clustering (Roca-Cusachs et al. 2009).

1.4.4 Mechanical force promotes integrin-dependent focal adhesion maturation and reinforcement

Increased force across the ECM-integrin-focal adhesion-cytoskeleton interface matures and strengthens focal adhesions. For example, integrins show increased clustering in response to increased ECM rigidity (Paszek et al. 2009), whereas the opposite trend is seen in soft matrices (Qian et al. 2010). Integrin clustering reinforces cell matrix adhesions (Roca-Cusachs et al. 2009). When integrins are subjected to external force, or interact with stiff matrices, a corresponding increase in focal adhesion size and strength is observed (Sniadecki & Chen 2007; Provenzano & Keely 2011).

At a focal adhesion level, maturation in response to force has been comprehensively demonstrated (Oakes et al. 2012); micropipette-induced force at adhesions promotes focal adhesion elongation (Riveline et al. 2001), stretching of single talin rods leads to exposure of vinculin binding sites (del Rio et al. 2009), and binding of vinculin stabilises the adhesion by preventing refolding of talin into an auto-inhibited conformation (Yao et al. 2014). At a cellular level, this response to increased matrix rigidity can increase the capacity of cells to migrate, and proliferate (Saez et al. 2007). This has profound functional consequences, for example the increased rigidity of the tumour microenvironment promotes cell proliferation (Provenzano et al. 2009), and increased matrix stiffness promotes myofibroblast differentiation in pulmonary fibrosis (X. Huang et al. 2012). However, the process of adhesion assembly, maturation and disassembly in response to force is dynamic, as opposed to a simple switch-like system (Hoffman et al. 2011). For example, the forces in vinculin-containing adhesions are polarised in cells, with increased traction forces located in adhesions undergoing assembly at the leading edge, and decreased forces in disassembling adhesions at the rear of cells, therefore allowing the cell to migrate (Grashoff et al. 2010).

1.4.5 Integrin-dependent responses to mechanical force are dynamic and depend on the degree of force applied

The processes by which adhesions interact with matrix ligands dynamically to control force transmission to the cytoskeleton were first conceptualised by the molecular clutch hypothesis (Mitchison & Kirschner 1988; Case & Waterman 2015). In this model, actin retrograde flow due to

myosin-generated contraction is constant, but without engagement of adaptor proteins to the integrin tail, does not result in traction forces, but rather a stationary “lamellipodial treadmill” (Craig et al. 2012). Engagement of the clutch is dependent on substrate stiffness: below a threshold stiffness, integrins unbind and the force is released, whereas above the threshold, talin unfolding occurs, the adhesion matures, and mechanotransduction can take place (Elosegui-Artola et al. 2016). The twin processes of actomyosin contractility, and of actin retrograde flow result in traction on the ECM, and actin polymerisation at the lamellipodium pushes the leading edge forward (Sun et al. 2016).

Two main types of integrin-matrix adhesive behaviour from force-induced changes in molecular kinetics have been conceptualised. Intuitively, and in correlation with many biological interactions (Dembo et al. 1988; Merkel et al. 1999; Li, Lee, et al. 2016), slip bond behaviour describes weakening of integrin-ligand bonds following application of force. This appears to occur at low levels of tension, whereas catch bond behaviour describes prolongation of integrin-ligand bonds in response to force (Thomas et al. 2008; Kong et al. 2009), possibly due to force-induced allosteric changes (Lou & Zhu 2007; Li, Kong, et al. 2016). This coincides with adhesion maturation behaviour described above. However, elegant atomic force microscopy and biomembrane force probe experiments suggest that cells exhibit slip bond behaviour at low forces, catch bond behaviour at a certain range of forces, then reversion to slip bond above a certain threshold (Marshall et al. 2003; Wayman et al. 2010). This is reflected in other integrin-fibronectin models that demonstrate low traction forces at low substrate

rigidity when the matrix is deformable by the cell. Decreasing bonding then occurs as rigidity increases, the matrix resists deformation and bonds break before new ones can be formed. Finally, a threshold stiffness is reached where force-induced bond strengthening occurs, i.e the clutch is engaged, and force transmission occurs (Elosegui-Artola et al. 2014; Elosegui-Artola et al. 2016) (Figure 1-7). Such dual or triphasic behaviour might help explain how cells regulate adhesion under conditions of varying mechanical tension, such as during leukocyte rolling and adhesion.

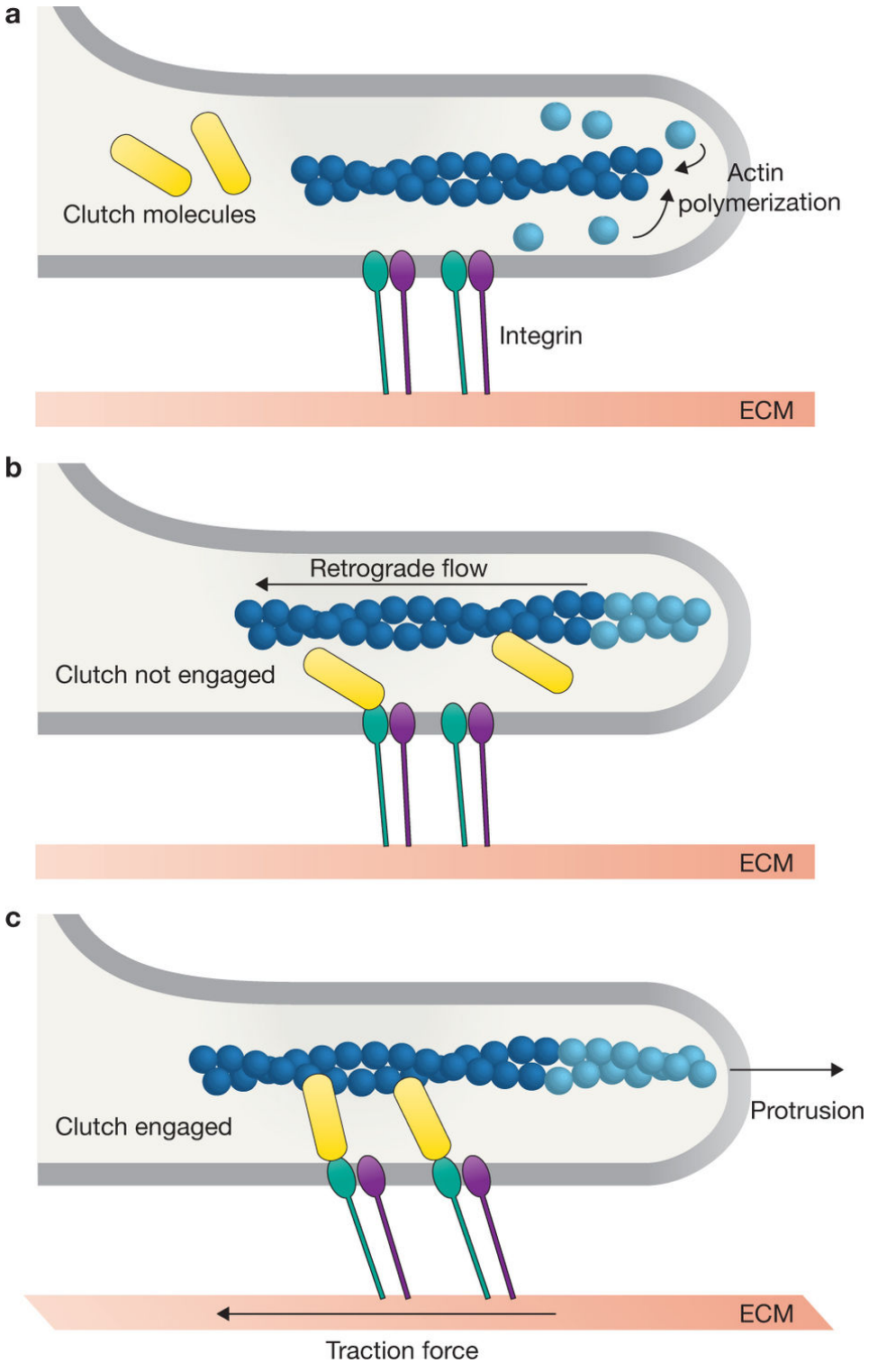


Figure 1-7 The molecular clutch hypothesis of integrin-matrix adhesion

Reprinted by permission from Nature Publishing Group: Nature cell biology (Case & Waterman 2015), copyright (2015). Under conditions of low force, actin is not engaged with the ECM, and actin flows retrogradely. Under conditions of increasing force (lower panel), force-induced bond strengthening occurs, the clutch is engaged, and the retrograde actin flow changes to traction on the ECM and cellular protrusion

1.4.6 Responses to externally-applied mechanical force

How cells regulate integrin-ligand adhesion in response to CMS might rely on these triphasic models of adhesion. Cyclic force on α5β1 integrin-fibronectin bonds prolonged their lifetimes 100-fold (Kong et al. 2013), suggesting force-induced bond 'memory'. A model for this type of 'cyclic mechanical reinforcement' suggests that each loading cycle induces changes in integrin conformation to a high affinity state, such that there is an accumulation of high-affinity bonds following repetitive, fast cycles (Li, Kong, et al. 2016). In correlation with this, atomic force microscopy of a single fibroblast bonded to a fibronectin-coated bead on a cantilever demonstrated that cyclic stretch rapidly promoted a decrease in bond tension, followed by an actomyosin-dependent gradual increase in tension over subsequent cycles (Watanabe-Nakayama et al. 2011).

Indeed, the application of different types of force induces different effects, suggesting that cells sense and respond not only to the degree of force applied, but also to the nature in which it is applied. This leads to different downstream effects: in endothelial cells, static or tonic (continuously-applied) stretch induces differential gene transcription to that from CMS, and the latter had a greater effect on vascular tube length and branch formation than static stretch (Zheng et al. 2008). Similarly, application of the two different modes of stretch in rabbit aortas induced differential tyrosine kinase phosphorylation (Lehoux et al. 2005). How different types of force induce distinct mechanotransduction is thought to be due to sensing of substrate

deformation at the focal adhesion-integrin-ligand interface (Hoffman et al. 2011), but the exact mechanism, and whether this is the case in the alveolar epithelium, is currently unclear.

1.5 Integrin-associated proteins

Whereas therapeutic targeting of leukocyte integrin-ligand binding has been met with success in some cases, inflammatory and auto-immune diseases for example, (Cantor et al. 2008), this method can have serious adverse consequences. For example, application of stretch in alveolar epithelial cells in which β1-integrin activity is inhibited can induce rapid cell detachment, and death (Liu et al. 2011). Therefore, modulation of integrin signalling via associated proteins presents an attractive option.

1.5.1 CD98hc

Mechanical force applied to β1-integrins promoted integrin activation and downstream RhoA signalling (Guilluy et al. 2011). Mechanical stretch applied to keratinocytes also increased β1 integrin-mediated adhesion through induction of integrin clustering (Knies et al. 2006), and this mechanism may promote stretch-induced epidermal thickening in skin (Tokuyama et al. 2015). More specifically, CMS of renal epithelial cells increased β1-integrin expression and signalling, promoting downstream TGF-β-mediated signalling (Hamzeh et al. 2015). That mechanical force can trigger β1-integrin-mediated signalling is evident in a variety of cell types, such as in cardiac myocytes where it is necessary for stretch-induced auto-phosphorylation of FAK (Lal et al. 2007).

Specific integrins may have distinct roles in mechanotransduction. Mechanical force modulates the adhesive strength of β1-integrin-fibronectin bonds (Friedland et al. 2009), and changes the conformational state of β1-integrins (Zhu et al. 2008). Increased ECM density specifically activated β1, but not β3, integrins in a ROCK and myosin II-dependent manner (Lin et al. 2013), and whereas the former may regulate cell adhesion and spreading, the latter appears necessary for stable focal adhesion formation (Schaufler et al. 2016).

CD98 (4F2, solute carrier family 3 member 2 - SLC3A2) is a transmembrane protein that regulates β-integrin signalling. Initially discovered as a marker for activated B and T lymphocytes (Haynes et al. 1981), it has since been discovered to have key roles in cell survival, adhesion and proliferation (Cantor & Ginsberg 2012). Expressed in all vertebrate cell types except platelets, the CD98 complex exists as a heterodimer of an 80kDa glycosylated heavy chain, linked by disulphide bridges to one of several 40kDa non-glycosylated light chains (Devés & Boyd 2000) (Figure 1-8). Whereas the light chains regulate amino acid transport and are dispensable for CD98 expression (Verrey et al. 1998), the heavy chain is essential and interacts with β-integrin tails (Fenczik et al. 2001). CD98hc is necessary for normal development, and genetic deletion is lethal at the early embryonic stage (Tsumura et al. 2003).

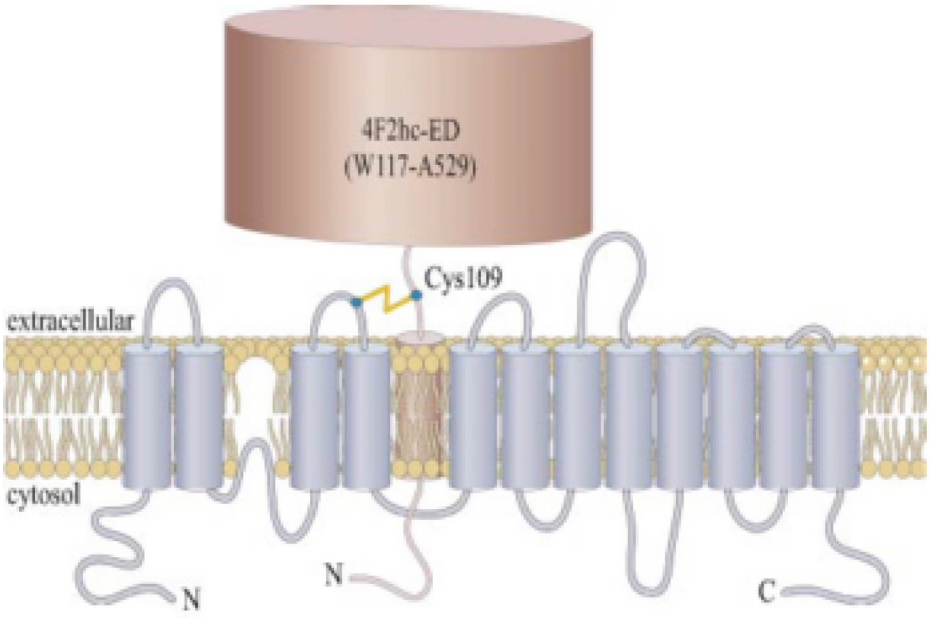


Figure 1-8 Structure of CD98

From (Fort et al. 2007) copyright American Society for Biochemistry and Molecular Biology – permissions not required. CD98 consists of a heavy chain (central – pink) linked to an N-glycosylated ectodomain by a conserved disulphide bridge (Cys 109) with a light subunit consisting of a 12 trans-membrane spanning non-glycosylated protein

Interaction between the CD98hc cytoplasmic tail and integrins promotes integrin signalling, and binding to β-integrin tails is required for adhesion-dependent spreading of cells (Prager et al. 2007). Specifically, the intracellular and transmembrane domains of CD98hc are necessary and sufficient for integrin binding and activity (Feral et al. 2005).

Given its capacity to modulate integrin signalling, CD98hc may play a key role in the regulation of the tumour microenvironment (Bajaj et al. 2016). As such it is up-regulated in many cancer types (Prager et al. 2009) and its expression correlates with aggressiveness of disease (Pöttler et al. 2011). This has led to the hypothesis that CD98hc expression amplifies integrin signalling such that cells can become anchorage independent and survive

and proliferate in soft matrix environments (Cantor & Ginsberg 2012), promoting tumourgenesis (Henderson et al. 2004). Indeed, CD98hc expression promotes renal epithelial cell proliferation via ERK signalling (Bulus et al. 2012), and suppression of CD98hc-mediated β1-integrin signalling has been shown recently to inhibit the progression of renal cell carcinoma (Poettler et al. 2013) and hepatocellular carcinoma *in vivo* (Wu et al. 2016).

CD98hc also regulates RhoA signalling. CD98hc null fibroblasts showed attenuated β1-integrin-driven RhoA activity (Féral et al. 2007), and CD98hc-mediated integrin activity regulated RhoA signalling to generate actomyosin contractility and traction on the ECM. Such CD98hc-regulated RhoA activity promotes keratinocyte proliferation and migration, and therefore skin homeostasis (Boulter et al. 2013). CD98hc deficiency also inhibits Ras-induced skin tumourgenesis via decreased ROCK signalling (Estrach et al. 2014) and, in this latter study, CD98hc-mediated ROCK signalling regulated epidermal stiffness and YAP/TAZ signalling, indicating CD98hc-RhoA activity as important for tuning mechanoresponses.

1.6 Actin cytoskeletal mechanotransduction

Coupled to focal adhesions via adaptor proteins, the actin cytoskeleton is a key component of force sensing and response (Burridge & Guilluy 2016). The microfilament F-actin is the major load-bearing element of the cellular architecture complemented by microtubules (such as tubulin) and intermediate filaments (such as desmin, vimentin and keratin) (Herrmann et al. 2007; Fletcher & Mullins 2010). Contractile actin stress fibres are bundles

of F-actin filaments, cross-linked by bipolar arrays of α-actinin and myosin II (Hu et al. 2017), and are emerging as being integral to cytoskeleton-mediated mechanotransduction. Ventral stress fibres, the long linear actin filaments that extend along the cell from one end to another, are anchored at each end by focal adhesions (Livne & Geiger 2016). Indeed, RhoA-mediated myosin driven contraction on actin filaments may be necessary for stress fibre assembly (Chrzanowska-Wodnicka & Burridge 1996; Even-Ram et al. 2007) in addition to focal adhesion maturation (Riveline et al. 2001), although recent evidence has suggested that myosin II-induced cross-linking of actin may be more important for nascent adhesion maturation than tension generation (Choi et al. 2008). Myosin-driven contraction of actin filaments induced α5β1 integrin conformational change to increase ligand binding affinity (Friedland et al. 2009), therefore directly coupling actin contractility on stress fibres to tension on the ECM.

Correspondingly, cytoskeletal remodelling and stress fibre development appear to be dependent on substrate rigidity *in vitro*. Fibroblasts cultured in gels contracted without stress fibre formation. However, when the gels were anchored to prevent deformation, stress fibre formation developed in the non-contracted fibroblasts (Tomasek et al. 1992), suggesting that stress fibres hold cells in isometric tension (Burridge & Guilluy 2016). Stress fibre formation in response to increased rigidity of the substrata is likely to be mediated by the small GTPase RhoA (Chrzanowska-Wodnicka & Burridge 1996), which shows increasing activity with increased stiffness of the matrix (Ridley & Hall 1992; Wozniak et al. 2003; Paszek et al. 2005). Tension on fibronectin-coated beads, which applied force to β1-integrins, induced RhoA

activation, and this was regulated through the action of two guanine nucleotide exchange factors (GEFs), leukaemia-associated Rho GEF (LARG) and GEF-H1 (Guilluy et al. 2011). The former is activated through Src tyrosine kinases, and the latter downstream of FAK and mitogen-activated protein kinase (MAPK)/ERK. Downstream ROCK-mediated activation of myosin II induced contractility and increased tension applied across the focal adhesion-ECM interface (Kimura et al. 1996). Stretch of F-actin filaments increased the affinity of actin for myosin II motors, thus creating a positive feedback loop in response to force (Uyeda et al. 2011).

Just as focal adhesions reorient in response to CMS, the actin cytoskeleton, as the major load bearing element of cellular architecture, demonstrates stretch-induced remodelling. Cyclic strain of endothelial cell monolayers induced rapid formation of stress fibres, tenting in the direction of least strain (J. H.-C. Wang et al. 2001). Force-induced actin remodelling appears to be specific to the type of strain applied: whereas uniform shear forces induced stress fibre reorientation parallel to the direction of force in endothelial cells (Tzima 2006), cyclic strain of fibroblasts promoted stress fibres to reorient perpendicular to the direction of force (Hayakawa et al. 2001). These responses were dependent not only on substrate rigidity (Faust et al. 2011), but also on the frequency and amplitude of cycles (Jungbauer et al. 2008). One possibility explored is that stress fibre reorientation occurs in response to a critical force threshold, followed by disassembly of bonds, and reorientation of actin to a more stable configuration (Chen et al. 2012).

Similarly, primary ATI subjected to CMS at high magnitude formed peri-junctional actin rings (PJAR), associated with rapid movement of integrin-bound arginylglycylaspartic acid (RGD) microbeads at the cell surface to track the displacement of anchored actin filaments (DiPaolo et al. 2010). These responses, the latter specific to CMS and dependent on the frequency of stretch applied, led to the suggestion that cells reorient actin cytoskeleton filaments to areas of least strain. Furthermore, rapid actin cytoskeleton movement and then attenuation during CMS was associated with stretch-induced fluidisation of the cytoskeleton, followed by a stiffening or reinforcement process. This dual phase response correlates with the finding that the focal adhesion protein zyxin is recruited to stress fibres in fibroblasts exposed to CMS (Yoshigi et al. 2005), and whereas it is not required for strain-induced cytoskeletal remodelling, which is Rho-dependent, it is necessary for repair and thickening of stress fibres in the reinforcement phase which is independent of RhoA (Hoffman et al. 2012).

However, the cytoskeleton may have a greater role in force transmission than passive remodelling. Human foreskin fibroblasts subjected to uniaxial sustained mechanical stretch showed reinforcement and reorientation of stress fibres along the direction of strain. Furthermore, stretch-induced activation of ERK localised to stress fibres and in correlation with the degree of strain applied, independently of myosin II-induced cell contractility (Hirata et al. 2015). In this way, stress fibres are a platform for force sensing and mechanotransductive signalling.

1.6.1 RhoGTPases

That CMS may induce RhoA signalling in fibroblasts via Rho GEFs (Guilluy et al. 2011) correlates with data obtained from CMS of lung endothelial cells (Gawlak et al. 2014). In this case, 15 minutes of CMS in human pulmonary artery endothelial cells (HPAEC) induced cytoskeletal remodelling as shown by paracellular gap formation, stress fibre formation, RhoA activation and downstream MLC phosphorylation. Crucially, immunoprecipitation revealed CMS-induced, and ERK 1/2-dependent, association of paxillin, ERK and GEF-H1 in the focal adhesion complex, which promoted RhoA activation. The authors proposed that CMS induced Src/FAK-dependent paxillin phosphorylation, exposing binding sites for the GEF-H1/ERK complex. Independently, CMS-induced ERK activity is necessary for paxillin-GEF-H1 binding, and this complex triggers Rho-dependent phosphorylation of MLC and actomyosin contraction.

Overlap between stretch-induced Rho-signalling and FAK and ERK activity has also been demonstrated in other cell types, such as in cardiomyocytes (Torsoni et al. 2005), but evidence for CMS-induced RhoA signalling in the alveolar epithelium has been conflicting and not so comprehensively demonstrated. ATII isolated from rats subjected to high tidal volume ventilation (25ml/kg) showed an increase in activated RhoA, as did treatment with hyperoxia or with the two treatments combined (Desai et al. 2007). *In vitro*, foetal ATII subjected to low magnitude CMS increased RhoA and Ras-related C3 botulinum toxin substrate 1 (Rac1) guanosine triphosphate (GTP) activity within 5 minutes in the former, and 15 mins for the

latter, and expression of dominant negative mutants of these GTPases inhibited CMS-induced stress fibre formation and cell realignment (Silbert et al. 2008). Interestingly, expression of these mutants abrogated CMS-induced ERK phosphorylation, suggesting that this process is dependent on Rho activity, in contrast to the data from endothelial cells. Conversely, biaxial CMS of rat ATI showed decreases in RhoA activity and MLC phosphorylation (DiPaolo & Margulies 2012), and also that CMS-induced cytoskeletal remodelling was dependent on Rac1-mediated phosphorylation of cofilin and LIMK (Dipaolo et al. 2013). How these differing CMS-induced cytoskeletal pathways can be reconciled is not yet clear, but differences may be due to cell type, and the actual magnitude of stretch when applied to cells of different sizes.

Murine lung epithelial cells (MLE)-12 cultured under hyperoxic conditions showed increased F-actin stress fibre formation, but also a corresponding and ROCK-dependent increase in elastic modulus, implying that hyperoxic-induced and RhoA-mediated cytoskeletal remodelling contributes to increased stiffness of cells. When these ‘stiffer’ cells were subjected to CMS, they detached more easily from the substrate, which again, was abrogated by ROCK inhibition (Wilhelm et al. 2014). This led the authors to believe that hyperoxia-induced ROCK activity increases cellular pre-stress, and therefore the susceptibility of ATII to deformation. These findings correlate with the previous observation that ATII decreased adhesion following stretch when a constitutively active RhoA mutant was used (Desai et al. 2007). Therefore, CMS-mediated regulation of RhoA may alter cellular stiffness, the deformability of cells, and subsequent mechanotransduction.

1.6.2 Mechanical properties of the cytoskeleton

Cytoskeletal responses of cells to force can be described in part by the 'tensegrity' model, whereby the cell is stable through a continuous balance between opposing tensile and compressive forces (Ingber et al. 2014). In this model, the compressive elements (microtubules) and tension elements (actin microfilaments) generate pervasive structural tension and stability (N. Wang et al. 2001). Force propagation along pre-stressed actin fibres is integral to mechanotransduction (Hu et al. 2005), but the orientation of stress fibres dictates the speed at which force can be transmitted throughout the cell. This is thought to be the mechanism by which cuboidal arterial endothelial cells with randomly-aligned fibres are more susceptible to the development of shear-stress associated atherosclerosis than elongated cells with highly aligned fibres (Hwang & Barakat 2012).

These models may explain force-induced stress-fibre reorientation (Hayakawa et al. 2001) as an attempt to escape, or adapt to, applied force. Cellular pre-stress increases linearly with cell rigidity (Wang et al. 2002), and tunes the sensitivity of the cell to respond to external force or stretch (Cirka et al. 2016). The rheology of the actin cytoskeleton responds to increasing substrate stiffness by increasing internal cellular stiffness. Both atomic force microscopy creep tests and kymographs of actin intensity of fibroblasts plated on substrates of increasing stiffness revealed decreasing retrograde actin flow with increasing substrate stiffness, indicating that the cytoskeleton behaves as fluid-like when plated on soft substrates, but as a solid-type material on stiffer substrates (Gupta et al. 2015).

Cytoskeletal remodelling in response to CMS is dynamic, possibly composed of an initial fluidisation or softening of the cytoskeleton, followed by stiffening or solidifying (Colombelli et al. 2009). This has been shown in airway smooth muscle cells subjected to optical magnetic twisting cytometry (OMTC) (Trepat et al. 2007), and in bladder smooth muscle cells (Chen et al. 2010). In the latter case, the fluidisation response appears to occur through the release of existing tensile forces leading to dissociation of weak bonds or of actin with binding partners. The degree by which the cytoskeleton becomes more fluid is determined by baseline stiffness, or pre-stress. Cells with higher initial pre-stress, such as following treatment with TGF-β, decrease traction forces in response to CMS, whereas cells with low baseline pre-stress, such as following myosin II inhibition, increase traction forces in response to stretch (Cirka et al. 2016).

1.7 Epithelial repair

1.7.1 Integrin and RhoGTPase signalling in epithelial repair

The lung shows significant capacity to regenerate following injury (Zeng et al. 2016). Recovery from lung injury requires, in part, restoration of the alveolar epithelium, and this process is dependent on cell spreading, migration and proliferation to recover the denuded basement membrane (Crosby & Waters 2010), Furthermore, evidence is emerging that populations of distal airway stem cells (DASC's), bronchoalveolar stem cells (BASCs) and lineage negative epithelial progenitor cells (LNEPs) all act as progenitor cells that proliferate, differentiate into ATII and migrate to the site of alveolar damage (Kim et al. 2005; Zuo et al. 2014; Vaughan et al. 2014; Zeng et al.

2016). These processes of migration and repopulation required for restoration of the injured lung alveolar epithelium both need to occur in the setting of continuous CMS experienced by the lung, and are mediated by many of the same pathways activated in CMS-induced injury, such as cytoskeletal-integrin-ECM interactions and RhoGTPase-driven signalling and traction forces (Crosby & Waters 2010).

β1-integrin signalling mediates migration of rat ATII on fibronectin and collagen (Kim et al. 1997), and is also necessary for airway epithelial migration on laminin (White et al. 1999). Inhibitors of downstream MAPK signalling, such as p38 MAP kinase, JNK and ERK 1/2, inhibited airway cell migration (White et al. 2005). Similarly, RhoA signalling is required for wound repair in A549 cells, and its inhibition resulted in cytoskeletal collapse and cell detachment at the wound edge (T. K. Geiser et al. 2001). Therefore, targeting such pathways to abrogate CMS-induced injury may adversely affect epithelial repair. Furthermore, CMS itself has been shown to negatively modulate epithelial repair processes (Desai et al. 2008).

1.7.2 The effect of CMS on epithelial repair

CMS significantly reduced the healing or migration of airway epithelial cells in response to a physical wound to the cell monolayer (Savla & Waters 1998; Crosby et al. 2011). This response may be mediated by CMS-induced inhibition of PI3K (Desai et al. 2010) and ameliorated by keratinocyte growth factor (KGF) (Waters & Savla 1999). In alveolar epithelial cells, similar CMS-induced inhibition of migration occurred at higher magnitudes of strain and was associated with decreased Rac1 activity dependent on membrane

localisation of T-cell lymphoma invasion and metastasis-inducing protein 1 (Tiam1) (Desai et al. 2008). Conversely, the inflammatory milieu of acute lung injury (ALI) or VALI may promote healing. IL-1β, a cytokine associated with lung injury, significantly increased rat ATII monolayer repair *in vitro*, via a MAPK-dependent mechanism (Geiser et al. 2000), and this process was also shown to be dependent on NF-κB signalling in airway cells (White et al. 2008). Therefore, the effect of lung injury and VALI on repair of the alveolar epithelium is complex and far from being comprehensively understood. Mechanical strain has also been associated with decreased cell adhesion. ATII from rats subjected to high tidal volume ventilation with hyperoxia showed decreased adhesion together with reduced FAK phosphorylation and increased RhoA activity (Desai et al. 2007). Expression of a dominant negative RhoA in these cells restored adhesion.

1.8 Hypothesis and aims

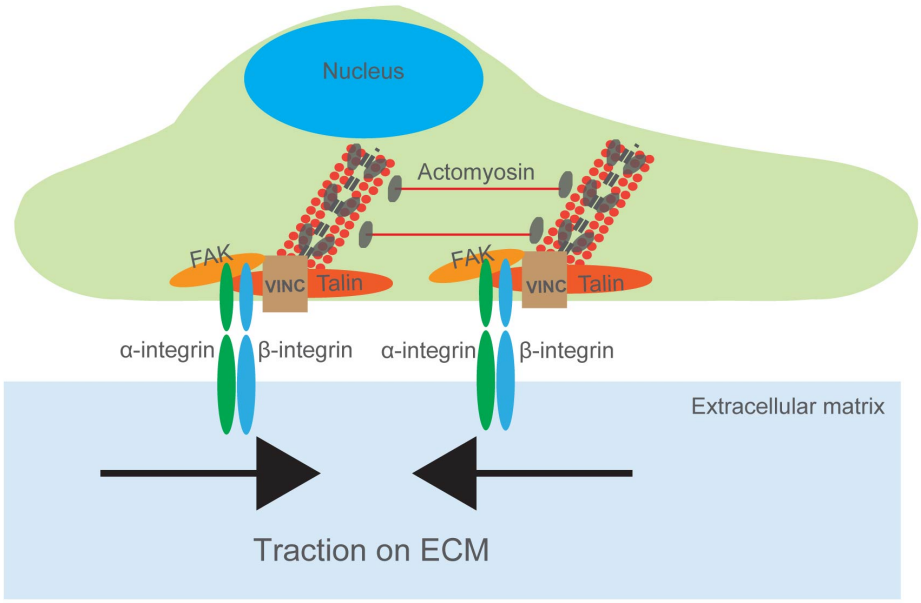
The work in this thesis tests the hypothesis that RhoA GTPase and integrin signalling mediate CMS-induced injury in alveolar epithelial cells (Figure 1-9).

Specifically, the aims of this project were to investigate:

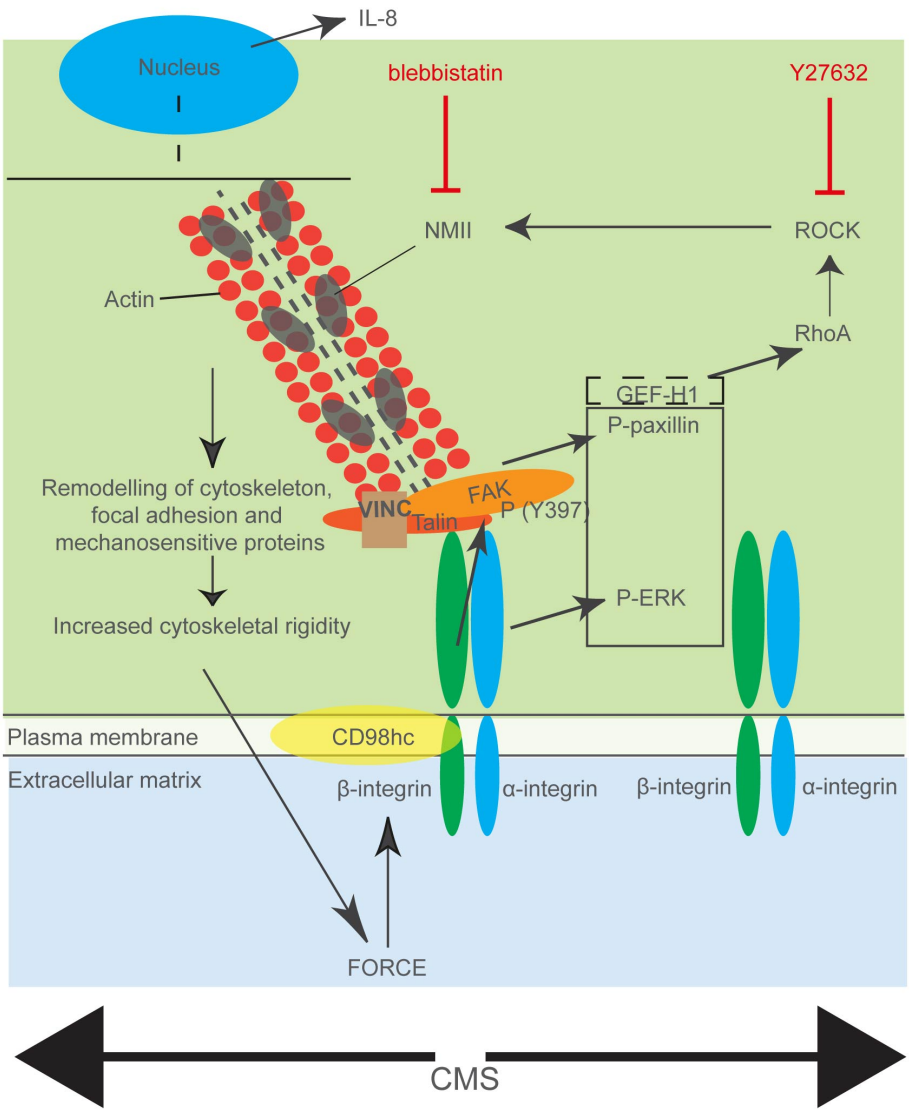
- how CMS affects cytoskeletal remodelling and RhoA GTPase signalling in alveolar epithelial cells (chapter 3)
- the role of the integrin-associated protein CD98hc in CMS-induced signalling, and in adhesion and migration in alveolar epithelial cells (chapter 4)

- to determine whether PCLS can be used as a platform in which to investigate CMS-induced RhoA GTPase and integrin signalling in alveolar epithelial cells (chapter 5)

a


Nucleus
Actomyosin
FAK
VINC
Talin
FAK
VINC
Talin
α-integrin
β-integrin
α-integrin
β-integrin
Extracellular matrix
Traction on ECM

b


IL-8
Nucleus
blebbistatin
Y27632
NMII
ROCK
Actin
RhoA
GEF-H1
P-paxillin
Remodelling of cytoskeleton,
focal adhesion and
mechanosensitive proteins
VINC
Talin
FAK
P (Y397)
P-ERK
Increased cytoskeletal rigidity
Plasma membrane
CD98hc
Extracellular matrix
β-integrin
α-integrin
β-integrin
α-integrin
FORCE

CMS

Figure 1-9 Putative mechanism by which integrin and RhoA GPTase signalling may mediate CMS-induced injury in alveolar epithelial cells

The work in this thesis tests the hypothesis that cyclic mechanical strain (CMS)-induced cytokine release is mediated through integrin and cytoskeletal Rho GTPase signalling. Panel A demonstrates how cellular integrins bind to ligands in the extracellular matrix (ECM), and are linked to the actin cytoskeleton through focal adhesion protein complexes. These are composed of a vast array of proteins, including focal adhesion kinase (FAK), vinculin (vinc) and talin. Inside out transmission of force from actomyosin contraction exerts traction on the ECM, allowing cells to become motile. Panel B shows how the application of strain on the ECM triggers activation of β1-integrins (Guilluy et al. 2011). Force-induced integrin activation promotes RhoA GTPase activity via the Rho GEF GEF-H1, possibly through FAK-dependent formation of an ERK-paxillin complex (Gawlak et al. 2014). Downstream activation of Rho-associated protein kinase (ROCK) activates non-muscle myosin II (NMII), promoting actin cytoskeletal tension and further conformational changes in mechanosensitive and focal adhesion proteins. This thereby affects cell matrix adhesion and downstream signalling, although how this may then lead to cytokine generation is currently unclear. ROCK can be inhibited by Y27632, and NMII by blebbistatin.

2 Chapter 2: Materials and methods

2.1 Reagents and materials

2.1.1 General reagents

2-mercaptoethanol	Sigma-Aldrich – M6250
2-propanolol	Sigma-Aldrich - 59304
Bovine Serum Albumin (BSA)	Sigma-Aldrich – A7030
Dimethyl sulphoxide (DMSO)	Sigma-Aldrich – D5879
Dithiothreitol (DTT)	Cell Signalling – 7016
Ethylenediaminetetraacetic acid (EDTA)	Invitrogen – AM9260G
Ethanol	Sigma-Aldrich – E7023
Glycine	Sigma-Aldrich – G7126
HEPES	Life Technologies - 15630080
Methanol	Fisher Chemical – M4000/17
Methylthiazolitetrazolium (MTT)	Sigma-Aldrich - 93482
Milk powder	Marvel
Phenylmethanesulphonyl fluoride (PMSF)	Sigma-Aldrich - 93482
Sodium Azide	Sigma-Aldrich – S2002

Sodium Chloride	Fisher Chemical – S/3161/60
Triton X-100	Sigma-Aldrich – X100
TRIZMA base	Fisher Chemical – BP152-1
TRIZMA hydrochloride	Sigma-Aldrich – T3253
Tween-20	Sigma-Aldrich – P2287

2.1.2 Cells and culture reagents

A549 alveolar epithelial cells	ECACC - 86012804
Dulbecco's Modified Eagles Medium (DMEM)	Life Technologies - 31885-049
Foetal Calf Serum (FCS)	Life Technologies
Penicillin/Streptomycin	Life Technologies – 15140122
Phosphate Buffered Saline	Life technologies – 10010-015
Trypsin - EDTA	Life Technologies - 25200056

2.1.3 Cytoskeletal reagents

Blebbistatin	Sigma Aldrich – B0560
Cytochalasin D	Sigma Aldrich – C8273

Lypophosphatidic acid (LPA)	Sigma Aldrich – L7260
Y27632 ROCK inhibitor	Sigma Aldrich – Y0503

2.1.4 Cytokines, inhibitors and other drugs

Human Interleukin-1β	R&D Systems – 201-LB-005
Human Tumour Necrosis Factor α (TNF- α)	Thermo Scientific – 10602 HNAE5

2.1.5 Molecular biology reagents

Culture broth (LB)	Sigma-Aldrich – L3022
DH5α bacterial cells	Invitrogen - 12297016
Lipofectamine p3000 transfection kit	Invitrogen – L3000001
Maxiprep kit	Invitrogen – K210016
Optimem medium	Life Technologies – 31985-062
Qiaprep miniprep kit	Qiagen – 27104

2.1.5.1 RNA extraction and processing

cDNA reverse transcription kit	Applied Biosystems - 4368814
Chloroform	Sigma-Aldrich - 319988

DNase 1	Qiagen - 79254
RNeasy mini kit	Qiagen - 74104
Taqman fast advanced mastermix	Life technologies - 4444556
Trizol reagent	Life technologies - 15596018

2.1.5.1.1 Taqman primers

Species	Gene	Primer code
Mouse	B2m	Mm00437762_m1
Mouse	HPRT	Mm01545399_m1
Mouse	CXCL1	Mm04207460_m1
Mouse	CXCL2	Mm00436450_m1
Mouse	IL-6	Mm00446190_m1
Human	B2m	Hs00984230_m1
Human	GAPDH	Hs03929097_g1
Human	ARHGAP6	Hs00241801_m1
Human	MAPK13	Hs00234085_m1
Human	CCNA1	Hs00171105_m1
Human	CDC42EP2	Hs00198943_m1
Human	AURKC	Hs00152930_m1
Human	LIMK2	Hs00948689_m1
Human	CD98hc	Hs00374243_m1
Human	IL-8	Hs00174103_m1

Table 2-1 Taqman Primers

All Primers were purchased from Life Technologies

2.1.5.2 siRNA reagents

Oligofectamine	Invitrogen - 58303
RNA/DNAse free water	Life Technologies - 10977049
siRNA buffer	Dharmacon - B-002000-UB-100

2.1.5.2.1 siRNA sequences

Gene	Code	Sequence
CD98hc	D-003542-01	UAAGGCUAUGAAGAGAUAC
Non-targeting	D-001210-02	AGAAUGGUCUGGUGAAGAU

Table 2-2 siRNA sequences used

All siRNA sequences were purchased from siGenome, Dharmacon

2.1.6 Antibodies

2.1.6.1 Primary antibodies

Target	Host	Company/code	Dilution
β1-integrins (active conformations – HUTS4)	Mouse	Merck Millipore/MAB2079Z	1:100 (IF)
β1-integrins	Rabbit	Abcam/EP1041Y	1:100 (IF) 1:1000 (WB)
CD98hc	Goat	Santa Cruz/sc 7095	1:5000 (WB)
CD98hc D603P	Rabbit	Cell signalling/13180S	1:400 (IF)
E-Cadherin	Rabbit	BD biosciences/610181	1:100 (IF)
phospho-ERK (Thr202/Tyr204)	Rabbit	Cell signalling/4377	1:100 (IF), 1:1000 (WB)

total-ERK	Rabbit	Cell signalling/9102	1:1000 (WB)
phospho-FAK (Tyr397) D20B1	Rabbit	Cell signalling/8556	1:1000 (WB)
total-FAK D2R2E	Rabbit	Cell signalling/13009	1:1000 (WB)
Gapdh	Rabbit	Millipore/ABS16	1:20,000 (WB)
GRO-α	Rabbit	Abcam/ab86436	1:100 (IF)
Paxillin Y113	Rabbit	Abcam/ab32084	1:100 (IF)
PH3	Rabbit	Millipore/06-570	1:1000 (IF)
PMLC2 2 Ser19	Rabbit	Cell signalling/3671S	1:50 (IF)
Pro-SPC	Rabbit	Millipore/AB3786	1:1000 (IF)

Table 2-3 Table of primary antibodies

IF – immunofluorescence, WB- Western Blot

2.1.6.2 Secondary antibodies

Target	Conjugate	Host	Company/code	Dilution
Goat	AF594	Donkey	Life technologies/A11058	1:500 (IF)
Goat	AF488	Donkey	Life	1:500 (IF)

			technologies/A11055	
Goat	HRP	Rabbit	Dako/P0449	1:5000 (WB)
Mouse	AF594	Goat	Life technologies/A11004	1:500 (IF)
Mouse	HRP	Donkey	R&D/HAF018	1:3000 (IF)
Rabbit	AF488	Goat	Life technologies/A11008	1:500 (IF)
Rabbit	AF594	Donkey	Life Technologies/A21207	1:500 (IF)
Rabbit	HRP	Goat	Cell signalling/7074	1:2000 (WB)

Table 2-4 Table of secondary antibodies

AF – Alexa Fluor, HRP – horseradish peroxidase, IF – immunofluorescence, WB- Western Blot

2.1.7 Precision Cut Lung Slices (PCLS)

Agarose-type IX-A ultra-low gelling temperature — Sigma-Aldrich – A9414

Hank's Balanced Salt Solution (HBSS) — Life technologies – 14025-050

2.1.7.1 Murine PCLS culture

Dulbecco's Modified Eagle Medium (low glucose, +phenol +L-glutamine) — Life technologies - 31885-023

Penicillin/Streptomycin	Life technologies - 15140122
Live/dead viability kit	Life Technologies – L3224

2.1.7.2Human PCLS culture

Gentamicin 10mg/ml solution	Sigma-Aldrich - G1272
RPMI 1640	Thermo Scientific - 11875-085

2.1.8 Imaging reagents

DABCO anti-fade DAPI stain	Sigma Aldrich – D2552
Mowiol	Sigma Aldrich - 81381
Paraformaldehyde	Thermo Scientific - 28906
Phalloidin stain (Alexa Fluor 488)	Molecular Probes (Life Technologies) - A12379
Prolong Gold anti-fade	Life Technologies – P36930

2.1.9 ELISA and MSD kits

Human IL-8 ELISA DuoSet	R&D - Dy208-05
Human IL-8 MSD (Vplex kit)	Mesoscale discovery - K151RAD
Murine KC/GRO MSD (Vplex kit)	Mesoscale discovery - K152QTD

2.1.10 Western Blot reagents

BCA assay	Thermo Scientific - 23227
Cell lysis buffer	Cell Signalling – 9803S
ECL western blot substrate	Thermo Scientific - 32132
Gel 4-12% Bis-Tris (Nupage)	Life Technologies - NP0322
Hyperfilm (Amersham)	GE healthcare - 289-068–36
LDS sample buffer (Nupage)	Life Technologies - NP0007
Protein ladder (Fermentas Spectra(TM)	Thermo Scientific - 26634
Polyvinylidene fluoride (PVDF) (Immobilon) Membrane	Merck Millipore - IPVH00010
Running Buffer (NuPAGE MES SDS)	Thermo Scientific – NP0002

2.1.11 Equipment

Appied Biosystems ViiA 7	Applied Biosystems
Centrifuge (Mistral 2000)	MSE
iCELLigence real-time cell analysis software	ACEA biosciences
FLIM detector	Becker Hickl
FX-5000T Flexercell *in vitro* strain	Flexcell

system

Microscope (confocal - Inverted) – Zeiss Zeiss LSM 510	
Microscope (epifluorescence inverted) – Zeiss Axiovert 200	– Zeiss
Microscope (confocal – upright) – Leica Leica SP5	– Leica
Multiphoton laser - Mai Tai 690-1020	Spectra-Physics
NanoDrop spectrophotometer	Thermo Scientific
Photospectrometer	TECAN life sciences
Tissue Slicer (VF-200)	Precisionary Instruments
Thermal Cycler (PTC-200)	MJ research
Western blot developer (XRay Film Processor JP-33)	JPI Healthcare

2.1.12 Software

FIJI (Image J)	Open source: https://imagej.net/Welcome
Prism 6.0	Graphpad software
Imaris	Bitplane
MSD workbench software	Mesoscale Discovery

Tri2	Paul Barber open source (University of Oxford) https://app.assembla.com/spaces/ATD_TRI/wiki/Download
Volocity 6.3	PerkinElmer

2.1.13 Company locations

ACEA biosciences	San Diego, CA, USA
Addgene	MA, USA
Agilent Technologies	Santa Clara, CA, USA
Alabama Research and Development	Munford, AL, USA
Applied Biosystems	California, USA
Becker Hickl GmbH	Berlin, Germany
Bitplane (Oxford Instruments)	Zurich, Switzerland
Cambridge Bioscience	Cambridge, UK
Cell Signalling Technologies	Beverley, MA, USA
Corning	New York, USA

Dharmacon	Colorado, United States
Eppendorf	Hamburg, Germany
Fisher Chemical	Loughborough, UK
Flexcell	Burlington, NC, USA
Graphpad software	La Jolla, CA, USA
Henkel	Hertfordshire, UK
Ibidi	Martinsried, Germany
Immune systems	Devon, UK
Invitrogen	Carlsbad, CA, USA
JPI	New York, USA
Lab tech International	East Sussex, UK
Leica	Solms, Germany
Life Technologies	Paisley, UK
Merial Animal Health	Harlow, Essex

Merck Millipore	Darmstadt, Germany
MJ research	Quebec, Canada
Mesoscale Discovery	Maryland, USA
Molecular Probes	Eugene, OR, USA
MSE	London, UK
Nunc	Roskilde, Denmark
PerkinElmer	Ohio, USA
Precisionary Instruments	Greenville, NC, USA
Qiagen	Limburg, Netherlands
R&D Systems	Abingdon, UK
Roche	Mannheim, Germany
Santa Cruz	Dallas, TX, USA
Sigma-Aldrich	Poole, UK
Spectra-Physics	Santa Clara, CA, USA

Tecan life sciences	Männedorf, Switzerland
VWR	Leicestershire, UK
Zeiss	Jena, Germany

2.2 General Methods

2.2.1 A549 cell line culture

A549 cells (ECACC), an adherent line of human lung adenocarcinoma cells, were cultured in Dulbecco's Modified Eagle Medium (DMEM). Medium was supplemented with foetal calf serum (FCS) (10%) and penicillin and streptomycin (1%), and cells cultured in T75 flasks at 37°C in a humidified incubator with 5% CO_2.

Passage of cells was performed by aspiration of medium and washing cells with phosphate buffered saline (PBS) (10mls) twice. Trypsin-EDTA (3ml of 0.05%) was added, and cells incubated for 3mins at 37°C. Cell detachment was observed by brightfield microscopy. FCS-replete DMEM (6mls) was added to neutralise the trypsin, and the resulting medium centrifuged (190g for 5 mins) to pellet the cells. Supernatant was then discarded, and cells resuspended in fresh culture medium (10mls). Cells were counted and cell suspension split accordingly, allowing for cells to be approximately 80% confluent after 48 hours.

2.2.1.1 Cell counting

Cells were counted using a haemocytometer (Immune systems FastRead 102, Devon, UK). Cell suspension (9µl) was added to the counting chamber, and cells counted under a phase-contrast microscope (Nikon, Surrey, UK). The counting chamber consists of ten large squares, each containing smaller squares in a 4x4 grid. Cells in each large square were counted by the total number of cells within each smaller square including cells

on the bottom and right borders only. The number of cells was then calculated using the following formula:

Cells/ml = total number counts／number of 4x4 grids counted $\times 10^4$

2.2.1.2 MTT determination of cell viability

Mitochondrial enzymes in metabolically active cells cleave yellow tetrazolium (MTT: 3-(4, 5-dimethylthiazolyl-2)-2, 5-diphenyltetrazolium bromide) into purple formazan, which can then be solubilised and quantified using spectrophotometry. The amount of formazan produced is directly proportional to the number of metabolically active cells present, when this technique is applied to a homogenous population of cells (Sylvester 2011).

Following treatment, cell supernatant was removed and the cells washed once with warm PBS. Cells were then incubated with MTT (1mg/ml) in medium for 15 minutes at 37°C. MTT solution was discarded, and the plates allowed to dry for 30 minutes. Cells containing formazan dye were then solubilised by incubation in DMSO with agitation for 10 minutes, following which excitation was read using a photospectrometer at 550nm.

2.2.2 Generation and culture of Precision Cut Lung Slices (PCLS)

2.2.2.1 Murine lung slices

Lung slices were obtained from CD1 mice euthanised by intraperitoneal injection of phenobarbital sodium (Euthatal; Merial) from the project licence ‘Mechanisms of acute and chronic inflammation’ (PPL 70/7643). Following euthanasia, the trachea was exposed and an intra-tracheal cannula inserted.

The thoracic cavity was exposed, and the lungs inflated under direct vision with low melting point agarose (1.2ml) supplemented with HEPES (25nM). A subsequent bolus of air (0.3ml) was injected to ensure full inflation of the lung parenchyma. Tissues soaked in ice-cold HBSS were draped over the lungs to cool and solidify the agarose. The lungs were excised and stored in HBSS on ice.

Lung lobes were embedded in agarose (2%) (which provides additional support during the slicing process). Lung lobes were cut in transverse section to a thickness of 300 μm using the tissue slicer (Precisionary Instruments Inc.), and individual slices were then cultured in DMEM (1ml) supplemented with penicillin and streptomycin (1%) in 1 well each of a 24-well plate for 1 hour at 37°C. Medium was then changed, and slices left overnight prior to treatment. This method is adapted from that described previously (Henjakovic et al. 2008).

2.2.2.2 Human lung slices

PCLS were generated from disease-free resection tissue obtained from the Biomedical Research Unit (BRU) human respiratory biobank (ethics, reference number 10/H0504/9 – study number MG13). Tissue was obtained in RPMI 1640 supplemented with penicillin and streptomycin (1%) and gentamicin (10mg/ml) at 4°C. PCLS were generated using an adapted agarose point-injection insufflation method described in (Sturton et al. 2007). Lung tissue submerged in HBSS was point injected with low melting point agarose (3%) in HBSS supplemented with penicillin and streptomycin (1%) in 100μl boluses stepwise throughout the tissue using a fine gauge needle, such

that the tissue inflated evenly. Approximately 1-2ml of agarose was required per gram of tissue. Inflated tissue was then submerged in HBSS, and allowed to cool at -20 °C for 10 minutes. The tissue was cored into 8mm diameter cylinders using a weighted coring tool (Alabama Research & Development). Cores were embedded in low melting point agarose, and sliced as for murine lung slices (2.1.7.1) but to thicknesses of 400μm (Figure 2-1).

Individual slices were placed into RPMI 1640 (1ml) supplemented with peniciilin, streptomycin and gentamicin as above, and incubated for 1 hour at 37°C. The medium was then changed 6 times at 30-minute intervals, and slices left overnight prior to treatment.

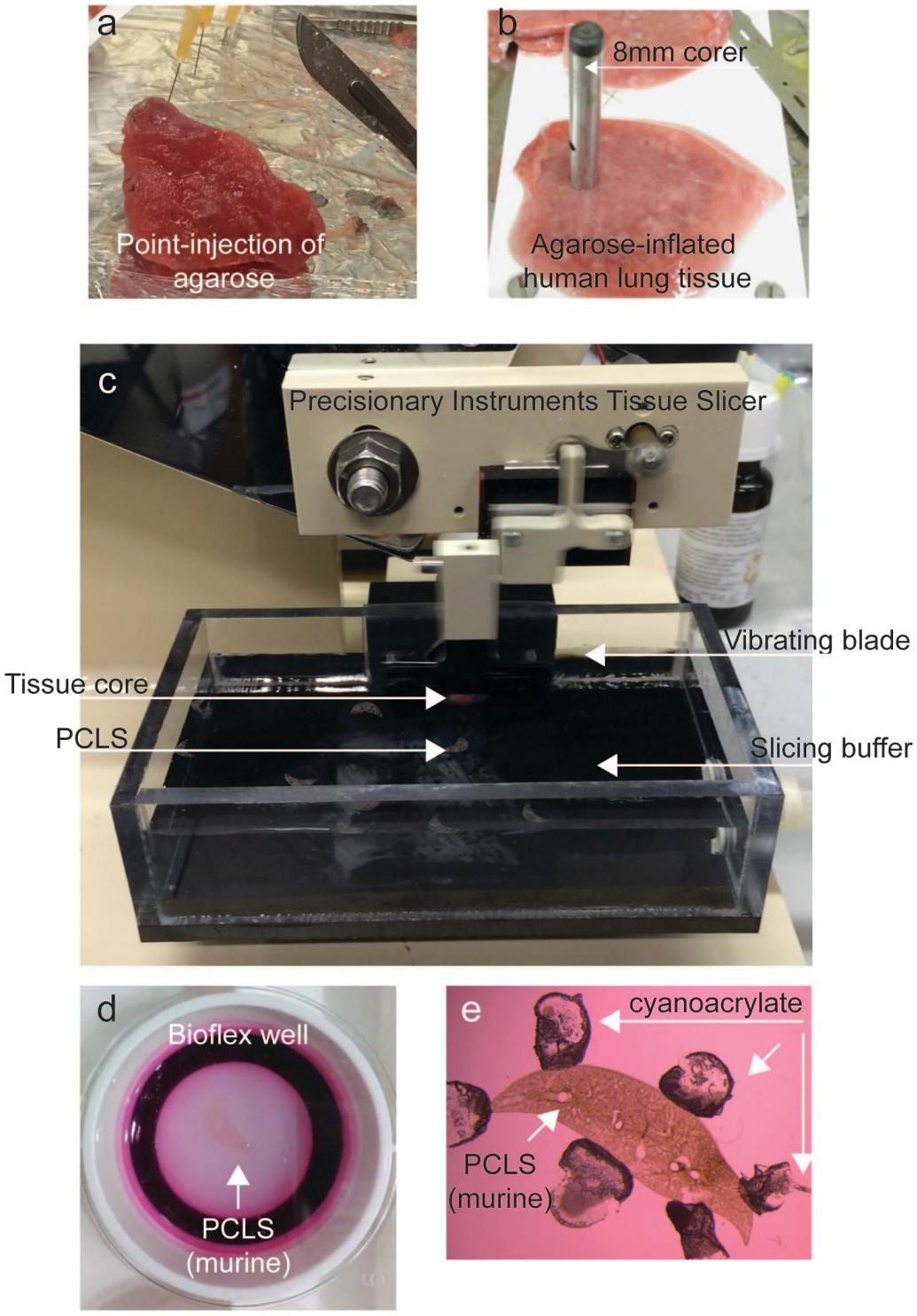


Figure 2-1 Generation and culture of Precision Cut Lung Slices (PCLS)

Human PCLS were point injected with agarose (panel A) and cored (panel B). Cores of human tissue, or whole murine lobes were loaded into the tissue slicer (Panel C) and PCLS generated. These were then adhered onto Bioflex plates (Panel D) using ethyl-cyanoacrylate (panel E) for Cyclic Mechanical Strain (CMS) studies. Photograph in Panel B courtesy of John-Poul Ng-Blichfeldt and Panel C courtesy of Joana Alçada.

2.2.2.3 PCLS viability studies

Fluorescent staining of live and dead cells provides an opportunity to explore the viability of excised and *ex vivo* tissues, not amenable to traditional cell-based viability assays (Johnson & Rabinovitch 2012). Treated PCLS were cut from silicone membranes, placed into 24-well plates with coverslip bottom (Ibidi µ-plate) and incubated with ethidium/calcein (4µM) in warmed PBS (Life Technologies) for 45 minutes at 37°C. They were then imaged immediately in an inverted confocal microscope using a 488nm laser for calcein, and 543nm laser for ethidium in HBSS. Cells treated with methanol (70% for 30 minutes) were used as a control: staining positive for ethidium nuclei (dead) staining but negative for calcein cytoplasm (live) staining (Figure 2-2).

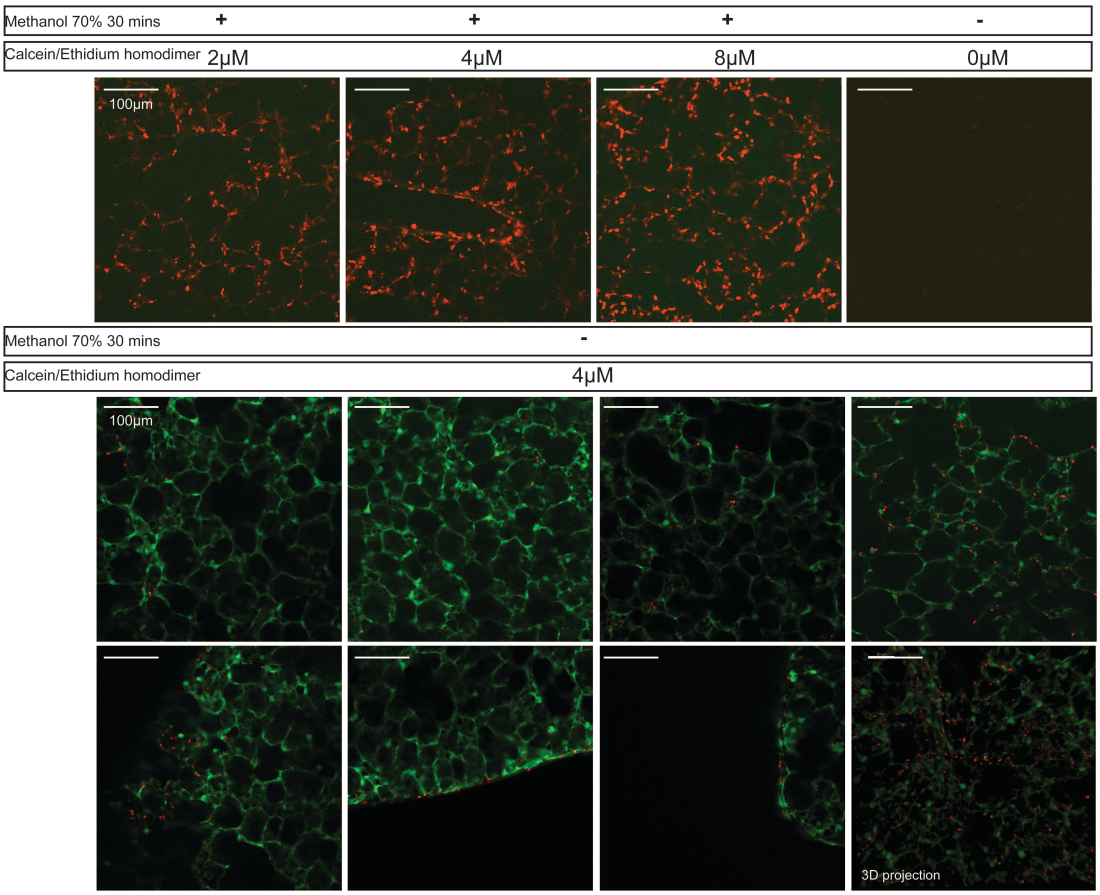


Figure 2-2 Optimisation of Calcein and Ethidium staining in murine Precision Cut Lung Slices (PCLS)

Murine PCLS were treated with methanol (70%) for 30 minutes, then stained with increasing concentrations of calcein and ethidium homodimer (top panel). The concentration that demonstrated clear ethidium homodimer (dead) nuclear staining without calcein (live) cytoplasm staining was selected as 4μM. This concentration was then applied to live PCLS (bottom panel). Scale bars represent 100μm.

2.2.3 Molecular Biology

2.2.3.1 Ribose nucleic acid (RNA) extraction

RNA was extracted from isolated cells by the addition of Trizol reagent (300μl, Life Technologies) to each well of a 6-well plate, and cells immediately scraped and the resultant solution placed into microcentrifuge tubes and

stored at -80°C for future use. Chloroform (300µl, Sigma-Aldrich) was added, samples agitated for 15 seconds, and then centrifuged (12,000g for 15 mins) at 4°C to separate organic and aqueous phases. 250µl of the top aqueous phase, in which total RNA is located, was removed and placed in a new microcentrifuge tube. An equal volume of ethanol (70%) was added to this solution to precipitate nucleic acids.

The RNeasy mini kit (Qiagen) was used to isolate RNA. The solution was transferred to an RNeasy mini column and centrifuged (8,000g for 15 seconds), and the effluent discarded. RW1 wash buffer (350µl) was then added to remove excess ethanol, and the column centrifuged for a further 15 seconds at 8,000g. DNase1 (80µl, Qiagen) was added to minimise genomic DNA contamination, and the solution incubated for 15 mins at room temperature (RT). A subsequent wash step by adding RW1 buffer (350µl) and centrifugation (8,000g for 15 seconds) followed, and the effluent was discarded. The column was then washed twice with RPE (500µl) and centrifuged (8,000g for 15 seconds in the first instance, and 2 minutes in the second). The effluent was discarded, and the columns transferred to a new collection tube. A further centrifugation step at full speed for 1 minute was used to remove excess ethanol, and then total RNA was eluted into a new microcentrifuge tube by adding RNAase-free water (50µl) and centrifugation (8,000g for 15 seconds). Concentration and purity of RNA was determined by using a NanoDrop spectrophotometer (Thermo Scientific).

2.2.3.2 Reverse transcription (RT) protocol

A high capacity cDNA reverse transcription kit (Life Technologies) was used to convert total RNA to cDNA. Eluted RNA (1µg) was made up to 10µl in RNase-free dH_2O, and then mixed with reverse transcription components containing (10µl): 10x RT buffer (2µl), 25x dNTPs (0.8µl), 10x random primers (2µl), reverse transcriptase enzyme (1µl) and RNAase-free dH_2O (4.2µl). A PTC-200 Peltier thermal cycler (MJ Research) was used to synthesise cDNA. First, random primers bind to the RNA during a heating step of 25 °C for 10 minutes, then cDNA conversion occurs during a subsequent heating step of 37°C for 120 minutes, followed by denaturing of the reverse transcriptase by heating the samples to 85°C for 5 minutes. cDNA obtained from the reaction was then diluted 1:5 by adding DNAase-free water (80µl). For all experiments, a reverse transcriptase control was used, where a reaction is performed without reverse transcriptase, therefore allowing for contamination of genomic DNA to be seen in downstream reactions.

2.2.3.3 Polymerase chain reaction (PCR)

2.2.3.3.1 Working principle

PCR amplifies sequences of DNA through recurrent cycles of DNA polymerase-catalysed reactions, and cDNA generated from RNA via the reverse transcriptase process as described above (2.2.3.2) can be subjected to PCR for the amplification of specific sequences derived from a gene of interest (Gibbs 1990). Primers, synthetic oligonucleotides complementary to each strand of DNA sequences surrounding the gene of interest, are selected

or designed, and bind to the DNA template. This allows Taq polymerase, a heat-stable DNA polymerase, to start catalysing the synthesis of a replicate DNA strand. Through repeated cycles, the newly synthesised DNA strands then become a template for subsequent synthesis, and the initial target DNA sequence can be amplified exponentially (Figure 2-3).

The three stages of PCR include:

1. Denaturation, where the two strands of DNA are broken apart by heating the reaction mixture to 94°C, which disrupts the hydrogen bonds between the strands.
2. Annealing, where hydrogen bonds from between the primer and single-stranded complementary DNA template by cooling of the reaction mixture to 55-65°C.
3. Extension, where Taq polymerase attaches to the cDNA at the 3' end of the primer, and extends it by adding complementary deoxyribonucleotide triphosphates (dNTPs) in a 5' to 3' direction, therefore doubling the amount of target DNA.
4. After all rounds of PCR are completed, a final elongation step extends any remaining single DNA strands

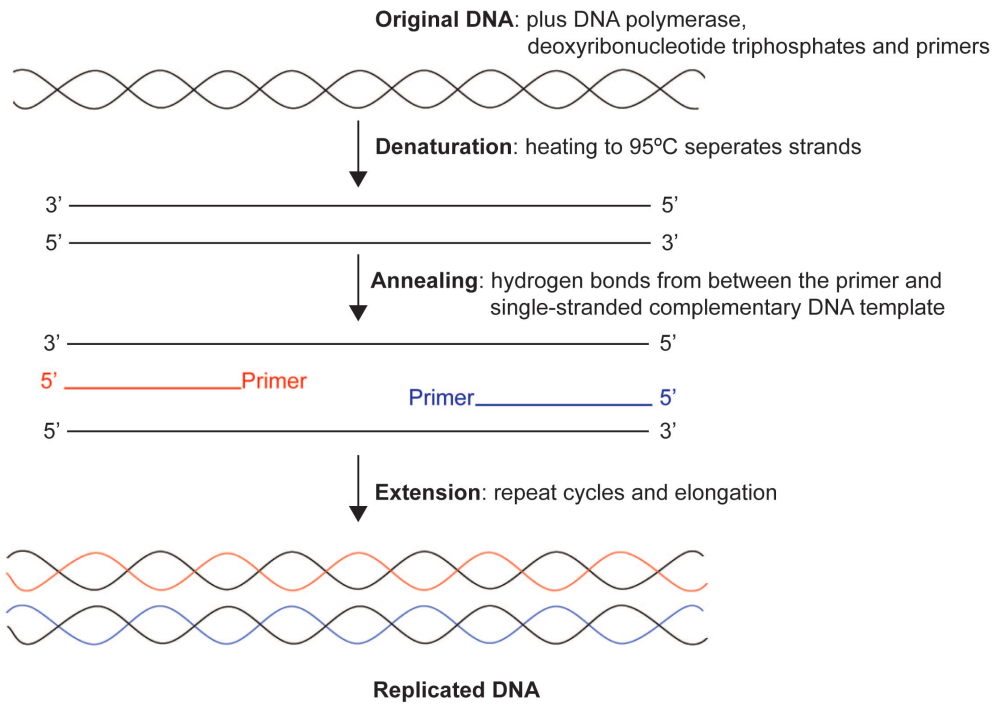


Figure 2-3 Principle of the Polymerase Chain Reaction

2.2.3.3.2 Quantitative real time PCR (qPCR)

By using oligonucleotide primers consisting of probes, which emit a fluorescent signal upon cleavage or hybridisation, PCR products can be quantified at each cycle (Kubista et al. 2006). The threshold cycle (CT) describes the cycle at which the fluorescent signal exceeds a threshold level, is arbitrarily set during exponential amplification, and is inversely related to the amount of amplicon in the reaction. Therefore, the lower the CT, the greater the amplicon (Pinhu et al. 2008). Data are presented either as absolute, where a standard curve allows for quantification of exact copy number, or relative to a reference gene, which does not change between conditions. The work in this thesis was conducted using real time qPCR, with two reference genes previously determined to show stability in A549 cells with CMS,

GAPDH and B2M (Pinhu et al. 2008). One form of RT-PCR probe, SYBR green, was used for gene array analyses, and another, Taqman, used for individual gene analyses. Both methods are described below.

2.2.3.3.3 SYBR Green 1

This process involves DNA binding dyes that fluoresce at 520nm when hybridised to double stranded DNA, but have undetectable fluorescence when in the un-bound state. Although simple and inexpensive, this technique is non-specific, in that SYBR green 1 will not only bind to amplified target DNA, but to all available dsDNA including genomic, non-specific PCR products and primer dimers.

The Cytoskeletal Regulators RT^2 PCR array (Qiagen #330231) used in this thesis (Section 1.1.1) is based on SYBR green qPCR. RNA from three independent experiments was isolated from cells as described above, and synthesised to cDNA using the RT^2 First Strand cDNA synthesis kit. Briefly, RNA (500ng) was made up to 10µl and genomic DNA eliminated by dilution in a 1:5 ratio with Buffer GE1. Samples were incubated for 5 mins in a thermocycler at 42 °C and subsequently kept on ice. Reverse transcriptase mixture (10µl) containing: 5x Buffer BC3 (4µl), Control P2 (1µl), RE3 Reverse Transcriptase Mix (2µl) and RNase-free water (3µl) was added to each sample, and reaction mixtures for each sample incubated at 42°C for 15 minutes for reverse transcription to occur. The reaction was stopped by a heating step of 95°C for 5 minutes. cDNA samples were then diluted by the addition of RNase-free water (91µl).

qPCR was performed using RT^2 SYBR Green Mastermix (Qiagen) supplied with the kit. Briefly, cDNA prepared as described (102µl) was added to a mixture of 2x RT^2 SYBR Green Mastermix (650µl) and RNase-free water (548µl), and 10µl of this mixture added to each well of the RT^2 Profiler PCR Array plate, which already contains primers for detection of specific genes of interest. qPCR was performed using an Applied Biosystems ViiA 7 machine with the following steps:

1. 95 °C for 10 minutes for activation of DNA Taq Polymerase
2. 95 °C for 15 seconds over 40 cycles for denaturation
3. 60 °C for 1 minute over 40 cycles for annealing and extension.

Relative gene product levels were quantified using SYBR green fluorescence at the end of each PCR cycle.

2.2.3.3.4 Taqman

This system uses oligonucleotide probes containing forward and reverse primers, and a Taqman probe dual-labelled with a fluorophore and quencher binding to a region between the primers. The probe and primer anneal to complementary sequences, and during extension, Taq polymerase cleaves the probe by exonuclease activity, dissociating the fluorophore from its quencher, allowing for its excitation and subsequent emission at 517nm (for 6-carboxyfluorescein (FAM)-labelled fluorophores).

For the work presented in this thesis, individual genes were assessed using Taqman probes. cDNA (2.4µl), synthesised as described (2.2.3.2), was added to each well of a 384-well block. Master mix (3.6µl), composed of

Taqman Fast Advanced Master Mix (3µl), Taqman primers (0.3µl) (2.1.5.1.1) and RNase-free dH_2O (0.3µl), was added to each well, and PCR performed using an Applied Biosystems ViiA 7 machine with the following steps:

1. 50 °C for 2 minutes for uracil N-glycosylase (UNG) incubation
2. 95 °C for 20 seconds for activation of Taq Polymerase
3. 95 °C for 1 second over 40 cycles for denaturation
4. 60 °C for 20 seconds over 40 cycles for annealing and extension.

2.2.3.3.5 Taqman primers

Primers were purchased from Life Technologies unless otherwise specified (Table 2-1). Primers were chosen that did not detect gene products with similar or off-target sequences. Furthermore, all primers that were selected were designed across exon-exon junctions, and therefore amplification of genomic DNA was minimised, and primers did not target 5' untranslated regions (UTR) (which have variable sequences between transcripts).

2.2.3.4 Quantification of gene expression

Gene expression was quantified using the comparative CT method (Schmittgen & Livak 2008), where the CT value of the gene of interest is normalised to the CT value of the housekeeping gene as described in the following equation (Livak & Schmittgen 2001).

$$2^{-\Delta\Delta CT} = [(\text{CT target gene} - \text{CT reference gene}) \text{ sample A}$$

$$- [(\text{CT target gene - CT reference gene}) \text{ sample B}$$

Equation 1 Comparative CT method

For the work presented in this thesis, sample A was the experimental condition, and sample B, untreated or controls. Therefore, quantitative PCR data are presented as the fold change from untreated controls, and averaged over two housekeeping genes. Although this technique makes the assumption that the PCR efficiency of the gene of interest and housekeeping genes are the same, it is a widely used and validated method (Schmittgen & Livak 2008).

2.2.3.5 RNA interference

2.2.3.5.1 Working principle

Double stranded RNA of less than 30 nucleotides can induce gene-specific silencing in mammalian cells as part of anti-viral defences (Elbashir et al. 2001). Small interfering RNA (siRNA) of these lengths are recruited into a multi-protein complex, the RNA-induced silencing complex (RISC) which guides these short strands of RNA to bind to complementary single stranded RNA. There, they mediate degradation of these RNA transcripts via catalytic cleavage, causing gene silencing. siRNA technology avoids the non-specific anti-viral responses induced by long double stranded DNA.

2.2.3.5.2 Transfection of siRNA into cells

Cells at approximately 30-50% confluence were transfected with siRNA targeting CD98hc or non-targeting controls (Dharmacon) (Table 2-2). For each well of a 6-well Bioflex plate, siRNA (10μM) was complexed with oligofectamine (Invitrogen) as described below (Table 2-5). Cells were left to transfect for 48 hours, and treated as necessary.

For each well of a 6-well plate, prepare - A: 10μl siRNA with 190μl media and B: 4μl oligofectamine with 196μl media
Allow complexes to incubate for 5 minutes at room temperature (RT)
Mix A and B by gentle pipetting, and allow to incubate for 20 minutes at RT
Aspirate media from wells, and wash twice with warm PBS.
Add 1600μl media to wells
Add 400μl complexes to wells
Change media at 5 hours to serum and antibiotic replete media.

Table 2-5 siRNA transfection protocol

Serum and antibiotic-free DMEM medium was used, as oligofectamine can introduce these components into cells.

2.2.4 *in vitro* cellular assays

2.2.4.1 Application of Cyclic Mechanical Strain (CMS)

2.2.4.1.1 Flexercell system and working principle

The FX-5000T system was used to apply CMS to monolayers of A549 cells or to PCLS adhered to flexible silicone membranes. The system is

composed of a Flexcell central computer system, baseplate and gaskets, Bioflex plates and corresponding loading stations. The system is calibrated to apply strain amplitudes of 0-30% elongation to cells, 0-20% when a central loading post is used, and 30% without a loading post. For our work, strain amplitudes of 0, 5, 20 and 30% elongation were applied.

Cells are cultured on 6-well Bioflex plates, the culture surface of which is a flexible and transparent silicone elastomer membrane. For the experiments described below plates pre-coated with collagen I were used. CMS is applied by the creation of a vacuum in the gasket in which the Bioflex plates are seated, which therefore deforms the flexible membrane on which cells are cultured (Schaffer et al. 1994; Gilbert et al. 1994). When loading stations are used, uniform radial and circumferential strain is applied across the membrane, with stretch of cells of up to 20% elongation possible. When loading stations are removed, stretch of cells up to 30% is possible, but the stretch applied is not equibiaxial across the strain field (Figure 2-4).

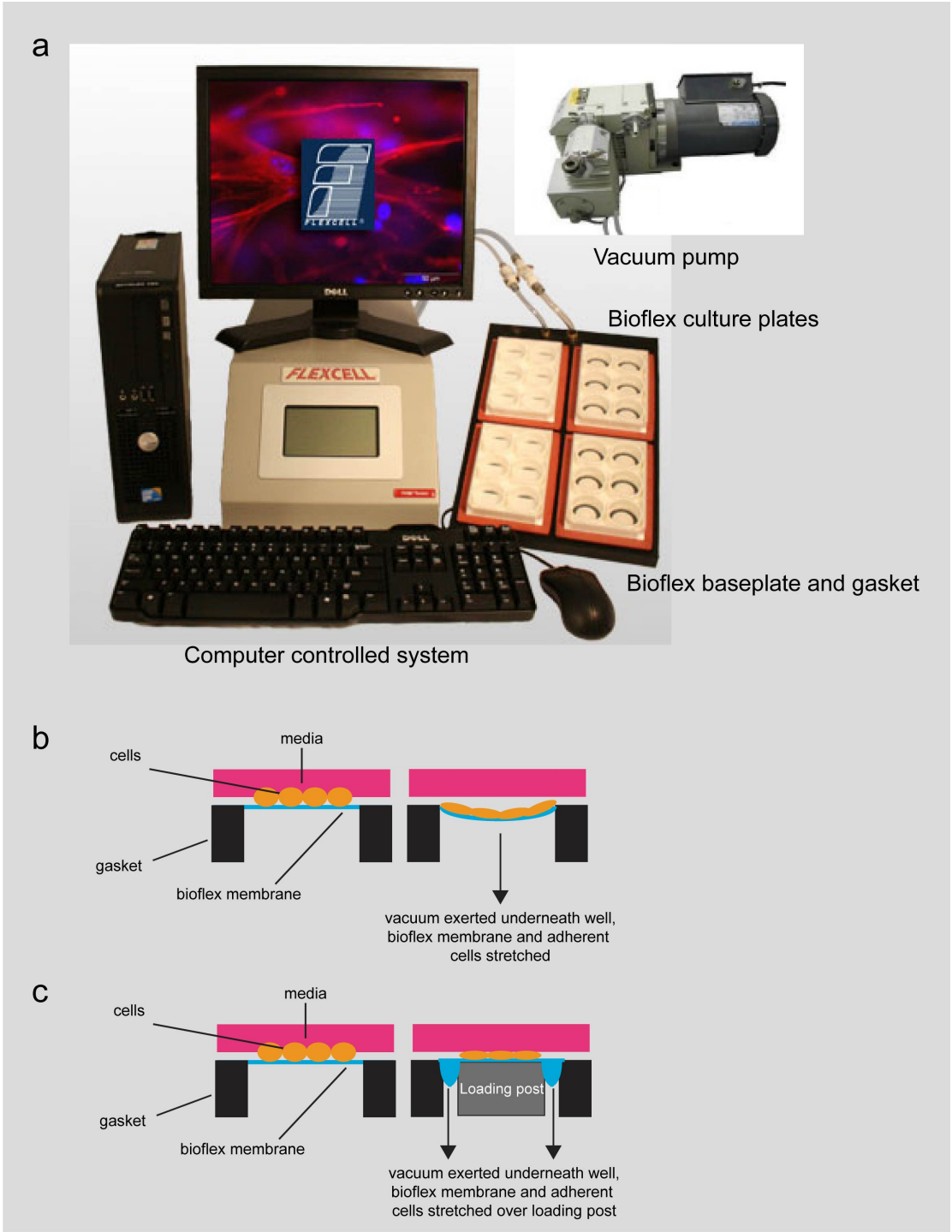


Figure 2-4 The Flexcell FX-5000™ system

Panel A shows the components of the Flexcell FX-5000™ system (courtesy of Flexcell product information), which is computer driven, and a vacuum exerted by the vacuum pump pulls cells plated on the Bioflex™ culture plates downwards, creating equibiaxial stretch. Panels B and C demonstrate the effect of a vacuum on plated cells, both without and with a loading post respectively.

2.2.4.1.2 Application of CMS to cells using the Flexercell system

Our group has previously determined that stretch of 30% elongation for up to 2 hours induced optimal IL-8 cytokine mRNA expression and protein generation (Pinhu 2008). Furthermore, a stretch/relaxation ratio of 1:1 and a frequency of 20 cycles per minute (0.33Hz) was applied, as these parameters were equivalent to those used during mechanical ventilation of patients. Unless otherwise stated, these parameters were used during the work in this thesis when applying mechanical strain to cells.

Alveolar epithelial cells during normal, tidal volume breathing are thought to experience magnitudes of strain between 1 and 5%, whereas during high tidal volume mechanical ventilation, cells might experience up to 30% strain (Vlahakis et al. 1999). Although these are approximations, inflation of the lung to total lung capacity (TLC) is estimated to increase strain to the range of 15-40% and potentially higher, and the heterogeneous nature of the state of inflation of injured lung results in some alveolar units experiencing deformation many times greater than neighbouring collapsed lung units (Roan & Waters 2011).

Although lung volume more than doubles when lungs are inflated to 100% TLC (Tschumperlin & Margulies 1999) some of this change in alveolar surface area derives from unfolding of alveolar septal pleats (Gil et al. 1979). Consequently, the epithelial basement membrane might only increase by as much as 50% or a strain of 22%. The elongation magnitudes used when applying mechanical strain in vitro are therefore approximations of normal and

injurious strain rates applied to healthy and injured lung by mechanical ventilation.

2.2.4.1.3 Preparation of A549 cells for application of cyclic mechanical strain

Seeding of A549 cells was optimised to enable the cells to be 30% confluent at the time of siRNA transfection, 50-70% confluent at the time of DNA transfection, and 80-100% confluent at the time of application of CMS. Cell seeding densities of 150 x 10^5 cells/well produced a confluent monolayer of cells at the time of CMS, and when compared to other seeding densities in preliminary experiments, although CMS-induced IL-8 release was not statistically significant at any seeding density, the mean increase at 150 x 10^5 cells/well was greatest (1.76 times baseline IL-8 release). The absence of statistical significance was attributed to high baseline IL-8 release in these experiments (Figure 2-5).

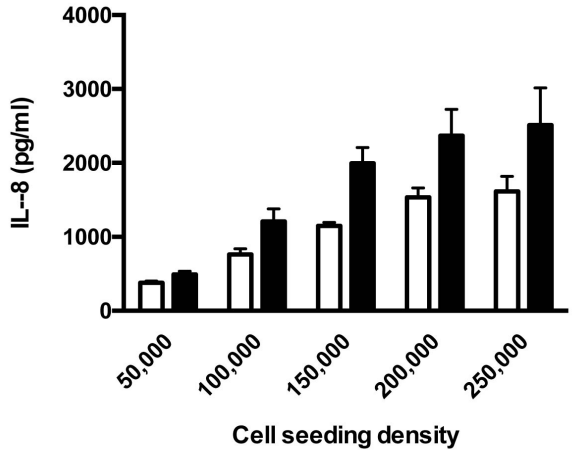


Figure 2-5 Optimising cell seeding density for CMS-induced IL-8 release

A549 cells were seeded at the above densities, and CMS applied equibiaxially at 30% elongation for 2 hours. Panel shows IL-8 generation as sampled from cell supernatant at 24 hours following either static conditions or CMS. Data are for three individual experiments, and are presented as mean ± SEM. Data analysis by Kruskal-Wallis test.

2.2.4.2 ‘Scratch assay’ epithelial migration model

Following treatment, monolayers of A549 cells plated and transfected in 6-well plates (Corning) were scratched with a P1000 pipette tip down the centre of each well to create a wound. Wells were washed with PBS to remove damaged or dead cells, and fresh culture medium replaced. Images were taken using a Zeiss Axiovert 200 (Zeiss: time 0 hours) inverted microscope with incubator, and the stage parameters noted to ensure the same field was imaged at later time points. Cells were cultured for a further 16-24 hours to allow for cell migration into the scratched area (Figure 2-6).

Wound area was calculated at each time point using Volocity software (PerkinElmer), and the difference in wound area between 0 and 16 hours calculated. Repair was expressed as a percentage of original wound area covered by cells.

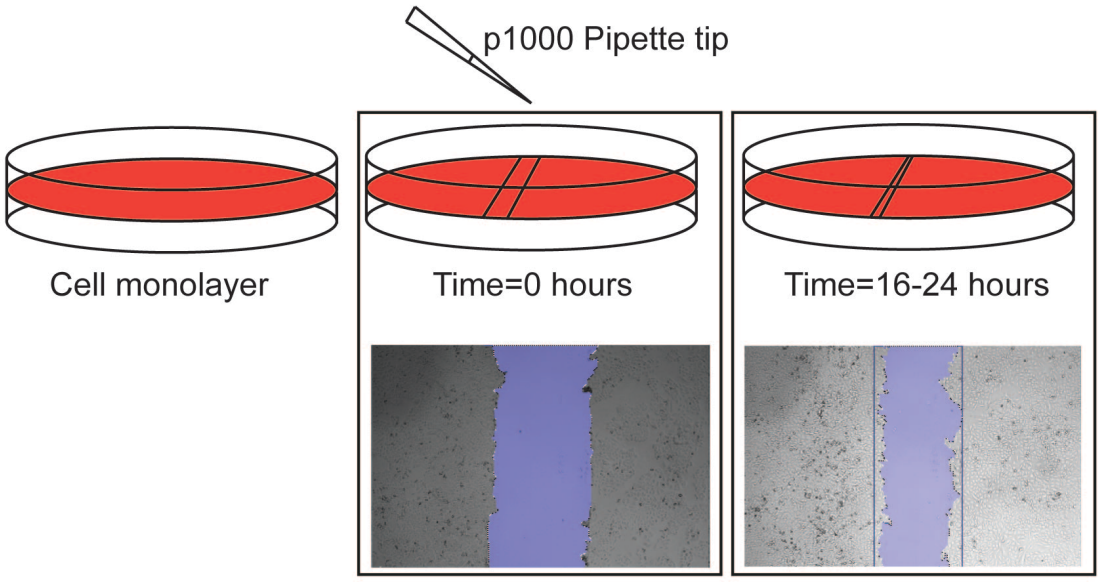


Figure 2-6 Outline of 'scratch assay' epithelial migration model

A confluent monolayer of cells was scratched with a pipette tip, imaged at time=0 hours, then again at time = 16-24 hours to observe cell migration into the scratched area.

As an indicator of cell spreading, inter-nuclear distance was calculated by fixation of cells in 4% PFA at 24 hours, and staining with DAPI (500mM). Cells were covered with Prolong Gold antifade mountant (Life Technology) and imaged using the DAPI filter on the Zeiss Axiovert 200 inverted microscope. Inter-nuclear distance was calculated using FIJI software using mean grey pixel intensity and centroid measurements, and the nearest neighbor distance (NND) calculated using the NND macro for Image J developed by Yuxiong Mao (Davis et al. 2016).

2.2.4.3 Electrical impedance assay

Epithelial barrier integrity was measured using the real-time cell analysis (RTCA) iCELLigence system (ACEA Biosciences). This model relies on the

passage of a current along electrodes at the bottom of a cell culture well. Cells plated in the well impede the passage of current, such that increasing density of cells with intact tight junctions increase resistance, termed the cell index (Figure 2-7).

To prime the system, cell culture medium (150µl) was added to iCELLigence 8 well E-Plates (ACEA Biosciences) and incubated for 30 min at 37°C. A measurement of impedance without cells was designated as the baseline. A549 cells seeded at a density of 12,000 cells/well in cell culture medium (150µl) were placed into the culture medium present in the wells, to give a total volume of cell culture medium of 300µl/well. Cell impedance measurements were recorded every 10 minutes and transfection and treatment steps performed over the next 160 hours. Cell index was normalised at specific points, such as prior to transfection or prior to wounding. The change in normalised cell index over time was calculated using RTCA iCELLigence software (ACEA Biosciences).

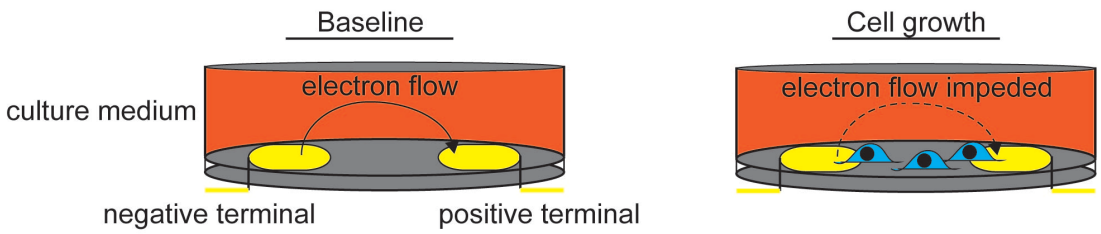


Figure 2-7 Electrical impedance assay

Cells are plated into wells containing impedance electrodes (yellow). At baseline conditions and prior to cell adherence and proliferation, electrical current flows un-impeded through the culture medium (orange). With cell adherence and proliferation, resistance to the flow of current is increased.

2.2.4.4 Cell adhesion assay

A549 cells seeded in 6-well plates (Corning) were grown to confluence, treated as required and then washed twice in PBS. Cells were fixed for 10 minutes in PFA (4%), then stained with crystal violet solution (0.1%) for 10 minutes. Stained cells were washed with running water until the run-off became clear, and left overnight to dry. Stained cells were then solubilised in methanol with agitation, and the solubilised crystal violet read in a plate reader at 570nm wavelength.

2.2.5 Imaging techniques

2.2.5.1 Confocal laser scanning microscopy

2.2.5.1.1 Working Principle

Confocal laser scanning microscopy scans specimens with focused beams of light, and uses a pinhole to reduce out of focus information at the point of detection (Poobalasingam et al. 2017). This allows for sharper images enabling greater detail, and optical sectioning of specimens in three dimensions (Pawley & Masters 2008). Using either antibody-based or direct fluorescence technology, laser-emitted light at particular wavelengths excites the fluorescent label, leading to emission at a higher wavelength, which is then collected through the objective lens, focussed through the pinhole, and recorded by a light-sensitive detector to generate an output signal transmitted to a computer for image acquisition (Figure 2-8).

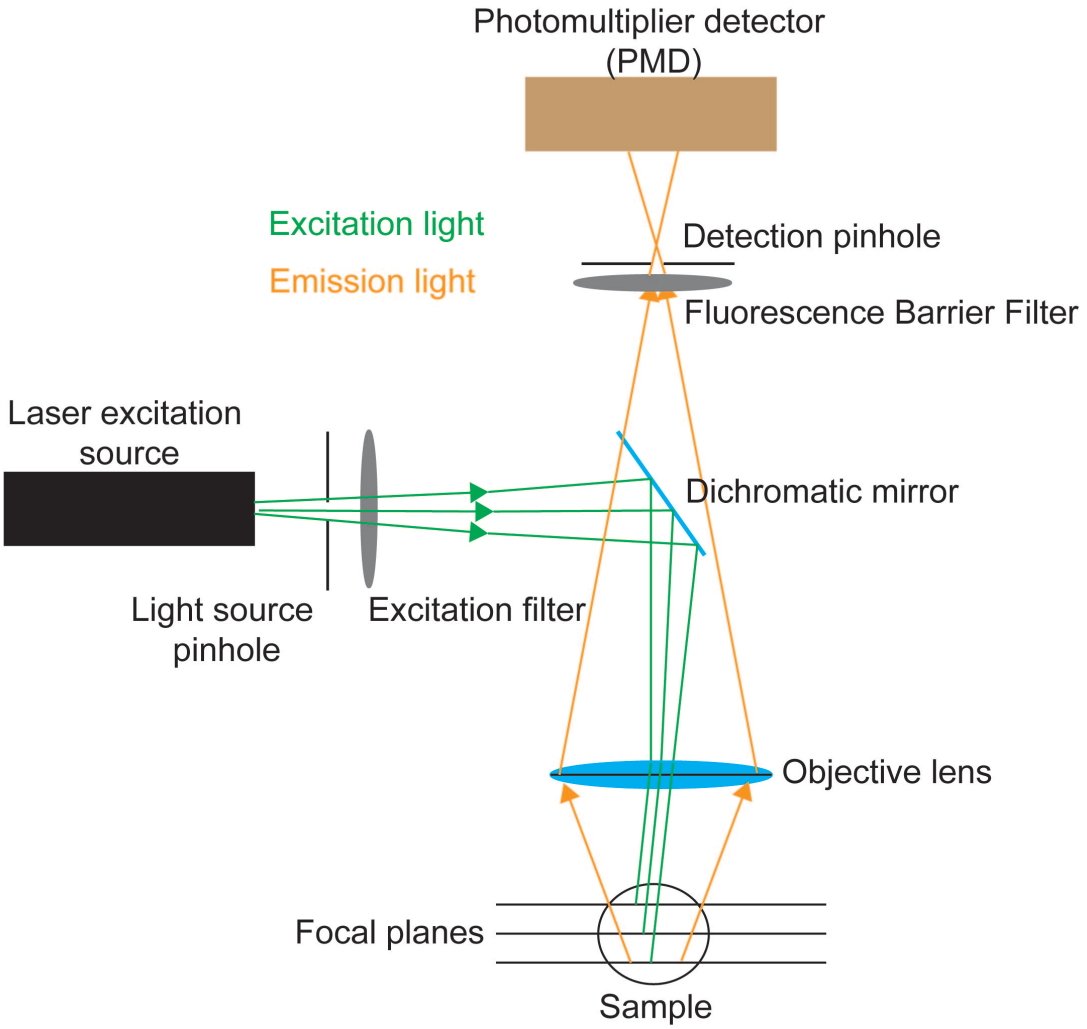


Figure 2-8 Line diagram representation of confocal microscopy process

Light from the excitation source passes through a pinhole aperture and is reflected by a dichromatic mirror. The light is then scanned across the specimen in a defined focal plane and emitted light from the excited fluorophore passes through the dichromatic filter and is focussed by the detection pinhole aperture. Imaging at focal planes occurs because out of focus light (above and below the focal plane being imaged) does not pass through the detection pinhole.

2.2.5.1.2 Fluorescence

Absorption of energy by a molecule can cause it to transition from a ground state (S0) to an excited-state (S1-S2). The molecule rapidly reverts its energy state back to S1 through internal conversion (vibrational relaxation)

and then from S1-S0. This latter transition produces fluorescence emission due to the energy release in the form of a photon (Figure 2-9).

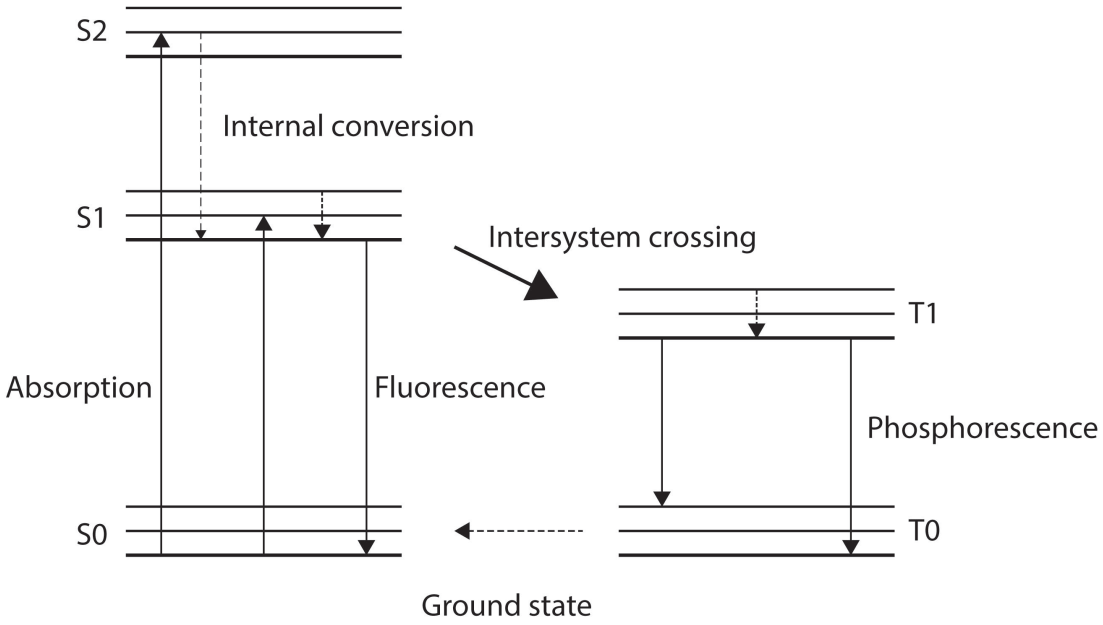


Figure 2-9 Jablonski diagram

Based on (Jablonski 1933). S0, S1 and S2 represent the ground, first and second electronic states respectively. Horizontal lines represent vibrational energy levels at each state. Vertical lines with arrows represent transition between states. Once a molecule absorbs energy in the form of electromagnetic radiation, the fluorophore transitions from S0 to S1 or S2. Fluorescence occurs when the fluorophore transitions from the lowest vibrational energy state of S1 to S0.

2.2.5.1.3 Preparation of cell samples for confocal immunofluorescence

For fixation, permeabilisation and labelling of cells for immunofluorescence, the following protocol was used unless otherwise specified.

Cells on coverslips or in Corning 24-well coverslip-grade plastic wells were fixed in PFA (4%) for 10 minutes at RT, and washed for 3 x 5 mins with gentle agitation. Cells were permeabilised by addition of Triton-X (0.2% in

PBS) for a further 5 minutes. At this stage, cells cultured in 6-well Bioflex plates were processed by cutting the membrane from the plate whilst immersed in PBS, and cutting into small 1cm square sections which were then placed into Corning 24-well plates. Blocking of non-specific antigens was facilitated by incubating fixed cells in BSA (1%) - Triton (0.1%) in PBS for 1 hour. Cells were then incubated in relevant primary antibody (Table 2-3) in blocking solution either overnight at 4°C or for 1 hour at RT. Cells were then washed as above, and secondary antibody (Table 2-4) together with phalloidin and DAPI stain added for 1 hour at RT, followed by a further wash step. At this stage, sections of membrane were removed from the 24-well plates, placed into slides in which artificial gaskets were made, covered with Mowiol solution and then covered with an imaging-grade coverslip. Cells on coverslips were simply covered with Mowiol and inverted to cure on slides. All samples were left to cure in the dark for 48 hours at room temperature.

Unless otherwise specified, samples were imaged using Leica SP5 upright confocal microscope, with 40x 1.25 or 63x 1.4 HCX PL APO oil objectives.

2.2.5.1.4 Preparation of tissue samples for confocal immunofluorescence

For fixation, permeabilisation and labelling of precision cut lung slices (PCLS) for immunofluorescence, the following protocol was used unless otherwise specified.

PCLS were fixed in PFA (4%) for 30 minutes at RT, and washed for 3 x 5 mins with gentle agitation. Cells were permeabilised and non-specific antigen binding blocked by Triton-X (0.3%) and BSA (1%) in PBS for either 2

hours at RT or overnight at 4°C. PCLS were then incubated in relevant primary antibody (Table 2-3) in blocking solution for 48 hours at 4°C. PCLS were then washed as above, and secondary antibody together with phalloidin and DAPI stain added for 2 hours at RT, followed by a further wash step. At this stage, PCLS were inverted, placed into Corning 24-well µ-plates, immersed in Prolong Gold solution, and then covered with a coverslip to compress the PCLS. All samples were left to cure in the dark for 24 hours at room temperature.

Unless otherwise specified, PCLS were imaged using a Zeiss LSM-510 inverted confocal microscope, using 20 X 0.8 EC Plan-Neofluar objective lens.

For immunofluorescence experiments using cell and tissue preparations, gain and offset were set such that no signal was obtained from secondary-antibody only conditions. These settings were then used for imaging experimental samples.

2.2.5.2 Fluorescence Lifetime Imaging

2.2.5.2.1 Förster Resonance Energy Transfer (FRET)

In lieu of transfer of energy to the external environment in the form of fluorescence, this process describes the situation in which energy released in the transition from the excited state to the ground state is transferred from a donor (D) to an acceptor fluorophore (A). This process, in which the donor is initially excited, occurs if the acceptor molecule is in close proximity to the donor, and energy is transferred via dipole-dipole interactions.

For FRET to occur, several conditions need to be met. First, both donor and acceptor need to be within nanometre range, and FRET is generally only observed at DA distances of less than 10nm (Pietraszewska-Bogiel & Gadella 2011). Consequently, FRET microscopy is ideal for measuring interactions in cellular biology. Second, there must be sufficient overlap between donor emission and acceptor absorption. Third, the acceptor transition dipole moment must not be perpendicular to the electric field of the dipole field of the donor (Pietraszewska-Bogiel & Gadella 2011). The efficiency of the energy transfer in FRET (E) is directly dependent on the distance between the donor and acceptor (Förster 1948), and is expressed in the following equation:

$$E = 1/(1 + \left(\frac{R}{R_0}\right)^6$$

Equation 2 FRET efficiency

Where E = fraction of photons absorbed by donors whose energy is transferred to acceptors, R = distance between donor and acceptor, R_0 = Forster radius (distance at which energy transfer is at 50%).

The Förster radius (R_0) is dependent on the orientation of transition dipoles, spectral overlap between donor and acceptor, and other environmental factors as described by the following equation:

$$R_0 = [k^2 \times J(\lambda) \times n^{-4} \times Q]^{\frac{1}{6}} \times 9.7 \times 10^2$$

Equation 3 Förster radius

Where k^2 = relative orientation of the transition dipoles between D and A, $J(\lambda)$ is the spectral overlap between donor emission and acceptor absorption (overlap integral, cm^6mol^{-1}), n = refractive index of intervening medium, Q = fluorescence quantum yield of the donor.

2.2.5.2.2 Fluorescence Lifetime Imaging Microscopy (FLIM)

FRET measurements can be confounded by several limitations, including direct excitation of acceptor fluorophores at donor excitation wavelengths and cross talk between donor and acceptor emissions. Many of these issues can be avoided by the use of FLIM, where the fluorescence lifetime (τ) of the donor is determined, reflecting the time taken for the population of excited donor fluorophores to decay to 1/e of the original value. The greater the efficiency of FRET between the donor and acceptor, the shorter the fluorescence lifetime of the donor (Koushik & Vogel 2008).

The two most common current methods for FLIM are time-domain and frequency domain lifetime imaging. The former method, used in this work, relies on donor excitation with pulses of light shorter than the donor lifetime, in the order of picoseconds. Donor fluorescence emission decay is then measured on the nanosecond scale, and donor fluorescence lifetime (τ_D) calculated by measuring the exponential decay in intensity. This is derived by counting the number of photons, either in time bins using gated detection, or from time-correlated single photon counting (TCSPC), where repetitive pulsed excitation of the sample leads to the emission of a single photon per pulse, which is timed at detection, and a histogram of decays can be produced. Excitation by multiphoton microscopy uses excitation pulses of near infra-red light. This causes non-linear absorption in fluorophores, which has the

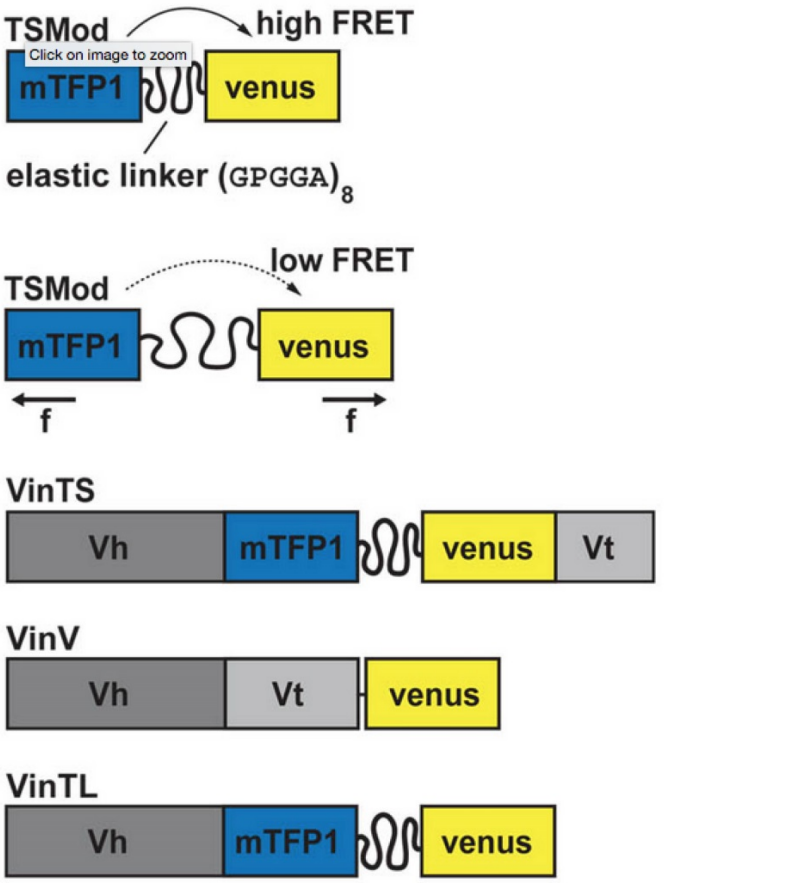
advantage of reducing excitation to a small area of the focal plane, reducing photobleaching.

2.2.5.2.3 Vinculin tension sensor (VinTS) FRET probes

Vinculin tension sensor and control probes were purchased from Addgene (plasmid 26019). The VinTS probe comprises a tension sensor module (TSMod) consisting of a 40-amino acid-long elastic domain linking a donor fluorophore (mTFP1) and an acceptor (venus) that FRET when in close proximity. The linker protein is formed from the spider silk protein flagelliform, the structure of which is composed of repetitive amino-acid motifs. These effectively act as ‘nanosprings’, making the structure suitable for measuring forces on the piconewton scale (Grashoff et al. 2010) (Figure 2-10).

The Vinculin construct was created by introducing TSMod cDNA into a chicken vinculin cassette, and the construct inserted into a pcDNA3.1 expression vector. The construct is such that the mTFP1 donor is associated with the vinculin head domain (Vh), followed by the flexible linker, and the venus acceptor associated with the tail domain (Vt). Therefore, tension across the vinculin protein would be expected to distend the linker, decreasing FRET efficiency between the two fluorophores. Controls included a construct devoid of a vinculin tail domain (tail-less/ VinTL – plasmid 26020), and one where the vinculin protein is intact, but associated to a venus fluorophore only (vinculin venus/VinV – plasmid 27300). The tension sensor module alone was also transfected into cells by the authors, and observed to localise throughout the cytoplasm (TSMod – plasmid 26021).

a


TSMod
high FRET
Click on image to zoom
mTFP1
venus
elastic linker (GPGGA)8
TSMod
low FRET
mTFP1
venus
f
f
VinTS
Vh
mTFP1
venus
Vt
VinV
Vh
Vt
venus
VinTL
Vh
mTFP1
venus

b

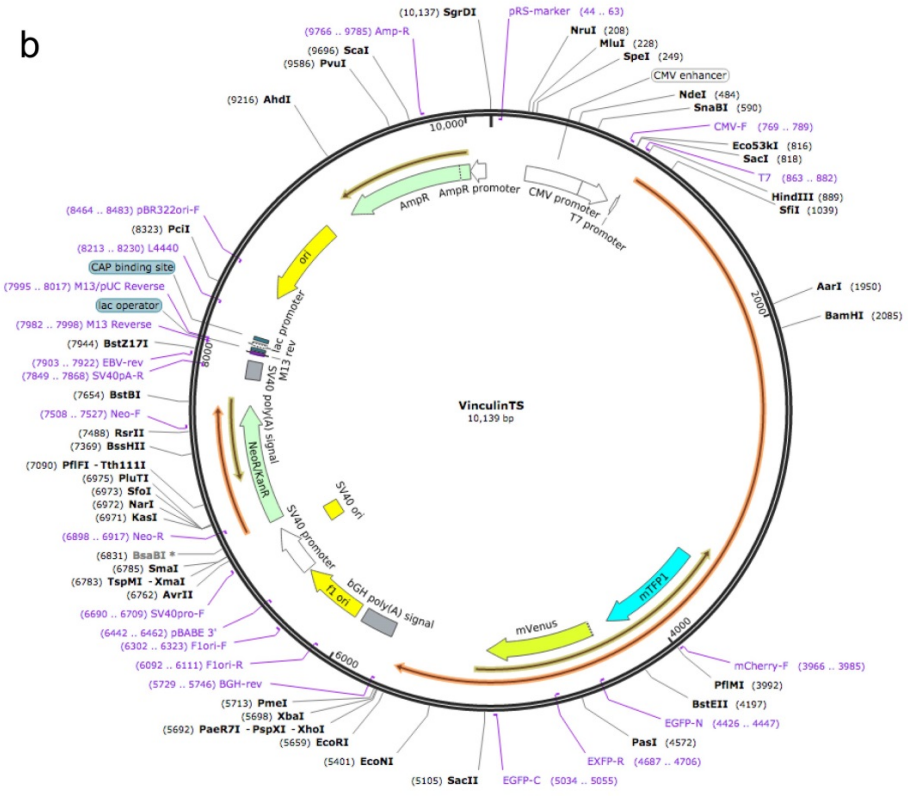

VinculinTS
10,139 bp
(10,137) SgrDI
pRS-marker (44 .. 63)
(9766 .. 9785) Amp-R
(9696) ScaI
(9586) PvuI
NruI (208)
MluI (228)
SpeI (249)
CMV enhancer
NdeI (484)
SnaBI (590)
(9216) AhdI
CMV-F (769 .. 789)
Eco53kI (816)
SacI (818)
T7 (863 .. 882)
HindIII (889)
SfiI (1039)
AmpR
AmpR promoter
CMV promoter
T7 promoter
(8464 .. 8483) pBR322ori-F
(8323) PciI
(8213 .. 8230) L4440
CAP binding site
(7995 .. 8017) M13/pUC Reverse
lac operator
(7982 .. 7998) M13 Reverse
(7944) BstZ17I
(7903 .. 7922) EBV-rev
(7849 .. 7868) SV40pA-R
(7654) BstBI
(7508 .. 7527) Neo-F
(7488) RsrII
(7369) BssHII
(7090) PflFI - Tth111I
(6975) PluTI
(6973) SfoI
(6972) NarI
(6971) KasI
(6898 .. 6917) Neo-R
(6831) BsaBI *
(6785) SmaI
(6783) TspMI - XmaI
(6762) AvrII
(6690 .. 6709) SV40pro-F
(6442 .. 6462) pBABE 3'
(6302 .. 6323) F1ori-F
(6092 .. 6111) F1ori-R
(5729 .. 5746) BGH-rev
(5713) PmeI
(5698) XbaI
(5692) PaeR7I - PspXI - XhoI
(5659) EcoRI
(5401) EcoNI
(5105) SacII
EGFP-C (5034 .. 5055)
EXFP-R (4687 .. 4706)
PasI (4572)
EGFP-N (4426 .. 4447)
BstEII (4197)
PflMI (3992)
mCherry-F (3966 .. 3985)
ori
lac promoter
M13 rev
SV40 poly(A) signal
NeoR/KanR
SV40 promoter
SV40 ori
f1 ori
bGH poly(A) signal
mVenus
mTFP1
2000
4000
6000
8000
10,000

Figure 2-10 Vinculin tension sensor (VinTS) constructs and plasmid map

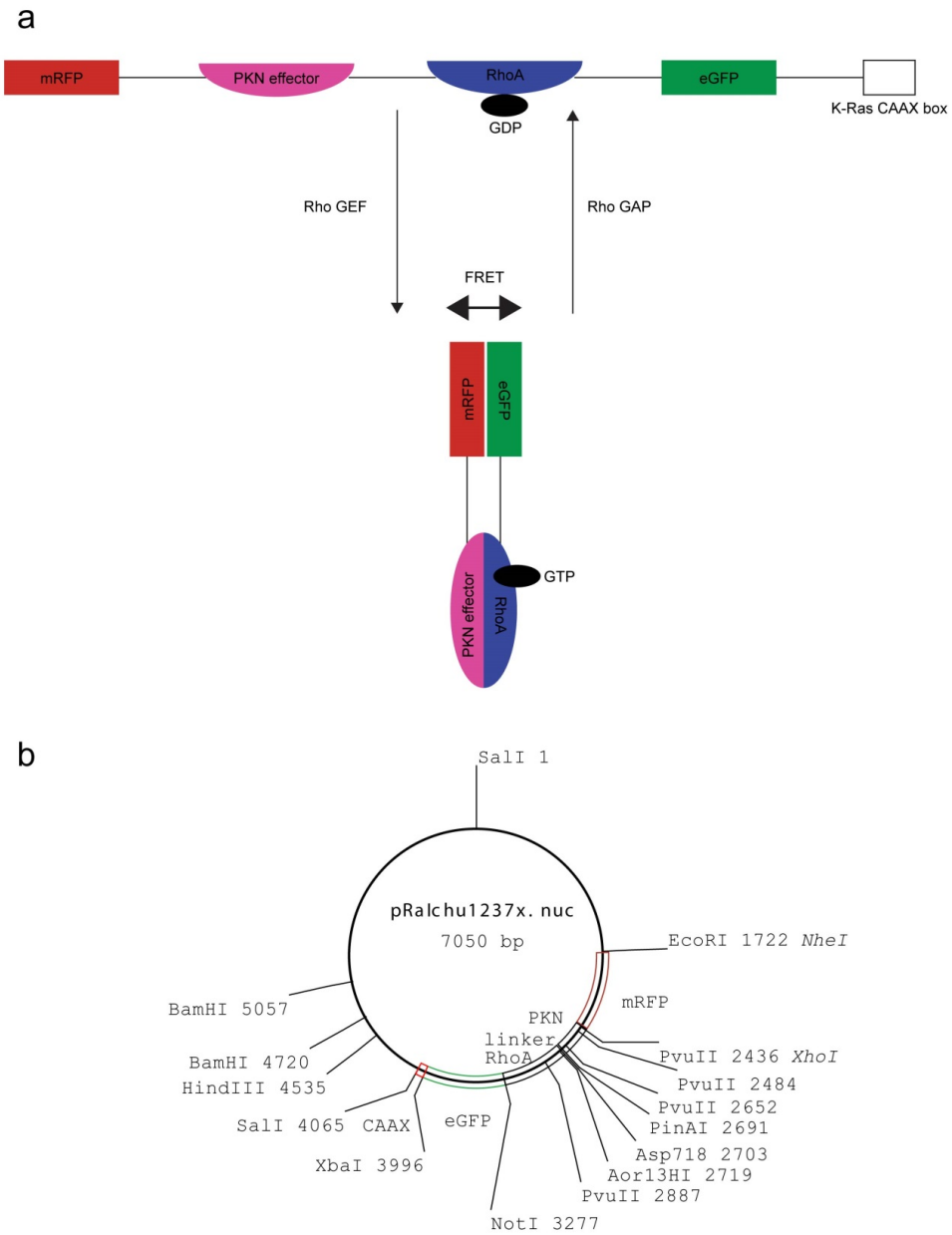
Panel A reprinted by permission from Nature Publishing Group: Nature (Grashoff et al. 2010), copyright (2010), shows the constructs: mTFP1 donor and venus acceptor are separated by a 40 amino acid-long flexible linker. Increasing force across the constructs separates the donor from the acceptor, decreasing FRET. Panel B shows the plasmid map containing the 708 base pair (bp) mTFP1 and 717 mVenus cassettes.

The authors found that in transfected cells, VinTS recruited to focal adhesions, and did not affect focal adhesion shape, size or f-actin association when compared with cells transfected with the venus-only construct, and that expression of vinculin in these cells was comparable to endogenous levels. Furthermore, expression of the construct did not affect vinculin activation status, and intermolecular FRET was negligible. Single-molecule fluorescence force spectroscopy was used to calibrate the sensor, and demonstrated that the sensor was sensitive with forces between 1-6pN, and that the average force in stationary focal adhesions was approximately 2.5pN.

2.2.5.2.4 Raichu RhoA GFP probes

Raichu RhoA probes were a gift from Professor Tony Ng, King's College London, and are a variant of the CFP-YFP RhoA probe reported previously (Makrogianneli et al. 2009), modified to express GFP-RFP FRET pairs (Heasman et al. 2010; Makrogianneli et al. 2009). The probe consists of a donor GFP domain associated with truncated RhoA, followed by RhoA-binding domain (RBD) of protein kinase-N (PKN). Intramolecular binding of GTP (active)-RhoA to the PKN effector changes the conformation of the probe, bringing the FRET pairs into closer proximity, and increasing FRET. In contrast, GDP-bound (inactive) RhoA holds the construct in an open position, diminishing FRET.

Raichu RhoA is anchored to the plasma membrane via the carboxy terminus region of k-Ras, and also cannot bind to RhoGDI (Guanine Nucleotide Dissociation Inhibitors), which maintain the GDP-bound form of RhoA in the cytosol. Raichu RhoA probes therefore monitor the activity of endogenous, and RhoGDI-unbound, RhoA at the plasma membrane, which has the advantage of reducing background signal from the cytosol. The probes consist of the Raichu RhoA probe itself (Figure 2-11), an inactive construct (T19N) where Asn was substituted for Thr^{19} of RhoA, therefore decreasing its affinity to guanine nucleotides, and a GFP-only construct.



Plasmid name: pRaichu1237x.nuc
Plasmid size: 7050 bp
Constructed by: H. Yoshizaki
Construction date: Sept. 2001
Comment&Reference: Modified 2006 by Konstantina Makgrogianneli
(King's College London)with modified RE sites italicised

Figure 2-11 pRaichu RhoA probe

Panel A shows the construct consisting of a donor GFP domain associated with truncated RhoA, followed by RhoA-binding domain (RBD) of PKN. Binding of GTP (active)-RhoA to the PKN effector changes the conformation of the probe to bring the FRET pairs into closer proximity, increasing FRET. GDP-bound (inactive) RhoA holds the construct in an open position, diminishing FRET. Panel B shows the plasmid map, with modified mRFP and eGFP domains.

2.2.5.2.5 Transfection of A549 cells with plasmid DNA

Cells at approximately 70% confluence were transfected with either the VinTS or Raichu FRET probes using lipofectamine reagent (Invitrogen). For each well of a 6-well Bioflex plate, 2.5µg DNA was complexed with opti-MEM medium (Life Technologies) and P3000/lipofectamine as described (Table 2-6). Cells were left to transfect for 48 hours then treated as described. Fixed cells were imaged on excised Bioflex membranes.

Component	Volume
Cells	0.25-1 x 10^6
Opti-MEM medium	125µl
Lipofectamine 3000 Reagent	3.75µl
DNA complex	
Opti-MEM medium	125µl
DNA	2.5ng
P3000 Reagent	5µl
Diluted DNA with P3000 reagent (125µl) added to lipofectamine reagent (125µl) and incubated for 10-15 minutes at room temperature	
250 µl added to well, and cells incubated for 28 hours at 37 °C	

Table 2-6 Protocol for lipofectamine-induced transfection of plasmid DNA into A549 cells

2.2.5.2.6 FLIM setup for Raichu and VinTS probes

Following transfection and treatment, cells were fixed in PFA (4%) for 10 minutes, membranes washed and cut as described for confocal imaging (2.2.5.1.3), immersed in Mowiol with DABCO (Sigma Aldrich) and placed onto slides with coverslip applied.

A Leica SP5 upright confocal microscope with a tunable infrared laser (Spectraphysics Mai Tai 690-1020) and Becker Hickl FLIM detector was used for the work in this thesis. A 63x 1.4 HCX PL APO oil objective was used. Measurements on fixed samples were performed at room temperature.

The two photon Mai Tai laser delivers under 100 femtosecond pulses at 80 ±1 MHz. Excitation for both probes was set at 890nm and data were collected at 500 ± 40nm for the VinTS probes, and 480 ± 20 nm for the Raichu probes, through a band-pass filter. Laser power, gain and offset were adjusted to give average photon counting rates of 10^4-10^5 photons/second. Acquisition times of 240s for VinTS probes, and 300s for Raichu probes, achieved photon statistics sufficient for fitting without observable photobleaching.

Instrument response was measured by imaging reflection scattering from urea crystals mounted on a coverslip, and used in data analysis by iterative re-convolution.

2.2.5.2.7 FLIM analysis

FLIM data acquired using Becker Hickl software were saved and processed using Time Resolved Analysis software (TRI2) (developed by Paul

Barber, University of Oxford, (Barber et al. 2009). Data for both probes were fitted to a Marquardt mono-exponential decay as described by the following equation:

$$f(t) = Z + A \exp\left(-\frac{t}{\tau}\right)$$

Equation 4 Marquardt mono-exponential decay model

Fit function (f), t = time variable, Z = background, A = peak strength of the exponential and τ = lifetime.

Pseudocolour images are generated showing the lifetime (tau) for each pixel of the original image, and histograms generated indicating the number of pixels with each lifetime. For VinTS probes, areas of focal adhesions were masked, and pre-processing applied such that 10^3 signal counts were obtained in all areas within the mask. For Raichu probes, masks were applied to the whole cell.

FRET efficiency was derived from lifetimes using the following equation

$$E = 1 - \frac{\tau_{FRET}}{\tau_D}$$

Equation 5 FRET efficiency

(FRET efficiency) is determined by the lifetime of the donor τ_D and the donor lifetime in the presence of the acceptor τ_{FRET}.

For the VinTS probe, I could not calculate FRET efficiency given that we did not have available an uncomplexed mTFP probe to measure donor

lifetimes. Although the average fluorescence lifetime of mTFP1 has previously been demonstrated to be 2.98s (Grashoff et al. 2010), this could not work for our system where all other parameters are likely to be different. For the Raichu probes, donor GFP lifetimes were calculated as 2.11ns and FRET efficiency calculated correspondingly.

2.2.6 Other antibody-based assays

2.2.6.1 Enzyme-linked Immunosorbent Assay (ELISA)

2.2.6.1.1 Working Principle

Enzyme-linked immunosorbent assay (ELISA) is a technique whereby antibodies are used to detect and quantify solid-phase bound proteins or proteins in solution. Two different types of ELISA are used commonly, including sandwich ELISAs, which detect proteins in solution by the use of an immobilised capture antibody, or a technique where the target protein is immobilised and captured by the antibody in solution (Figure 2-12).

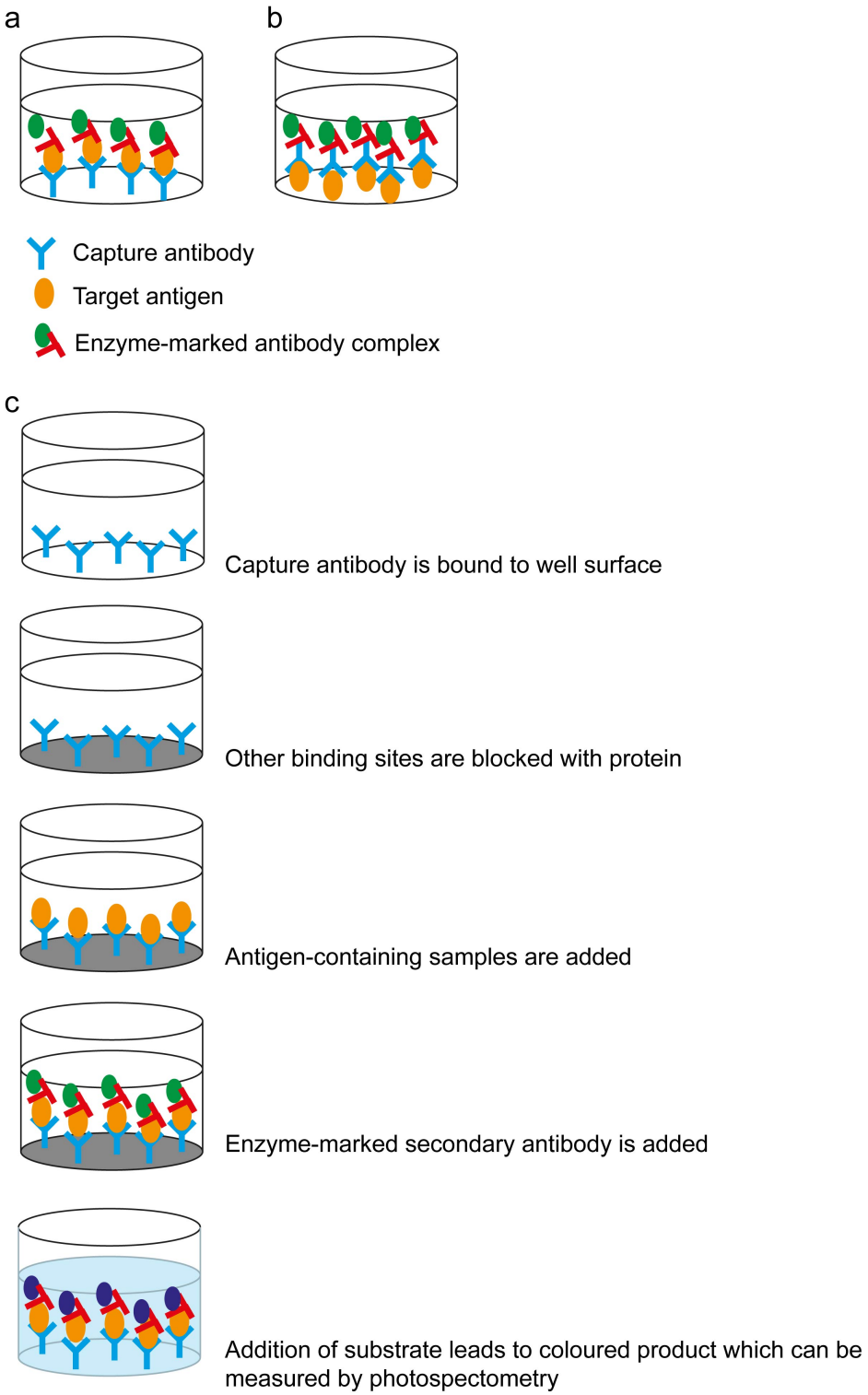


Figure 2-12 Enzyme-linked immunosorbent assay (ELISA) working principle

Panel A shows the basis for a sandwich ELISA and B shows target protein immobilisation and capture in solution. Panel C shows the basic steps of a sandwich ELISA.

2.2.6.1.2 Duoset ELISA

Sandwich ELISAs for the detection of human IL-8 on A549 cells were performed using a standard protocol provided by the manufacturer (R&D Systems, UK).

Wash buffer	Block buffer	Reagent diluent	Substrate solution	Stop solution
0.05% Tween 20 in PBS	1% BSA in PBS (0.2µm filtered and pH 7.2-7.4)	Tris-buffered saline (20mM Trizma base, 150mM NaCl), 0.1% BSA, 0.05% Tween-20	Reagents A and B	2N H_2SO_4

Table 2-7 Duoset ELISA reagents

Wells were coated with 4µg/ml capture antibody (100µl) diluted in sterile, filtered PBS, and the plate was sealed and incubated at room temperature overnight. The following day, wells were aspirated and washed 3 times with wash buffer (Table 2-7), and plates were dried on a paper towel. Wells were blocked with block buffer (300µl) for 2 hours. A subsequent wash step was performed, and 100µl of either standard or sample (diluted in reagent buffer) was added to appropriate wells, and the plate sealed and incubated for a further 2 hours. Following a further wash step, 20ng/ml biotinylated detection antibody (100µl) was added to wells, and the plate sealed and incubated at room temperature for a further 2 hours. Following a subsequent wash step, streptavidin horseradish peroxidase (HRP) (100µl) was added to each well, and the plate sealed and incubated for 20 minutes. A final wash step was

performed, substrate solution (100µl) was added, and the plate incubated for 20 minutes at room temperature. Stop solution (50µl) was added to each well to end the reaction, and the plate absorbance was read using a plate reader (TECAN) at 450nm with a correction of 570nm.

2.2.6.2 Electrochemiluminescence (MSD)

2.2.6.2.1 Working Principle

Mesoscale Discovery multiplex plate technology allows for the detection of multiple proteins from the same biological sample, and at concentrations far below those seen with standard ELISA techniques. The microplate consists of wells, each with micro-spots containing capture antibody for specific proteins of interest. Sample is added to the wells, and the technique follows that of a standard ELISA. In this case, the detection antibody is conjugated to a Sulfo-Tag™ group, and following addition of READ buffer, the plate reader pulses a small electric current across each micro-spot. By electrochemiluminescence, voltage applied to the plate electrodes causes the captured labels to emit light in proportion to the quantity of Sulfo-tagged antibody bound to the protein of interest in each well. The luminous intensity is then measured by the plate reader instrument (Figure 2-13).

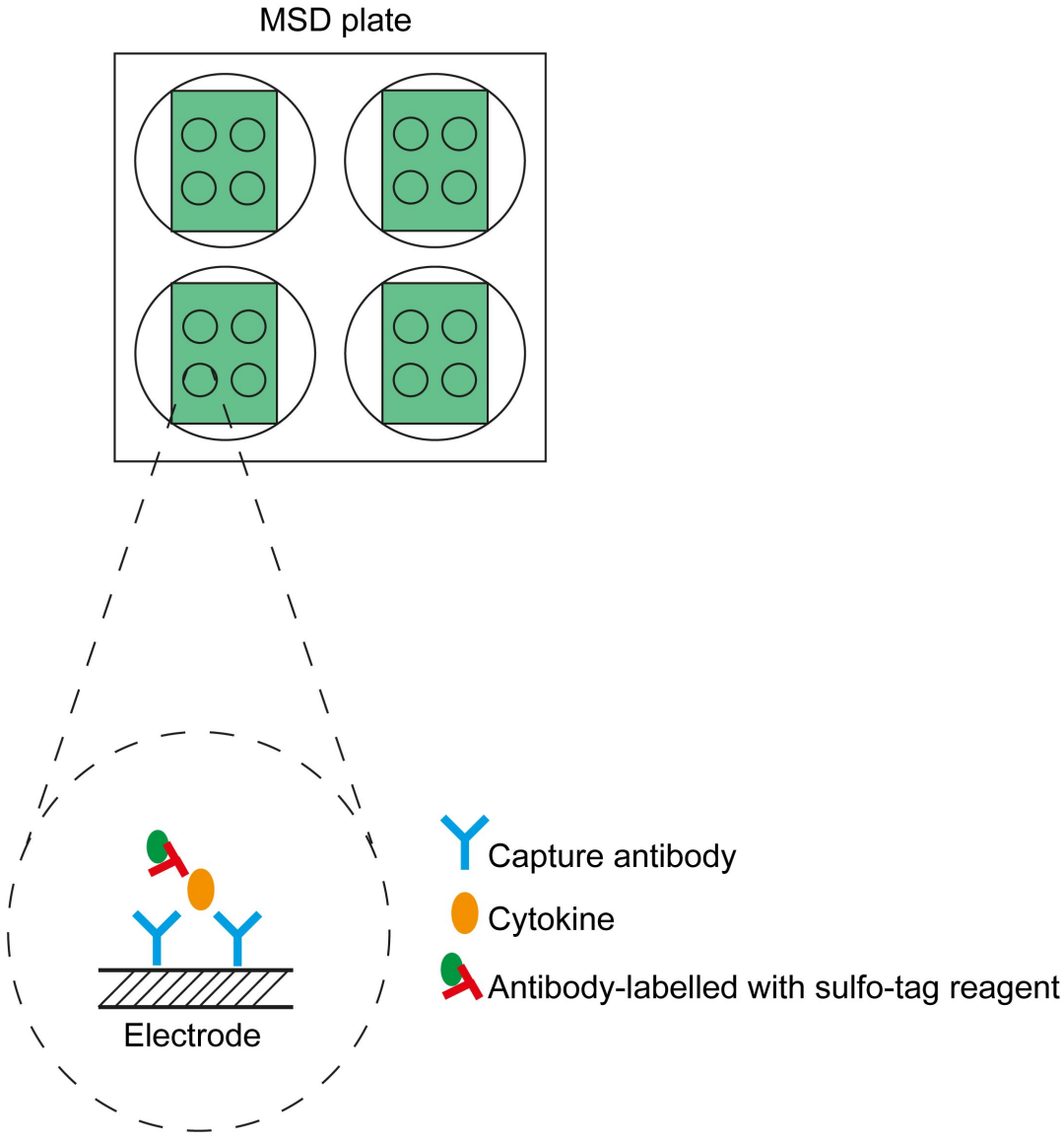


Figure 2-13 Mesoscale Discovery (MSD) electrochemiluminescence

Samples are incubated in the multi-spot plate, each spot containing a capture antibody for a specific cytokine. Quantity of cytokine is measured using cytokine-specific detection antibody labelled with Sulfo-tag™ reagent.

2.2.6.2.2 MSD protocol

Supernatant following treatment of either murine or human PCLS were analysed for KC/GRO-α or IL-8 respectively using the designated V-PLEX MSD kit. Reagents were prepared as per manufacturers' instructions, and

calibrators (standards) diluted as required. 50µl of the sample (diluted 2-fold in diluent 2) or calibrator standard was added to respective wells, and the plate sealed and incubated at room temperature for 2 hours with shaking. Wells were then washed 3 times with wash buffer (PBS + 0.05% Tween 20), and detection antibody (25µl) added to each well. The plate was sealed and incubated for a further 2 hours with shaking. Following a final wash step, 2x Read buffer-T (150µl) was added to each well, and the plate read on the SECTOR ^{TM} reader. Standard curves were fitted using the MSD Workbench software (version 4.0) and samples fitted to the curve.

2.2.6.3 Western Blotting

2.2.6.3.1 Working Principle

Western or immunoblotting allows for the identification and quantification of proteins from cell or tissue lysates. The technique relies on fractionation of the protein mixture by gel electrophoresis, giving a breakdown of protein components by molecular weight. These fractionated proteins are transferred to either a nitrocellulose or PVDF membrane, which is incubated with a blocking protein to shield non-specific binding sites. The membrane is then incubated in a primary antibody, which captures the target protein. Wash steps remove unbound antibody, after which the membrane is incubated with HRP-conjugated secondary antibody to bind the primary antibody-immobilised protein complex. Following a subsequent wash step, addition of a specific chemiluminescent substrate generates a light signal, the intensity of which is dependent on the quantity of HRP-primary antibody-target protein complex (Figure 2-14).

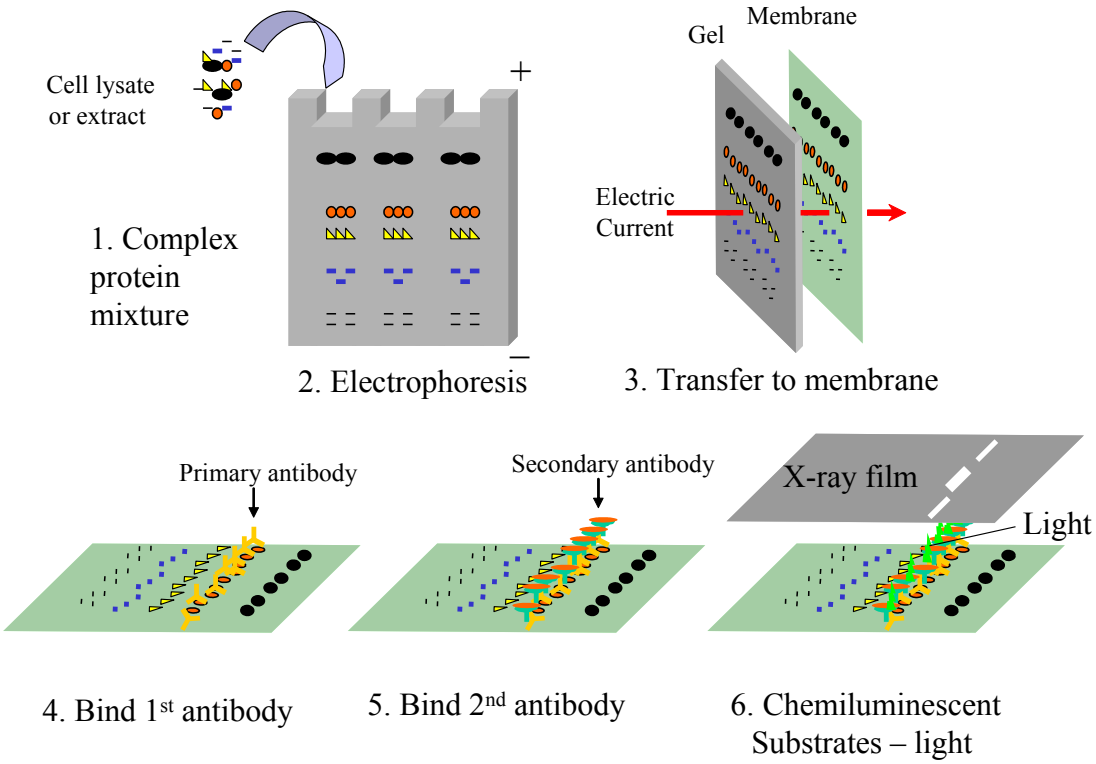


Figure 2-14 Western Blot general principle

Courtesy of L.Pinhu (Pinhu 2008) and A. Proudfoot (Proudfoot 2014)

2.2.6.3.2 Western Blot protocol

Following treatment, A549 cells were washed once in ice-cold PBS, then lysed in cell lysis buffer (Cell Signalling) supplemented with complete EDTA-free protease inhibitors (Roche), PhosSTOP phosphatase inhibitors (Roche), and PMSF (1µ, Sigma-Aldrich) to inhibit degradation and dephosphorylation of proteins, and scraped from wells. Lysed cells were collected into microcentrifuge tubes, and kept on ice for 30 minutes, with agitation every 10 minutes. Samples were then centrifuged (14,000g for 10 min) at 4 °C. Pellets were discarded, and the supernatant (containing protein) was placed in microcentrifuge tubes, and stored on ice or at -80 °C.

Protein concentration was determined using the Pierce bicinchoninic acid (BCA) assay (Thermo Scientific). This method relies on the reduction of Cu^{+2} to Cu^{+1} by protein in an alkaline medium. The purple product formed by chelation of bicinchoninic acid by Cu^{+1} is then measured by calometry. Diluted sample (25µl) or BSA standard (ranging in concentration from 2000 to 0 µg/ml) were added to individual wells of a 96-well plate (Costar). Supplied BCA working reagent (200µl) was then added to each well, and the plate agitated for 30 seconds, followed by incubation at 37°C for 30 minutes. The plate was then cooled, and read using a spectrophotometer at 562nm. Protein concentration was calculated by comparing absorbance of samples to a linear standard curve of the absorbance of known BSA standards.

10-20 µg of sample protein were diluted in ddH_2O and NuPage 4x LDS Sample Buffer (4µl) (with 2.5% β-mercaptoethanol for reducing samples, Sigma-Aldrich) to a total volume of 16µl. For denaturing conditions, samples were heated at 95 °C for 5 minutes on a heat block. Protein samples were loaded into wells of a pre-cast Bis-Tris gel (4-12 %, Invitrogen) and a molecular weight marker added to one well to monitor progress of electrophoresis. The samples were then resolved by gel electrophoresis in running buffer (125V), separating proteins by molecular weight. Protein was transferred to a PVDF membrane using wet electro-transfer in transfer buffer (30 minutes at 100V). To block non-specific protein binding on the PVDF membrane, blots were incubated with either BSA (5 %, Sigma-Aldrich) or non-fat dried milk powder (Marvel) in Tris-buffered saline (Table 2-8) containing Tween 20 (0.1%) for 1 hour at room temperature.

Membranes were incubated with primary antibody overnight at 4°C in blocking solution with gentle agitation at the appropriate concentration (Table 2-3). Blots were washed three times for 15 minutes each, to remove unbound antibody, using TBS-T with agitation. Blots were then incubated with an appropriate HRP conjugated secondary antibody (Table 2-4) diluted in blocking solution for 1 hour at room temperature, followed by a final wash step.

Bound antibodies were visualised by incubation with ECL western blot substrate (1ml, Thermo Scientific) for 5 min in the dark. This reaction relies on the catalysis by HRP of the oxidation of luminol into a light-emitting compound. Blots were exposed to Amersham Hyperfilm ECL (GE Healthcare) in the dark to visualise protein bands, and densitometry calculated using Fiji software.

Transfer buffer	Tris-buffered saline
25mM Trizma base, 192mM glycine, 20% methanol in ddH_2O	20 mM Trizma base, 137 mM NaCl (pH7.4)

Table 2-8 Western blot reagents

2.2.7 Statistical analysis

2.2.7.1 Data processing

Data were collated in excel spreadsheets and analysed using Prism software v6.0 (GraphPad software, CA, USA).

2.2.7.2 Data presentation and analysis

Unless otherwise stated, data assumed to be non-parametric were presented as the median and interquartile range (IQR). Non-parametric analysis was used (Kruskal Wallis, Mann Whitney, Wilcoxon-paired) as normal distribution of data could not be assessed due to smaller sample sizes. Normally distributed (parametric) data were presented as the mean and standard error of the mean (SEM). P-values were adjusted for multiple comparisons and a p-value of <0.05 was considered significant.

3 Chapter 3: Cyclic Mechanical Strain (CMS)-induced cytoskeletal remodelling, RhoGTPase signalling and force transduction in alveolar epithelial cells

3.1 Introduction

The cellular actin cytoskeleton, as the major load-bearing apparatus of the cell, is a key regulator of mechanotrandsduction (Burridge & Guilluy 2016). Application of external force induced remodelling of the actin architecture, with re-orientation of stress fibres and focal adhesions in both endothelial cells (J. H.-C. Wang et al. 2001; Tzima 2006) and fibroblasts (Wang et al. 2004). In epithelial cells, CMS promoted rapid actin remodelling (DiPaolo et al. 2010) dependent on the frequency of applied strain. However, the actin cytoskeleton does not passively remodel in response to force. Stretching of individual actin fibres promoted downstream signalling (Hayakawa et al. 2008), In fibroblasts, CMS-induced ERK activation was localised to actin stress fibres in a strain-dependent manner (Hirata et al. 2015), suggesting that the cytoskeleton acts as a platform for CMS-induced signalling.

CMS-induced actin remodelling is highly dependent on Rho-GTPases, and RhoA signalling in particular. RhoA activation, which is a critical mediator of mechanotransduction in spreading cells (Plotnikov et al. 2012), was increased in rats subjected to high tidal volume ventilation (Desai et al. 2007) and regulated stretch-induced downstream signalling in cardiomyocytes (Torsoni et al. 2005). Furthermore, CMS-induced β1-integrin activation may directly promote activation of a Rho-GEF, GEF-H1 (Guilluy et al. 2011), which formed a stretch-induced complex with paxillin and ERK 1/2 to promote

activation of RhoA and trigger downstream myosin II-mediated actomyosin contraction (Gawlak et al. 2014).

These cytoskeletal and Rho-GTPase responses to CMS affect the mechanical properties of cells. RhoA activity is associated with increases in the stiffness of alveolar epithelial cells (Wilhelm et al. 2014). Baseline stiffness tuned the sensitivity of cells to externally-applied force (Cirka et al. 2016), suggesting that RhoA-mediated alterations in cytoskeletal dynamics may affect the susceptibility of cells to stretch-induced injury. Indeed, cellular responses to CMS are comprised of both softening (Trepat et al. 2007) and reinforcement (Krishnan et al. 2009; Colombelli et al. 2009) of the cytoskeleton, with the former being independent of RhoA signalling (Chen et al. 2010).

However, there are few consistent data to demonstrate CMS-induced cytoskeletal remodelling and RhoA signalling in alveolar epithelial cells (DiPaolo & Margulies 2012), and particularly in response to pathological stretch. The work in this chapter is based on the hypothesis that CMS-induced cytokine release in alveolar epithelial cells is dependent on cytoskeletal remodelling and RhoA signalling. Specifically, the aims of the work in this chapter are:

a. To determine whether CMS-induced cytokine release in alveolar epithelial cells is associated with cytoskeletal and focal adhesion remodelling

b. To investigate the association between CMS-induced cytoskeletal remodelling and changes in traction forces across focal adhesions in these cells
c. To investigate the role of RhoA-ROCK signalling in CMS-induced mechanotransduction in these cells.

Cellular integrins bind to ligands in the extracellular matrix (ECM), and are linked to the actin cytoskeleton through focal adhesion protein complexes. These are composed of a vast array of proteins, including focal adhesion kinase (FAK), vinculin (vinc) and talin. Inside out transmission of force from actomyosin contraction exerts traction on the ECM, allowing cells to become motile (Figure A). The application of strain on the ECM triggers β1-integrin-mediated activation of RhoGEFs, leading to activation of RhoA and Rho-associated protein kinase (ROCK). ROCK activates non-muscle myosin II (NMII), affecting actin cytoskeletal tension, and promoting further conformational changes in mechanosensitive and focal adhesion proteins, thereby affecting cell matrix adhesion and downstream signalling leading to cytokine generation. ROCK can be inhibited by Y27632, and NMII by blebbistatin (Figure B).

3.2 Specific methods

3.2.1 Cytoskeletal gene regulation following CMS

A549 cells seeded on collagen I-coated BioFlex™ 6-well plates were exposed to CMS for 2 hours at 0.33Hz, and cells immediately lysed and processed for RT-PCR by the cytoskeleton array PCR assay as described (2.2.3.3.3).

3.2.2 ROCK and myosin II inhibition, and analysis of CMS-induced cytokine generation

A549 cells seeded on collagen I-coated BioFlex™ 6-well plates were treated with relevant inhibitors, exposed to CMS for 2 hours at 0.33Hz, and supernatant collected at 24 hours for assessment of cytokine release as described (2.2.6.1.2). For inhibition of ROCK, myosin II and actin polymerisation, cells were incubated with either: Y27632 (10μM, 1 hour); Blebbistatin (20μM, 30 minutes); or cytochalasin D (0.5μM, 30 minutes) respectively prior to CMS. For LPA–induced RhoA agonism, cells were incubated for 30 minutes prior to CMS with lypophosphatidic acid (LPA) (10μM). For assessment of chemical-induced cytokine release, cells were treated with TNF-α (10ng/ml) for 24 hours prior to sampling of supernatant. Cell viability was determined as described (2.2.1.2).

3.2.3 Immunofluorescence for cytoskeletal and focal adhesion remodelling after CMS

Cells were subjected to CMS for 0, 10, 30 or 60 minutes, fixed, stained and imaged by confocal microscopy as described (2.2.5.1.3). Antibodies for paxillin (rabbit 1:100) and PMLC2 (rabbit 1:50) (Table 2-3) and stains for f-actin (phalloidin 1:50) and nuclei (DAPI 500mM) (2.2.5.1.3) were used. Fixed and stained cells were mounted in Mowiol plus DABCO anti-fade. Areas of cells and cell-free area calculations were performed using Image J software, and the latter with a macro developed in-house. Corrected total cell fluorescent measurements were performed using Image J software by taking the integrated density of selected cells and subtracting the area of a background selection multiplied by its mean fluorescence as described previously (McCloy et al. 2014).

3.2.4 Analysis of CMS-induced FAK phosphorylation

Cells subjected to CMS as above were lysed at their respective time points and protein levels calculated by BCA protein assay as described (2.2.6.3.2). Western Blot under reducing and denaturing conditions was performed using rabbit anti-pFAK Y397 (1:1000), total FAK (1:1000) or GAPDH (1:20,000) (Table 2-3).

3.2.5 Measurement of CMS-induced cell traction forces and RhoA activity

Cells were transfected with the VinTS FRET tension sensor DNA (Grashoff et al. 2010) or the Raichu RhoA activity probe (Heasman et al. 2010) using lipofectamine reagent (Table 2-6), fixed following either 0 or 1 minute CMS, and mounted as described (2.2.5.1.3). FLIM microscopy was performed using a multiphoton upright microscope (Leica SP5) with a two photon Mai Tai laser (690-1040nm) (Newport spectra-physics), and Becker Hickl FLIM photon detector as described in (2.2.5.2.6).

3.3 Results

3.3.1 CMS-induced cytoskeletal remodelling

To examine the effect of CMS on F-actin cytoskeletal remodelling, cells were subjected to CMS for 0 (static), 10, 30 or 60 minutes, fixed, stained with phalloidin and imaged by confocal immunofluorescence microscopy. At baseline, cells demonstrated rhomboid-type morphology, with random orientation of stress fibres. By 10 minutes CMS, cell-cell attachment diminished as measured by an increase in cell-free area by approximately 12%. By 60 minutes CMS, cell-free area had significantly increased to 32% of the total area. The size of individual cells also decreased significantly with increasing duration of CMS. Stress fibres adopted more co-ordinated alignment after 10 and 30 minutes CMS. By 60 minutes CMS, phalloidin staining was only visible at the periphery of cells (Figure 3-1).

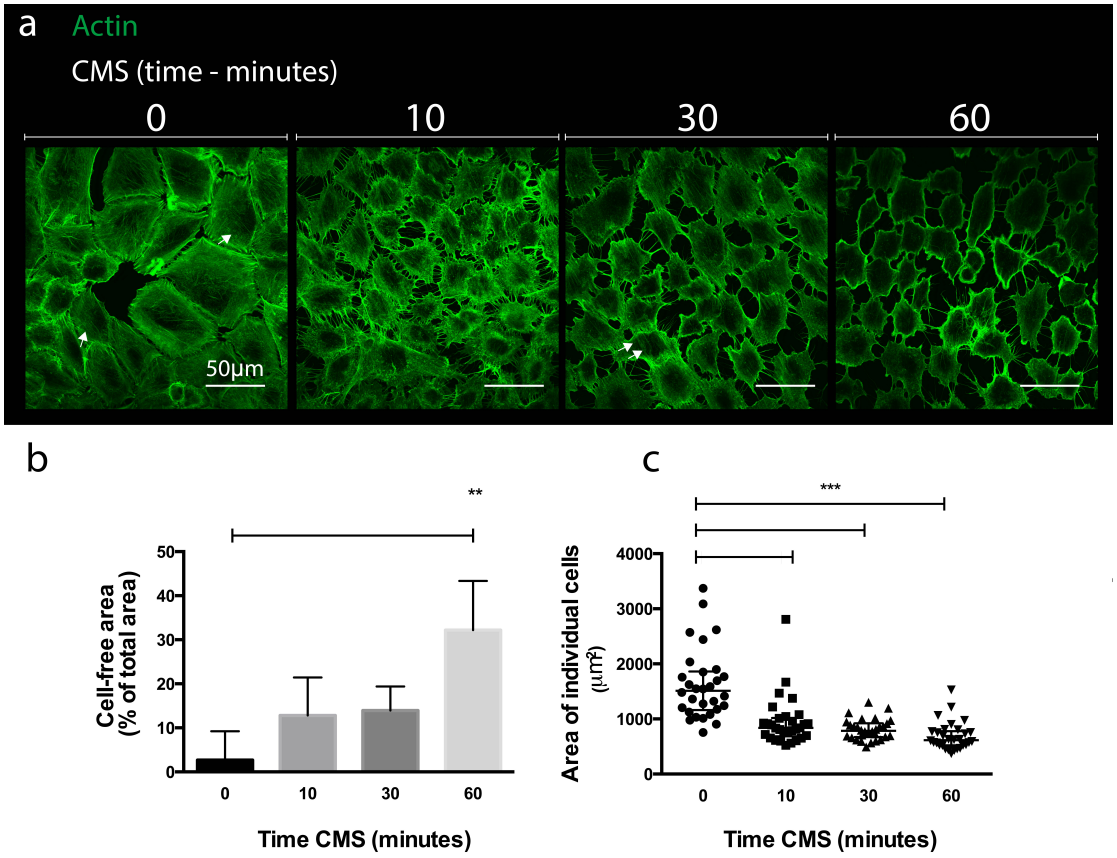


Figure 3-1 Effect of Cyclic Mechanical Strain (CMS) on cytoskeletal architecture

A549 cells were subjected to 30% equibiaxial CMS for 0 to 60 minutes, fixed and the actin cytoskeleton stained with phalloidin for confocal immunofluorescence microscopy. Panel A shows phalloidin-actin staining over a time course of CMS. Panel B shows the cell-free area at each respective time point and C shows the area in μm^2 of individual cells. Scale bar represents 50µm. Arrows indicate actomyosin stress fibres. Data are for two fields per time point from three individual experiments, and images representative of those from all experiments. Area of individual cells calculated from maximum intensity projection images of 5 cells per field of view. Data are presented as the median ± IQR analysed by Kruskall-Wallis test, **p<0.01, ***p<0.001

3.3.2 CMS-induced focal adhesion remodelling

At baseline, paxillin-stained focal adhesions could be seen at the ends of stress fibres, at the periphery of cells. Following 10 and 30 minutes CMS, numerous focal adhesions could be seen capping small stress fibres at the periphery and throughout the interior of cells. By 60 minutes CMS, stress

fibres could not be seen within the cell, and focal adhesions were less elongated and predominantly at the cell periphery (Figure 3-2).

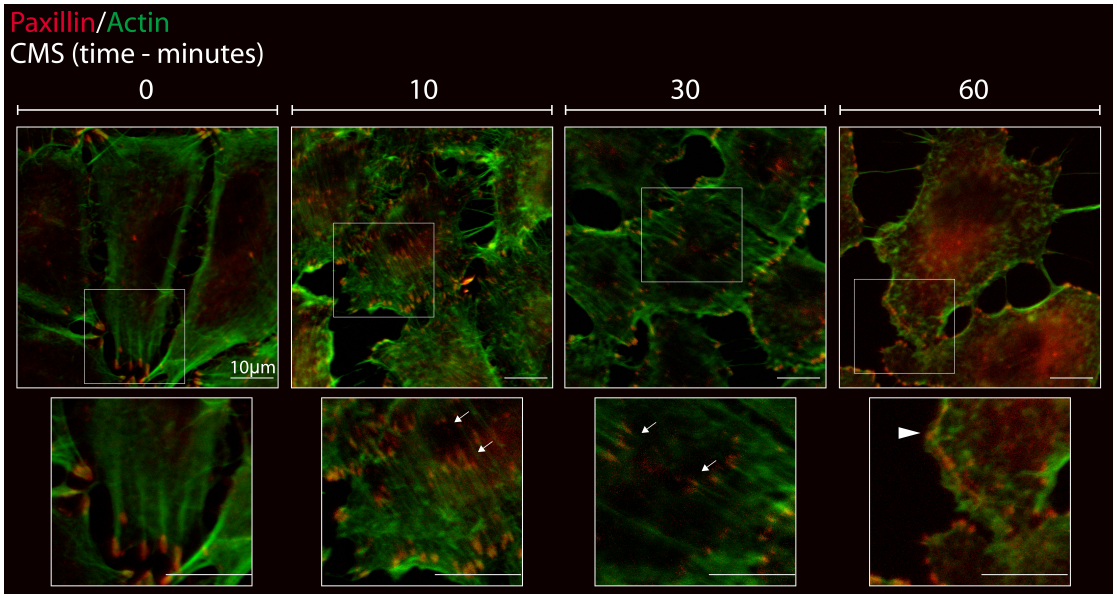


Figure 3-2 Cyclic Mechanical Strain (CMS)-induced focal adhesion remodelling

A549 cells were subjected to 30% equibiaxial CMS for 0 to 60 minutes and fixed. The actin cytoskeleton was stained with phalloidin (green), and focal adhesions with paxillin (red) for confocal immunofluorescence microscopy. Arrows show focal adhesions capping small stress fibres present throughout the cell. Arrowhead shows small focal adhesions at the peripheries of the cell following 60 minutes CMS. Scale bar represents 10µm. Images representative of three individual experiments.

3.3.3 The effect of ROCK inhibition on CMS-induced cytoskeletal and focal adhesion remodelling

Whereas application of CMS to A549 cells induced both cytoskeletal remodelling and focal adhesion redistribution, cells treated with Y27632 did not demonstrate similar CMS-induced reorganisation. Under baseline conditions, cells were larger than their untreated controls and did not decrease in size with CMS as demonstrated in untreated cells. There were no visible stress fibres either at baseline or during CMS, and no correlation

between small paxillin-stained focal adhesions, and phalloidin-stained F-actin (Figure 3-3).

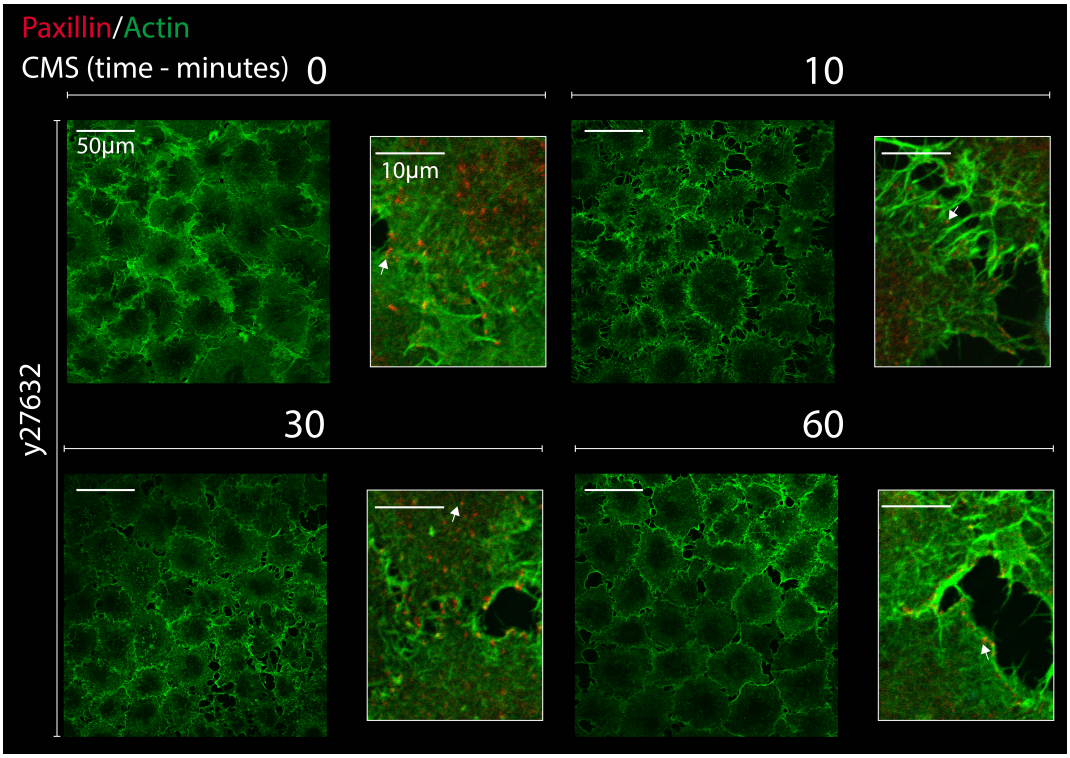


Figure 3-3 Effect of Rho-associated protein kinase (ROCK) inhibition on CMS-induced cytoskeletal and focal adhesion remodelling

A549 cells were treated with Y27632 (10μM) for 1 hour, subjected to 30% equibiaxial CMS for 0 to 60 minutes, then fixed. The actin cytoskeleton was stained with phalloidin (green), and focal adhesions with paxillin (red) for confocal immunofluorescence microscopy. Arrows show small focal adhesions dissociated from any organised actin structure. Scale bar represents 50 and 10μm as indicated.

3.3.4 The effect of ROCK inhibition on CMS-induced IL-8 release

Inhibition of ROCK by Y27632 (10uM for 1 hr) led to a significant reduction in CMS-induced IL-8 release in A549 cells, and to a level comparable with un-stretched cells, when compared to the untreated group (Figure 3-4 – a). Application of Y27632 did not affect cell viability as assessed by MTT assay at 24 hours following CMS (Figure 3-4 – b). In order to test

whether Y27632-induced abrogation of IL-8 release was specific to mechanical stimulation, untreated or Y27632-treated cells were exposed to TNF-α (10ng/ml). These experiments demonstrated that IL-8 generation was at a level comparable with untreated cells (Figure 3-4 - c).

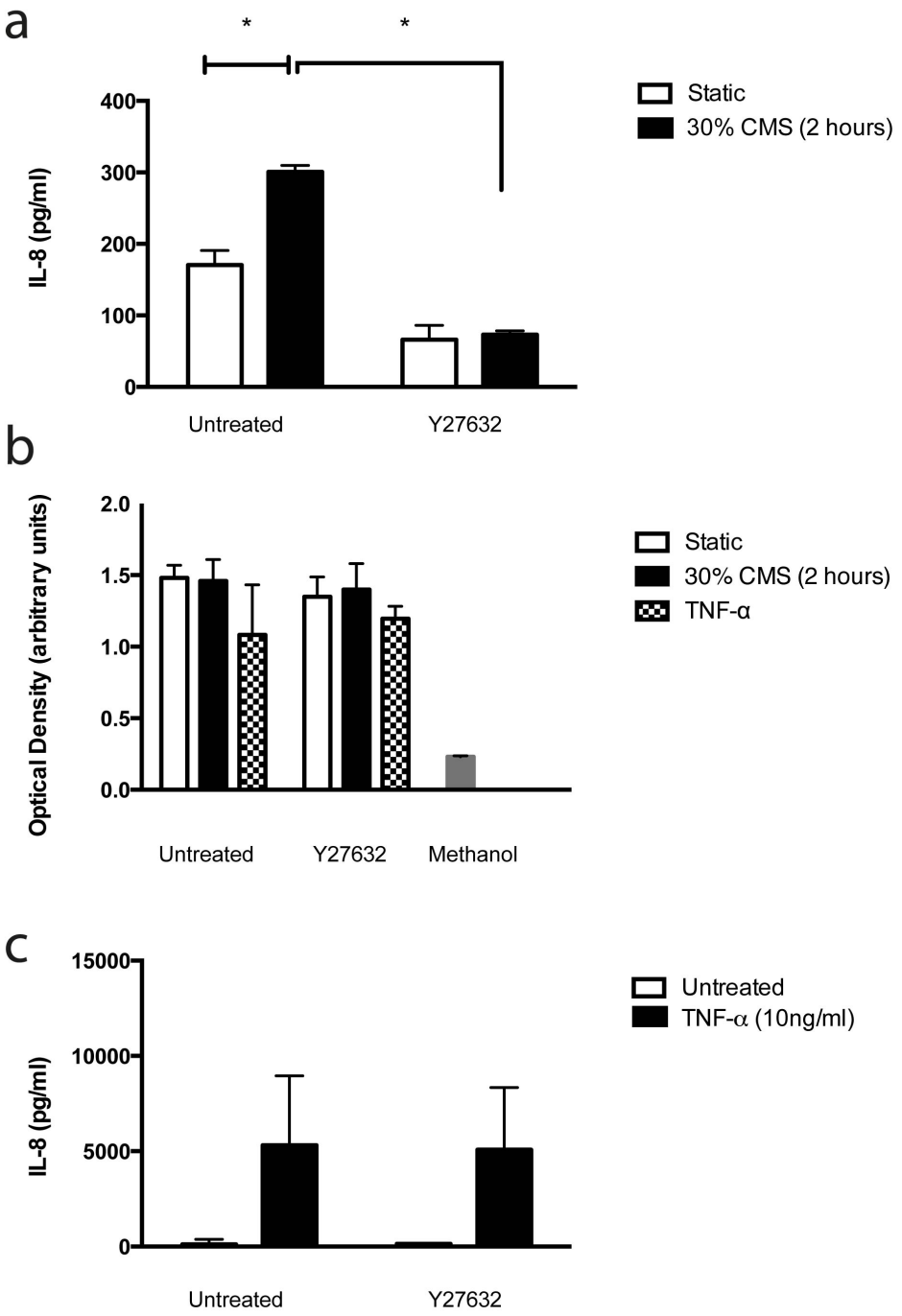


Figure 3-4 The effect of ROCK inhibition on CMS-induced cytokine release

A549 cells were either untreated or Y27632 (10μM) was applied for one hour. CMS was applied equibiaxially at 30% elongation for 2 hours. Panel A shows IL-8 generation as sampled from cell supernatant at 24 hours following CMS. Panel B shows cell viability at 24 hours following CMS as assessed by MTT assay. Panel C shows IL-8 release in respective treatments at 24 hours following TNF-α treatment Data are for n=3 from three individual experiments for panel A, and n=4 from two experiments for panels B and C, and are presented as median ± IQR. Data analysis by Mann Whitney test, *$p<0.05$.

3.3.5 The effect of LPA and cytochalasin D on CMS-induced IL-8 release

Treatment with the RhoA agonist lypophosphatidic acid (LPA) (10μM), or the inhibitor of actin polymerisation, cytochalasin D, (0.5μM), for 30 minutes had expected morphological effects on actin cytoskeletal architecture as demonstrated by phalloidin F-actin staining. Increased density of actin-fibres was observed with LPA treatment, whereas cytochalasin-D reduced cellular F-actin content, leaving no visible stress fibre architecture (Figure 3-5 - a). Treatment with LPA did not lead to statistically significant increases in CMS-induced IL-8 release. Similarly, cytochalasin D did not abrogate nor lead to a statistically significant increase in CMS-induced IL-8 release (Figure 3-5 - b).

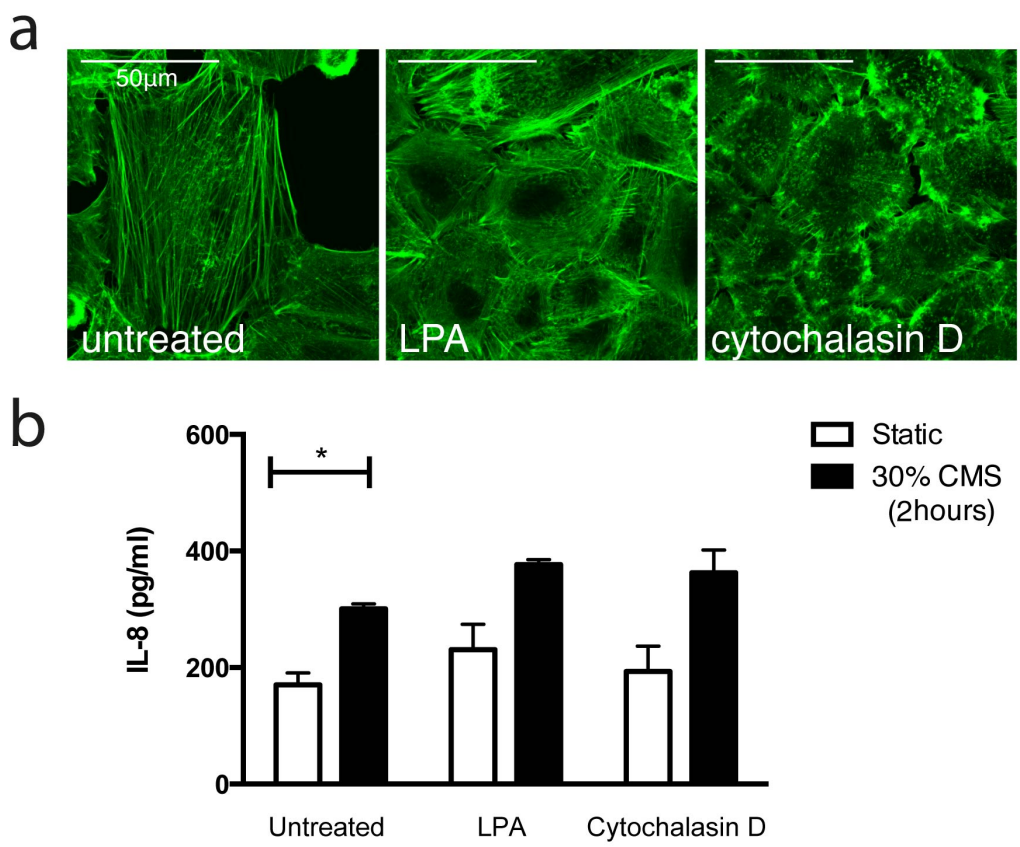


Figure 3-5 LPA treatment does not increase CMS-induced IL-8 release

A549 cells were either untreated, lypophosphatidic acid (10µM) or cytochalasin D (0.5µM) applied for 30 minutes. CMS was applied equibiaxially at 30% elongation for 2 hours. Panel A shows phalloidin staining of the f-actin cytoskeleton in respective treatments at baseline (static) conditions. Panel B shows IL-8 generation as sampled from cell supernatant at 24 hours following CMS. Data are for three individual experiments, and are presented as median ± IQR. Data analysis by Mann Whitney test, *p<0.05

3.3.6 The effect of CMS and ROCK inhibition on FAK phosphorylation

To determine the effect of CMS (0 to 60 minutes) and ROCK inhibition on FAK activation (autophosphorylation at tyrosine 397) western blots were performed. FAK phosphorylation was minimal at baseline (static) in untreated cells. Following application of 30% CMS, FAK phosphorylation was

approximately 3 times that of baseline at 30 minutes and 60 minutes, although these results were not statistically significant. ROCK inhibition (Y27632) was associated with FAK phosphorylation at baseline and at 10 minutes, but with a decrease at 30 and 60 minutes CMS (Figure 3-6).

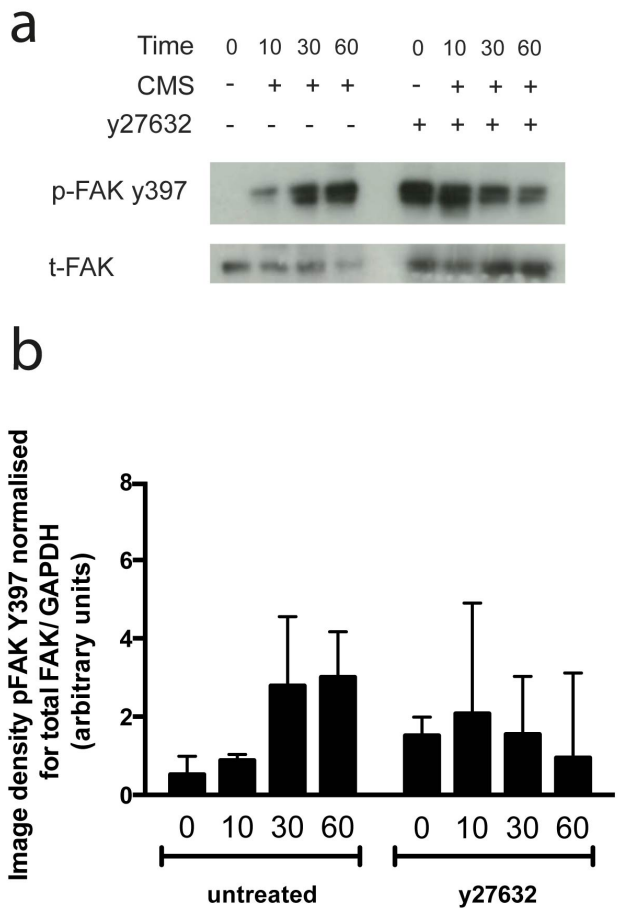


Figure 3-6 The effect of CMS and ROCK inhibition on FAK phosphorylation

A549 cells were either untreated, or subjected to y27632 (10μM) for 1 hour. CMS was applied equibiaxially at 30% elongation for 0-60 minutes. Panel A shows western blot images of both phosphorylated and total FAK over the time course of CMS. Panel B shows calculated image densities for respective blots. Data are presented as the median and IQR for 4 independent experiments. Statistical analysis by Kruskal-Wallis test.

3.3.7 The effect of myosin II inhibition on CMS-induced cytokine release

To test the effect of inhibition of downstream ROCK signalling on CMS-induced mechanotransduction, myosin II activity was blocked with blebbistatin (20μM). Whereas CMS-induced IL-8 generation was intact in vehicle-treated controls, this effect was abrogated in blebbistatin-treated cells (Figure 3-7 – a). Blebbistatin treatment did not affect cell viability as assessed by MTT assay (Figure 3-7 – b), and the ability of blebbistatin-treated cells to generate IL-8 in response to chemical stimulation (10ng/ml TNF-α) was preserved (Figure 3-7 - c).

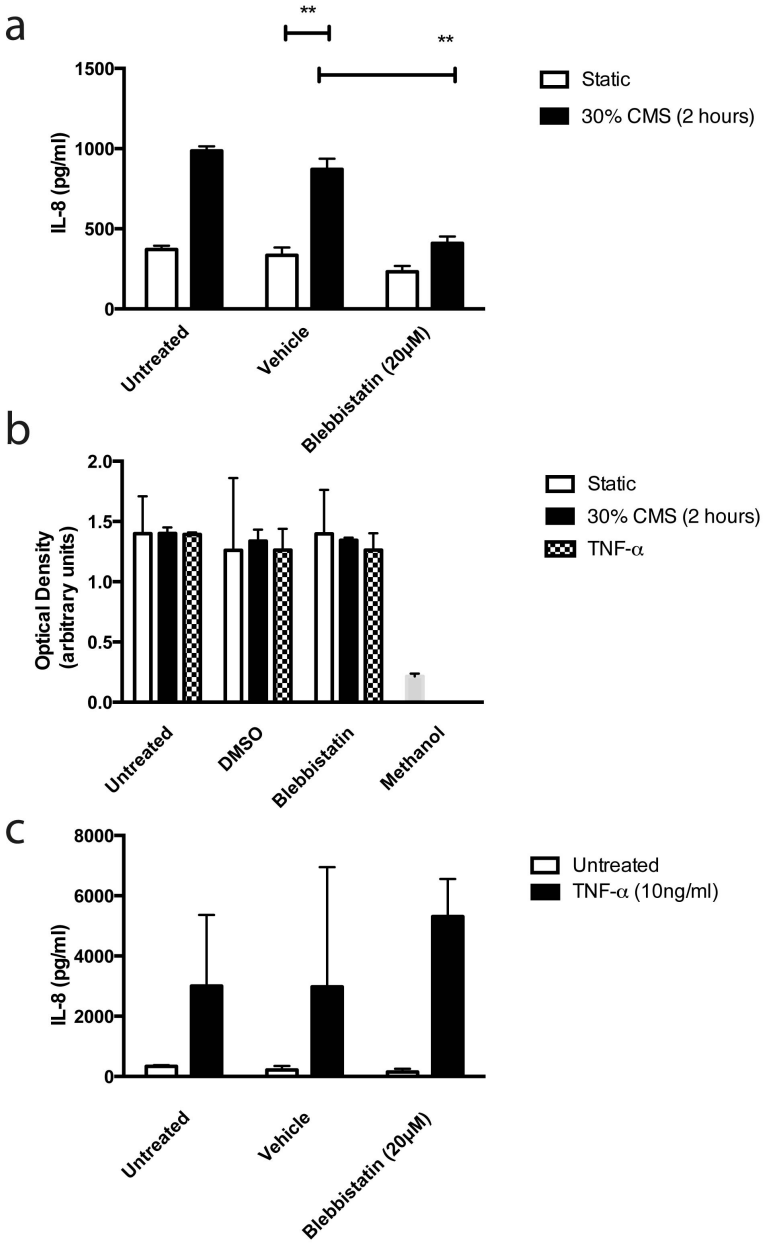


Figure 3-7 The effect of myosin II inhibition on CMS-induced cytokine release

A549 cells were either untreated or blebbistatin (20μM) was applied for 30 minutes. CMS was applied equibiaxially at 30% elongation for 2 hours. Panel A shows IL-8 generation as sampled from cell supernatant at 24 hours following CMS. Panel B shows cell viability at 24 hours following CMS as assessed by MTT assay. Panel C shows IL-8 release in respective treatments at 24 hours following TNF-α treatment Data are for n=6 from three individual experiments for panel A, and n=3 from three individual experiments for panels b and c, and are presented as median ± IQR. Data analysis by Mann Whitney test, **p<0.01

3.3.8 The effect of myosin II inhibition on CMS-induced cytoskeletal and focal adhesion remodelling

To assess the effect of blebbistatin treatment on CMS-induced cytoskeletal remodelling, cells were stained for actin and paxillin after CMS (0-60 mins). At baseline, blebbistatin-treated cells exhibited similar baseline morphology to Y27632-treated cells, with few visible stress fibres and small focal adhesions associated with disorganised actin architecture. Following 60 minutes CMS, cell-cell detachment and cellular contraction seen in vehicle-treated controls was not evident in blebbistatin-treated cells (Figure 3-8).

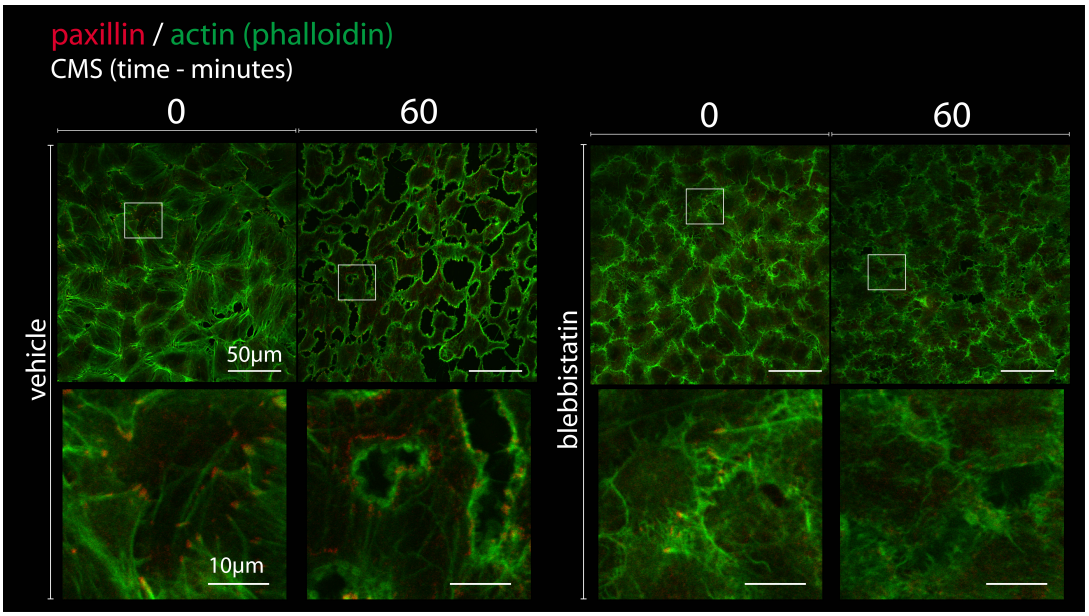


Figure 3-8 The effect of myosin II inhibition on CMS-induced cytoskeletal and focal adhesion remodelling

A549 cells were treated with blebbistatin (20μM) for 30 minutes, subjected to 30% equibiaxial CMS for 0 to 60 minutes, then fixed. The actin cytoskeleton was stained with phalloidin (green), and focal adhesions with paxillin (red) for confocal immunofluorescence microscopy. Scale bars represent 50 or 10μm.

3.3.9 The effect of CMS on cellular traction force

To assess the effect of CMS on tension forces experienced by cells, cells were transfected with the vinculin TS tension sensor FRET probe. FLIM microscopy was performed to ascertain fluorescence lifetimes for either unstretched (static) cells, or cells exposed to CMS for 1 minute. Venus-only probes had lifetimes of approximately 2.3, tail-less controls and static cells of 1.8. When CMS was applied for 1 minute, mean fluorescent lifetime decreased to 1.6, indicating a reduction in tension across vinculin. However, given the absence of an uncomplexed mTFP1 probe, we could not calculate FRET efficiency, and these results can only be indicative of CMS-induced changes in cellular tension (Figure 3-9).

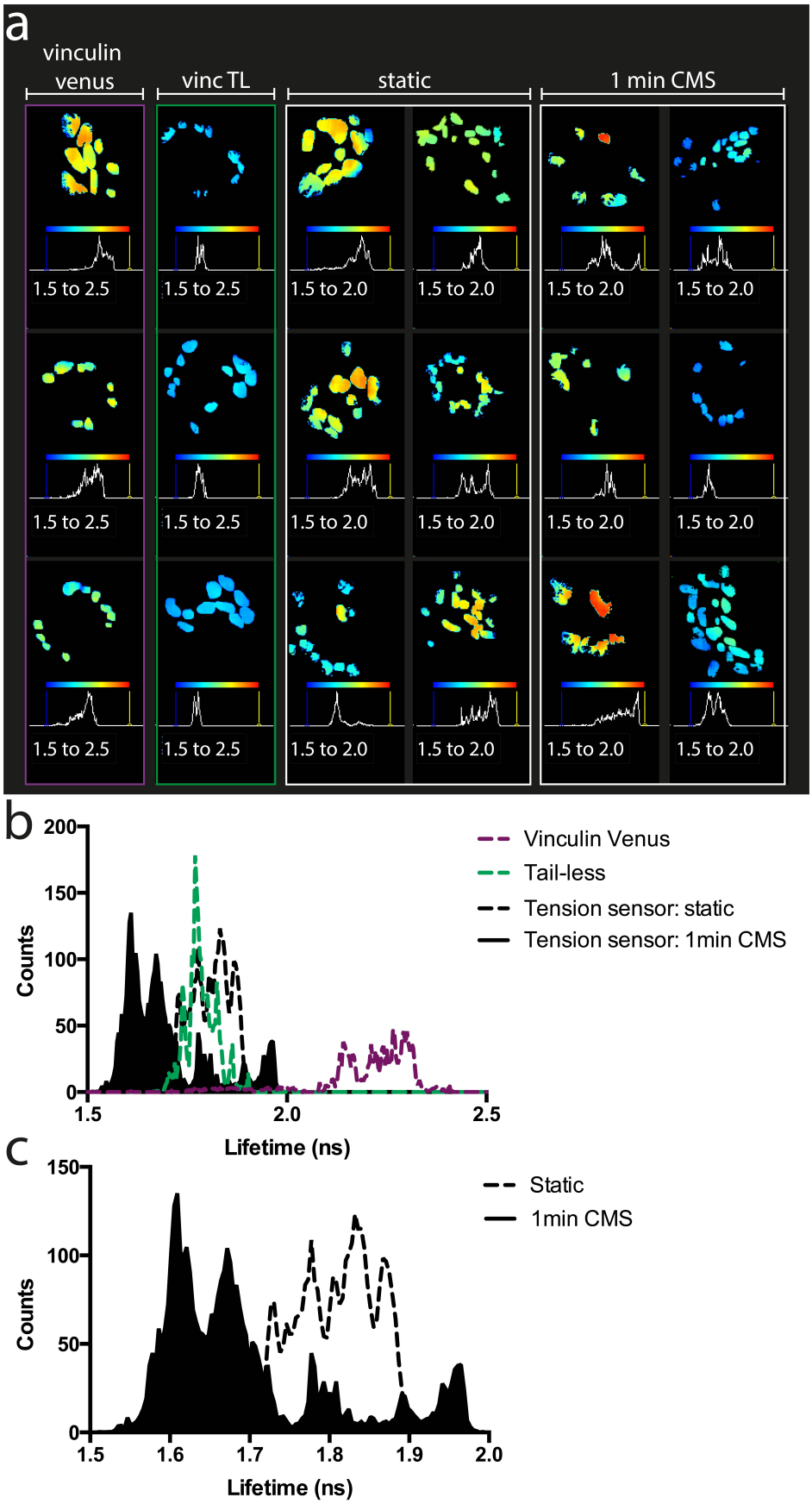

a
vinculin venus
vinc TL
static
1 min CMS
1.5 to 2.5
1.5 to 2.0
b
Vinculin Venus
Tail-less
Tension sensor: static
Tension sensor: 1min CMS
Counts
Lifetime (ns)
c
Static
1min CMS
Counts
Lifetime (ns)

Figure 3-9 The effect of CMS on cellular traction force

Cells were transfected with the Vinculin TS tension FRET probe, and cells either unstretched (static), or subjected to CMS for 1 minute. At each time point, cells were fixed, and FLIM microscopy used to ascertain respective fluorescent lifetimes. Panel A shows 'heat map' colouring of lifetimes for venus-only, and tailless controls, and for static cells or those subjected to CMS. Lower lifetimes are on the blue end of the spectrum as detailed below each heat map.. Panel B shows collated histograms of fluorescent lifetimes for all conditions. Panel C shows collated histograms of fluorescent lifetimes for cells under static and CMS conditions. Data are from n=6 cells, and images representative.

3.3.10 The effect of CMS on RhoA activity

Experiments were designed to test the effect of CMS on RhoA activity in alveolar epithelial cells using the Raichu FRET probe. Cells were transfected and CMS applied for either 0 (static) or 1 minute. FLIM was performed to ascertain fluorescence lifetimes for cells under respective conditions. Rho-GFP-only probes had mean lifetimes of 2.1, inactive Rho (T19) probe of 2.1 and static cells of 1.9. When CMS was applied for 1 minute, mean fluorescent lifetime decreased to 1.86. 1 minute CMS significantly increased FRET efficiency in these cells, implying a CMS-induced increase in RhoA activity (Figure 3-10).

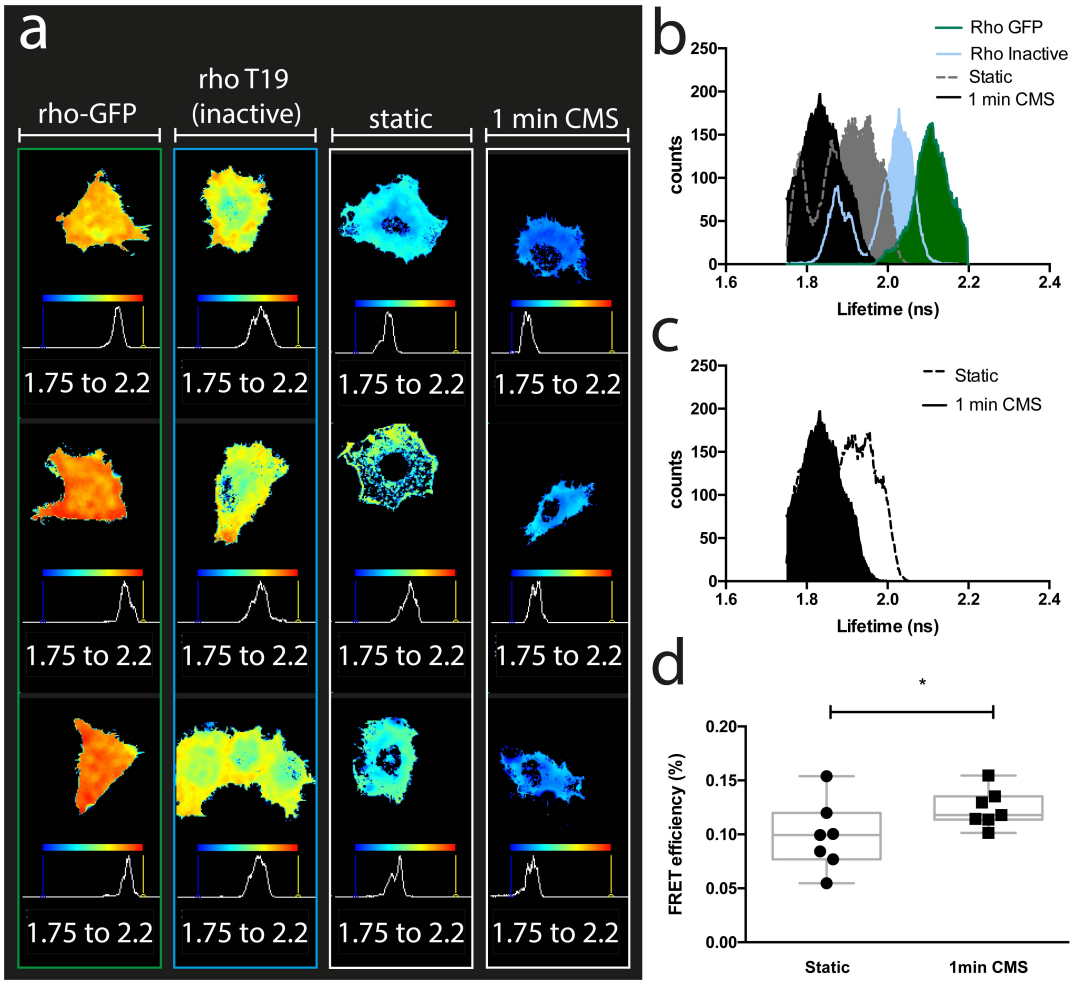


Figure 3-10 The effect of CMS on RhoA activity

Cells were transfected with the Raichu RhoA FRET probe, and either unstretched (static), or subjected to CMS for 1 minute. At each time point, cells were fixed, and FLIM microscopy used to ascertain respective fluorescent lifetimes. Panel A shows heat maps of lifetimes for Rho-GFP, Rho-inactive controls (T19N) and for static cells or those subjected to CMS. Lower lifetimes are on the blue end of the spectrum. Panel B shows collated histograms of fluorescent lifetimes for all conditions. Panel C shows collated histograms of fluorescent lifetimes for cells under static and CMS conditions. Panel D shows calculated FRET efficiencies for cells subjected to static or CMS conditions. Data are presented as median ± interquartile range for 7 cells per condition, and analysed by Wilcoxon paired test, *p<0.05. Images shown are representative of respective conditions.

3.4 Discussion

3.4.1 Summary of important findings

CMS applied to cells induced cytoskeletal remodelling, including stress fibre re-orientation in one direction, a reduction in the area of individual cells and increases in cell-free area. CMS also induced focal adhesion redistribution to the ends of stress fibres seen throughout cells. Inhibition of ROCK with Y27632 abrogated CMS-induced IL-8 generation, but without affecting cell viability, or the ability of cells to generate IL-8 in response to chemical stimuli (TNF-α). This correlated with a decrease in CMS-induced FAK phosphorylation. Downstream inhibition of myosin II with blebbistatin also abrogated CMS-induced IL-8 generation in a manner similar to that seen with Y27632, and was associated with similar morphological features. Finally, preliminary experiments using FRET sensors demonstrated that CMS for 1 minute was associated with decreased cell traction forces, and significantly increased RhoA activity.

3.4.2 CMS-induced cytoskeletal and focal adhesion remodelling

CMS induced cytoskeletal reorganisation, with loss of random orientation of stress fibres, decreased cellular area and increased cell-free area. Stress fibre reassembly and realignment is a well-documented response of endothelial cells (J. H.-C. Wang et al. 2001) and fibroblasts (Greiner et al. 2013) subjected to mechanical stresses or increased ECM rigidity. In these cells, mechanical force-induced cytoskeletal remodelling occurred via integrin-mediated Rho signalling (Guilluy et al. 2011; Tzima et al. 2001). CMS-induced

Rho signalling in particular promoted reorientation of stress fibres and focal adhesions perpendicular to the direction of uniaxial force (Goldyn et al. 2009; Abiko et al. 2015; Kaunas et al. 2005). This mechanism has been proposed as an adaptation to reduce injury from external forces (Faust et al. 2011; Hwang & Barakat 2012).

Evidence of similar CMS-induced actin remodelling in epithelial cells is less extensive. In equibiaxial CMS of foetal ATII, stress fibre reorientation was induced along the long axis of the cell, and was dependent on RhoA signalling (Silbert et al. 2008). Another study of biaxial CMS of rat ATI found perijunctional actin ring (PJAR) formation within 10 minutes in a manner dependent on magnitude of stretch and frequency, and associated with spontaneous movement of actin-focal adhesion-bound microbeads (DiPaolo et al. 2010). In the latter study, the authors concluded that this effect was specific to the cell type used, as PJAR were evident in A549 at baseline, and not altered by CMS. Our results may be different due to differences in the degree of CMS applied, the method used to apply CMS and the fact that the authors serum-starved cells prior to application of CMS, which is known to impede Rho-dependent stress fibre formation (Machesky & Hall 1997).

Furthermore, our observations indicated that CMS promotes a decrease in cellular area, perhaps indicating an increase in cellular contraction. This was associated with an increase in denuded, or cell-free, area. These observations correlate with those of CMS-induced gaps in monolayers of rat ATII (Crosby et al. 2011), and with those demonstrating that VALI is associated with denudation of the lung epithelial basement membrane or

epithelial ‘leak’ (Frank et al. 2002; Matthay et al. 2012; Hamlington et al. 2016). While CMS-induced injury to the lung epithelium is generally associated with cell apoptosis and death (Crosby et al. 2011), our work demonstrates that A549 viability is not reduced following CMS. We were not able to ascertain whether the increase in cell-free area and decrease in cell size were secondary to primary cellular contraction in response to CMS, or due to broken cell-matrix and cell-cell adhesions and unopposed cell contraction. However, work in endothelial cell monolayers lends weight to the latter, suggesting that whereas cytokine-induced injury contributes to vascular permeability, a separate Rho and focal-adhesion-dependent contractile process also induces endothelial gap formation (Birukova et al. 2016).

ROCK and myosin II inhibition abrogated CMS-induced cytoskeletal remodelling. That this pathway mediates CMS-induced cytoskeletal remodelling has been demonstrated previously in ATII (Silbert et al. 2008), where dominant negative expression of RhoA abrogated CMS-induced stress fibre assembly or realignment. In fibroblasts subjected to uniaxial CMS (Hoffman et al. 2012), Y27632 (3μM for 2 hours) both abrogated stress fibre production at basal states, and reduced formation and perpendicular realignment following CMS. Our observations of inhibited stress fibre assembly and CMS-induced reorientation in cells following ROCK and myosin II inhibition correlate with those of fibroblasts (Greiner et al. 2013), endothelial cells (Lee et al. 2010; Kaunas et al. 2005) and ATI (DiPaolo & Margulies 2012) but in the latter case no differences in CMS-induced cytoskeletal remodelling were seen when compared to untreated controls. Again, these differences may be secondary to the degree of CMS applied. Indeed, in

endothelial cells, Rho-mediated CMS-induced stress fibre construction and reorganisation was dependent on strain rate (Lee et al. 2010).

Our experiments also indicated that CMS induced the appearances of ‘breaks’ in stress fibres within cells, with reorganisation of focal adhesions to the free ends of the actomyosin fibre. The application of mechanical force promotes focal adhesion maturation (Riveline et al. 2001; Gawlak et al. 2014), but also myosin-dependent realignment (Greiner et al. 2013). However, focal adhesions also transiently assemble and disassemble in response to externally-applied force, such as with primary ATII subjected to tonic stretch (Liu et al. 2011), and this behaviour may be protective. In this case, cells transiently contracted, disassembled adhesions and partially detached, but without cell death. Reducing integrin-ECM binding increased this transient stretch-induced cell contraction but abrogated cell death. Conversely, increasing integrin activity reduced transient disassembly contraction, but increased cell death, suggesting that transient focal adhesion disassembly allows cells to escape stretch-induced injury.

In our case, focal adhesions associated with stress fibres within the cell during CMS. A similar phenotype occurs when stress fibres are mechanically broken, and in that case, the adaptor protein zyxin relocated from focal adhesions to newly maturing adhesions at the severed ends as the filament retracts (Colombelli et al. 2009). Crucially, zyxin redistributed to areas of high strain (Smith et al. 2010). This phenomenon occurred in response to CMS where it contributed to stress fibre cytoskeletal re-enforcement (Yoshigi et al. 2005) by recruiting actin-binding proteins α-actinin and *Drosophila* enabled

(Ena) / vasodilator-stimulated phosphoprotein (VASP) (Hoffman et al. 2012). In this case, zyxin was not required for CMS-induced cytoskeletal re-orientation, but for subsequent re-enforcement of stress fibres. Therefore, the focal adhesion reorientation seen in our model may represent CMS-induced relocation of zyxin to repair damaged stress fibres.

3.4.3 Rho-ROCK-myosin II signalling is required for CMS-induced cytokine generation

My data (3.3.4, 3.3.7) indicate that ROCK and myosin II are required for CMS-induced cytokine generation in alveolar epithelial cells. Inhibition of both elements, with 10μM Y27632 in the former and 20μM blebbistatin in the latter, significantly abrogated CMS-induced IL-8 release in these cells. Furthermore, the doses used were comparable with previous studies *in vitro* (Torsoni et al. 2005) and did not reduce cell viability in comparison to untreated cells. Finally, cells were still able to generate IL-8 in response to chemical stimulation from TNF-α, suggesting that ROCK and myosin II regulate pathways specific to strain-induced cytokine generation.

Neutrophil chemokines like IL-8 play an important role in the pathogenesis of ARDS, which is sensitive to high tidal volume stretch of the alveolar epithelium (Ranieri et al. 1999). This corresponds with data suggesting that CMS of alveolar epithelial cells *in vitro* induced IL-8 generation (Vlahakis et al. 1999). My data correlate with work in bronchial epithelial cells (Thomas et al. 2006), where CMS-induced IL-8 release was abrogated by inhibition of ROCK. Similarly, the application of 18% CMS to endothelial cells over 48-72 hours resulted in an increase in IL-8 release,

abrogated by siRNA knockdown of the Rho GEF GEFH1 (Tian et al. 2016). This also abrogated CMS-induced actin remodelling, indicating the role of RhoA signalling in stretch-induced mechanotransduction.

How might CMS-induced cytokine generation progress via ROCK signalling? Rho-ROCK-myosin II-driven contractility increases cellular pre-stress (Cirka et al. 2016) and elastic modulus (Wilhelm et al. 2014). Both of these effects could increase the susceptibility of the cell to externally-applied strain. However, how this process links with previously determined ERK/oxidative stress pathways is not clear. CMS promoted expression of the Rho activating protein GEF-H1 downstream of FAK activation (Guilluy et al. 2011), which forms a complex with ERK and paxillin to stimulate Rho activity (Gawlak et al. 2014). GEF-H1 is required for CMS-induced cytokine generation in endothelial cells (Tian et al. 2016). Rho-GEF-H1 and RhoA are upstream of ROCK, indicating either the possibility of a positive feedback loop driven by myosin-induced contractility, or of independent effects of ROCK/myosin II and GEF-H1/RhoA.

Given the strong possibility of RhoA-mediated mechanotransduction indicated by these results, I attempted to ascertain if treatment with LPA would agonise CMS-induced cytokine release. Phalloidin staining suggested that treatment with LPA (10μM for 30 mins) promoted increased stress fibre formation (3.3.5), as previously described in Swiss 3T3 cells (Ridley & Hall 1992). However, there was no increase in CMS-induced IL-8 generation following this treatment. There are numerous potential reasons for this. First, I could not confirm that LPA treatment did increase RhoA activity: results from

rhotekin-bead pull-down and the raichu RhoA probe were inconclusive. Another possibility is that RhoA activity is already maximal in untreated cells, and therefore cannot be potentiated further.

I also aimed to determine whether inhibition of actin polymerisation by cytochalasin D would have a similar effect to ROCK inhibition on CMS-induced cytokine release. However, despite phalloidin-stained morphology consistent with cytochalasin-D-mediated inhibition of actin polymerisation, the cytokine response to CMS was preserved, and not abrogated as I expected. Although there are few data examining the effect of cytochalasin-D on CMS-induced mechanotransduction, previous work by our group suggests that the same dose inhibited CMS-induced ERK phosphorylation and oxidative stress in A549 cells (Pinhu 2008). Cytochalasin D has also been shown to decrease the elastic modulus of cells subjected to hyperoxia (Roan et al. 2012). Taking all this into account, it would be expected to reduce stretch-induced cytokine generation.

I cannot preclude the possibility that this indicates a role for RhoA and myosin II signalling in CMS-induced IL-8 release, but independent of cytoskeletal integrity. One possibility may be that mechanical force promotes IL-8 gene transcription or protein translation, possibly via direct force transduction to the nucleus (Guilluy et al. 2014). Another potential explanation is that actin polymerisation has a minor role in stress fibre and focal adhesion assembly (Chrzanowska-Wodnicka & Burridge 1996), when compared to Rho-driven myosin contractility. However, given that contrasting data implies that polymerisation is critical for the development of stress fibre and focal

adhesion mechanosensitive elements (Hotulainen & Lappalainen 2006; Oakes et al. 2012), I cannot fully explain these results. Finally, CMS may contribute to actin polymerisation itself, counteracting the effect of cytochalasin-D, and restoring the ability of cells to sense and respond to external force (Riveline et al. 2001). In conclusion, these data suggest that the role of the cytoskeleton in CMS-induced IL-8 release may be more complex, and the possibility for direct nuclear mechanotransduction, potentially with a role for RhoA-ROCK-myosin II activity, cannot be ignored.

Mechanical force (Friedland et al. 2009), and specifically CMS is associated with increased β1-integrin activity (Wernig et al. 2003) (Hamzeh et al. 2015) (Sanchez-Esteban et al. 2006). Force-induced β1-integrin activity activated RhoA via FAK and GEF-H1 activation (Guilluy et al. 2011). FAK is critical for integrin-mediated adhesion and response to substrate rigidity (Provenzano et al. 2009), and is activated by autophosphorylation at Y397 in response to CMS as demonstrated in lung endothelial cells. This then phosphorylates paxillin, enabling GEF-H1-paxillin-ERK complex formation (Gawlak et al. 2014). Indeed, inhibition of FAK abrogated force-induced GEF-H1 activation (Guilluy et al. 2011).

In our system, FAK phosphorylation at Y397, as a read-out of mechanoresponse to CMS, increased following 30 minutes of stretch. However, baseline phosphorylation was observed in cells following ROCK inhibition which contrasts with observations from mouse lung epithelial cells (Wilhelm et al. 2014) and cardiomyocytes (Torsoni et al. 2005). A CMS-dependent increase in phosphorylation was not observed in these cells, such

as at 30 minutes. Considering the above schema of CMS-induced RhoA activation, ROCK activation can be considered downstream of FAK, and its inhibition would not be expected to affect FAK phosphorylation in response to mechanical force. Therefore, these effects of CMS on FAK phosphorylation may be considered to be secondary to Rho-ROCK-mediated reinforcement following repeated loading cycles, i.e an indication of the ability of the cell to tune traction forces in response to force. Indeed, FAK may not regulate CMS-induced stress fibre remodelling or ERK activation as these occur even in the absence of FAK in aortic endothelial cells subjected to CMS (Hsu et al. 2010), and CMS-induced cell reorientation is myosin II-dependent (Greiner et al. 2013). Therefore, we can consider CMS-induced FAK signalling in this case as occurring both upstream of RhoA-ROCK activation, and as a dynamic response to mechanosensation. However, as seen following cytochalasin D treatment, the possibility of mechanotransduction directly affecting IL-8 transcription, translation or trafficking cannot be ignored.

3.4.4 Cellular tension during CMS-induced mechanotransduction

From preliminary experiments of cellular tension measurements using FRET constructs, we cautiously conclude that CMS of 1 minute induced a decrease in tension across vinculin focal adhesions. If these results prove to be consistent, they would suggest that force transmission is decreased very rapidly following the onset of externally applied force. These observations are in agreement with previous descriptions of mechanical responses to CMS. Cell traction forces of human airway smooth muscle cells demonstrated acute decreases following transient stretch, implying rapid cytoskeletal ‘softening’ or

fluidisation (Trepat et al. 2007; Krishnan et al. 2009). Similarly, transient stretch of human bladder smooth muscle cells promoted the same rapid fluidisation response, followed by a slow increase in traction force and cell stiffness as measured by elastic modulus (Chen et al. 2010). Indeed, macroscopically, the lung shows evidence of strain-induced hardening with an exponential increase in stress with applied strain to isolated lung parenchymal strips (Navajas et al. 1995).

This dual response also correlates with actin dynamics seen in various systems. For example, a rapid increase in movement of actin filaments was observed within 1 minute CMS in rat ATI, which then slows down, suggesting acute malleability of the actin cytoskeleton followed by recovery or reinforcement (DiPaolo et al. 2010). Fibroblasts subjected to uniaxial stretch demonstrated a two-phase response composed of initial stress fibre reorientation followed by zyxin-mediated reinforcement (Hoffman et al. 2012). Mechanisms that could account for initial cytoskeletal fluidisation are not entirely clear. Possibilities include purely physical properties of the cell, force-induced dissociation of actin from binding partners such as α-catenin or VASP, or activation of cofilin (Chen et al. 2010). Whether rapid dissociation of zyxin from focal adhesions to stress fibres can account for fluidisation also remains to be seen, although initial actin reorganisation is zyxin-independent (Hoffman et al. 2012).

Initial fluidisation as a physical response of the cell to acute strain in our model may be related to CMS-induced changes in stress fibre and focal adhesion dynamics. Acute strain on individual stress fibres decreases their

ability to transmit force through their corresponding focal adhesion, followed by a zyxin-dependent restoration phase corresponding to stress fibre repair (Smith et al. 2010). Accordingly, severing of individual stress fibres with femtosecond laser nanoscissor techniques revealed an immediate retraction of the fibre associated with a dissipation of force to the ECM. Crucially, in this case the degree of recoil corresponded with tensile pre-stress: when this was reduced by inhibition of ROCK-myosin II-driven contractility, elastic recoil of stress fibres also decreased (Kumar et al. 2006; Colombelli et al. 2009). We therefore suggest that CMS-induced damage to stress fibres corresponds with prompt relaxation of tension throughout the cell, and that this elastic recoil may be inhibited by decreasing myosin II driven cellular pre-stress.

Our aim to measure cellular tension in cells following ROCK inhibition was impeded by the small focal adhesions in those cells as seen in previous studies (Rápalo et al. 2015), which made it difficult to establish fluorescent lifetimes. However, Grashoff et al. overcame this issue, and ascertained that tension following ROCK and myosin II inhibition is decreased (Grashoff et al. 2010). This reinforces our belief that these cells are less susceptible to CMS-induced injury because their baseline pre-stress is reduced. Similar observations were seen when ROCK inhibition protected alveolar epithelial cells from susceptibility to hyperoxia and CMS, possibly by preventing hyperoxia-induced increases in cellular pre-stress (Wilhelm et al. 2014). In this context, we would expect to see no fluidisation of ROCK-inhibited cells following onset of CMS, but rather an increase in tension such as that observed in valvular interstitial cells with reduced pre-stress following myosin

II inhibition (Cirka et al. 2016). In this context, cells tune traction forces to maintain an optimum equilibrium in response to external forces.

That inhibition of Rho alters baseline cytoskeletal properties to tune susceptibility to CMS is in agreement with observations by Yalcin et al. Where actin was depolymerised with latrunculin A, alveolar epithelial cells subjected to CMS exhibited both increased cell adhesion and cell viability. Using optical tweezer techniques, the authors demonstrated that the rheology of the latrunculin-treated cells was 'softer' and more visco-elastic and fluid-like than that of untreated cells. It was proposed that this softer rheology predisposed the latrunculin-treated cells to deform more slowly and 'dampen' out the applied force. This effect could be replicated by heating the cells to 37°C (Yalcin et al. 2009).

However, my results must be interpreted with caution. First, the complexity of the experimental technique limited the data gathered to that from 6 cells at present. Second, I note that the fluorescent lifetimes from 1 minute CMS are lower than those of the tail-less probe, suggesting lower tension. Given that no tension can be applied across this control probe, my hypothesis is that either the control probe does not function correctly in my set-up, or that CMS at the magnitude applied in my case led to breakage of the filamentous linker between FRET donor and acceptor, allowing for greater proximity between the two, and therefore increased FRET. This may be possible, given that the TSMod is sensitive to forces in the range of 1-6 pN (Grashoff et al. 2010), and the force required to stretch actin stress fibres from relaxed length to original length is thought to be in the region of 10nN

(Kassianidou & Kumar 2015). The force required to break individual stress fibres may be even greater, given that stress fibres appear to undergo local increases in tension in zones liable to break (Smith et al. 2010).

3.4.5 CMS-induced regulation of RhoA activity

In this context, I sought to establish the relationship between early changes in cellular traction forces and RhoA activity. Using a previously described raichu RhoA FRET probe (Heasman et al. 2010), preliminary results demonstrated that 1 minute CMS increased RhoA activity. These observations contrast with other attempts to characterise RhoA-ROCK activity during CMS of alveolar epithelial cells.

MLC2 phosphorylation and RhoA activity decreased in rat ATI subjected to CMS of 37% elongation for 10 and 60 minutes (DiPaolo & Margulies 2012). When Silbert et al. subjected foetal ATII to low magnitude (5%) CMS, RhoA activity initially decreased at 1 minute, followed by an increase at 5 minutes (Silbert et al. 2008). My results correlate more closely with those observed in cardiomyocytes, where CMS induced RhoA activity by 1 minute, which persisted until 10 minutes (Kawamura et al. 2003). Differences again may be accounted for by cell type, but also the method used to ascertain RhoA activity. I used a FRET sensor on the basis that it would provide greater spatio-temporal information that a standard pull-down assay (Pertz et al. 2006).

That RhoA expression may be up-regulated within 1 minute CMS corresponds with stretch-induced β1 integrin activation and FAK-regulated

GEF-H1 expression (Guilluy et al. 2011). Downstream of RhoA, ROCK activation promotes myosin II activity through MLC2 phosphorylation (Totsukawa et al. 2000). Myosin-driven contractility increases cellular pre-stress, and possibly the cell stiffening response to externally-applied force (Guilluy et al. 2011) (Watanabe-Nakayama et al. 2011). Although increased pre-stress and stiffening are thought to be a cellular adaptation to maintain cellular integrity in the face of externally applied force (Watanabe-Nakayama et al. 2011) (Guilluy et al. 2011), such a response may mediate cytokine generation following increased susceptibility to transmitted force across a tense cytoskeleton.

The effect of RhoA-mediated cytokine release in alveolar distension may have implications for the pathogenesis of lung injury. Pre-treatment of rats with Y27632 in a caecal ligation model of sepsis reduced lung injury parameters including interstitial oedema, lung architectural damage and inflammatory cell infiltration (Cinel et al. 2012). Although the animals in this case were not ventilated, and the authors did not discuss the effect of modulation of alveolar distension-induced cytokine release in the progression of lung injury, this ties with other observations of Rho-mediated and CMS-induced 'second-hit' lung injury. Y27632 attenuated Rho and CMS-mediated augmentation of IL-6 induced endothelial cell permeability *in vitro*, and lung injury *in vivo* (Birukova et al. 2012), and knockdown of GEF-H1 abrogated CMS-induced endothelial disruption in an LPS two-hit model of lung injury (Tian et al. 2016). These data add to a growing body of evidence from endothelial cells that VALI follows this two-hit model, composed of a Rho-independent IL-6 mediated disruption of endothelial integrity, such as from

sepsis, augmented by a focal adhesion and Rho-dependent stretch-induced injury (Birukova et al. 2016).

Finally, that RhoA signalling may mediate stretch-induced lung injury correlates with previously observed signalling pathways in lung mechanobiology. Mitochondrial ROS, the generation of which has been linked to CMS-induced mechanotransduction pathways in the lung (Pinhu 2008; Nurit Davidovich et al. 2013; Rápalo et al. 2015) were shown to activate ROCK and MLC-mediated cytoskeletal remodelling in a drosophila model of wound healing (Muliyil & Narasimha 2014), and may also be responsible for increasing the pre-stress of cells via this pathway (Wilhelm et al. 2014).

3.4.6 Limitations

Application of CMS to cells using the Flexcell system, particularly when applying stretch magnitudes of over 30%, is associated with heterogeneity of the strain field. In a system such as mine, where sections of the flexible silicone membrane are cut for immunofluorescence microscopy or FLIM, these heterogeneities will lead to inconsistencies in observations or measurements. One possible solution to this is to use stretch magnitudes of 20%, and only section the membrane lying over the loading post (Ursekar et al. 2014). Furthermore, when considering the effect of CMS on cells, it must be appreciated that there may be shear forces applied as the cells are stretched within the media (Pinhu 2008).

When measuring the effect of CMS on cellular size and on cell-free area, an actin dye was used. However, results may have been confounded by the

effects of CMS on actin composition at the lamellipodium. The use of a membrane dye may provide more accurate information on the precise boundaries of cells.

Finally, investigating the effects of CMS at fixed times may only offer ‘snapshots’ of what may be a dynamic and constantly-adapting picture. Therefore, the effects of CMS on cytoskeletal and focal adhesion remodelling, cellular traction forces and RhoA activity may only be relevant at the time points measured, and may not reflect complex, rapid and evolving signalling over time. The combination of high-speed FRET imaging (Poland et al. 2015), with recent development of platforms for real-time imaging (Rápalo et al. 2015) may provide more insight into CMS-induced signalling in future.

3.4.7 Conclusions

I have shown that CMS promoted cytoskeletal remodelling and focal adhesion re-distribution in alveolar epithelial cells, and that remodelling and cytokine generation are dependent on RhoA-ROCK-myosin II signalling. Furthermore, preliminary results suggest that CMS induced rapid (1 minute) decreases in cellular tension at focal adhesions, and increased RhoA activity.

I believe that RhoA-ROCK signalling may mediate CMS-induced mechanotransduction and cytokine generation by altering baseline cytoskeletal tension (pre-stress), which alters the susceptibility of cells to transmission of force from CMS. However, the fact that cytochalasin D did not affect CMS-induced IL-8 release, if consistent, reveals a potential greater

level of complexity than the pathway hypothesised, possibly including direct nuclear mechanotransduction.

3.4.8 Future directions

Although I have ascertained preliminary results for the effects of CMS on a short time-scale (1 minute) on cellular traction and RhoA activity, evidence suggests that cells exhibit biphasic responses to CMS, with an initial reduction in traction forces followed by a slow reinforcement. Therefore, I aim to measure these effects over longer time periods of CMS, from 1 minute to 10 minutes, with the aim of developing a more robust picture of cellular responses over time. Furthermore, I aim to use frequency domain FLIM to accelerate data acquisition.

Another future aim is to use staining for zyxin to determine whether focal adhesion redistribution and remodelling correlates with zyxin mobilisation from focal adhesions to sites of stress fibre repair, and if this is associated with CMS-induced remodelling and stiffening.

In order to ascertain how the role of cellular pre-stress correlates with the results seen following application of cytochalasin D, it would be prudent to apply the cellular tension measurements to cells in this condition.

Finally, these investigations have focussed on the role of signalling within single cells during CMS. However, a sub-confluent monolayer of cells does not respond to CMS with a significant cytokine response (2.2.4.1.3). Therefore, cell-cell interactions are likely to play a major role in CMS-induced injurious mechanotransduction. Assessment of the roles of α and β catenin, in

addition to other cell-cell adhesion markers, will be critical for understanding the interplay between cell-cell and cell-matrix adhesions in CMS-induced mechanotransduction signalling.

4 Chapter 4: The role of CD98hc in responses of the lung alveolar epithelium to Cyclic Mechanical Strain (CMS)

4.1 Introduction

Results from the previous chapter indicated that CMS induced RhoA activation in alveolar epithelial cells. Previous studies demonstrated that mechanical force-induced β1-integrin activation promoted RhoA signalling (Guilluy et al. 2011), and that β1-integrin activation in response to increased ECM rigidity required ROCK-myosin II signalling (Lin et al. 2013).

The transmembrane protein, CD98hc, interacts with β-integrin tails (Fenczik et al. 2001), mediates β-integrin-dependent adhesive signalling, and regulates adhesion-dependent spreading of cells (Prager et al. 2007). In embryonic stem cells, CD98hc, and specifically the intracellular and transmembrane domains that interact with β1-integrins, was required for adhesion-induced and integrin-dependent activation of Akt and Rac GTPase (Feral et al. 2005). These integrin-mediating properties of CD98hc may underlie its capacity to promote anchorage-independence and tumourgenesis (Cantor & Ginsberg 2012) (Henderson et al. 2004). Furthermore, CD98hc regulated β1-integrin-mediated RhoA activity (Féral et al. 2007), and ROCK signalling (Estrach et al. 2014) in fibroblasts.

Although depletion of β-integrin induced cell detachment and death in ATII exposed to tonic stretch (Liu et al. 2011), the targeting of integrin-mediating proteins, such as CD98hc, to affect downstream integrin signalling is an attractive prospect (Cantor et al. 2008). CD98hc may therefore represent a potential target for CMS-induced injurious mechanotransduction occurring

via β-integrin and RhoA signalling processes. However, recovery of the lung from injury is dependent, in part, on adhesion, migration and proliferative restoration of the alveolar epithelium (Crosby & Waters 2010). Given that β1-integrin signalling (Kim et al. 1997), and RhoA signalling (Reffay et al. 2014) regulate epithelial cell migration, the effect of CD98hc depletion on adhesion, migration and epithelial barrier integrity must be carefully evaluated before credence is given to its potential as a therapeutic target in VALI.

Therefore the work in this chapter is based on the hypothesis that CMS-induced cytokine release in alveolar epithelial cells is mediated via CD98hc-induced baseline RhoA activity and cellular tension. Specifically, the aims of the work in this chapter are:

a. To investigate the effect of CD98hc knockdown on CMS-induced mehcanotransduction, integrin activity and downstream FAK signalling

b. To establish whether knockdown of CD98hc mediates baseline RhoA activity and cellular tension

c. To determine whether knockdown of CD98hc decreases the migratory and adhesive capacity of alveolar epithelial cells, which is essential for repair of the injured alveolar epithelium.

To achieve these aims, I will use siRNA to knockdown CD98hc, and will apply biaxial CMS to A549 cells *in vitro,* using FRET techniques already described to ascertain RhoA signalling and traction forces.

4.2 Specific methods

4.2.1 Effect of CD98hc knockdown (kd) on CMS-induced IL-8 protein, gene expression and cell viability

A549 cells seeded on collagen I-coated BioFlex™ 6 well plates were transfected with either non-targeting or CD98hc siRNA at 24 hours when 30-50% confluent as described (2.2.3.5.2). Efficiency of knockdown was assessed by immunoblotting of protein (2.2.6.3) for CD98hc (1:10,000) referenced to β-actin expression (1:1000) (2.1.6.1).

At 48 hours following transfection, cells were exposed to 30% CMS for 2 hours at 0.33Hz, and supernatant collected at 24 hours for assessment of cytokine release by ELISA as described (2.2.6.1). For gene expression analyses, cells were lysed in Trizol reagent immediately following CMS, and reverse transcription and RT PCR steps followed as described (2.2.3.3).

For assessment of cell viability following CMS, cells with respective treatments were treated with MTT reagent 24 hours after CMS, and processed as described (2.2.1.2). Finally, for assessment of the ability of CD98hc kd cells to generate IL-8 in response to chemical stimulation, cells were treated with IL-1β (500 pg/ml). Supernatant was collected at 24 hours following CMS and analysed by ELISA as described (2.2.6.1).

4.2.2 β1-integrin-mediated signalling and mechanotransduction in CMS

Cells, either untreated or transfected with non-targeting or CD98hc kd siRNA, were subjected to CMS for 0-120 minutes, and cells immediately lysed and protein extracted for immunoblotting as described (2.2.6.3). Protein was incubated with antibodies against activated β1-integrin (Wu et al. 2015). (Luque et al. 1996) (HUTS4, non-reducing and non-denaturing, 1:1000), total β1-integrin (1:1000), pFAK Y397 D20B1 (1:1000), total FAK (1:1000), CD98hc (1:10,000), p-ERK p42/44 (1:1000), total ERK p42/44 (1:1000) or GAPDH (1:20,000) (2.1.6.1, Table 2-3).

Immunofluorescence of activated β1-integrin in cells transfected with non-targeting or CD98hc kd siRNA was performed by concurrent fixation and permeabilisation of cells with 4% PFA in the presence of 0.1% triton, followed by blocking in 1% BSA for 1 hour and incubation in HUTS4 antibody (1:100) for 1 hour at room temperature. Subsequent wash, incubation in secondary antibody and imaging steps were followed as described (2.2.5.1.3).

To assess the effect of exposure of cells to ambient conditions on β1-integrin activity in cells, A549 cells were plated in separate petri-dishes. Medium change was conducted in all cells, and cells lysed for protein analysis either immediately (0 minutes) or at 5, 30 or 60 minutes. Immunoblotting for activated β1-integrin activity was then performed as described previously (2.2.6.3).

4.2.3 Assessment of the effect of CD98hc kd on cellular tension and RhoA activity

Cells were transfected with either non-targeting or CD98hc kd siRNA at 24 hours after seeding as described (2.2.3.5), then subsequently transfected with either the vinculin FRET tension sensor DNA (Grashoff et al. 2010) or the Raichu RhoA activity probe (Heasman et al. 2010) (2.2.5.2.3, 2.2.5.2.4, 2.2.5.2.5) 48 hours after seeding at approximately 60-75% confluence. Cells were fixed after either 0 or 1 minute CMS, mounted, and FLIM microscopy performed as described (2.2.5.2).

4.2.4 Assessment of epithelial cell migration in CD98hc kd cells

Monolayers of A549 were seeded in 6-well plates and transfected with either non-targeting or CD98hc kd siRNA at 24 hours as described (2.2.3.5). Monolayers were scratched at 72 hours following seeding, and epithelial migration assessed immediately (t=0 hours) or at 16 hours as described (2.2.4.2). For inter-nuclear distance measurements, cells were fixed at 24 hours and images taken at equal points along the wound. Inter-nuclear distances were calculated using the 'nearest neighbour' plugin for Image J imaging software (Fiji, http://fiji.sc/Fiji).

4.2.5 Assessment of epithelial monolayer integrity in CD98hc kd cells

A549 cells were seeded at 0.01 $x10^6$ cells/well in 8-well RTCA iCELLigence electrical impedance plates as described (2.2.4.3). siRNA

transfection was performed at 24 hours (2.2.3.5) and the wells scratched with a P200 pipette tip when cell index reached a plateau (indicating monolayer integrity) at approximately 106 hours. For monolayer growth following transfection, indices were normalised at a point following transfection, and the slope (change in normalized cell index/hr) was calculated from the point prior to scratch to the normalization point. For recovery of monolayer integrity after scratch, indices were normalised at the plateau point, and the slope calculated for the difference between this point and at 24 hours following scratch.

4.2.6 The effect of CD98hc kd on cell-matrix adhesion after CMS

To ascertain sensitivity of the assay to differences in cell density, cells were seeded at either 150, 75, 37.5, 18.75, 9.375 x 10^3 cells per well, and incubated for 72 hours. At 72 hours, 5 mM EDTA in calcium and magnesium deplete PBS was added to another well seeded at 150 x 10^3 cells for 2 hours as a negative control. Cells were washed, fixed and stained with 0.1% crystal violet solution as described (2.2.4.4). Stained cells were solubilised in methanol, and the solubilised crystal violet read in a plate reader at 570nm wavelength.

To assess the effect of CD98hc knockdown on cell-matrix adhesion following CMS, plated cells were transfected 24 hours following seeding (2.2.3.5) then exposed to either static conditions, or 30% CMS for 2 hours. Cells were then immediately washed, fixed and stained with crystal violet solution, and the optical density of solubilised solution measured as described above.

4.3 Results

4.3.1 The effect of CD98hc knockdown on CMS-induced IL-8 protein and gene expression

To examine the role of CD98hc in CMS-induced mechanotransduction, CD98hc was knocked down by siRNA gene silencing, achieving efficient and consistent knockdown at 48 hours following transfection (Figure 4-1 - a). CD98hc knockdown cells demonstrated significantly reduced CMS-induced IL-8 release when compared to siRNA control or untreated cells (Figure 4-1 - b). Furthermore, cell viability as assessed by MTT assay was not significantly different between conditions (Figure 4-1 - c) and there was no difference in the ability of CD98hc knockdown cells to generate IL-8 in response to IL-1β treatment than controls. Finally, CD98hc kd demonstrated a significant ability to reduce CD98hc mRNA expression in addition to protein, but there was a limited decrease in IL-8 mRNA expression following application of CMS (Figure 4-1 – e-f).

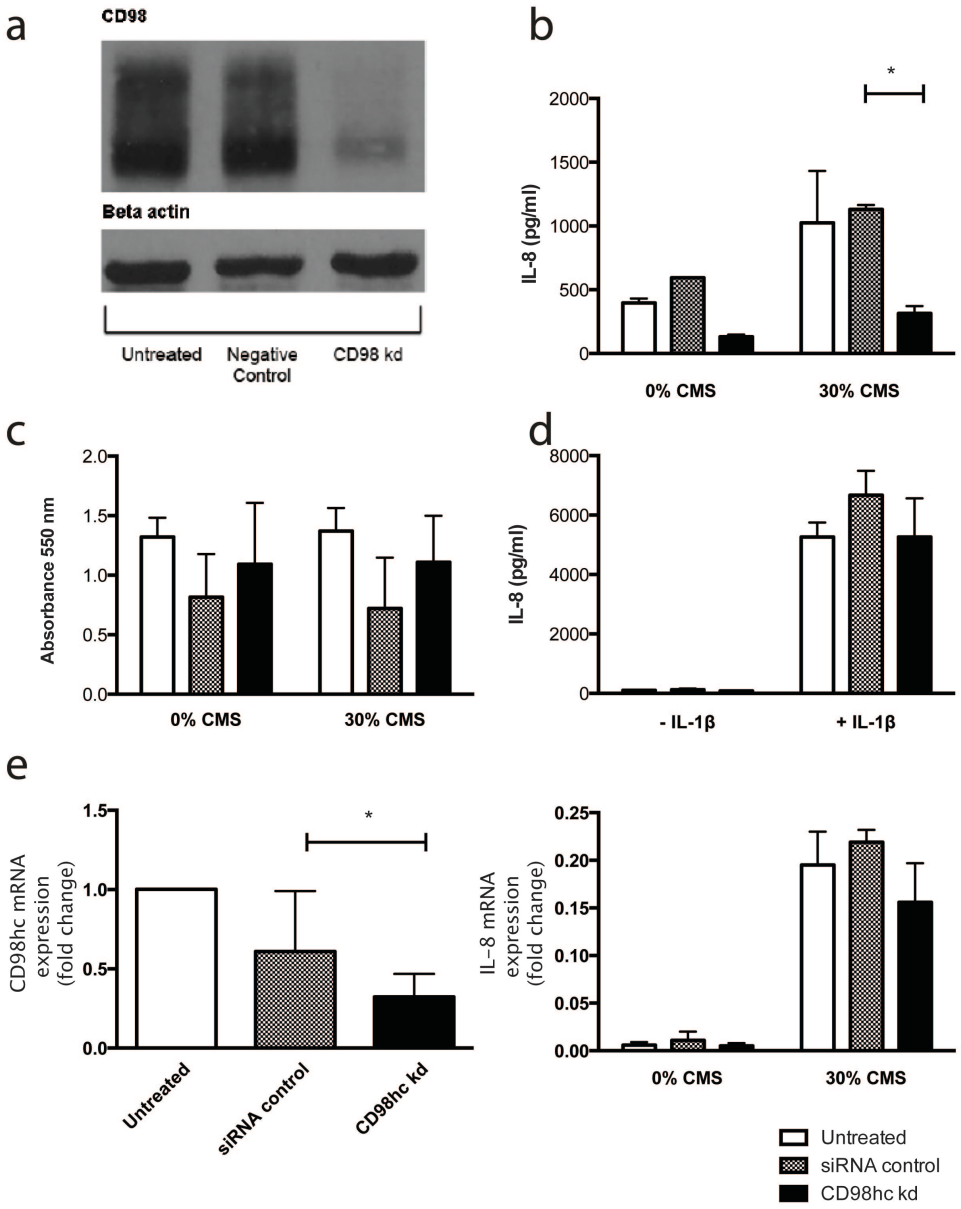


Figure 4-1 The effect of CD98hc knockdown on CMS-induced IL-8 protein and gene expression

Panel A shows densitometry from western blot for CD98hc following either no treatment (untreated), vehicle + scrambled siRNA sequence (siRNA control) or CD98 knockdown (CD98hc kd) relative to β–actin. Panel B shows IL-8 cytokine released from cells following exposure to either static (0% CMS) or 30% CMS conditions. Panel C shows cell viability as assessed by MTT assay of cells with respective treatments under either static or CMS conditions. Panel D shows IL-8 cytokine release for cells from respective conditions treated with either control or IL-1 β. Panel E shows CD98hc mRNA expression relative to untreated cells for cells treated with either siRNA control or CD98hc kd. Panel F shows IL-8 mRNA expression for cells with respective treatments exposed to either static or CMS conditions. For panels E—F, data are presented as fold change in expression (ΔΔCT) for the average of two housekeeping genes (GAPDH and B2M), and normalized for untreated control conditions. All data are presented as the median ± IQR of three independent experiments. Statistical analysis was by Friedman's test with Dunn's post-test correction for Panel B and by Wilcoxon test for Panel E, * $p<0.05$.

4.3.2 The effect of CD98hc knockdown on CMS-induced β1-integrin and MAPK p42/44 (ERK 1/2) activity

CMS induced RhoA activity via activation of β1-integrin in fibroblasts (Guilluy et al. 2011), and CD98hc interacts with β1-integrins to modulate downstream signalling (Feral et al. 2005). To determine whether CMS promoted β1-integrin activation in alveolar epithelial cells, the HUTS4 antibody for β1 integrin in an extended (activated) conformation was used. At 5 and 10 minutes CMS, activated β1 integrin blots were more dense than for static conditions, although the differences in calculated optical density did not reach significance. At 30-120 minutes CMS, there was minimal difference seen in blot activity between conditions. To determine whether the application of CMS correlated with known pathways of CMS, blots were also probed for MAPK p42/44 at these time points, demonstrating an increase in blot density at 10 minutes CMS as expected (Figure 4-2 – a-b).

When this was repeated with untreated, siRNA control and CD98hc knockdown conditions, this trend did not occur and there was no observable gross difference between β1 integrin activity in all conditions, from 10-60 minutes CMS (Figure 4-2 – c-d). Immunofluorescence for β1 integrin demonstrated staining at focal adhesions, indicating that β1 integrin activity is not affected by CD98hc knockdown (Figure 4-2 – e).

In order to determine whether the difference in activated β1-integrin activity with CMS from untreated cells alone (Figure 4-2 – a-b) and control

cells following transfection (Figure 4-2 – c-d) was due to experimental setup, cells were plated in individual petri dishes, and integrin activity assessed at varying times following medium change. β1-integrin activation was greatest 5 minutes after medium change, suggesting that the results obtained in (Figure 4-2 – a-b) may be due to exposure of cells to ambient conditions, as this was not the case in (Figure 4-2 – c-d) due to experimental setup.

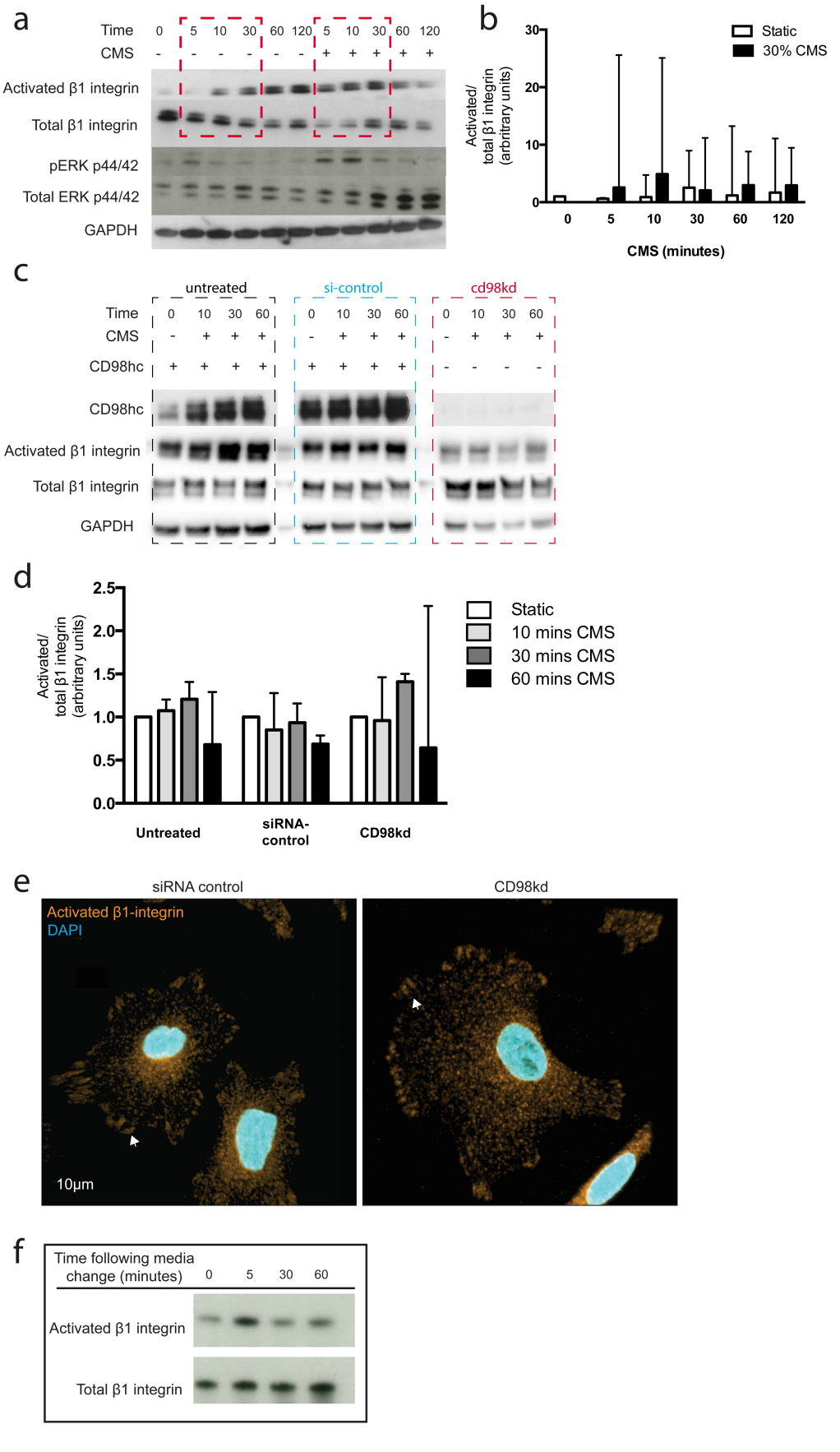

a
Time 0 5 10 30 60 120 5 10 30 60 120
CMS - - - - - - + + + + +
Activated β1 integrin
Total β1 integrin
pERK p44/42
Total ERK p44/42
GAPDH
b
Static
30% CMS
Activated/ total β1 integrin (arbritrary units)
30
20
10
0
0 5 10 30 60 120
CMS (minutes)
c
untreated
si-control
cd98kd
Time 0 10 30 60 0 10 30 60 0 10 30 60
CMS - + + + - + + + - + + +
CD98hc + + + + + + + + - - - -
CD98hc
Activated β1 integrin
Total β1 integrin
GAPDH
d
Activated/ total β1 integrin (arbritrary units)
2.5
2.0
1.5
1.0
0.5
0.0
Static
10 mins CMS
30 mins CMS
60 mins CMS
Untreated
siRNA-control
CD98kd
e
siRNA control
CD98kd
Activated β1-integrin
DAPI
10μm
f
Time following media change (minutes) 0 5 30 60
Activated β1 integrin
Total β1 integrin

Figure 4-2 The effect of CD98hc knockdown on CMS-induced β1-integrin activity

Panel A shows a time course of CMS whereby A549 cells were either static (CMS -) or stretched to 30% CMS (CMS +) from 0 to 120 minutes, and cells lysed and immunoblotted for activated β1-integrin (HUTS4). Panel B shows densitometry for blots at respective time points, normalised for 0 minute baseline. Panel C shows time course of blots for cells either untreated, treated with non-targeting siRNA (si-control) or with CD98hc knockdown siRNA. Panel D shows respective densitometry, normalised for 0 (static) time point for each condition. Panel E shows immunofluorescence staining for activated β1-integrin in si-control or CD98hc knockdown cells. Panel F shows immunoblots for activated β1-integrin in cells following medium change. Panels A-D: data for 3 individual experiments, shown as median ± IQR. Panel E-F: data for one experiment, scale bar = 10μm, arrowheads show positive staining at focal adhesions.

4.3.3 The effect of CD98hc knockdown on CMS-induced FAK and ERK activity, and on actin cytoskeletal integrity

Previous studies have shown CD98hc- β1-integrin interactions to induce FAK activation. Therefore, a time course of CMS was assessed for FAK phosphorylation with CD98hc knockdown. FAK phosphorylation at Y397 was increased by 60 mins in non-targeting control conditions as per previous results. CD98hc knockdown showed baseline phosphorylation with minimal changes over time, similar to that observed when cells were treated with Y27632. Phosphorylation of ERK 1/2 by 10 minutes CMS was preserved with CD98hc knockdown (Figure 4-3 – a). Furthermore, phalloidin staining of CD98hc knockdown cells demonstrated intact actin stress fibre formation, in comparison with cells treated with the ROCK inhibitor Y27632 (Figure 4-2– b).

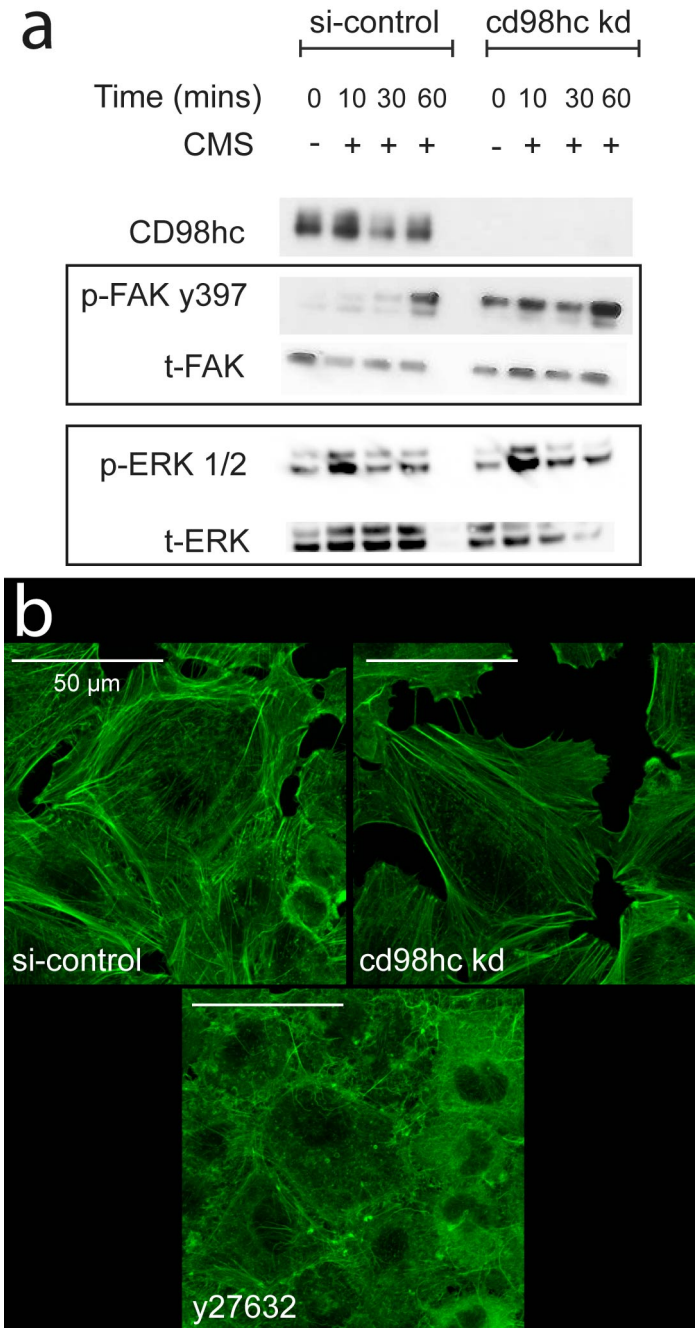


Figure 4-3 The effect of CD98hc knockdown on CMS-induced FAK and ERK activation, and on actin cytoskeletal integrity

Panel A shows immunoblots for FAK and ERK activation following treatment with either non-targeting siRNA (si-control) or with CD98hc knockdown siRNA (CD98hckd). Cells were lysed over a time course of 30% CMS from 0 mins (static) to 60 mins. The top panel shows expression of CD98hc in si-control or knockdown conditions. The middle panel shows phosphorylation of FAK (y397) in comparison with total FAK, and the bottom panel shows phosphorylation of ERK 1/2 in comparison with total ERK. Data are representative of three experiments performed per condition. Panel B shows immunofluorescence of phalloidin-stained cells treated with either non-targeting siRNA (si-control) or with CD98hc knockdown siRNA (cd98hc kd). Cells treated with the ROCK inhibitor Y27632 are shown for comparison. Scale bar – 50 µm.

4.3.4 The effect of CD98hc knockdown on baseline and CMS-induced cellular tension

CD98hc-null cells have demonstrated both reduced RhoA activity and tissue tension (Estrach et al. 2014). In order to assess the effect of CD98hc knockdown on baseline cellular tension and RhoA activity, dual transfection of cells with each FRET sensor combined with siRNA knockdown was attempted. An initial aim was to obtain FLIM data for respective sensors and to also image for CD98hc in order to determine whether cells in which FLIM data was acquired were expressing CD98hc. Both dual transfection and imaging was successful, and immunofluorescence for CD98hc demonstrated knockdown in cells expressing FRET sensors (Figure 4-4). However, FLIM acquisition of cells in these conditions was poor, and this was attributed to leaching of the FRET probe from cells due to the methanol fixation required for CD98hc immunofluorescence. When the experiment was repeated with PFA fixation, FLIM activity was similar to that seen in untreated cells.

Several observations were made from FLIM analysis of cells transfected with the VinTS probe. First, although a degree of heterogeneity was seen in the lifetimes of probes in all conditions, the mean lifetimes of both non-targeting siRNA control cells (1.77 ns) and of CD98hc cells (1.71ns) overlapped in the static state, with a trend towards decreased lifetimes (indicating decreased tension) with CD98hc kd. Following 1 minute of CMS, the mean lifetime of si-control cells was decreased to 1.75, and that for CD98hc kd cells increased to 1.93, indicating decreased and increased

tension respectively, following onset of CMS Figure 4-5. FRET efficiencies could not be calculated as described previously given the lack of an mTFP probe with which to derive uncomplexed donor lifetimes.

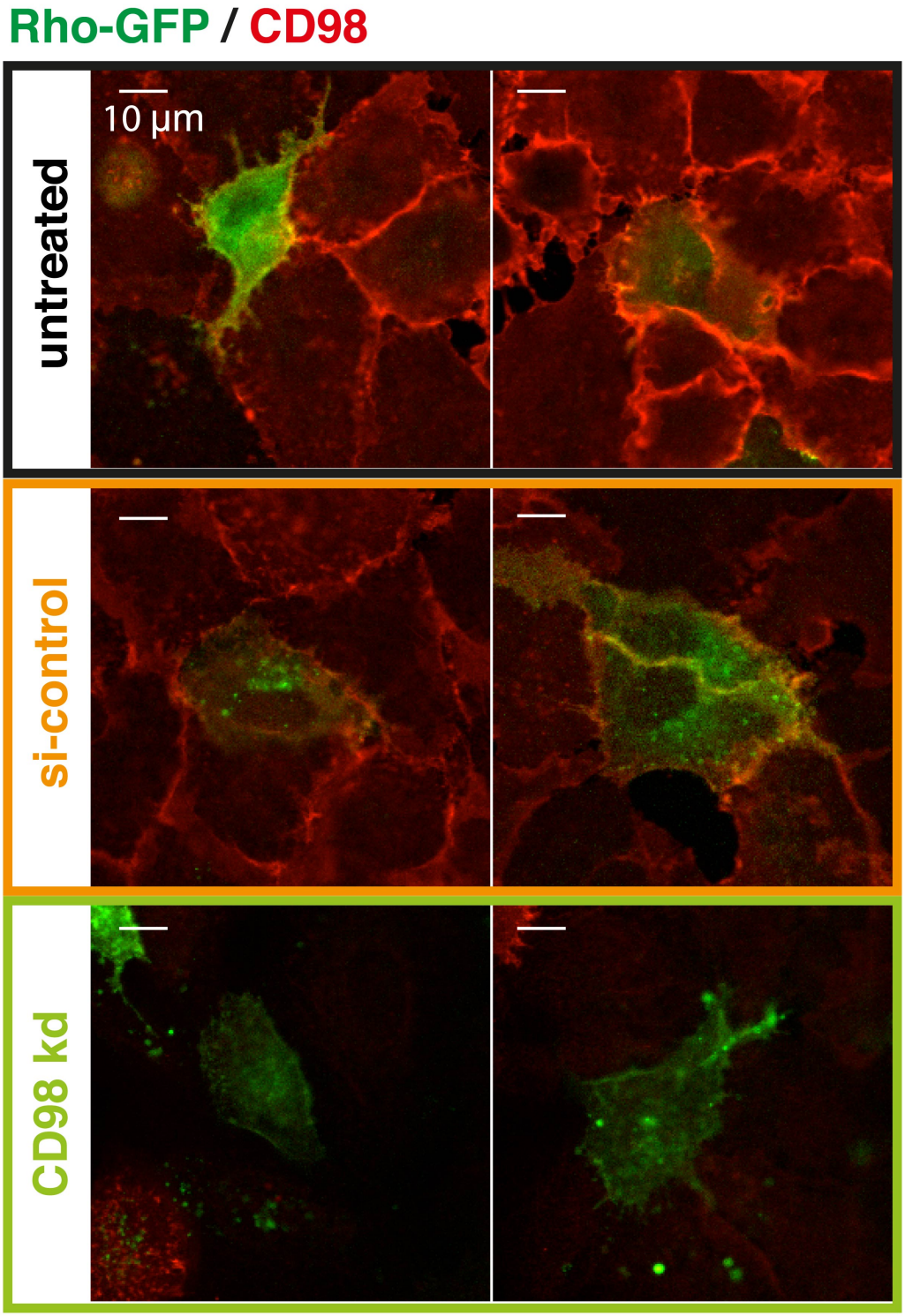


Figure 4-4 Dual transfection of A549 cells with CD98hc knockdown siRNA and RhoGFP FRET probe

Dual transfection of A549 cells with both CD98hc knockdown siRNA and Rho-GFP FRET probe, and immunofluorescence staining for CD98hc (red) and Rho-GFP (green). The top panel shows untreated cells, the middle panel shows cells treated with non-targeting control siRNA (si-control) and the bottom panel, cells treated with CD98hc knockdown siRNA. Images representative of 3-5 cells per condition. Scale bar - 10µm.

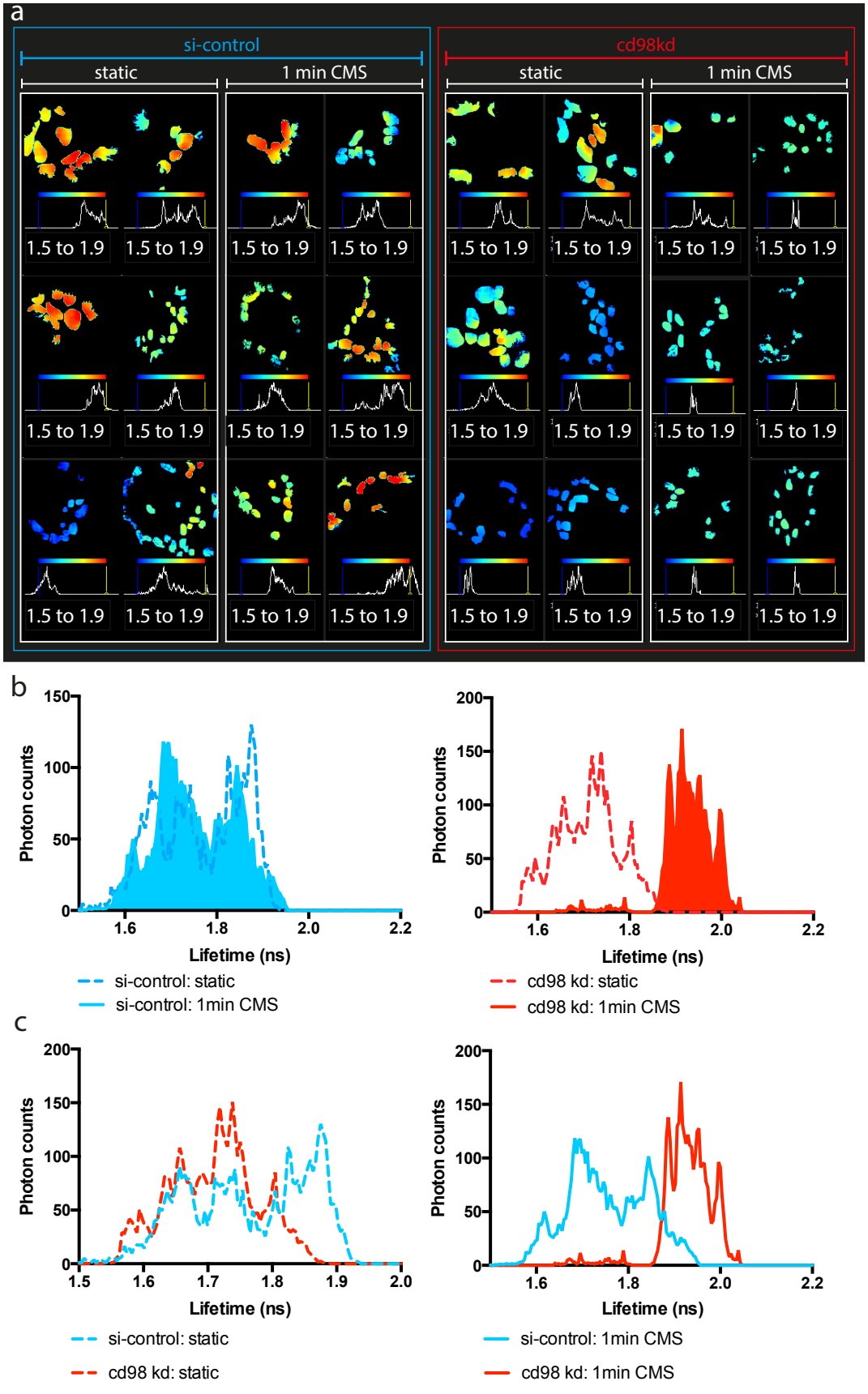
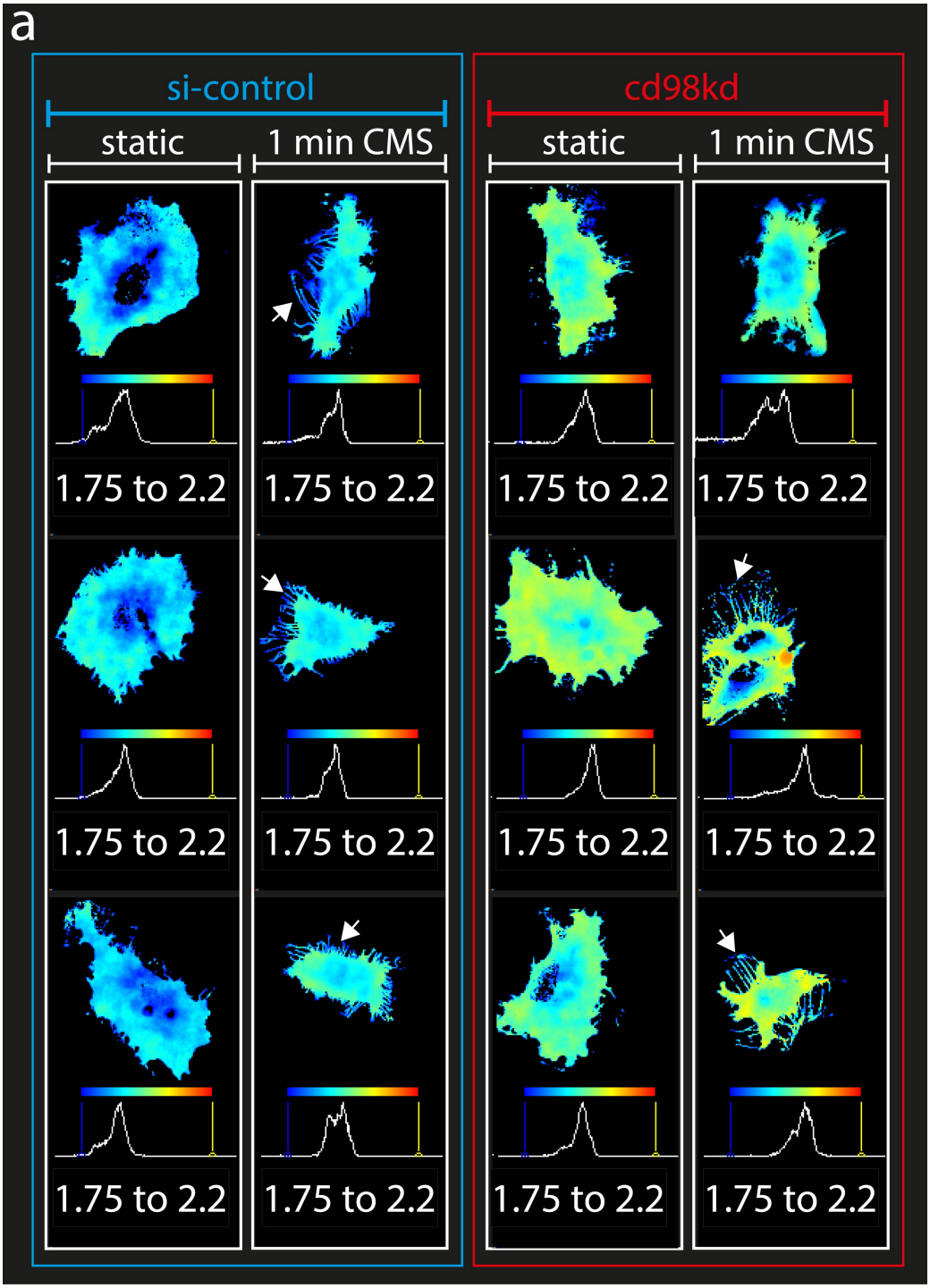


Figure 4-5 The effect of CD98hc knockdown on cellular traction forces

A549 cells were transfected with both CD98hc knockdown siRNA or non-targeting control (si-control), and the VinTs tension sensor, and subjected to either static conditions or 30% CMS for one minute. Panel A shows FLIM heat maps of cells from respective conditions. The blue end of the spectrum indicates short fluorescent lifetimes, whereas the red end suggests long lifetimes. Panel B shows combined histograms of lifetimes for cells treated with non-targeting controls for both static and 1 min CMS conditions on the left, and for CD98hc kd on the right. Panel C shows how histograms compare for both non-targeting controls and CD98hc kd under static conditions (left) and following 1 min CMS (right). Data shows histograms from 6 cells per condition.

4.3.5 The effect of CD98hc knockdown on RhoA activity

In order to ascertain the effect of CD98hc knockdown on RhoA activity, cells were transfected with both CD98hc kd siRNA and the Raichu RhoA probe. Results indicated that with both non-targeting controls and CD98hc knockdown treatment, 1 min of CMS induced the cellular protrusions seen with untreated cells. From these preliminary results, CD98hc knockdown significantly reduced baseline FRET efficiency (and therefore RhoA activity) in CD98hc kd cells when compared to controls. Following 1 minute CMS, there was no significant difference between both groups, although FRET efficiency (indicating RhoA activity) was noted to trend towards a decrease in si-control cells, and an increase in CD98hc cells, with CMS (Figure 4-6).


a
si-control
cd98kd
static
1 min CMS
static
1 min CMS
1.75 to 2.2
1.75 to 2.2
1.75 to 2.2
1.75 to 2.2
1.75 to 2.2
1.75 to 2.2
1.75 to 2.2
1.75 to 2.2
1.75 to 2.2
1.75 to 2.2
1.75 to 2.2
1.75 to 2.2

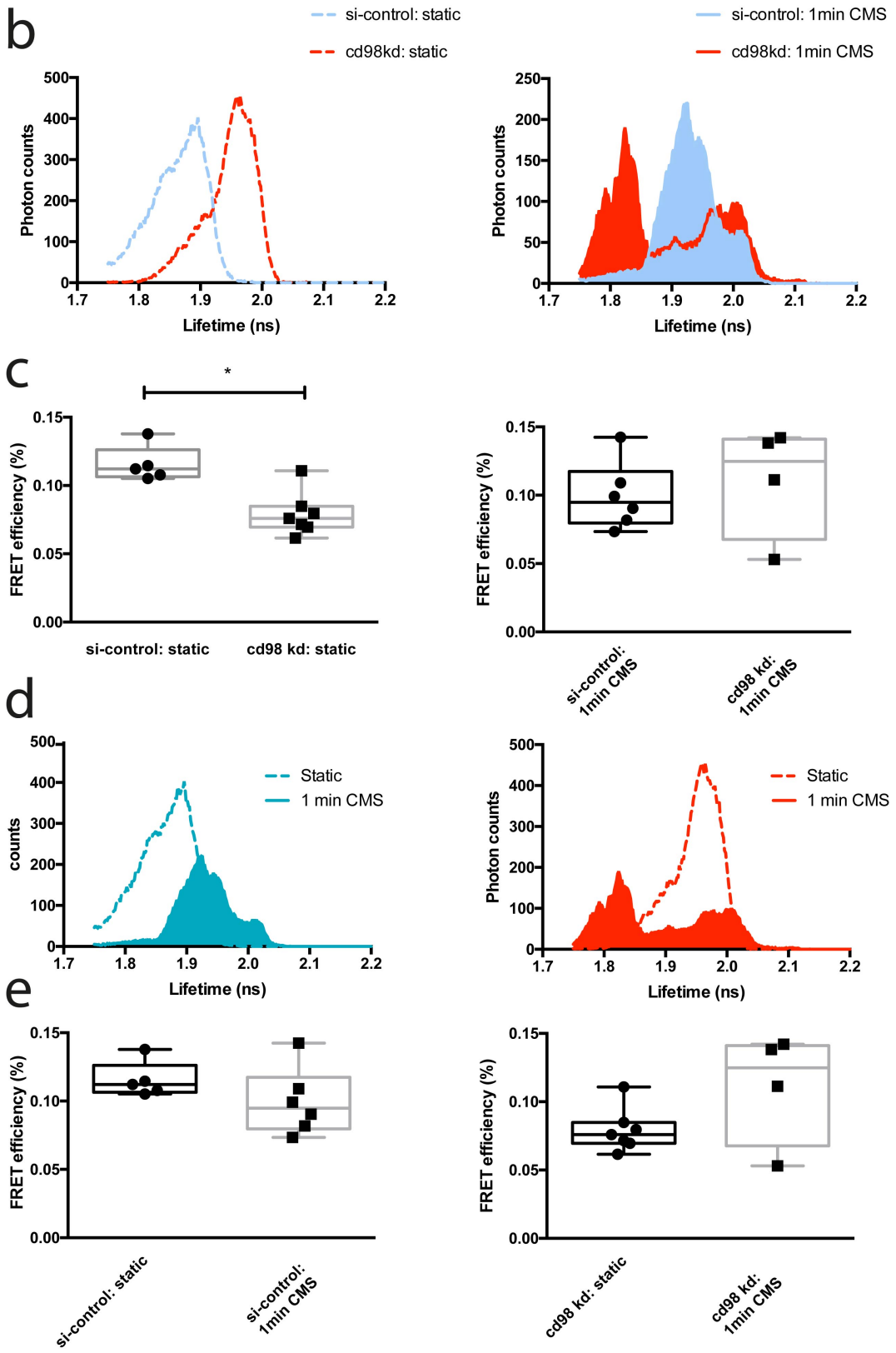


Figure 4-6 The effect of CD98hc knockdown on RhoA activity

A549 cells were transfected with both CD98hc knockdown siRNA or non-targeting control (si-control), and the Raichu RhoA FRET sensor, and subjected to either static conditions or 30% CMS for one minute. Panel A shows FLIM heat maps of cells from respective conditions. The blue end of the spectrum indicates short fluorescent lifetimes, whereas the red end suggests long lifetimes. Arrows indicate cellular protrusions noted following application of CMS. Panel B shows combined histograms of lifetimes for cells treated with non-targeting controls or CD98hc kd under static conditions on the left, and following 1 minute CMS on the right. Panel C shows FRET efficiencies for both treatments under static conditions on the left, and following 1 minute CMS on the right. Panel D shows combined histograms for non-targeting controls (left) and CD98hc knockdown (right) following both static and 1 min CMS conditions. Panel E shows FRET efficiencies for non-targeting controls (left) and CD98hc knockdown (right) following both static and 1 minute CMS conditions. Data are presented as the median ± IQR for 5 cells (si-control: static), 6 cells (CD98hc kd:static and si-control: 1 min CMS) and 4 cells (CD98hc kd: 1 min CMS). Data were analysed by Mann-Whitney test, *p<0.05.

4.3.6 The effect of CD98hc knockdown on epithelial cell migration in a wound healing model

Decreased expression of CD98hc reduced migration and survival in various cell types (Feral et al. 2005; Poettler et al. 2013). However, intact cell migration is critical for restoration of the injured alveolar epithelium (Atabai et al. 2002). Any potential therapeutic modality for VALI that disrupts alveolar epithelial cell migration may therefore be counterproductive.

To determine the effect of CD98hc kd on epithelial migration in response to a wound, a scratch wound was applied to confluent monolayers of transfected cells and controls that were either untreated, or treated with serum-free medium or IL-1β (20ng/ml). Although there was no difference in the percentage area healed at 16 hours between non-targeting control and CD98hc knockdown cells, there was also no difference found between untreated and IL-1β controls. Conversely, application of serum-free medium significantly reduced epithelial migration as expected (Figure 4-7 – a-b). To further elucidate the effect of different treatments on the migration of cells, the distance between DAPI-stained nuclei at the wound edge was assessed. In

this case, there were significant differences in internuclear distance between untreated and positive (IL-1β) or negative (serum-free) controls, but CD98hc did not significantly alter cell spreading (Figure 4-7 – c-d).

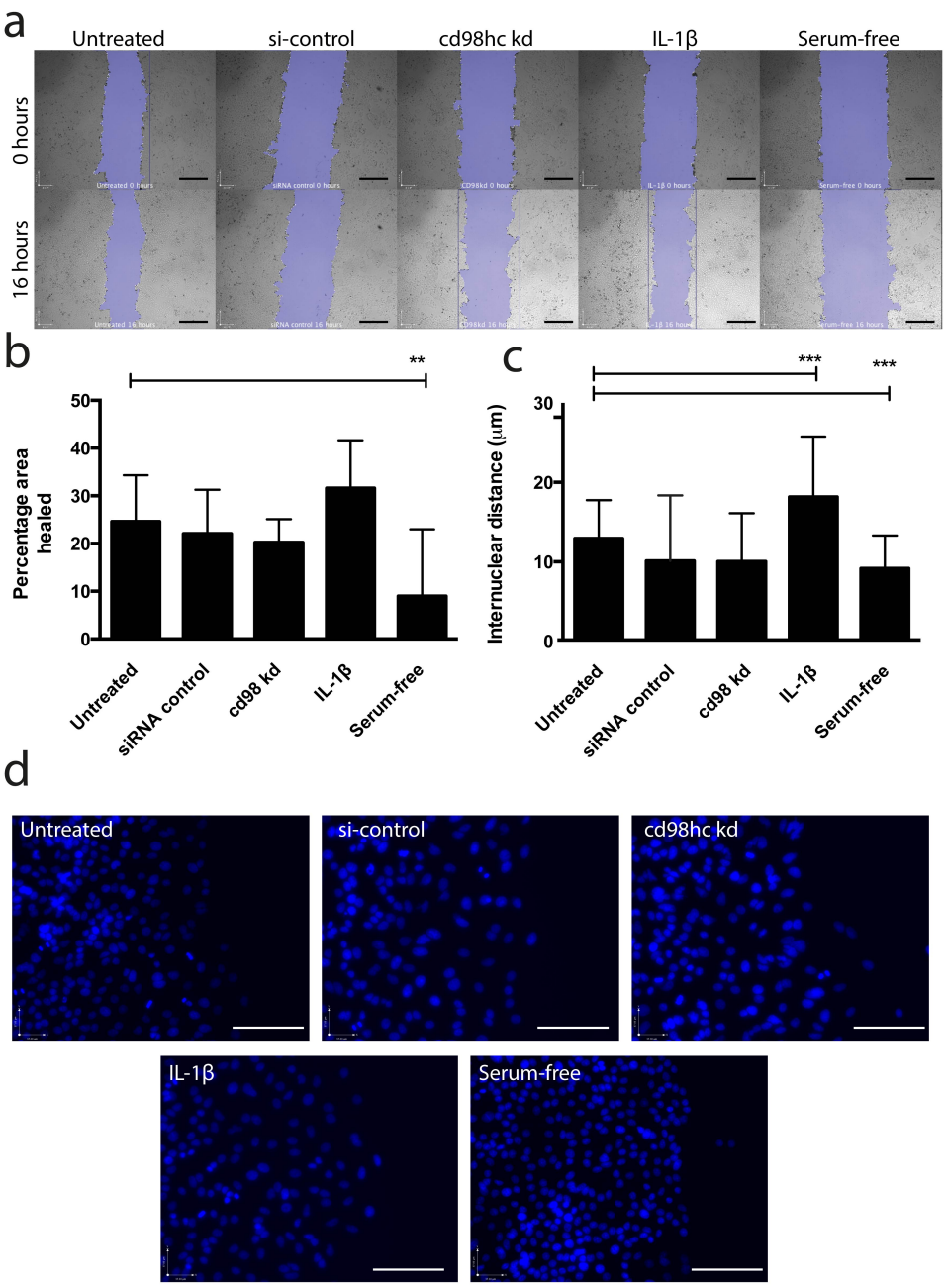


Figure 4-7 The effect of CD98hc knockdown on epithelial cell migration in a wound healing model

A549 cells seeded on 6-well plates were either untreated or transfected with non-targeting (si-control) or CD98hc siRNA (cd98hc kd), and grown to confluence. A scratch wound was applied across the well, controls treated with either serum-free medium or IL-1β (20ng/ml), and the percentage area healed calculated. Panel A shows representative images of wounds at 0 and 16 hours following scratching. Panel B shows calculated percentage of the area healed, and panel C the internuclear distance as a measure of cell spreading at the wound edge. Panel D shows representative images of DAPI-stained nuclei at the wound edge. Data are presented as the median ± IQR for three independent experiments for A and B, and analysed by paired Friedman test with Dunn's multiple comparison correction, and nuclei from one experiment for C and D, analysed by Kruskal-Wallis test with Dunn's multiple comparison correction, **p<0.01, ***p<0.001. Scale bars represent 100μm.

4.3.7 The effect of CD98hc knockdown on epithelial monolayer integrity

To measure epithelial monolayer integrity following CD98hc knockdown, trans-epithelial resistance to an electric current was used. Following transfection, there was an increase in the rate of increase of monolayer integrity with CD98hc kd cells compared to non-targeting siRNA-treated cells, but no differences between untreated controls and CD98hc knockdown cells (Figure 4-8 – a-b). Following the application of a wound to the monolayer, CD98hc had a slower rate of recovery of the wound when compared to non-targeting controls. IL-1β treated cells had a significantly increased recovery when compared to untreated controls Figure 4-8 – c-d).

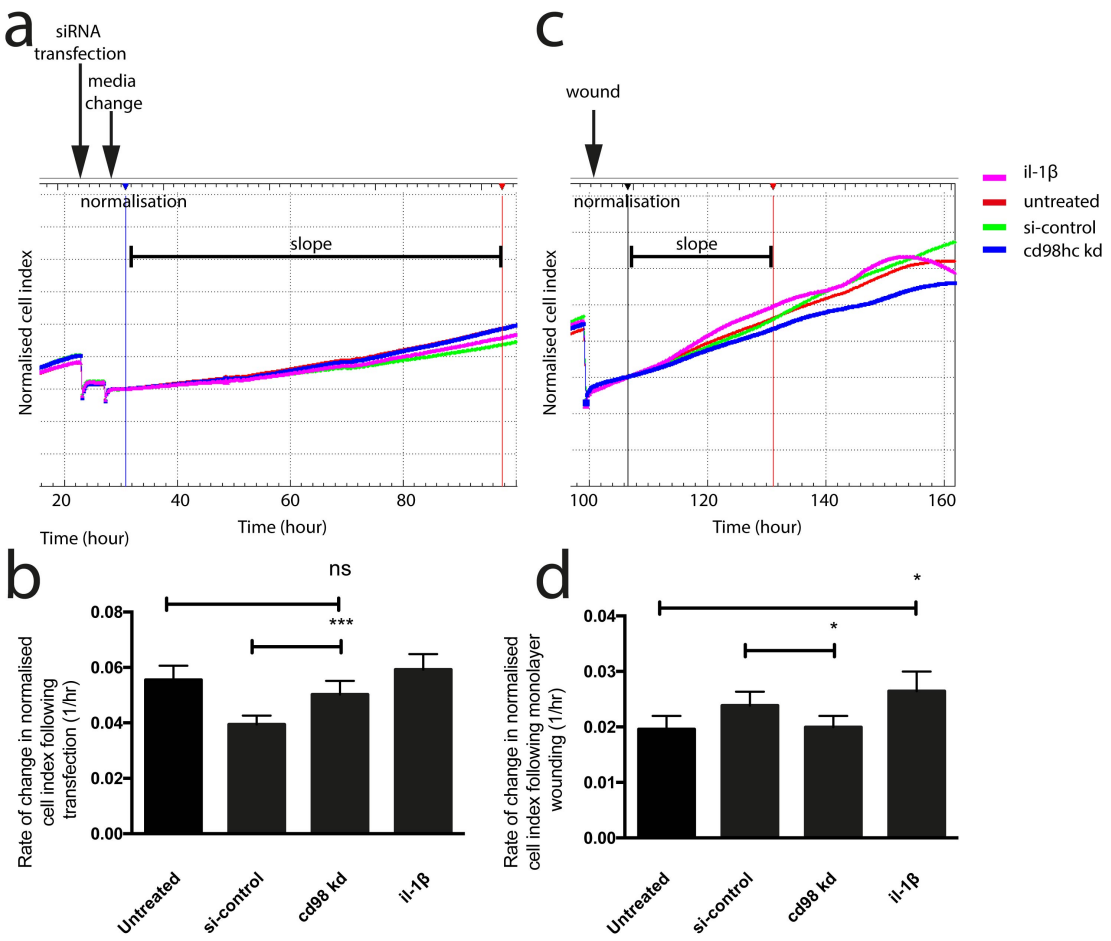


Figure 4-8 The effect of CD98hc knockdown on epithelial monolayer permeability as measured by trans-epithelial resistance

A549 cells seeded on collagen-coated ICELLigence 8-well electrode array plates were either untreated or transfected with non-targeting or CD98hc siRNA, and trans-epithelial resistance measured and presented as normalised cell index to represent resistance of the epithelial monolayer to an electric current. Panel A shows representative normalised cell index for the respective treatments following transfection for a period of approximately 60 hours until confluence was achieved. Panel B shows slope as a measure of change in normalised cell index over the measured time for respective treatments. Panel C shows representative normalised cell index for respective treatments over 24 hours following wounding of the monolayer. At this point, one well was treated with IL-1β (20 ng/ml). Panel D shows slope for respective treatments. Cell index measurements were collected every 10 minutes. Indices were normalised at the lines shown. Data are presented as the mean ± SEM and analysed by paired one-way ANOVA for the interactions shown, with Holm-Sidak's multiple comparison correction for n =12 from 4 independent experiments. *p<0.05, ***p<0.001.

4.3.8 The effect of CD98hc knockdown on cell-matrix adhesion

Inhibition of β1-integrin function can induce cell detachment from the ECM (Liu et al. 2011). A crystal violet assay was used to establish the effect

of CD98hc knockdown on cell-matrix adhesion and cell detachment following CMS. Firstly, optical densities of solubilised crystal violet decreased stepwise with decreasing cell seeding density, indicating that the assay was sensitive to decreases in cell number (Figure 4-9 – a-b). Secondly, CD98hc knockdown cells did not significantly affect cell adhesion following CMS when compared to static conditions, or untreated and non-targeting siRNA controls (Figure 4-9 – c-d).

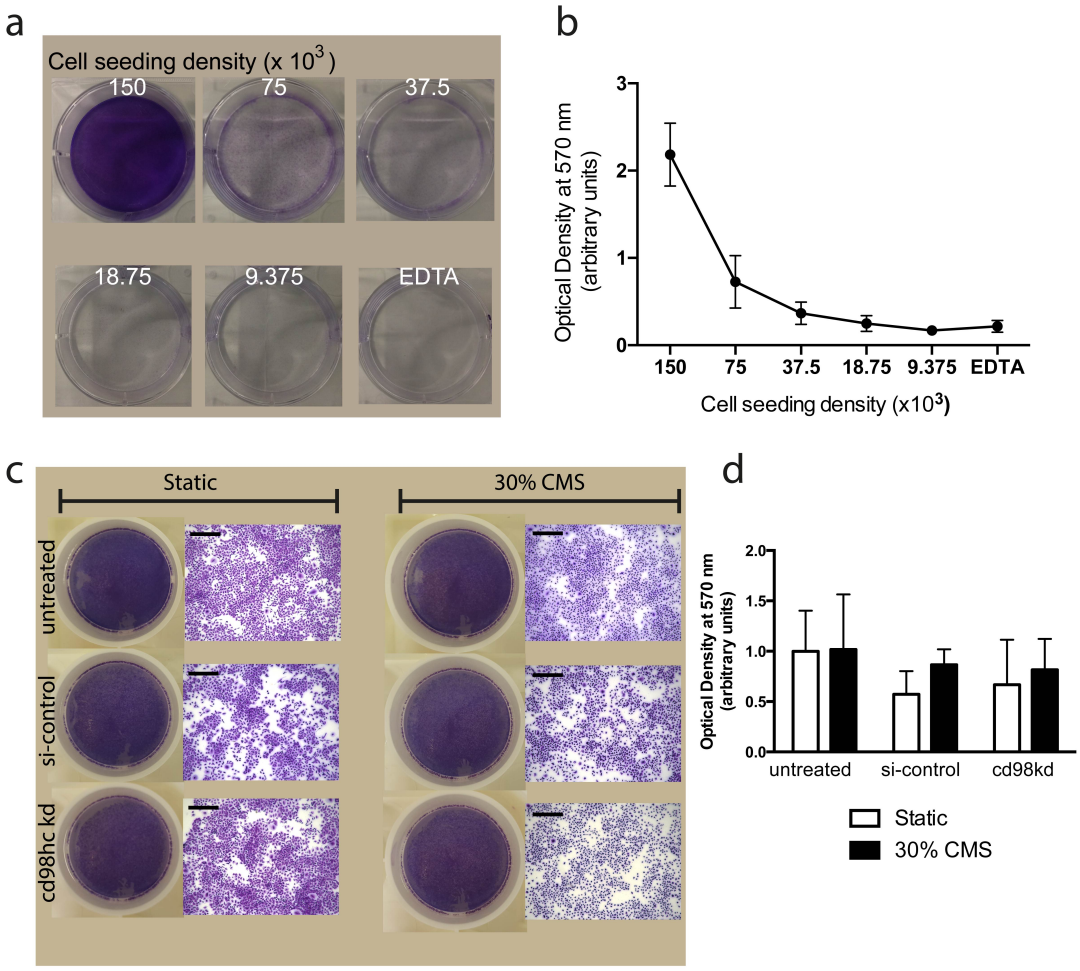


Figure 4-9 The effect of CD98hc kd on cell-matrix adhesion following CMS

Panel A shows photographs of wells containing crystal violet-stained cells seeded at different densities, with 5mM EDTA control (on cells seeded at 150 x 10^3). Panel B shows optical densities of solubilised crystal violet at the different seeding densities, read at 570nm wavelength. Panel C shows photographs of wells containing crystal violet-stained cells either untreated, or treated with non-targeting control siRNA (si-control) or with CD98hc knockdown siRNA (cd98 kd) and exposed to either static conditions, or 30% CMS for 2 hours. Insets show bright field microscopy at 5x magnification. Scale bars – 500µm. Panel D shows solubilised crystal violet from the different conditions, read at 570nm wavelength. Data shown as median ± IQR for 3 independent experiments for panels A-B, and n=6 from 3 independent experiments for C-D.

4.4 Discussion

4.4.1 Summary of results

The work in this chapter first aimed to establish the effect of CD98hc knockdown on mechanotransduction, integrin activity, and FAK activation in response to CMS. I demonstrated that CD98hc siRNA reduced expression of CD98hc on a protein and mRNA transcript level. CD98hc kd reduced CMS-induced IL-8 generation, without decreasing cell viability or the ability of cells to generate IL-8 in response to chemical stimulation. CD98hc knockdown did not reduce β1-integrin activity. However, knockdown did abrogate CMS-induced FAK autophosphorylation in a manner similar to that observed with inhibition of ROCK, but without the morphological changes seen with inhibition of that pathway. Phosphorylation of ERK 1/2 at 10 minutes CMS was preserved in knockdown cells.

I also aimed to determine whether CD98hc inhibition affected Rho-ROCK signalling by altering RhoA activity. I found that, from preliminary FLIM data using a RhoA FRET biosensor, CD98hc significantly reduced RhoA activity in comparison to non-targeting siRNA controls. Furthermore, there was a trend towards decreased cell-matrix tension in the knockdown cells when compared with controls, and whereas untreated cells demonstrated a decrease in tension following onset of CMS, the opposite was observed in CD98hc knockdown cells.

Finally, I also aimed to investigate the effect of CD98hc knockdown on the migratory and adhesive capacity of alveolar epithelial cells, and found

that, although CD98hc kd did not affect cell migration in an *in vitro* wound healing model, it did decrease the rate of healing in an impedance-based assay. However, CD98hc kd did not affect cell-matrix adhesion, and did not induce cell detachment following 2 hours CMS.

4.4.2 Mechanotransduction, integrin and focal adhesion signalling

My results demonstrated that CD98hc knockdown significantly reduced CMS-induced IL-8 generation without affecting cell viability or the ability of cells to release IL-8 in response to chemical stimulation. Interestingly, the effect of CD98hc kd on CMS-induced IL-8 mRNA transcription was minimal, which might suggest a post-translational effect of CD98hc on CMS-induced IL-8 release. However, the IL-8 response to chemical stimulation, in this case IL-1β, was intact following knockdown. This indicates that CD98hc kd does not affect IL-8 protein trafficking to such an extent as to inhibit this response. However, although these data might reflect the relative abundance of IL-8 mRNA transcript available for translation, the potential effect of CD98hc on post-translational modification in the context of these data must be taken into account. IL-8 undergoes significant post-translational NH2-terminal proteolytic processing (Mortier et al. 2008), and CD98hc kd may have an effect on this process.

Integrin β1 activity was preserved in CD98hc kd cells, indicating that CD98hc does not affect the activation of integrins in response to matrix rigidity (inside-out signalling) but may affect signalling downstream of integrin activation (outside-in signalling). Furthermore, CD98hc kd cells abrogated CMS-induced FAK activity in a manner similar to that observed with inhibition

of ROCK, without affecting CMS-induced ERK activation. However, although I initially observed a non-significant increase in β1- integrin activity with CMS in untreated cells, these observations were not repeated when the experimental setup was changed.

Mechanical force has been shown to promote β1-integrin function and downstream focal adhesion kinase signalling (Friedland et al. 2009), and tension applied directly to β1-integrins induced downstream RhoA activity (Guilluy et al. 2011). In the former study, α5β1-integrin bonds with fibronectin changed from a 'relaxed' state to tensed, cross-linkable bonds following the application of external force (centripetal force from a centrifuge), suggesting that mechanical force on integrins can increase bond or adhesion strength. Furthermore, inhibition of cytoskeletal tension by pharmacological inhibition of myosin II activity decreased the number of initial tensed bonds, but these could be induced with force, indicating that external force is sufficient to promote integrin-fibronectin bonding under tension as a model of outside-in signalling. Other studies corroborate such mechanical force-induced integrin activity. Cyclic stretch of renal epithelial cells increased β1-integrin mRNA expression (Hamzeh et al. 2015) to regulate downstream fibrotic signalling, and mechanical stretch of keratinocytes increased β1-integrin-mediated adhesion to substrate and ERK 1/2 activation, and promoted clustering of β1-integrins on the basal cell membrane (Knies et al. 2006). β3-integrins were also shown to activate in response to shear stresses (Tzima et al. 2001).

These phenomena may represent force-induced strengthening of integrin-ligand bonds. Experiments using atomic force microscopy of both

isolated integrin α5β1-fibronectin bonds and in K562 cells exposed to repetitive cyclic forces demonstrated an increase in bond strength in a manner described as cyclic mechanical reinforcement (Kong et al. 2013). Moreover, this reinforcement was positively correlated with increased strain rate, it required a flexible integrin hybrid domain, and was also specific to cyclic strain as opposed to tonic or linear strain.

CD98hc constitutively binds to the c-terminal domain of β1 and β3 integrin cytoplasmic tails (Zent et al. 2000; Rintoul et al. 2002; Prager et al. 2007) and regulates downstream β1-integrin signalling. Cross-linking CD98hc increased β1-integrin-mediated adhesion of small cell lung cancer cells (Fenczik et al. 1997), and stimulated downstream integrin signalling in an FAK-dependent manner (Rintoul et al. 2002). Moreover, it is the β1-integrin-binding cytoplasmic domain of CD98hc which promotes downstream integrin FAK and ERK activation, and tumour growth. Accordingly, transfection of dominant active FAK into CD98hc-null cells rescued CD98hc and integrin-dependent cell spreading behaviour (Poettler et al. 2013). These data suggest that CD98hc co-operates with β1-integrins to regulate integrin signalling via FAK.

To assess integrin activation status, I used the HUTS-4 antibody which detects β1-integrin in a high affinity conformation (Luque et al. 1996), specifically the hybrid domain (Byron et al. 2009) (Figure 4-10). This becomes exposed following the increase in hinge angle between the βA and hybrid domains when the integrin has high affinity for ligand (Luo et al. 2003).

Therefore, HUTS-4 has been used to detect activated β1-integrins by immunoblotting (Yao et al. 2013).

My results correspond with previous observations that β-integrin activity is not affected by CD98hc regulation as detected by a monoclonal antibody to an active conformation of β3 integrins, WOW -1 (Poettler et al. 2013), and CD98hc-null cells did not affect β1-integrin expression or β1-integrin-dependent fibronectin binding (Feral et al. 2005). Taken together, these observations suggest that CD98hc does not regulate inside-out integrin activity, but rather affects downstream integrin signalling.

Conversely, others have observed that CD98 knockdown in hepatocellular carcinoma cells significantly decreased β1- integrin activity, as demonstrated by the HUTS4 probe and downstream FAK activity. Overexpression of CD98hc had the opposite effect (Wu et al. 2015). These different observations may be accounted for by differences in experimental setup. First, hepatocellular carcinoma cells were used, which have a distinct ECM profile (Giannelli et al. 2001). Second, stable hairpin (shRNA) knockdown was used. Finally, membrane fractions were measured by flow cytometry.

I initially observed an (non-significant) increase in β1-integrin activity with 5-10 minutes CMS, which was not repeated when a different experimental technique was used. This led me to question whether repeated removal of cells from the incubator might increase β1-integrin activity. When individual petri dishes of cells were removed from the incubator and subjected to medium change, increased β1-integrin activity was observed 5 minutes

later, suggesting that changes in the ambient conditions of cells might affect integrin activity. Indeed, cells exposed to acidic environments demonstrated increased β3-integrin activity (Paradise et al. 2011). Furthermore, changes in oxygen concentration affects ECM composition (Vogel et al. 2017) and cell-matrix adhesion (Roan et al. 2012).

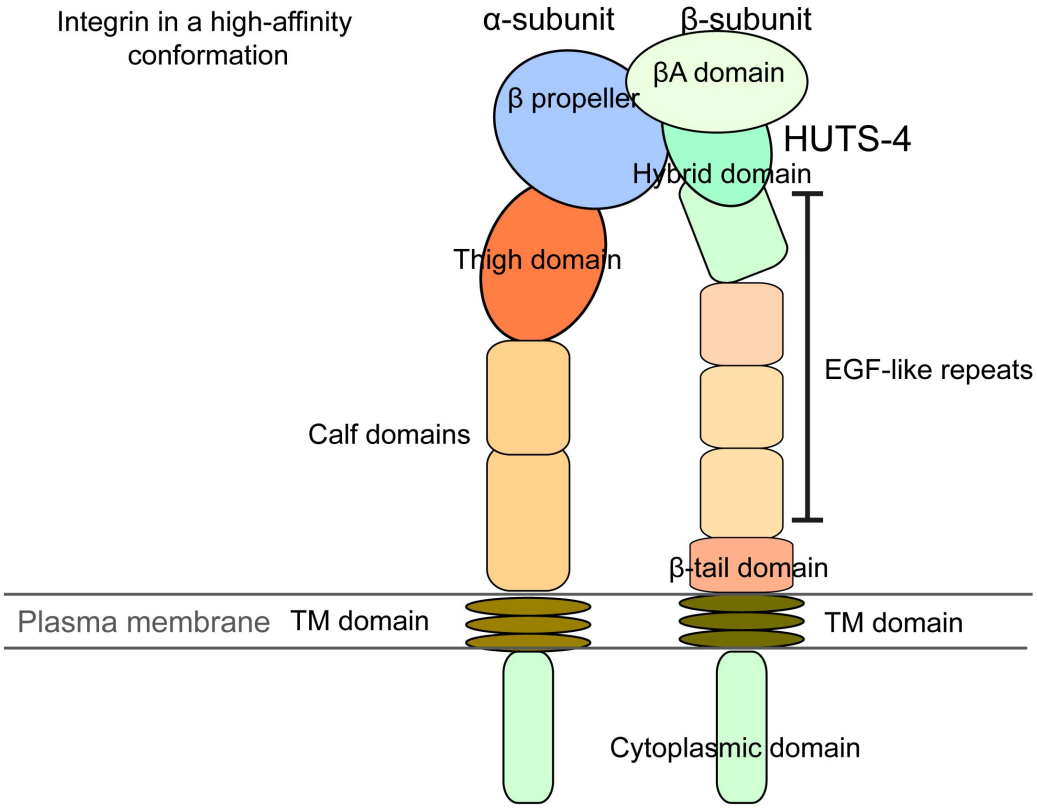


Figure 4-10 The HUTS4 antibody detects β1-integrin activation at the exposed hybrid domain in the high-affinity state

Based on (Byron et al. 2009). TM – transmembrane, EGF – epidermal growth factor.

I have investigated the activation status of β1-integrins only, and β1-integrins clearly play a critical role in mechanotransduction, particularly as β1, and not β3-integrins mediated traction forces in a Rho kinase and myosin-dependent manner in fibroblasts plated onto micropost arrays (Lin et al.

2013). However, it is becoming clear that the interplay between different integrin subtypes mediates different elements of cell adhesion and motility. Inhibition of integrin αvβ3 activation may not affect initial adhesion and spreading, which is mediated by α5β1 as shown in human osteosarcoma cells, but it is essential for the formation of stable focal adhesions (Schaufler et al. 2016). Furthermore, both α5β1 and αvβ6 integrins regulated rigidity sensing and the integrin-ECM bond dynamics in response to matrix stiffness (Elosegui-Artola et al. 2014) Other studies have shown that αvβ3 can fully compensate for loss of α5β1 integrins, and that both subtypes can support traction forces albeit at different magnitudes and with different cellular functional responses (Balcioglu et al. 2015). Therefore, it would be prudent to assess the activation states on an array of different integrin subtypes during CMS.

Finally, attempts were made to establish the efficacy of the probe by using positive controls of Mn^{2+} and Mg^{2+} to induce integrin activation, and this, together with the use of integrin-inhibiting antibodies, is part of ongoing work. Therefore, these results must be interpreted with caution until the sensitivity of the probe can be validated by robust controls such as these.

4.4.3 CD98hc–regulated tension at focal adhesions and RhoA activity

My previous results suggested a potential decrease in cell-matrix tension, as expressed across vinculin following 1 minute CMS (3.3.9). These changes correlated with an increase in RhoA expression following 1 minute CMS. Results from this chapter indicate that CD98hc may have an effect on

decreasing baseline cellular tension, but this cannot be concluded from these results. I can cautiously conclude from these data that CD98hc reduces baseline RhoA activity in A549 cells, but I aim to increase the rate of data collection from these FRET probes by using frequency domain FLIM before further conclusions can be made.

An initial decrease in cellular tension with onset of mechanical stretch may represent part of a dual response to CMS, reflecting an initial actin-mediated fluidisation of the cytoskeleton followed by cyclic force-induced strengthening, as previously discussed (1.6.2, 3.4.4). It may also represent a rupture in stress fibres, integrin-ECM bonds, or even of the FRET probe itself. CD98hc expression is associated with anchorage-independence and tumour progression in a manner thought to derive from its ability to amplify β1-integrin-mediated downstream signalling, therefore allowing cells to survive and proliferate in softer matrix environments (Cantor & Ginsberg 2012). In a Ras-driven model of squamous cell carcinoma, CD98hc-deficiency reduced epidermal thickness as demonstrated by AFM measurements, and this correlated with tumour regression (Estrach et al. 2014). The authors demonstrated that CD98hc-mediated β1-integrin signalling increased the stiffness of the tumour environment through increased RhoA activity and YAP/TAZ signalling. Similarly, CD98hc-mediated RhoA contractility has also been shown to regulate fibronectin matrix assembly (Féral et al. 2007), therefore further affecting integrin-ECM binding and also cellular traction forces.

In my model, CD98hc kd cells demonstrated a small reduction in baseline tension when compared to controls, but without affecting the morphological appearance of the actin cytoskeleton. That decreased baseline tension can reduce CMS-induced injurious signalling has been shown in alveolar epithelial cells subjected to hyperoxia, where an increased elastic modulus augmented CMS-induced cellular detachment (Roan et al. 2012), and this effect was prevented by inhibition of ROCK (Wilhelm et al. 2014).

I also witnessed a subsequent increase in tension when CD98hc kd cells were subjected to 1 min CMS when compared to controls. This could either be attributed to the fact that these cells have fewer broken stress fibres or adhesions, or that this follows universal mechanical properties governing cell pre-stress and response to strain. For example, when valvular interstitial cells were treated with inhibitors of myosin II to decrease their pre-stress, they increased traction forces in response to CMS, whereas cells with higher baseline pre-stress following TGF-β treatment dropped their traction forces with CMS (Cirka et al. 2016). This response was attributed to homeostatic maintenance of constant tension levels. My results give a preliminary indication that CD98hc knockdown cells may have behaved in this way, and that their reduced baseline pre-stress protected them from CMS-induced injury, as occurs following ROCK inhibition.

I therefore tried to ascertain RhoA activity in CD98kd before and during CMS, and from preliminary observations using FRET constructs, found that CD98hc knockdown reduced RhoA activity when compared with controls. These results correlate with previous observations in different cell types.

CD98hc-null fibroblasts failed to increase RhoA activity in response to interaction with a 3D matrix, but did in response to LPA (Féral et al. 2007). This led the authors to conclude that CD98hc is required for RhoA activation in response to cell-matrix adhesion. Subsequent studies demonstrated that RhoA activation was reduced in the CD98hc-deficient epidermis of mice (Boulter et al. 2013), and that downstream ROCK-mediated phosphorylation of the regulatory subunit of myosin phosphatase was also decreased (Estrach et al. 2014). These results suggest that CD98hc regulates cell stiffness via RhoA-ROCK and downstream myosin II and YAP/TAZ activity. This may influence stiffness-dependent injury in alveolar epithelial cells by increasing the elastic modulus (Wilhelm et al. 2014). Therefore, CD98hc may regulate RhoA-ROCK activity in alveolar epithelial cells to tune cellular stiffness and susceptibility to injury.

However, these results must be interpreted in the context of several limitations to my approach. First, cells were fixed at either static conditions or at 1 minute following CMS. Therefore, measurements of both cellular tension and RhoA activity can only be interpreted as a ‘snapshot’ at that time and may even be affected by the process of transfer from the flexcell bioreactor and of fixation. I attempted to develop a live stretch model using the Flexcell apparatus, but unfortunately to date have been unsuccessful due to difficulties with maintaining a focal plane during CMS. Newer methods of live-cell imaging with CMS should help overcome this (Rápalo et al. 2015).

Second, although I attempted to stain transfected cells for CD98hc to assess RhoA activity or cellular tension in cells positive or negative for

CD98hc, the methanol fixation required for CD98hc imaging precluded this due to effects on the image quality of the respective FRET probes. Therefore, I cannot be certain that each of the cells assessed as CD98hc kd are actually deplete of CD98. Finally, as encountered in other aspects of this work, it appears that the non-targeting siRNA used as a control has effects that differentiate it from untreated controls. This is not uncommon, is largely due to effects on complementary sequences, and may be overcome in future by the use of smart pool siRNA (Hannus et al. 2014).

Third, although I attempted to use inhibitors of RhoA and ROCK to validate the FRET probes, these proved problematic in reducing the size of focal adhesions which therefore precluded measurement of cellular tension. However, both the RhoA inhibitor, C3 transferase, and the RhoA activator, calpeptin or LPA, will be used for ongoing investigation of RhoA activation in CMS and the role of CD98hc. These positive and negative controls will increase the robustness of the results obtained using the probes.

Therefore, I cannot be absolutely certain that CD98hc kd reduces baseline RhoA activity to reduce myosin II-mediated cellular stiffness and therefore susceptibility to CMS-induced injury without addressing these issues. The FRET-based approach was selected as it provides greater spatial information on RhoA activity on a cell-by-cell basis (Heasman et al. 2010) (Pertz et al. 2006). However, I also attempted to use rhotekin-bound pulldown techniques to assess active, GTP-bound RhoA with CD98hc knockdown but internal controls demonstrated that the technique did not work consistently. An alternative approach is an ELISA-based assay, previously used to

ascertain the role of CD98hc on RhoA activity (Féral et al. 2007). A combination of all three methods would be expected to provide better clarity. Finally, a ‘rescue’ of RhoA activity in CD98hc kd cells, possibly using calpeptin or LPA, would also provide more evidence in favour of a RhoA-mediated effect of CD98hc on cell stiffness and mechanotransduction.

4.4.4 Migration and adhesion

Alveolar epithelial cell migration is critical for restoration of the denuded basement membrane following injury (Crosby & Waters 2010), and β1-integrin and RhoA signalling are instrumental for this process (Shen et al. 2015). Therefore, I expected any interference in these signalling pathways to have a prohibitive effect on alveolar cell migration in response to a wound, and on cell adhesion during CMS. CD98hc depletion inhibited β1-integrin-dependent spreading and migration in renal epithelial cells (Poettler et al. 2013), in embryonic stem cells via the RhoGTPase Rac (Feral et al. 2005), and in epidermal cells via impaired RhoA signalling in response to a wound (Boulter et al. 2013).

A scratch assay is a well-documented experiment allowing assessment of epithelial migration in response to a ‘wound’ in a monolayer of cells (Liang et al. 2007) and has previously been used in alveolar epithelial cells (Geiser et al. 2000; T. Geiser et al. 2001). 16 hours was selected as the optimal time point to detect closure rates, as longer durations led to complete closure of wounds, with the risk of contact inhibition confounding results (Puliafito et al. 2012). Other studies with alveolar epithelial or A549 cells used an 18 hour time point (Ng-Blichfeldt et al. 2017; T. Geiser et al. 2001).

There were no differences detected in the percentage area of the wound healed between CD98hc kd cells and untreated or non-targeting controls, or in inter-nuclear distance between cells at the wound edge. The fact that IL-1β treatment did not elicit a significant increase in healing in comparison to untreated controls, in contrast to previous observations (Geiser et al. 2000), suggests an impairment in the sensitivity of this assay in my hands. This was improved when inter-nuclear distance was measured, and significant differences between untreated, IL-1β –treated and serum-free controls were observed as expected from previous studies (Galiacy et al. 2003).

To improve sensitivity of the assay further, a method of continuous electrical impedance of the monolayer was assessed as a measure of monolayer permeability. Cell index is an arbitrary value derived from the real-time electrical impedance to electric current from the monolayer, and is proportional to the area of the well covered by cells (Rahim & Üren 2011). This method has previously been used to characterise cell adhesion in airway epithelial cells (Heijink et al. 2010). The rate of increase in electrical impedance following application of a wound to the monolayer was assessed, and in this case, CD98hc kd was observed to decrease the rate of wound healing when compared to siRNA controls in accordance with our hypothesis.

One explanation for this discrepancy between techniques may be that, as the use of 10% FCS increases wound healing significantly from serum-free conditions (Galiacy et al. 2003), the use of 10% serum throughout the conditions amplifies wound healing to such an extent that this overrides other factors, and differences between conditions cannot be easily detected. Serum

contains additional factors such as LPA that can promote wound healing and cell migration (Mills & Moolenaar 2003), and the use of a lower concentration of serum (such as 2%, 1% or serum starvation) may increase the sensitivity of the assay (Ng-Blichfeldt et al. 2017).

Another factor is that wound healing in this model may not be due to epithelial cell migration alone, as proliferation along the wound edge cannot be excluded. To overcome this issue, hydroxyurea has previously been used to inhibit proliferation (Grochot-Przeczek et al. 2009), and this will be considered in future experiments. However, previous assays of wound healing with ATII have demonstrated that proliferation does not mediate wound closure in these cells (Galiacy et al. 2003), although staining for proliferative markers such as ki67 or phospho-histone H3 (PH3) at the wound edge would confirm or refute this.

It was noted that the non-targeting siRNA control reduced cell impedance following transfection, whereas there were no observed differences between CD98hc kd cells and untreated controls. This again would suggest either off-target effects of the siRNA control, or cytotoxicity that is prevented by CD98hc kd. I previously observed no differences in cell viability between the different conditions as measured by MTT assay, suggesting that the defect is not due to cell death, but perhaps due to impairments in cell-matrix or cell-cell adhesion.

β1-integrin signalling can mediate cell adhesion to collagen fibrils (Jokinen et al. 2004), and therefore we aimed to determine whether targeting CD98hc would affect cell adhesion in the context of CMS in our system.

CD98hc mediates β1-integrin-mediated adhesion in renal epithelial cells (Cai et al. 2005), and lung (Fenczik et al. 1997) and breast (Chandrasekaran et al. 1999) cancer cells. Furthermore, high tidal volume ventilation (under hyperoxic conditions) decreased alveolar epithelial cell adhesion (Desai et al. 2007), and whereas transient disassembly of cell-matrix adhesions has been shown to be protect cells from stretch-induced injury, complete disassembly or inhibition of β1-integrin signalling does not, and actually promotes cell detachment and death (Liu et al. 2011).

My results suggest that CD98hc kd does not reduce adhesion in cells following CMS, using crystal violet staining and solubilisation immediately following CMS as previously described (Cai et al. 2005). However, whereas crosslinking or increased expression of CD98hc has been shown repeatedly to augment adhesion, other studies have found that decreased CD98hc expression does not necessarily decrease cell-matrix adhesion. For example, CD98hc null ES cells did not have impeded adhesion to fibronectin (Feral et al. 2005), and depletion of CD98hc did not affect keratinocyte adhesion to type I collagen (Boulter et al. 2013). This latter study also noted that CD98hc absence *in vivo* in the epidermis did not resemble adhesion defects resulting from β1-integrin loss. Taken together these data confirm results demonstrating that CD98hc does not affect β1-integrin activity *per se*, and therefore does not modulate the ability of cells to adhere or not. Its role may be to modulate strength of adhesions resulting from rigidity sensing and mechanotransduction via β1-integrin-mediated downstream signalling.

Whereas the adhesion protocol used correlated optical density of solubilised crystal violet staining with cell seeding density in a linear fashion (4.3.8), this does not confirm that it is sensitive to small reductions in cell number resulting from adhesion defects. More sensitive approaches may include staining fixed and adherent cells following CMS with live/dead markers, such as the calcein/ethidium homodimers, and counting cells per field, or reading the luminescence on a plate reader. This would have the additional advantage of identifying dead cells following CMS (Pipparelli et al. 2013). However, for the purposes of this study, this straightforward assay revealed no reduction in adhesion following CMS in CD98 knockdown cells when compared with controls.

4.4.5 Summary and limitations

In summary, I have shown that, although CD98hc knockdown did not affect β1-integrin activity, it did reduce CMS-induced cytokine generation and baseline RhoA activity in A549 cells compared to non-targeting controls. CD98hc kd also appeared to reduce baseline tension across focal adhesions, and this increased in response to 1 minute CMS unlike that observed in untreated and siRNA control cells. However, there was a reduction in the rate of epithelial migration to recover a wound in the epithelial monolayer (as measured by the electrical impedance assay). Therefore, my putative model for CD98hc-mediated mechanotransduction involves CD98hc regulating downstream RhoA and myosin II activation in the quiescent state, reducing cellular pre-stress and therefore the force propagated throughout the cell.

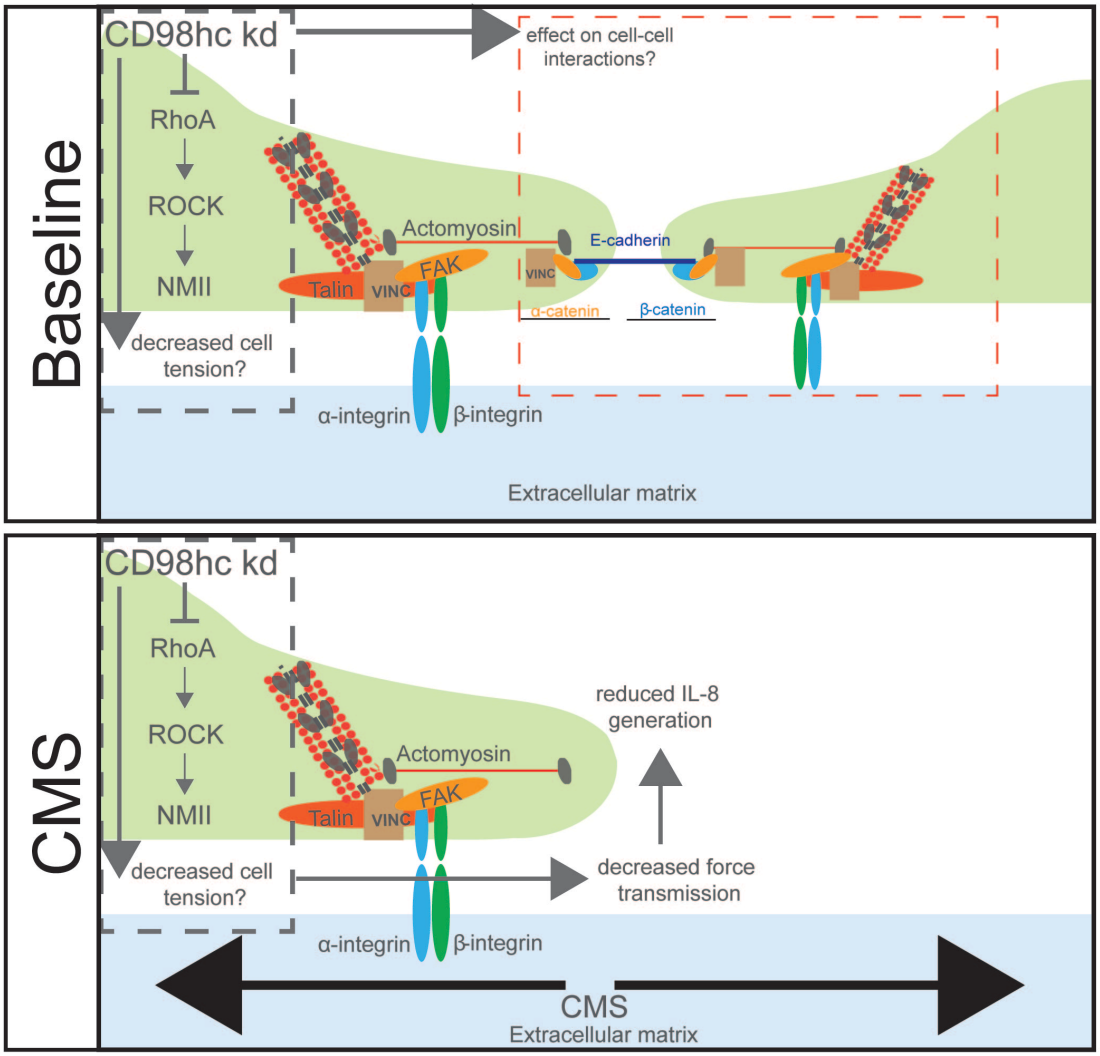


Figure 4-11 Putative mechanism for the effect of CD98hc kd on reducing CMS-induced injurious signalling

This putative mechanism involves CD98hc kd-mediated reduction of RhoA activity, reducing baseline 'pre-stress' or cellular tension via ROCK and non-muscle myosin II-mediated cellular contractility (upper panel). Therefore, when CMS is applied, there is decreased transmission of force throughout the cell, and a reduction in CMS-induced IL-8 generation (lower panel). The role of CD98hc on cell-cell adhesion/interactions has not been explored, and the effect of CD98hc kd on α- and β-catenin and E-cadherin, and subsequent effects of tension of the epithelial monolayer, would be an interesting avenue for further research (upper panel).

However, beyond the limitations of *in vitro* mechanotransduction experimentation using the Flexcell system discussed previously (3.4.6), the model of transfection could be optimised. Single-target siRNA to induce gene silencing are efficient, practical and cost effective, but limited by off-target

effects. We have seen that the non-targeting control siRNA induced differences in epithelial layer integrity, cellular tension and RhoA activity from untreated controls. One possible way to avoid such off-target effects in future is to use siRNA pools containing up to 60 low concentration siRNA sequences (Hannus et al. 2014).

The limitations of the work using the VinTS and RhoA FRET sensors have already been discussed both in general and when considering the CD98hc knockdown (4.4.3). Furthermore, the inability to image cells both for presence or absence of CD98hc and for FLIM of VinTS or RhoA constructs mean that results for cellular tension or RhoA activity for individual cells have to be assumed to be for CD98hc kd cells. The use of frequency domain FLIM will allow for a greater number of cells to be imaged in a shorter time, increasing the likelihood of the CD98hc kd population representing true knockdown.

4.4.6 Future directions

In addition to the optimisation steps discussed above, immediate future work would involve investigating the effect of CD98hc on signalling downstream of RhoA. RhoA activates myosin II through either phosphorylation of myosin light chain (Amano et al. 1996), or through inhibition, by phosphorylation, of myosin phosphatase (MYPT1) (Kawano et al. 1999). Brief attempts were made to ascertain the effect of CD98hc kd on ROCK-mediated activation of myosin II, via immunostaining for phosphorylation of myosin light chain 2 (pMLC2), but unfortunately without consistent results. Future investigations could focus on either pathway of

ROCK-mediated myosin regulation. Indeed, CD98hc deficiency decreased MYPT phosphorylation in murine epidermis (Estrach et al. 2014).

Furthermore, given that the RhoGEFs LARG and GEFH1 regulate mechanical force-induced integrin signalling and subsequent RhoA activation (Guilluy et al. 2011), a prudent step would be to examine the effect of CD98hc kd and CMS on expression of these two activation factors by mRNA or protein analysis. Furthermore, although I have shown that inhibition of NMII activation using blebbistatin decreased CMS-induced IL-8 generation, RhoGTP-ROCK activity can also regulate YAP/TAZ signalling, which act as mechanosensors and nuclear relays to dictate cellular size, proliferation and transformation in response to the cellular microenvironment (Dupont et al. 2011). CD98hc depletion decreased expression of the YAP/TAZ target genes, mANKRD1 and mCTGF in murine epidermis (Estrach et al. 2014). Therefore, further work would aim to examine the effect of CMS on YAP/TAZ signalling and nuclear translocation, and the effect of CD98hc kd on this.

One major aspect of CMS-induced mechanotransduction signalling that needs further exploration is the role of cell-cell adhesion and interactions. Silencing of CD98hc in HeLa cells triggered β-catenin degradation (Santiago-Gómez et al. 2013). Therefore, cell-cell tension, pre-stress and subsequent injurious mechanotransduction may be decreased in CD98hc kd cells through this mechanism.

Finally, silencing of CD98hc can be applied to more physiologically relevant models of CMS-induced injury. For example, blocking antibodies for CD98hc function were acquired with a view to application in PCLS subjected

to CMS, and although this was not possible in the lifetime of this thesis, it is still an option for future work in this field. Interestingly, siRNA technology was used to target CD98hc in intestinal cells *in vivo*. CD98hc siRNA complexed with polyethyeneimine (PEI), loaded into nanoparticles and administered as a hydrogel orally to mice decreased intestinal epithelial expression of CD98hc and reduced inflammatory colitis (Laroui et al. 2014). These exciting data demonstrate that CD98hc silencing can be realistically applied to *in vivo*, *ex vivo* or PCLS studies of injurious ventilation or CMS.

5 Chapter 5: Application of Cyclic Mechanical Strain (CMS) to Precision Cut Lung Slices (PCLS)

5.1 Introduction

Results from preceding chapters were obtained from the application of CMS to a monolayer of cultured cells. These therefore must be interpreted in the context of the limitations of this method, described earlier (2.2.4.1, 3.4.6). Although such an approach is valuable for understanding mechanistic processes in the alveolar epithelium, different approaches are needed to develop understanding of mechanotransduction in alveolae *in vivo*. Alveolar epithelial cells not only exist as part of an interconnected 3D structure (Ochs et al. 2004), they function in concert with a variety of different cell types, including fibroblasts, macrophages, and endothelial cells (Bagnato & Harari 2015). Therefore, to understand the effect of CMS on alveolar epithelial cell biology, a method incorporating these elements needs to be developed.

The generation and culture of precision cut lung slices (PCLS) allow for investigation of viable animal or human lung tissue, with near physiological characteristics. Properties of the ECM, and contacts between cells and matrix are grossly preserved (Liberati et al. 2010; Song et al. 2016). Furthermore, multiple PCLS can be generated from a small amount of lung (Dassow et al. 2010), enabling large-scale studies on valuable human lung material, and preservation of animal tissue. For these reasons, PCLS have been extensively used for toxicology, pharmacological and gene therapy studies (Sanderson 2011; Griesenbach et al. 2012; Liberati et al. 2010).

The work in this chapter is based on the hypothesis that PCLS can be used to investigate CMS-induced mechanotransduction in alveolar epithelial cells. Specifically, the aims of the work in this chapter are to determine whether:

a. CMS can be applied to PCLS without adversely affecting PCLS architecture or viability

b. application of CMS can induce cytokine generation in PCLS

c. PCLS can be used to investigate CMS-induced cell signalling and mechanotransduction processes.

To achieve these aims, I generated murine and human PCLS, and applied biaxial CMS using the Flexcell system.

5.2 Specific methods

Human or murine samples of lung were agarose-inflated and PCLS generated as described (2.2.2). For all experiments, PCLS generated from contiguous sections of lung were used as control and treatment groups. In this way, differences in anatomy between PCLS could be minimised. PCLS were adhered to the silicone membrane and CMS applied using application of ethyl-cyanoacrylate (Henkel) at points around the periphery of the PCLS using a dissection microscope (Figure 5-1). CMS was either not applied (0%/static) applied at 5% (CMS low) or applied at over 15% (CMS high) for the durations specified.

5.2.1 PCLS architecture following CMS

PCLS subjected to either static or CMS conditions were detached from the membrane and fixed in 10% neutral buffered formalin for 30 minutes, then washed and incubated in 70% ethanol prior to xylene washes and embedding in paraffin wax. Paraffin blocks containing embedded tissue were sectioned at 4μm thickness and stained for Haematoxylin and Eosin (H&E).

Surfactant Protein C (Pro-SPC) staining of PCLS was performed as described for immunofluorescence of PCLS (2.2.5.1.4), with incubation in rabbit Pro-SPC primary antibody (1:1000, Millipore) (Table 2-3).

5.2.2 CMS-induced cytokine release

Following CMS, PCLS were either left for specified durations or for 24 hours, and the supernatant obtained, clarified and stored at -80°C. MSD analysis was performed as described (2.2.6.2) for KC/GRO (murine) or IL-8 (human).

5.2.3 Assessment of PCLS viability

PCLS attached to silicone membranes were cut out, placed into ibidi 24-well plates with coverslip bottom (Ibidi µ-plate), and incubated with 4µM ethidium/calcein as described (2.2.2.3). They were then imaged immediately using an inverted microscope.

5.2.4 Cell proliferation in PCLS

PCLS were subjected to either static or CMS conditions, then fixed and processed for immunostaining at 24 hours as described (2.2.5.1.4). PCLS were incubated in primary antibody (rabbit anti-PH3, 1:1000, Millipore) (Table 2-3). The number of DAPI or PH3 positive nuclei was calculated using Imaris (Bitplane) software, and the ratio of the two determined.

To characterise the proliferating cells, PLCS were co-incubated with mouse anti E-cadherin antibody (1:1000, CST) (Table 2-3).

5.2.5 Visualisation of cytokine release in PCLS

PCLS were either untreated, or incubated with TNF-α at 10ng/ml or 100ng/m for 4 hours. PCLS were then fixed, permeabilised and blocked as described (2.2.5.1.4), and immunostaining for GRO-α performed. (Table 2-3).

Attempts were made to visualise intracellular GRO-α by adding brefeldin A (10μg/ml) with the TNF-α, and the above procedure was then followed.

5.2.6 Cytokine gene regulation in PCLS

To assess gene regulation in PCLS, slices were either untreated, or incubated with TNF-α at 10 or 100ng/ml. Following incubation for 4 hours, 3 PCLS for each condition were lysed in Trizol and homogenised. RNA was extracted as described (2.2.3.1) and assessed for quantity and quality using the high sensitivity RNA Tapestation system (Agilent Genomics). RT-PCR was performed as described (2.2.3.3) using the primers listed in (Table 2-1).

5.2.7 Assessment of ERK phosphorylation downstream of CMS

PCLS were either incubated in EGF (20ng/ml) for 30 minutes, or exposed to 0% CMS (static) or CMS high for 10 minutes. PCLS were then fixed, permeabilised, blocked and stained and imaged as described (2.2.5.1.4). The ratio of p-ERK positive nuclei to total, DAPI-stained, nuclei was calculated using Imaris software.

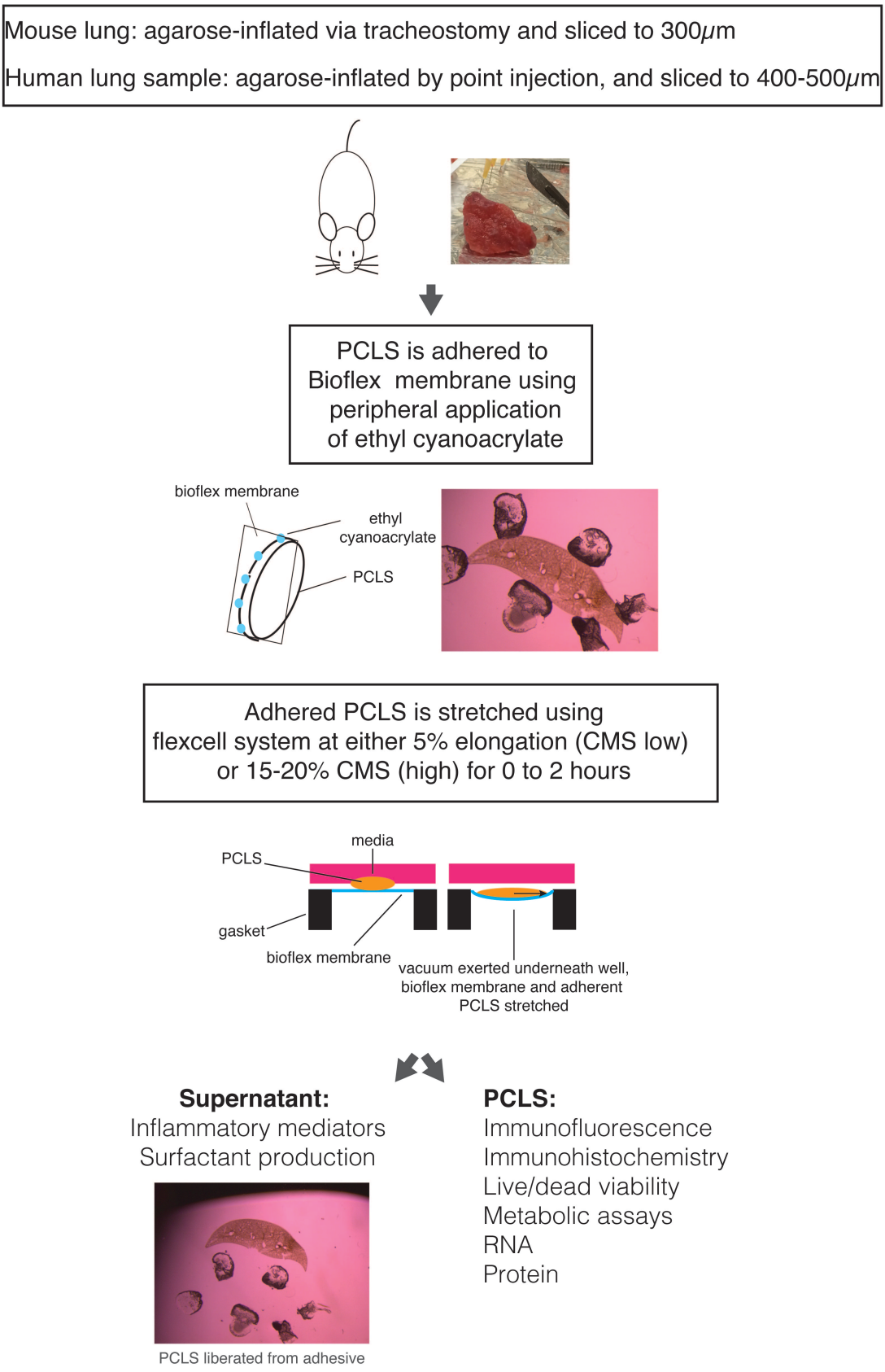


Figure 5-1 Proposed workflow for investigating CMS-induced signalling using PCLS

5.3 Results

5.3.1 PCLS architecture following CMS

Initial experiments were performed to assess the integrity of alveolar epithelial architecture following generation of murine PCLS, and application of CMS. H+E staining demonstrated preservation of the architecture of lung parenchyma. The presence of cell nuclei within alveolar septal walls was noted (Figure 5-2 - a).

Confocal immunofluorescence imaging of PCLS for cytoplasmic Pro-SPC showed numerous positive cells at baseline conditions, indicating the presence of ATII cells (Figure 5-2 - b).

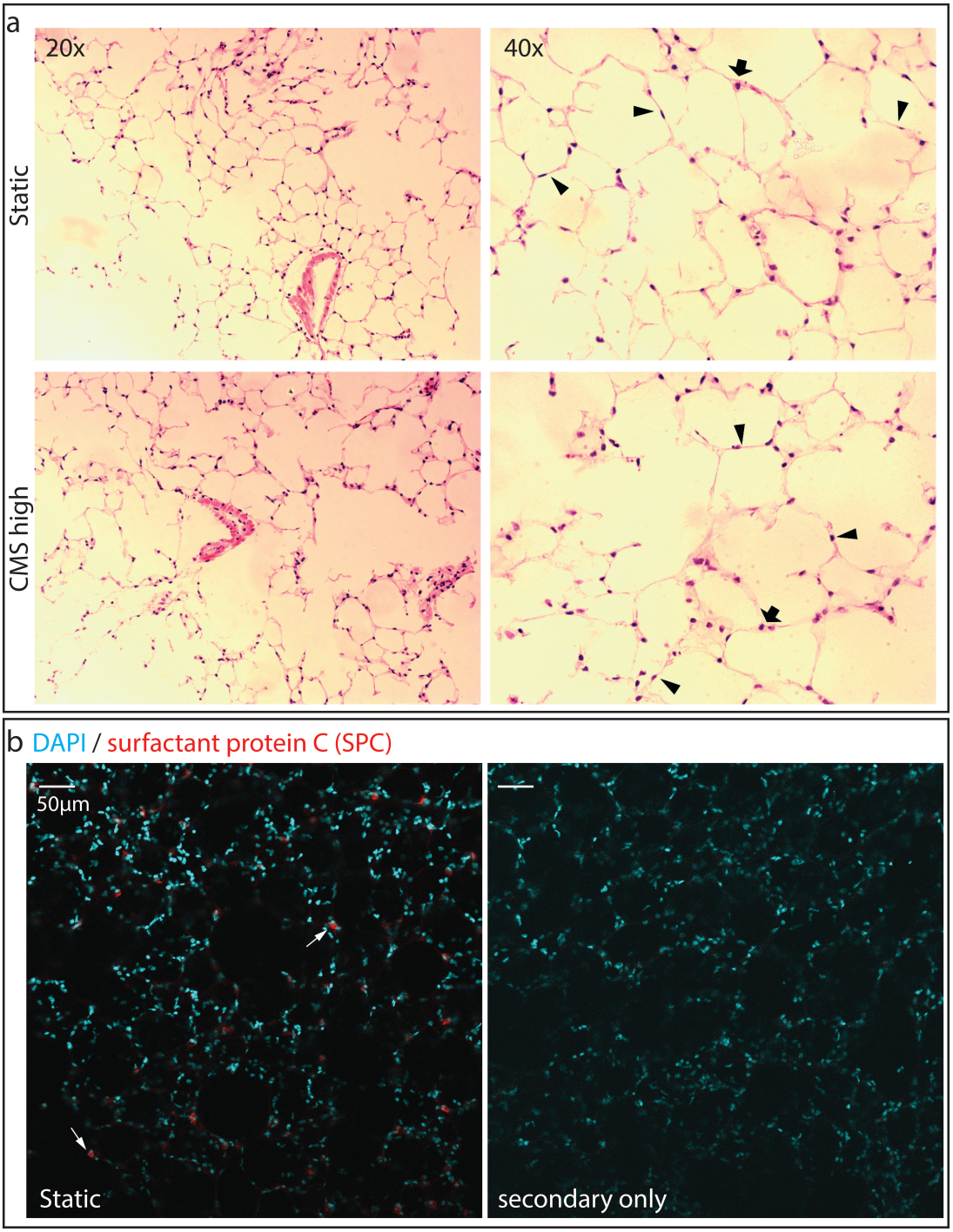


Figure 5-2 PCLS architecture following CMS

Panel A shows murine PCLS either un-stretched (static) or exposed to CMS high for 2 hours. PCLS were detached from the silicone membrane, fixed, paraffin-embedded and stained for haematoxylin and eosin (H&E). Phase contrast images shown are at 20x (left) and 40x (right) original magnification. Arrowheads show nuclei of ATI, and arrows ATII. Panel B shows confocal immunofluorescence images for murine PCLS stained for nuclei with DAPI (cyan) and pro-surfactant protein C (red) indicated by arrows. Images show baseline, static conditions on the left, and secondary-antibody only conditions (right). Scale bar – 50 µm.

5.3.2 CMS-induced cytokine release in murine PCLS

Murine PCLS were either unstretched, or subjected to CMS high for 2 hours. Supernatant was sampled at 4, 8 and 24 hours following this and KC/GRO release assessed by MSD assay. At 24 hours, KC/GRO was approximately 2 times greater than static controls, and so this time point was used for future assessments of CMS-induced cytokine release (Figure 5-3). One outlier was removed from these results due to KC/GRO release over 100 fold greater than other results.

Further studies revealed a CMS-dependent increase in KC/GRO release, with CMS-high significantly increasing cytokine generation by 1.8 times above static controls (Figure 5-3- b). The results for one experiment were removed due to grossly increased KC/GRO values across all conditions, attributed to technical anomalies.

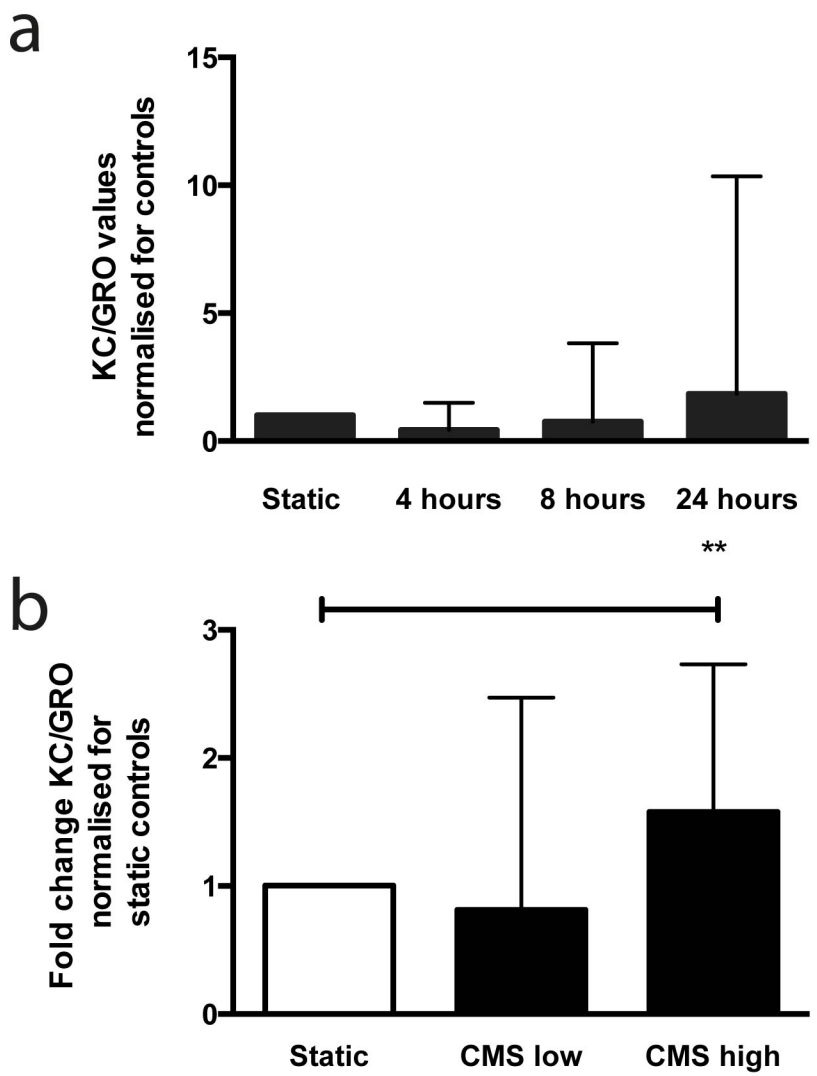


Figure 5-3 CMS-induced cytokine release in murine PCLS

Murine PCLS were subjected to either static conditions or CMS, and cytokine release assessed by MSD assay. Panel A shows fold changes in cytokine release at 4, 8 and 24 hours following CMS high of 2 hours duration when compared to static controls at those time points. Data represented as median ± IQR from 4 PCLS per time point (n=1) (one outlier excluded at 4 hours). Panel B shows IL-8 release at 24 hours in PCLS subjected to CMS low and high (fold change over static controls). Data represented as median ± IQR from 19 PCLS (CMS low) and 18 PCLS (CMS high), from 5 individual experiments (n=5), ** = $p<0.01$, Kruskal Wallis test with Dunn's post test.

5.3.3 CMS-induced cytokine release in human PCLS

To determine whether CMS induced relevant cytokine release in human PCLS, hPCLS were generated and subjected to CMS as described for 1-2 hours. 1 hour CMS induced a significant 5-fold increase in measured IL-8 release over static controls (Figure 5-4 – a), whereas 2 hours CMS induced a 75-fold increase (Figure 5-4 – b).

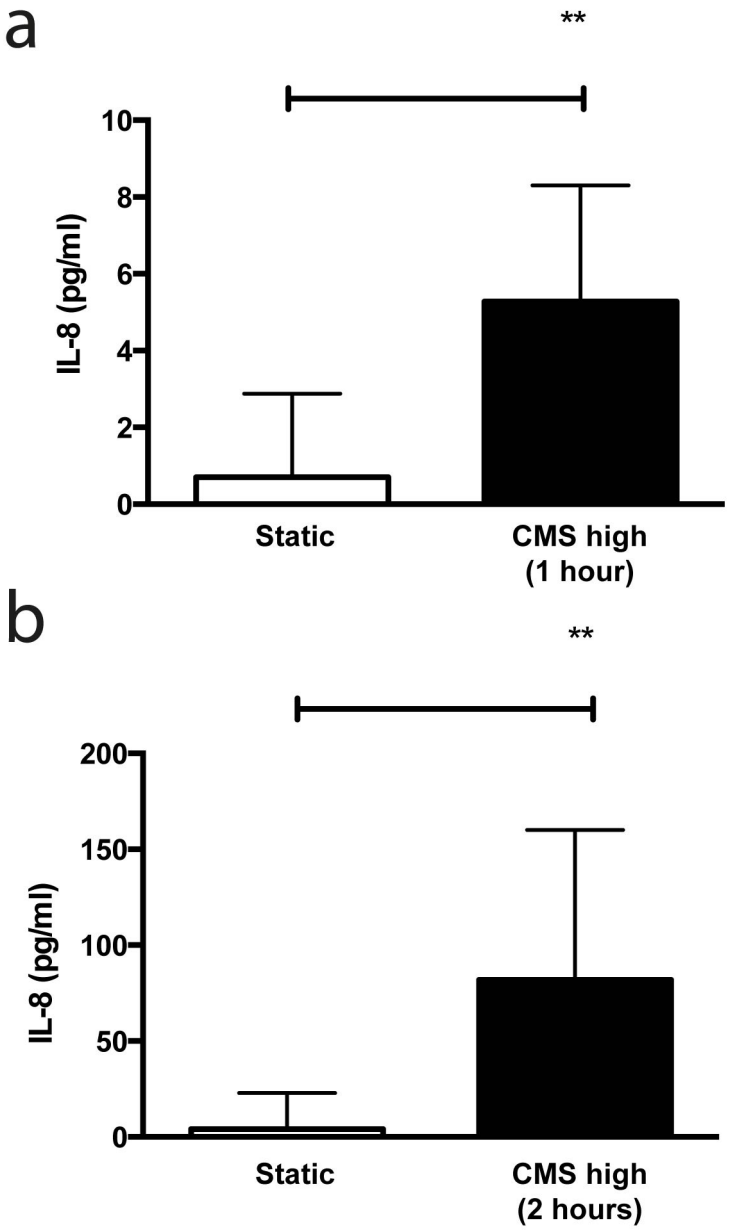


Figure 5-4 CMS-induced cytokine release in human PCLS

Human PCLS were generated and subjected to either static conditions or CMS for 1-2 hours. IL-8 release was assessed at 24 hours by MSD assay. Panel A shows IL-8 values (left) and fold changes in IL-8 release (right) for PCLS subjected to 1 hour CMS high when compared to static controls. Data represented as median ± IQR from 9 PCLS per time point from two individual specimens of lung (n=2). Panel B shows IL-8 values (left) for PCLS subjected to 2 hours CMS high when compared to static controls. Data represented as median ± IQR from 12 PCLS from 2 individual specimens of lung (n=2), ** = $p<0.01$, Wilcoxon paired analysis.

5.3.4 Viability of PCLS

Viability as assessed by staining live murine PCLS with calcein and ethidium homodimer, demonstrated numerous dead, ethidium-stained nuclei in PCLS following static, and CMS low and high conditions. However, calcein staining revealed viable cells in all conditions. In contrast, PCLS incubated with methanol were replete with ethidium-stained nuclei, but no calcein-stained cytoplasm (Figure 5-5).

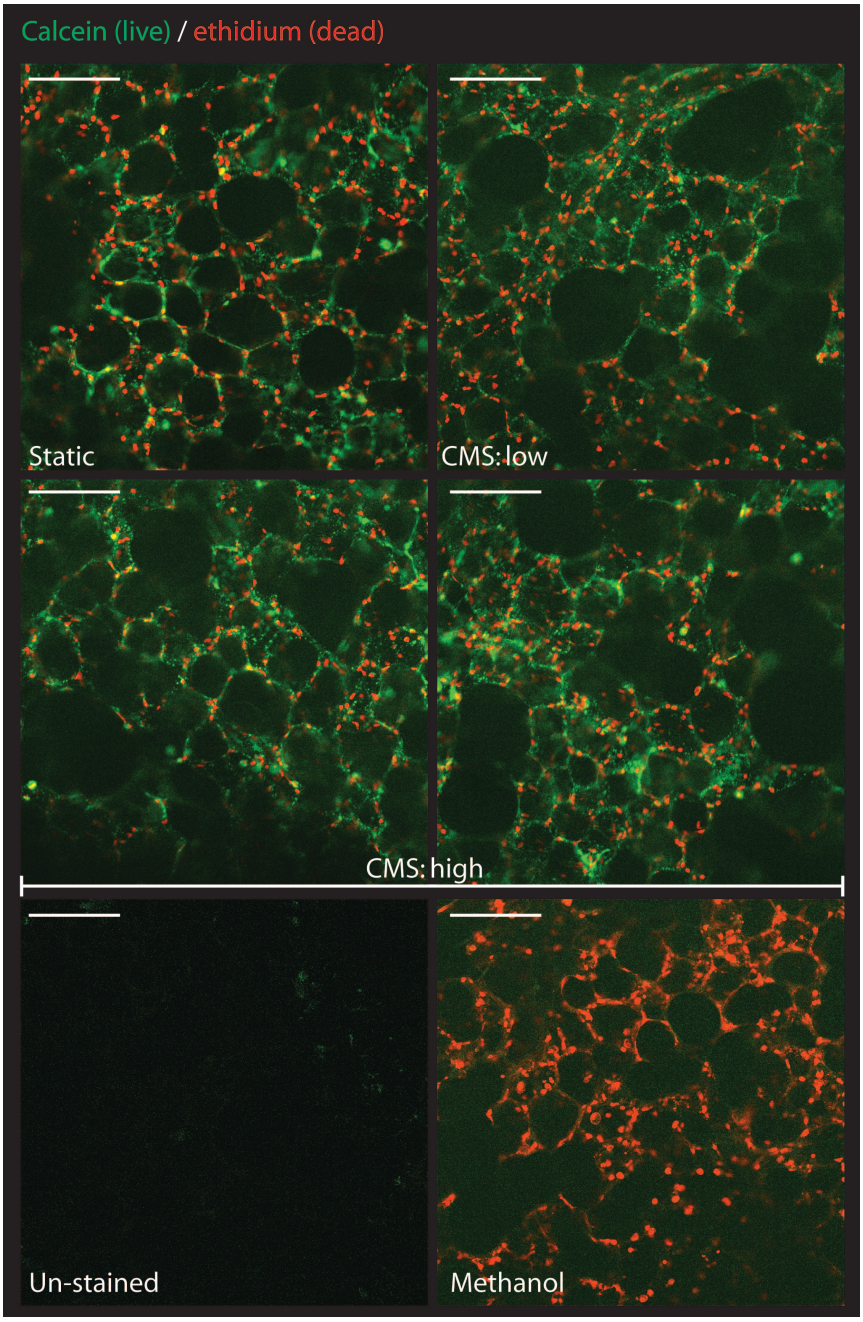


Figure 5-5 Viability of PCLS

Murine PCLS subjected to either 0% CMS (static – top left), CMS low (top right) or CMS high (central two images) were incubated with calcein and ethidium homodimer, then imaged using an inverted confocal microscope. Green, calcein-stained cytoplasm represent live cells, whereas red, ethidium-stained nuclei represent dead cells. Conditions were compared with either un-stained PCLS (bottom left) or methanol-treated PCLS (bottom right). Images representative of two PCLS per condition, scale bar – 100 μm).

5.3.5 Cell proliferation in murine PCLS exposed to CMS

To determine whether CMS affects alveolar epithelial cell proliferation, murine PCLS at either static, CMS low or CMS high conditions were fixed and imaged for the proliferation marker PH3 and the ratio of PH3-positive nuclei against total DAPI-stained nuclei calculated using Imaris software. CMS low conditions induced a 3-fold increase in proliferating cells compared to static controls, although a high SEM was observed. CMS high conditions induced a 1.8 times increase (Figure 5-6).

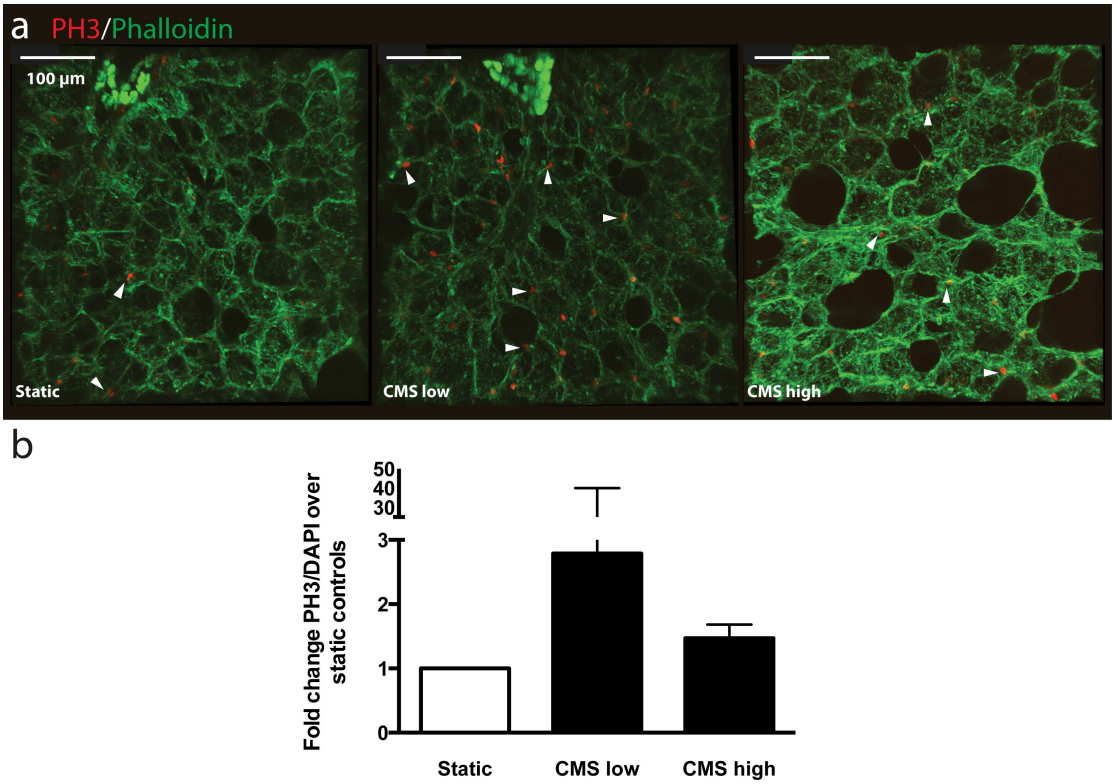


Figure 5-6 Cell proliferation in murine PCLS exposed to CMS

Murine PCLS subjected to either 0% CMS (static – left), CMS low (centre) or CMS high (right) were imaged for PH3 and the ratio of these cells against total nuclei assessed. Panel A shows PH3 stained nuclei (red) and phalloidin-stained actin architecture (green) for each condition. Arrowheads indicate PH3-stained nuclei, scale bar – 100 µm. Panel B shows fold change in PH3/total nuclei ratios for CMS low and high against static conditions. Data represented as median ± IQR for 3 PCLS from 2 individual mice (n=2) for CMS low and 6 PCLS from 3 individual mice (n=3) for CMS high.

CMS – cyclic mechanical strain, PH3 – phosphohistone H3

5.3.6 Cell proliferation in human PCLS exposed to CMS

To determine whether CMS-induced proliferation in human PCLS, slices were either un-stretched (static), or subjected to CMS-high, and the ratio of PH3-positive nuclei against total nuclei calculated as for murine PCLS. CMS-high induced a non-significant increase in proliferating cells when compared to static controls (Figure 5-7).

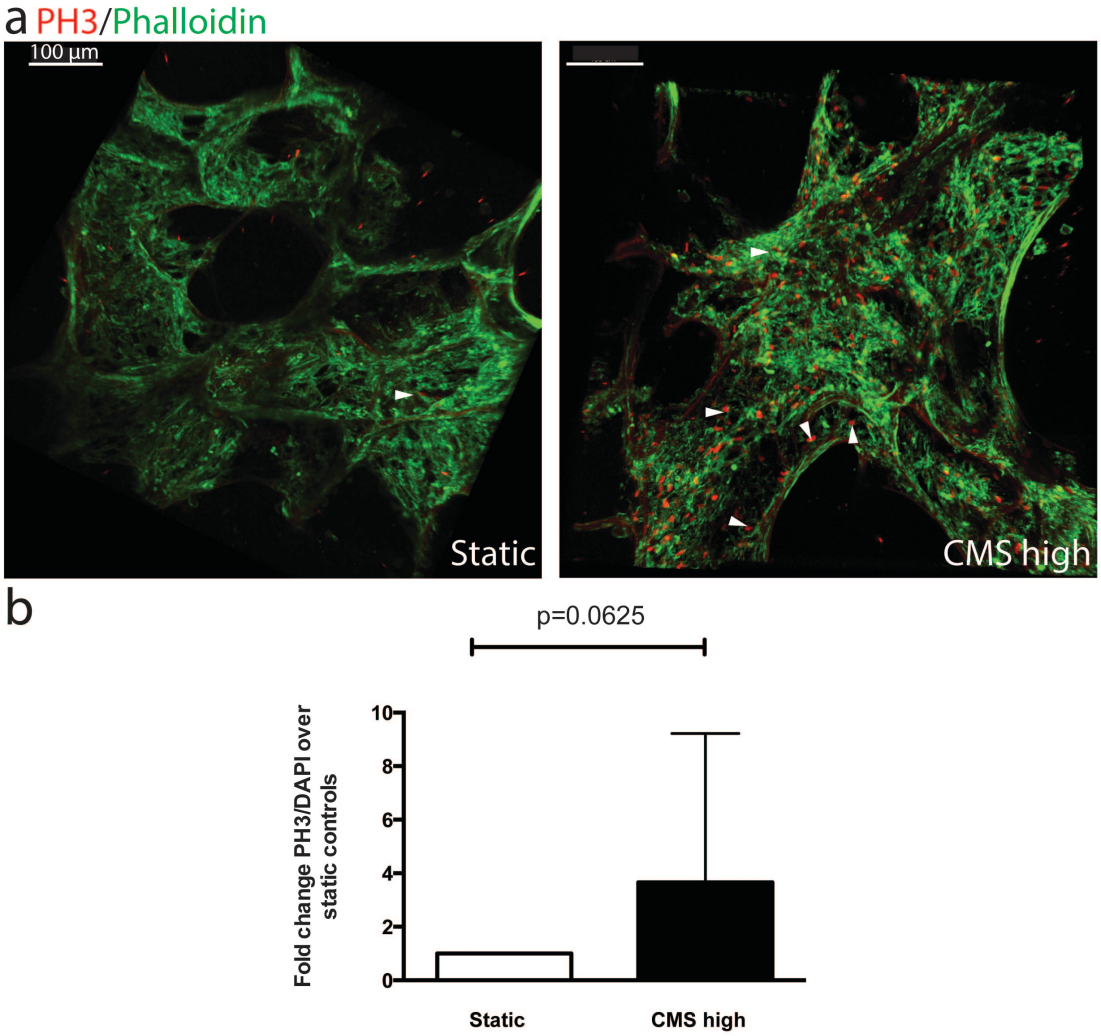


Figure 5-7 Cell proliferation in human PCLS exposed to CMS

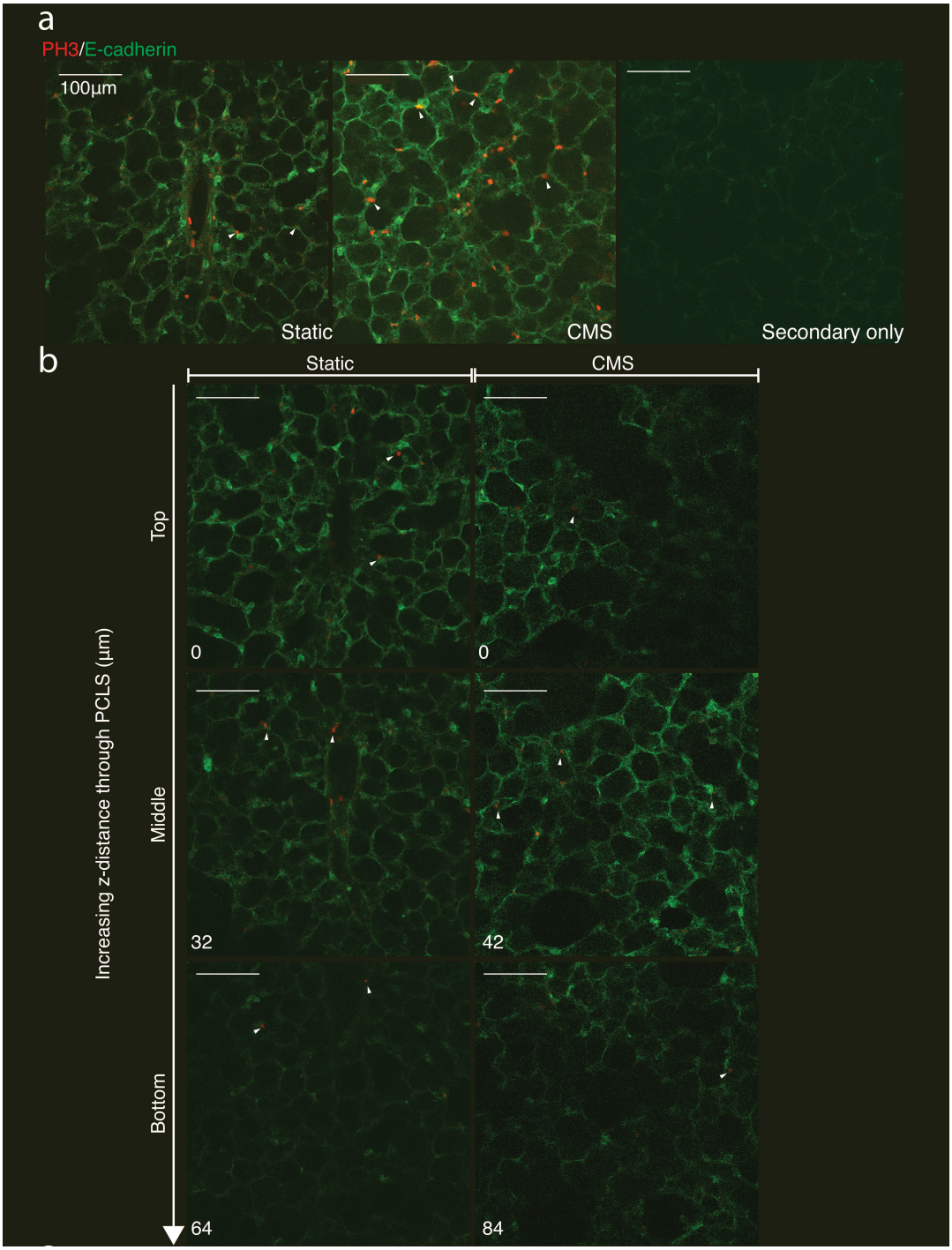
Human PCLS subjected to either 0% CMS (static – left), or CMS high (right) were imaged for PH3 and the ratio of these cells against total nuclei assessed. Panel A shows PH3 stained nuclei (red) and phalloidin-stained actin architecture (green) for each condition. Arrowheads indicate PH3-stained nuclei, scale bar – 100 µm. Panel B shows fold change in PH3/total nuclei ratios for CMS high against static conditions. Data represented as median ± IQR for 5 PCLS from 3 individual lung specimens (n=3), and analysed with Wilcoxon's test.

CMS – cyclic mechanical strain, PH3 – phosphohistone H3

5.3.7 Characterisation of proliferating cells

To characterise the proliferating cells, murine PCLS exposed to either static or CMS conditions were fixed and dual-stained for the epithelial-cell marker, E-cadherin, and PH3. PH3-positive nuclei were co-localised with E-

cadherin-positive staining (Figure 5-8 - a). Furthermore, PH3 staining was visible throughout the slice thickness, rather than simply at the cut edges (Figure 5-8 – b). Brightfield images overlaid with PH3–stained nuclei indicated that PH3-positive nuclei were spatially located in the corners of alveoli, where ATII cells would be expected (Figure 5-8 - c).


a
PH3/E-cadherin
100µm
Static
CMS
Secondary only
b
Static
CMS
Top
Middle
Bottom
Increasing z-distance through PCLS (µm)
0
0
32
42
64
84

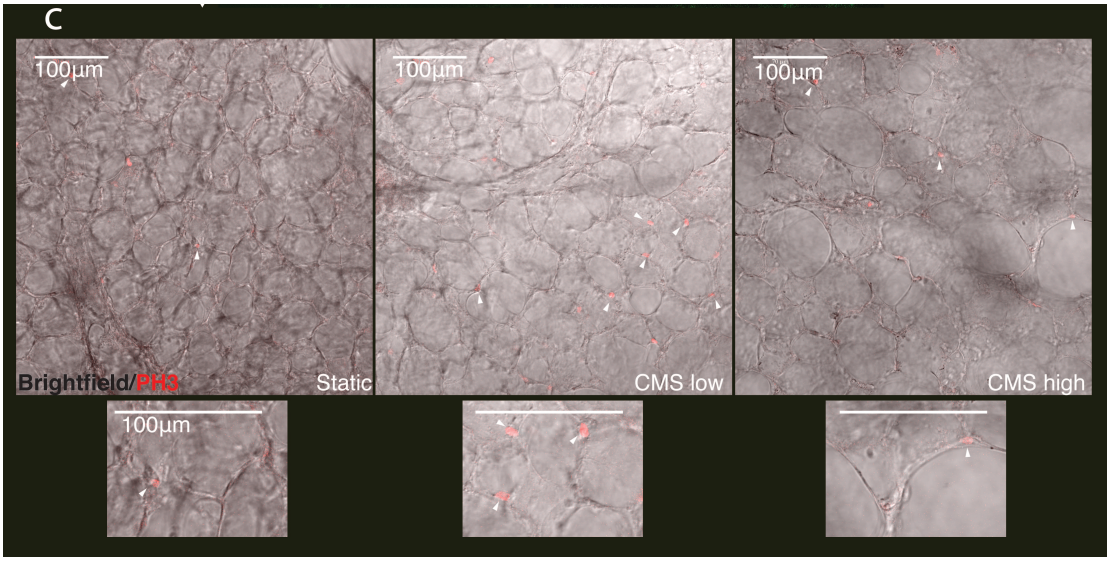


Figure 5-8 Characterisation of proliferating cells

Murine PCLS subjected to either 0% CMS (static) or CMS were imaged and stained for both PH3 and the epithelial cell marker E-cadherin. Panel A shows PH3 stained nuclei (red) and E-cadherin-stained cytoplasm (green) for static vs. CMS. Panel B shows images throughout the z-stack thickness at the top, middle and bottom of the slice. Panel C shows brightfield and PH3 overlay. Arrowheads in all panels indicate PH3-stained nuclei, scale bar – 100 µm.

5.3.8 Visualisation of cytokine release in PCLS

To characterise which cells express GRO-α, trial experiments were conducted where murine PCLS were treated for 4 hours with TNF-α at either 0 (untreated), 10 or 100ng/ml. PCLS were fixed and stained for GRO-α. Initial results demonstrated widespread GRO-α expression, even in untreated conditions, although image intensity was visibly greater in PCLS following TNF-α treatment (Figure 5-9 - a). In an attempt to visualise TNF- α –induced intracellular generation of GRO-α, PCLS were treated with brefeldin A (10µg/ml) to inhibit golgi-ER trafficking of GRO-α. Although all conditions again demonstrated widespread generation and release of GRO-α, discreet cellular generation was visible within alveolar septa, and in many cases, spatially correlated with ATII cells (Figure 5-9 – b).

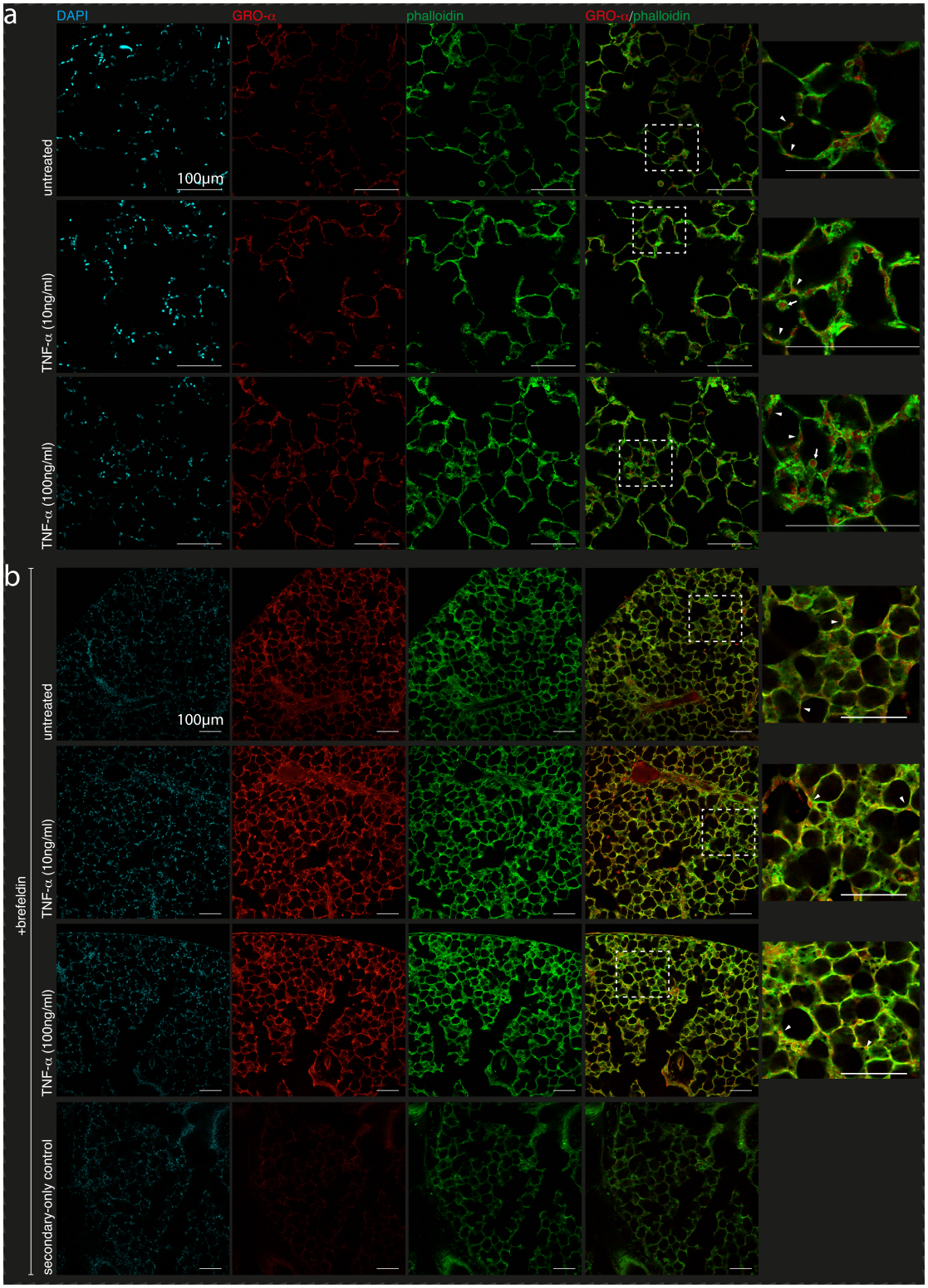


Figure 5-9 Visualisation of cytokine release in murine PCLS

Murine PCLS either untreated, or treated with TNF-α at either 10 or 100ng/ml were fixed and stained for GRO-α (red) and co-stained for phalloidin (green) and DAPI (cyan). Panel A shows murine PCLS treated in the absence of brefeldin (10µg/ml), stained for GRO-α, and imaged at 40x original magnification. Panel B shows PCLS treated in the presence of brefeldin, and imaged at 20x original magnification. Additional 2.5x digital magnification of

overlay is also shown to the right of each condition. Arrowheads indicate GRO-α -stained cells and arrows show GRO-α-expressing structures resembling macrophages. Scale bar – 100 μm.

5.3.9 Cytokine gene regulation in PCLS

To determine whether cytokine generation could be determined at an RNA level in PCLS, trial experiments were undertaken where murine PLCS were treated with 0 (untreated), 10 or 100ng/ml of TNF-α for 1 hour, and lysed for quantification of CXCL1, CXCL2 and IL-6 mRNA. Quality of PCLS mRNA was assessed using the high sensitivity Agilent Genomics RNA Tapestation system. PCLS mRNA was of good quality, with RNA Integrity Number equivalent (RIN^e) values consistently above 8 (Figure 5-10 – a-b). Moreover, although TNF-α treatment at 10ng/ml did not induce a demonstrable fold change in cytokine gene expression over untreated controls, TNF-α at 100ng/ml induced a four-fold increase in CXCL1, a 1.7-times increase in CXCL2, and a 1.6-times increase in IL-6 gene expression (Figure 5-10 – c).

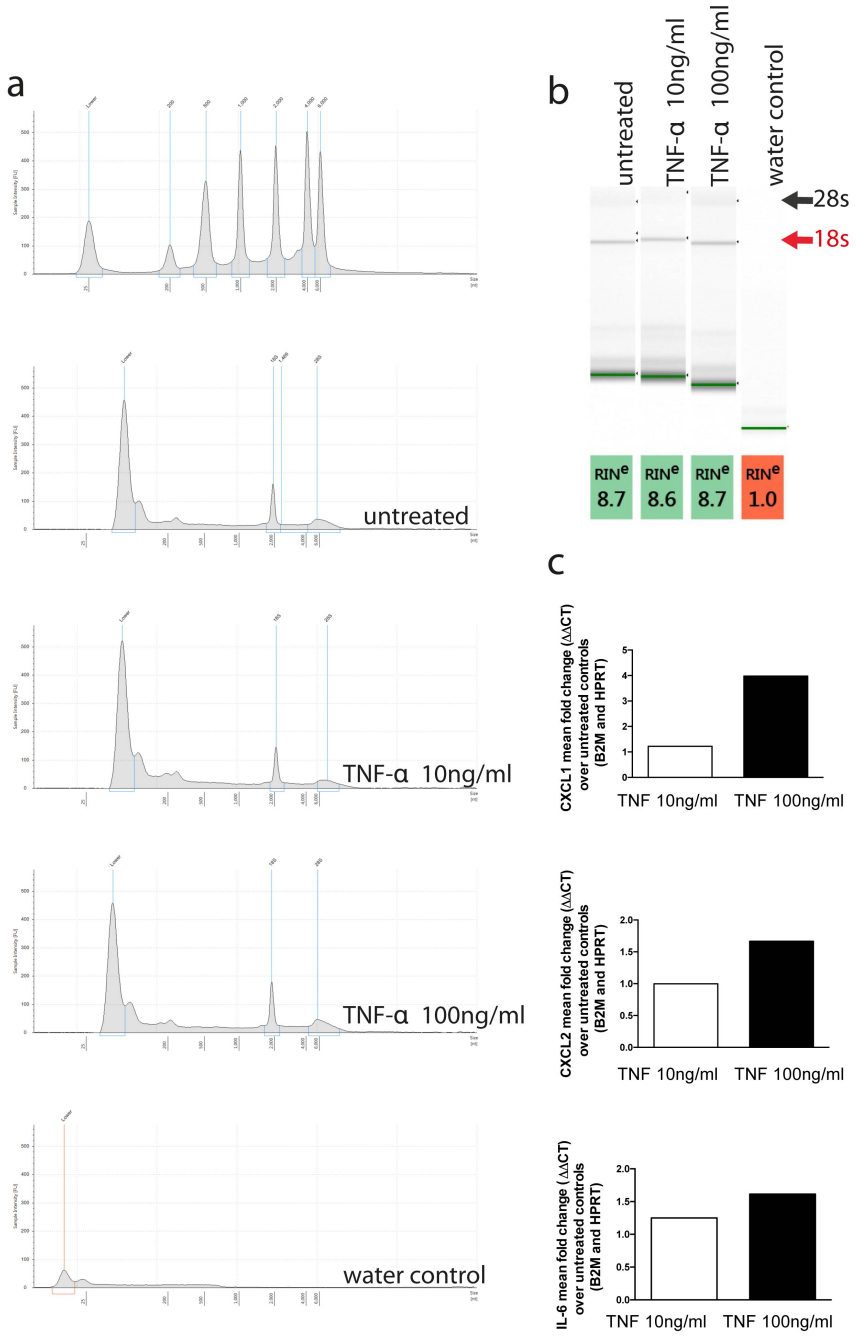


Figure 5-10 Cytokine gene regulation in PCLS

Murine PCLS were untreated, or exposed to TNF-α at 10 or 100 ng/ml for 1 hour, then lysed for mRNA quantification by RT-PCR. Panel A shows electropherogram of PCLS ribosomal (r)RNA showing 28s (right hand peak) and 18s (middle peak) and lower RNA (left-hand peak) at 5000, 2000 and <50 base pairs respectively, and compared to a ladder (top). Panel B shows these results as demonstrated on a gel. Black arrow indicates 28s bands and red arrow 18s bands. RIN^e values are shown below samples. Panel C shows fold change in mRNA expression over untreated PCLS for CXCL1 (top), CXCL2 (middle) and IL-6 (bottom) mRNA, for TNF-α at either 10 or 100ng/ml. mRNA quantified as ΔΔct where CT values are first normalised to that of two housekeeping genes (B2M and HPRT), then the average of these values normalised to that of untreated controls.

5.3.10 CMS-induced downstream signalling in PCLS

To determine whether CMS of PCLS induced downstream signalling that correlated with that seen in A549 cells, murine PCLS treated with either 20ng/ml epidermal growth factor (EGF) for 30 mins, or exposed to static conditions or CMS high for 10 minutes. The ratio of pERK-positive to total, DAPI-stained, nuclei in fixed and stained PCLS was calculated. EGF treatment induced a four-fold increase in p-ERK/total nuclei over static, untreated PCLS, and CMS induced a three-fold increase (Figure 5-11).

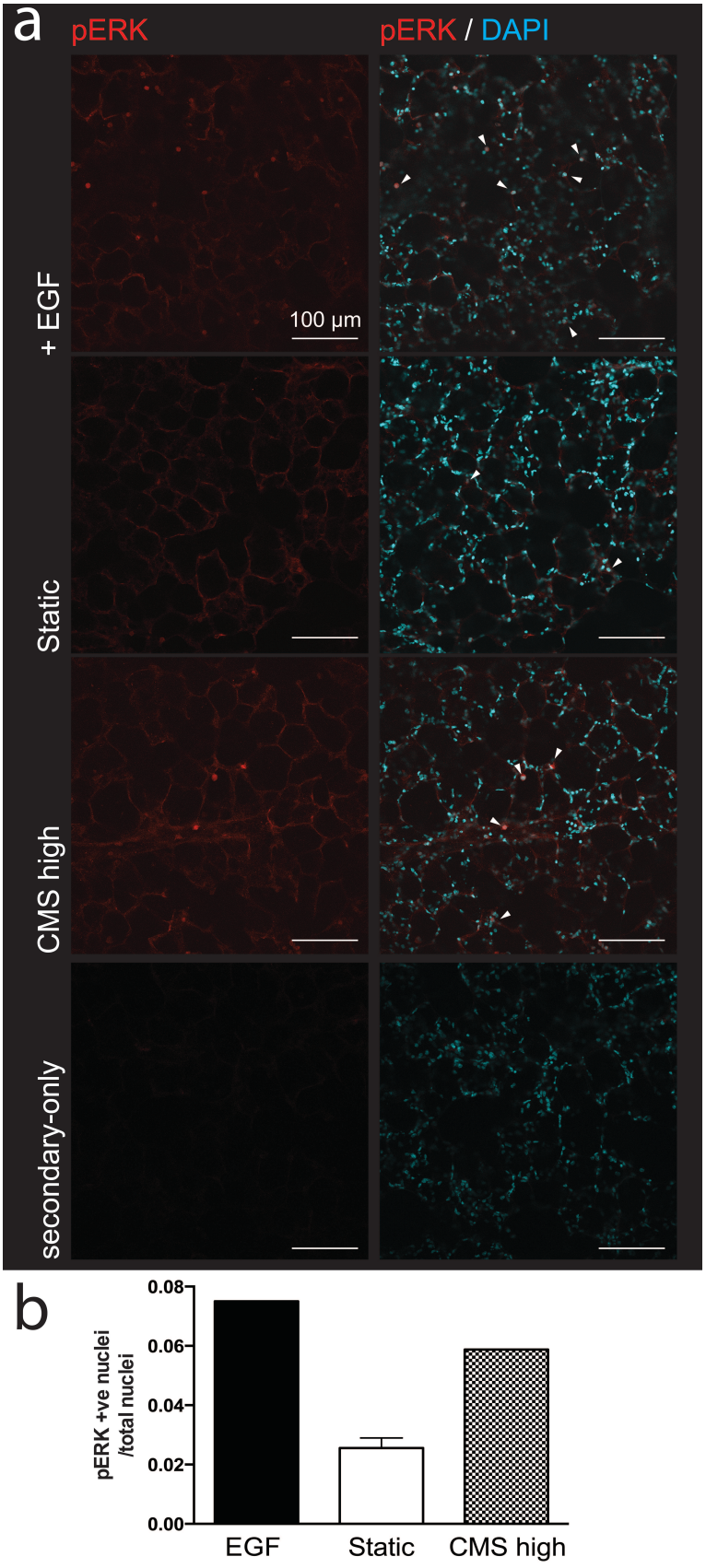


Figure 5-11 CMS-induced ERK phosphorylation in murine PCLS

Murine PCLS were either treated with epidermal growth factor (EGF), or exposed to static or CMS high conditions. Panel A shows confocal images of PCLS under different conditions, stained for p-ERK (red) and imaged by confocal immunofluorescence at 20x original magnification. Arrowheads show p-ERK positive nuclei. Scale bar – 100μm. Panel B shows the ratio of p-ERK positive nuclei to total nuclei for respective conditions. Data represented as mean for two images from one PCLS per condition (n=1).

5.4 Discussion

5.4.1 Summary of results

The aims of the work in this chapter were to determine whether PCLS could be used to model CMS-induced cell signalling in alveolae. Specifically, I aimed to determine whether CMS could be applied to PCLS without adversely affecting architecture or viability, and if CMS could induce cytokine generation and downstream signalling in PCLS.

Generation of murine PCLS preserved alveolar epithelial integrity, and nuclei spatially correlating with ATI and ATII were visible by H&E staining. Evidence of ATII was confirmed by confocal immunostaining for Pro-SPC. CMS-induced CXCL-1 release was found at 24 hours post-CMS in murine PCLS, and was dependent on the degree of CMS applied. Similarly, high degree CMS for over 1 hour induced significant IL-8 production by human PCLS at 24 hours. Basic ethidium and calcein staining of cells showed no gross differences in alveolar cell viability in PCLS exposed to CMS when compared to static controls, but a low degree of applied CMS induced proliferation of cells that spatially correlated with ATII, and a high degree of CMS induced a similar trend in human PCLS, although a statistically significant increase could not be determined in both cases.

I have shown from preliminary experiments that cytokine mRNA can be isolated from PCLS at good quality, and that TNF-α-induced increases in CXCL1 and CXCL2 mRNA can be detected. Finally, I have shown that CMS-induced phosphorylation of ERK can be detected in PCLS.

5.4.2 Application of CMS to PCLS

I have successfully generated both murine and human PCLS that demonstrate preservation of cellular architecture in agreement with previous work from our group (Alçada et al. 2014; Ng-Blichfeldt et al. 2017) and also demonstrated reactivity to CMS without gross structural damage. I used 400μm thickness for human PCLS, and 300μm for murine, correlating with thicknesses used in previous studies (Dassow et al. 2010), although 250μm thick slices have also been used (Song et al. 2016; N Davidovich et al. 2013).

The application of adhesive and the method used to apply CMS also differs from that used in other studies. I found that application of cyanoacrylate in discrete areas along the periphery of the PCLS allowed adhesion to the silicone membrane of the Flexcell system, and biaxial stretch of the PCLS could be visualised. However, one group stitched the PCLS to a deformable silicone membrane and an indenter was then used to cyclically deform the membrane (J. Huang et al. 2012; N Davidovich et al. 2013). This generated consistent alveolar deformation to 30% of alveolar surface area. Another technique, although without a similar degree of uniformity of deformation, successfully stretched PCLS by clamping to a pliant PDMS membrane, which was then deformed by applying pressure beneath from compressed air (Dassow et al. 2010). Deformation of individual alveoli

increased linearly with applied pressure to approximately 35% original surface area.

In my case, attempts were made to quantify the mean degree of stretch when pressures calibrated for stretch of cells to 5% original surface area (CMS low) and 15-20% (CMS high) were applied. This was done by live microscopy, and attempting to measure alveolar size at baseline and during a single stretch. Unfortunately, the onset of CMS moved the PCLS out of view in both the Z and XY directions, impeding our ability to successfully measure alveolar dimensions. For future studies, membrane stains will be used, and the average area of alveoli in a field of view at baseline compared with the average sizes during a period of tonic stretch. Therefore, at present, I cannot say with confidence by what degree application of CMS deforms individual PCLS, and how consistent that might be.

Work from our group has previously shown that both ATI and ATII markers are visible in human PCLS for up to 7 days using markers for podoplanin and Pro-SPC respectively (Alçada et al. 2014). Moreover, both PECAM staining for endothelial cells within alveolar septal walls and larger vessels, and alpha smooth muscle actin (α-SMA) around vessels and airways have been described in human and porcine PCLS (Ng-Blichfeldt 2014). In rat PCLS, Pro-SPC staining is visible for up to 6 days in culture, at which point levels decline, suggesting possible de-differentiation to ATI cells (Dassow et al. 2010), whereas staining for the ATI marker, aquaporin-5 (AQP5), remained constant throughout the 6 day period. Type I and II alveolar epithelial cell phenotypes were similarly maintained in culture for up to 3 days in rat PCLS

(N Davidovich et al. 2013) and in murine PCLS for 5 days (Uhl et al. 2015). Therefore, it is assumed that, as CMS is applied to PCLS at 24 hours following slicing, tissue characteristics are well preserved.

PCLS offer the advantage of generating a large sample size from a small amount of lung, therefore preserving animal and human tissue. However, when producing slices, significant variations can occur between PCLS in anatomy, such as the presence of large vessels or airways. Furthermore, both point-instillation of agarose to human PCLS, or tracheal instillation for murine PCLS, is likely to generate different distending forces throughout lung tissue, with some areas potentially exposed to high strain. In order to minimise heterogeneity between control and corresponding treatment PCLS, adjacent slices were used as control or treatment, and normalised for each other when calculating CMS-induced differences.

5.4.3 CMS-induced cytokine release

These results indicated that CMS promoted generation of KC/GRO-α (CXCL1) and IL-8 (CXCL8) from murine and human PCLS respectively. In previous murine studies, CXCL1 generation in adult mice was induced by high tidal volume ventilation, which paralleled neutrophil sequestration and lung injury scores and was sensitive to the degree of ventilation applied (Belperio et al. 2002). In adult studies, IL-8 generation in BAL fluid correlates with onset of ARDS (Donnelly et al. 1993), and low tidal volume (lung-protective) ventilation reduced BAL IL-8 concentration (Ranieri et al. 1999). These observations indicate that these cytokines are sensitive to the degree of mechanical strain applied to the lung. *In vitro,* application of CMS to human

alveolar epithelial cells promoted IL-8 generation (Vlahakis et al. 1999), and these cytokines have therefore been used as a ‘readout’ of CMS-induced injury in our models.

The putative mechanism of CMS-induced cytokine release in ATII cells is dependent on ERK 1/2 signalling, and inhibition of ERK signalling using UO126 inhibits downstream IL-8 generation in A549 cells (Pinhu 2008). Furthermore, actin cytoskeletal tension is required for mechanotransduction-induced cytokine release, as shown by earlier results using inhibition of ROCK and myosin II (3.3.4). Finally, A549 cells grown without mitochondria cannot generate cytokine in response to CMS (Pinhu 2008) correlating with observations suggesting that mitochondrial superoxide has a role in CMS-induced mechanotransduction responses. Recent work demonstrated ROS generation in PCLS exposed to CMS, and that superoxide scavenging attenuated CMS-induced tight junction dissociation (Song et al. 2016).

However, the benefit of using PCLS to investigate CMS-induced injury is the presence of all cell types normally resident in the alveolar epithelium. Increased nuclear translocation of p65 in ATI was seen in rat PCLS stretched to 37% (N Davidovich et al. 2013), and the authors stated their intent to also examine responses in other lung cells such as endothelial cells, and ATII. We attempted to visualise GRO-α in murine PCLS treated with TNF-α, in an attempt to localise cytokine release to cell type, but the diffuse staining seen in both control and TNF-α–treated PCLS made quantification and localisation difficult, even in the presence of the protein-transport inhibitor Brefeldin A. The concentration of Brefeldin A used in my experiments (10μg/ml) blocked

intracellular transport of proteins from hepatocytes by impedance of ER to golgi trafficking (Misumi et al. 1986). However, I could not confirm that this dose was effective in PCLS and therefore dosage and timing will need to be optimised when applied to PCLS in culture.

Preliminary characterisation of ERK activation in PCLS was promising, suggesting a positive response to epidermal growth factor (EGF) and increase following 10 minutes CMS as observed with immunoblotting in A549 cells (4.3.3). However, as with other work in this chapter, the cells staining positive for phosphorylation need to be characterised fully when this work is repeated. Therefore, a mechanistic explanation for CMS-induced cytokine generation in PCLS cannot be provided at present, but this work suggests that this may be attainable.

Finally, attempts to obtain cytokine mRNA expression profiles from PCLS exposed to injury were relatively successful. The RNA integrity number (RIN) scores RNA integrity based not only on the ratio of 28s:18s ribosomal RNA degradation bands, but also other factors including the height of the 28s peak and the fraction of the areas in the region of the peaks compared to the total area under the curve, and provides robust prediction of RNA integrity (Schroeder et al. 2006). Values over 7.4 are likely to be of acceptable quality for RNA sequencing analyses, although evidence suggests the effects of RNA degradation in these specimens can be controlled for (Gallego Romero et al. 2014). Nonetheless, RIN values for all PCLS samples analysed fell over 8.5, suggesting that RNA expression profiles can be collated from pooled samples of 3 PCLS. A dose dependent increase in CXCL1, CXCL2 and IL-6

expression was seen in samples treated with TNF-α, suggesting that this can be used as a positive control in future studies of CMS-induced cytokine generation in PCLS.

5.4.4 Viability of PCLS

CMS-induced responses in PCLS tissue are dependent on the preservation of cell viability following the slicing, adhesion and CMS process. I used a variety of different methods, including MTT assay of PCLS tissue, determination of the ratio of ethidium-stained dead nuclei to total, DAPI or Hoechst-stained, nuclei. However, dual ethidium and calcein staining of PCLS to determine dead nuclei and cytoplasm of live cells respectively, was found to be quick and effective, and could be visualised in live cells allowing for real-time viability studies during CMS in the future. Difficulties with this method result from the technical process of microscopy in adhered slices, and in quantifying viability from the images obtained. My preliminary data suggest that there are no gross differences in viability between PCLS exposed to static or CMS conditions at both low and high degrees of stretch when compared to methanol-treated PCLS. However, these conclusions are made cautiously, given both the large quantities of dead nuclei in all conditions, and the inability to derive quantifiable data from this work at present.

Viability of lung slices as assessed by lactate dehydrogenase release, thymidine incorporation and MTT assay in rat (Martin et al. 1996) and guinea pig slices (Ressmeyer et al. 2006) have demonstrated that PCLS maintain viability in culture for at least 72 hours. Maintenance in culture beyond 7 days can affect physiological function, such as random twitching of airway smooth

muscle due to calcium store overloading and subsequent release (Bergner & Sanderson 2002; Sanderson 2011). Furthermore, previous work from our group suggests that human PCLS maintain viability in culture for up to one week as determined by the WST-1 metabolic assay (Alçada et al. 2014).

The application of 4 hours CMS to rat PCLS clamped into a bioreactor did not significantly reduce viability as assessed by both ethidium/calcein staining and MTT assay (Dassow et al. 2010), although it must be noted that the PCLS appear better preserved in all conditions, with fewer dead cells evident compared with my data. This may be attributed to our use of ethyl-cyanoacrylate to adhere PCLS to the silicone membrane. Indeed, stitching of the PCLS to a deformable membrane led to a similar viability profile to that obtained in our experiments (N Davidovich et al. 2013), indicating that both methods have an impact on PCLS viability without revealing an effect of CMS on cell viability.

Recent data suggested that the short chain cyanoacrylate, ethyl-2-cyanoacrylate, may reduce surgical and haemostasis time, and reduce inflammation when compared to the use of sutures in pulmonary partial lobectomy surgery (Szkudlarek et al. 2011), and a similar profile was obtained in vascular surgery studies (Kaplan et al. 2004). However, in general, shorter chain cyanoacrylates are known to induce local toxicity due to degradation of their alkyl chains into cyanoacetate and formaldehyde (García Cerdá et al. 2015). Longer chain cyanoacrylates, such as *n*-butyl-2-cyanoacrylate (Indermil) have slower rates of degradation, with better toxicity profiles but with increased rates of dehiscence. My on-going and future work is using *n*-

butyl-2-cyanoacrylate to reduce cell death in PCLS studies when compared to ethyl-2-cyanoacrylate, with PCLS that remain adhered during CMS. Another alternative currently being tested is 'Cell-Tak' (Corning) adhesive, which consists of polyphenolic proteins from the bivalve mollusc, *Mytilus edulis*, which enable it to adhere to structures (Waite 1983). The advantages of this compound in PCLS studies are that it has a low cytotoxicity profile, and can be subsequently degraded, facilitating detachment of the PCLS from the deformable membrane. However, optimisation is needed to identify the best concentration of this product to maintain PCLS adherence during CMS.

Therefore, although preliminary work has demonstrated viability of PCLS following adhesion and CMS, further optimisation must be undertaken with both the type of adhesive and quantification of viability profiles. Imaris software (Bitplane, Zurich, Switzerland) can be used to 'reconstruct' and quantify the volume of tissue occupied by the calcein-stained cytoplasm, and count the number of ethidium-stained dead nuclei. A ratio can therefore be derived from the two measurements, allowing for some quantification of PCLS viability. In this way, we aim to determine whether CMS has an effect on PCLS viability. Finally, recent data suggest that murine PCLS maintain viability even following freeze-thawing (Rosner et al. 2014). Use of this technique in human PCLS could allow for long-term preservation and use of human tissue in CMS studies.

5.4.5 CMS-induced proliferation

Although not reaching statistical significance at present, these preliminary results suggest that CMS of murine and human PCLS induced an increase in the proliferation of cells that correlated spatially with ATII cells. These results support the hypothesis that lung re-growth following pneumonectomy in humans is driven by overdistension of the remaining lung (Butler et al. 2012), but repeat studies will determine if this trend in PCLS is consistent and significant. Furthermore, there is a growing body of evidence to suggest that lung development is driven by mechanical stretch. Foetal breath movements are necessary for the normal development of the lung (Wigglesworth & Desai 1979), exposure to continuous positive airways pressure (CPAP) promoted a 40% increase in total lung capacity in 6-week old ferrets when compared to controls (Zhang et al. 1996), and mechanical forces across epithelial tissues direct branching morphogenesis of the developing lung (Gjorevski & Nelson 2010; Varner et al. 2015).

These observations correlate with increased alveolar cell proliferation both *in vitro* and *in vivo*. In both H441 and A549 pulmonary epithelial cells, low degree CMS over 24-72 hours increased cell numbers (Chaturvedi et al. 2006), and mechanical ventilation of mice resulted in a 3-fold increase in the G1 and S-phase marker proliferating cell nuclear antigen (PCNA), and a 6.5-fold increase in the cell cycle entry marker ki67 in cells identified morphologically as ATII (Chess et al. 2010). Furthermore, pneumonectomy is associated with a subsequent increase in alveolar cell density (Jain et al. 2015) (Butler et al. 2012), and in murine lung induced a regression in

transcriptomic profile similar to late stages of development (alveolar stage), comprised of a small regression backwards (de-differentiation phase) then subsequent re-development phase (Kho et al. 2013).

It is currently not clear by which mechanism mechanical stretch might induce epithelial cell proliferation, but in mammary epithelial cells, the *Yorkie* homologue proteins YAP and TAZ were activated in response to increasing ECM stiffness and corresponding RhoGTPase signalling (Dupont et al. 2011). In more recent studies, such stretch-induced YAP/TAZ activation promoted S-phase re-entry (Aragona et al. 2013) and mechanical strain of MDCK epithelial cells induced cell cycle re-entry and progression through S phase (Benham-Pyle et al. 2015). This was dependent on Yap1 activation, and β-catenin expression was necessary for S-phase progression. Furthermore, E-cadherin extracellular engagement was required for strain-induced β-catenin transcriptional responses, suggesting its role as both a mechanical and signalling platform for mechanical strain-induced responses in epithelial cell monolayers.

Recently, stretch-induced mitosis was also seen to be dependent on the transmembrane protein Piezo1, which activates in response to stretch to promote calcium-dependent phosphorylation of ERK 1/2, activating cyclin B transcription to drive cell cycle entry from G2 phase (Gudipaty et al. 2017). Piezo1 in this case may act as a mechanosensor and promote different responses to mechanical tension on epithelial cells, from extrusion of cells in response to overcrowding on one hand, to cell division in response to mechanical stretch on the other, depending on the magnitude of force applied.

Another possibility is that proliferation may be a regenerative response to CMS-induced injury or apoptosis. Although alveolar epithelial cell turnover in the quiescent adult lung is low (Barkauskas et al. 2013; Hogan et al. 2014), evidence suggests that the alveolar epithelium will regenerate with cell proliferation following injury. Bleomycin-induced fibrotic lung injury (Kawamoto & Fukuda 1990), and pulmonary fibrosis itself are associated with increased alveolar epithelial cell proliferation (Königshoff 2014; Weng et al. 2014). Cigarette smoke injury is associated with increased bronchial epithelial proliferation as demonstrated by ki-67 labelling (Lee et al. 2001; Hittelman et al. 2007). ATII proliferated 3 days after LPS and haemorrhagic shock in a rodent model of ALI, in a HGF and c-Met-dependent manner (Zeng et al. 2016). These effects are thought to be secondary to cell apoptosis in fibrotic models of injury (Königshoff 2014), but whether this is the case in stretch-mediated injury is not clear (Crosby et al. 2011).

Although ATII self-renew and de-differentiate to repopulate the depleted alveolar epithelium following injury (Barkauskas et al. 2013), recent evidence suggests that the majority of ATII present following injury are not derived from self-renewal, but rather from differentiation and proliferation of club cells (Zheng et al. 2017). This may include previous candidates for alveolar epithelial stem cells, including lineage negative progenitor cells (Vaughan et al. 2014) and distal airway integrin α6β4+ cells (Chapman et al. 2011). Furthermore, the differentiation between ATII and ATI may be bi-directional, and ATI may be directly differentiated from Krt+ progenitor tracheal cells (Yee et al. 2017). These data suggest a significant degree of plasticity and complexity in the regeneration and self-renewal capacity of the alveolar

epithelium (Jain et al. 2015). Therefore, the cells identified as proliferating in response to CMS need extensive further characterisation.

To identify cell proliferation, I used the G2/M-phase marker PH3, which was used in studies of CMS-induced alveolar epithelial cell proliferation (Gudipaty et al. 2017). Phosphorylation at ser10, 28 and thr11 of histone h3 correlates with chromosome condensation during mitosis and meiosis (Hendzel et al. 1997; Goto et al. 1999), but I appreciate that the use of markers to identify cell cycle entry (ki67) and S-phase (EdU) would increase the robustness of these results.

Additionally, although previous studies have both demonstrated (Crosby et al. 2011) and failed to identify (Chess et al. 2010) CMS-induced apoptosis *in vitro* and *in vivo* respectively, our results would benefit from a correlation with an apoptosis or necrosis profile as measured by terminal deoxynucleotidyl transferase dUTP nick end labeling (TUNEL), cleaved caspase 3 and propidium iodide staining. These were attempted, and require further work to fully elucidate the balance between cell death and proliferation stimulated by CMS.

Finally, as with cytokine generation, attempts to characterise proliferating cells as epithelial were impeded by difficulties with combining ATII epithelial markers such as TTF-1 and Pro-SPC with proliferation markers. These may be overcome in future by the use of a Fluorescein isothiocyanate (FITC)-conjugated epithelial cell adhesion molecule (EPCAM) antibody, or by using PCLS from an epithelial-GFP tagged mouse line (Lee et al. 2013).

Although E-cadherin allowed for a preliminary identification of epithelial proliferating cells, the staining was diffuse and not definitive (5.3.7).

5.4.6 Summary and limitations

The aim of the work in this chapter was to determine whether PCLS could provide a platform to study mechanotransduction processes in the human alveolar epithelium with near *in vivo* conditions. To an extent, I have partly achieved this by demonstrating CMS-induced cytokine release in murine slices. Furthermore, I have described, to my knowledge, the first example of CMS-induced cytokine generation in human PCLS. I also made preliminary observations of TNF-α –induced cytokine mRNA expression to provide impetus for further work regarding CMS-induced injury, and of CMS-induced proliferation and ERK activation.

However, the major limitation to this work has been my inability to characterise activated cells as epithelial and of any particular subtype. Attempts were made to co-stain with TTF-1, pancytokeratin, Pro-SPC, and E-cadherin. Although some success was obtained with E-cadherin staining, results when using these markers were inconclusive. This was partly due to species incompatibility between proliferation or cytokine antibody and epithelial marker, but also due to poor penetration into the lung slice itself, and 488-channel auto-fluorescence from elastin. Improvements have been made since this work, with EPCAM providing a consistent and specific epithelial cell stain, and the use of alveolar-epithelial–GFP expressing mice to generate PCLS.

Similarly, optimisation of PCLS viability studies will help ensure optimal conditions for further mechanotransduction work in PCLS. One issue with the work presented here is the high index of ethidium-stained dead nuclei, and this has been attributed to the use of ethyl-cyanoacrylate adhesive. Although there were no gross differences observed in the ratio of ethidium and calcein – stained cells between static and CMS conditions, this method to assess cell viability does not allow for easy quantification of cell viability parameters. Other methods were attempted, including measurement of the ratio of ethidium-positive to Hoechst-positive nuclei, but without consistent and reliable results. Two improvements have therefore been made to progress this work. The first is substitution of n-butyl-cyanoacrylate for ethyl-cyanoacrylate to reduce the adhesive-related toxicity to PLCS. The second is use of the MTT assay, which has now been optimised and validated in PCLS by work from our group.

Finally, a better characterisation of the degree of CMS experienced by PCLS is required. Although PCLS were observed to stretch, our previous attempts at calculating the degree of CMS applied by measuring alveoli in relaxed and stretched states was inhibited by movement of the PCLS in and out of focus. One possibility in future work is to film PCLS undergoing stretch, and calculate change in surface area of the PCLS itself.

5.4.7 Future directions

The aim of the work in this chapter was to advance my model of mechanotransduction in the alveolar epithelium to near *in vivo* conditions in the human lung. Therefore, I hoped to assess the role of RhoGTPases and

CD98hc in CMS-induced injury in PCLS. Although further optimisation of the model is required as described above, the long-term aim is to be able to characterise cytokine generation, apoptosis and proliferation on a cell-by-cell basis in the PCLS. Inhibitors of the Rho-ROCK-NMII pathway, CD98hc blocking antibodies (Bhuyan et al. 2014) and ERK inhibitors can then be used to assess response.

One of the key benefits of the PCLS model is the potential to assess alveolar epithelial function in a near physiological cellular environment. Therefore, the interaction of alveolar epithelial cells with other cell types in response to CMS can be assessed. Interestingly, flow cytometric profiling of murine lung following high tidal volume ventilation indicated that endothelial cells responded with inflammatory signalling most rapidly (within 1 minute), followed by epithelial cells and then macrophages (Woods et al. 2015). These results indicate that the kinetic profiling of inflammatory responses to stretch of different lung cells is important, and the use of PCLS provides an opportunity to examine the role of the epithelium in what is likely to be complex and dynamic inter-dependent signalling between different cells.

6 Chapter 6: Discussion and further work

6.1 Summary of important results from this thesis

The work in this thesis demonstrated that CMS induced actin cytoskeletal remodelling, promoting a reduction in cell size, an increase in the cell-free area between cells, and redistribution of focal adhesions to, what appeared to be, damaged stress fibres within the cell. Furthermore, inhibition of ROCK and NMII abrogated CMS-induced cytokine release, and CMS induced early increases in RhoA activation, suggesting that Rho-ROCK-NMII is critical for CMS-induced injurious signalling in alveolar epithelial cells.

I also found that knockdown of the transmembrane integrin-associated protein, CD98hc, abrogated CMS-induced cytokine release and was associated with loss of CMS-induced autophosphorylation of FAK. Significantly, knockdown of CD98hc reduced baseline RhoA activity. Preliminary results using a FRET probe to indicate tension across focal adhesions suggested that knockdown may be associated with lower tension at baseline, with increased tension following CMS. Finally, knockdown was associated with a decreased rate of migration of cells to recover a wound in the epithelial monolayer, as indicated by an impedance-based assay.

Although the application of CMS to a monolayer of epithelial cells *in vitro* is useful for understanding mechanistic responses, it is vital to understand the mechanobiology of the *in vivo* alveolar epithelium, as affected by cellular repertoire, cell-matrix and cell-cell interactions. I developed a method by which CMS could be applied to precision cut lung slices (PCLS). These PCLS

demonstrated preserved alveolar epithelial integrity. CMS-induced cytokine release was evident in both murine and human PCLS, and was dependent on the degree of CMS applied. A low degree of applied CMS was associated with cell proliferation that spatially correlated with ATII in murine PCLS, and a high degree of CMS induced a similar trend in human PCLS, although a statistically significant increase could not be determined in both cases.

Finally, I demonstrated that cytokine mRNA can be isolated from PCLS, and that PCLS increased expression of CXCL1 and CXCL2 mRNA in response to TNF-α. Preliminary work also demonstrated that it is possible to detect CMS-induced phosphorylation of ERK in PCLS. I believe that this work in PCLS opens the door to further, more physiologically relevant, investigations of mechanobiology in the alveolar epithelium, using live human tissue.

6.2 The role of the CD98hc-RhoA-NMII axis in alveolar epithelial mechanobiology

6.2.1 Cellular tension and pre-stress

The findings that inhibition of ROCK, NMII or CD98hc abrogated CMS-induced cytokine release led me to hypothesise that baseline pre-stress affects the response of alveolar epithelial cells to CMS. Although I was unable to confirm the effect of these treatments on the dynamics of cellular tension before and during CMS, this is to form the basis of on-going work. The data presented in this thesis suggest that cells with lower pre-stress, such as from

inhibition of ROCK or NMII, may be less susceptible to the sensation and transduction of mechanical force into injurious biological signalling.

Pre-treatment of animals with Y27632 protected animals from lung injury in models of sepsis-induced injury (Cinel et al. 2012; Birukova et al. 2012). Moreover, hyperoxia-induced increases in cell stiffness were Rho kinase dependent and associated with CMS-induced cell detachment, which was abrogated by inhibition of ROCK (Wilhelm et al. 2014).

Patients with chronic interstitial lung disease, who have lungs with less elasticity and greater stiffness (Liu et al. 2010), have poor tolerability of mechanical ventilation with a subsequent increased mortality (Saydain et al. 2002; Fernández-Pérez et al. 2008). Although there are many reasons why patients with the gross pathological changes observed in interstitial lung disease may have poor outcomes following mechanical ventilation, it would be interesting to ascertain if this was due to increased VALI in this cohort of patients, and if this in turn was due to higher baseline pre-stress in alveolar epithelial cells. Use of *ex vivo* lung perfusion (EVLP) or PCLS studies may be helpful in this regard. Interestingly, Rho-ROCK signalling has been demonstrated to regulate fibroblast to myofibroblast differentiation in the pathogenesis of pulmonary fibrosis, and its inhibition using a ROCK inhibitor, fasudil, protected animals from experimental fibrosis (Zhou et al. 2013).

The tensegrity model of the cell as a pre-stressed structure predicts that the transmission of force throughout the cell is dependent on the degree of baseline pre-stress (Wang & Ingber 1994; Hu et al. 2005; Matthews et al. 2006). Evidence for the effect of increased cellular pre-stress on susceptibility

to high tidal volume stretch may be seen in hyperoxia, which increased the elastic modulus of alveolar epithelial cells (Wilhelm et al. 2014; Roan et al. 2012), and worsened VALI (Makena et al. 2010; Li et al. 2007). Furthermore, these effects of hyperoxia-induced cell stiffening, and CMS-induced cell detachment following hyperoxia were abrogated by inhibition of ROCK signalling using Y27632 (Wilhelm et al. 2014).

6.2.2 Mitochondrial ROS and ERK signalling

My finding that ablation of F-actin polymerisation using cytochalasin D did not reduce CMS-induced IL-8 release suggests an additional factor of the Rho-ROCK-NMII signalling pathway integral to mechanotransduction in CMS, beyond mechanical integrity of the pre-stressed actin cytoskeleton. Physical forces may directly influence nuclear mechanotransduction of cytokine signalling (Lammerding et al. 2004). Furthermore, the generation of mitochondrial ROS has been associated with CMS-induced cytokine generation in the lung, and A549 cells grown without mitochondria do not generate cytokine in response to CMS (although they do in response to chemical stimulation) (Pinhu 2008). PCLS exposed to CMS generated ROS, the attenuation of which abrogated CMS-induced tight junction disruption (Song et al. 2016).

There are also data to suggest that mitochondrial ROS activate ROCK and MLC-mediated remodelling of the cytoskeleton in drosophila (Muliyil & Narasimha 2014), suggesting a direct interaction between the Rho-ROCK and mitochondrial ROS pathways. Activation of the NF-κB pathway mediated CMS-induced ROS release in monolayers of alveolar epithelial cells and in

ATI and ATII in PCLS (Nurit Davidovich et al. 2013; N Davidovich et al. 2013). That hyperoxia is associated with mitochondrial ROS generation (Kallet & Matthay 2013), and that hyperoxia-induced cell stiffening and increased susceptibility to CMS-induced injury were abrogated by inhibition of ROCK (Wilhelm et al. 2014), lends further evidence of an interaction between mitochondrial ROS, ROCK signalling, cellular pre-stress and susceptibility to CMS-induced injury.

Moreover, inhibition of ERK signalling also abrogated CMS-induced cytokine responses (Pinhu 2008), and CMS-induced p65 nuclear translocation in PCLS was prevented by ERK inhibition (Song et al. 2016), suggesting a possible overlap between mitochondrial ROS and ERK pathways. CMS of human lung endothelial cells was associated with the formation of a paxillin-ERK-GEF-H1 complex to stimulate Rho signalling with subsequent actomyosin contraction and endothelial permeability. Formation of this complex was abolished by inhibition of ERK by UO126 (Gawlak et al. 2014). Therefore, given that NF-κB and mitochondrial ROS-induced cytoskeletal remodelling occurs via ROCK, I would suggest ROCK as the point of overlap between these pathways in CMS-induced injury. This could be tested by the use of LPA or other Rho and NMII 'rescue' of mechanotransduction following ERK inhibition.

6.2.3 CD98hc signalling

I have shown that CD98hc kd is associated with lower baseline RhoA activation in a preliminary FRET-based assay, suggesting that CD98hc-mediated alteration of baseline RhoA activity, and possibly pre-stress, has a

role in the regulation of CMS-induced mechanotransduction. This correlates with previous observations that CD98hc-deficient cells demonstrate reduced RhoA (Féral et al. 2007; Boulter et al. 2013) and ROCK (Estrach et al. 2014) activity. Furthermore, overexpression studies of CD98hc demonstrated increased ERK and p38 MAPK signalling, and proliferation, in a mechanism dependent both on CD98-mediated-amino acid transport, and the CD98hc cytoplasmic tail (Bulus et al. 2012). Although this was in the context of serum-dependent proliferation responses, it would be interesting to determine whether CD98hc overexpression stimulated RhoA activity, as my hypothesis would suggest (Figure 6-1).

Although this thesis has focussed on the cytoplasmic CD98hc association with β1-integrins, the ectodomain of the heavy chain associates with any of 6 light chain subunits LAT1, LAT2, xCT, y+LAT1, y+LAT2, asc1 (Fotiadis et al. 2013) responsible for amino acid transport across the cell. Inhibition of the light-chain binding capacity of CD98hc leads to accumulation of ROS, indicating the role of CD98 in regulating redox balance (de la Ballina et al. 2016). How this might relate to mechanobiology pathways remains to be seen. Finally, an actin bundling protein Fascin-1 was observed to target SLC3A2 (CD98hc) gene expression and transcription to regulate mTor activity to affect cell growth and survival via aberrant amino acid transport (Saad et al. 2016). That the actin-fascin interaction may be dependent on Rho-ROCK signalling (Jayo et al. 2012) and that CD98hc activation might lie downstream of fascin suggests the exciting possibility of a force-sensing feedback loop mediated in part by CD98hc.

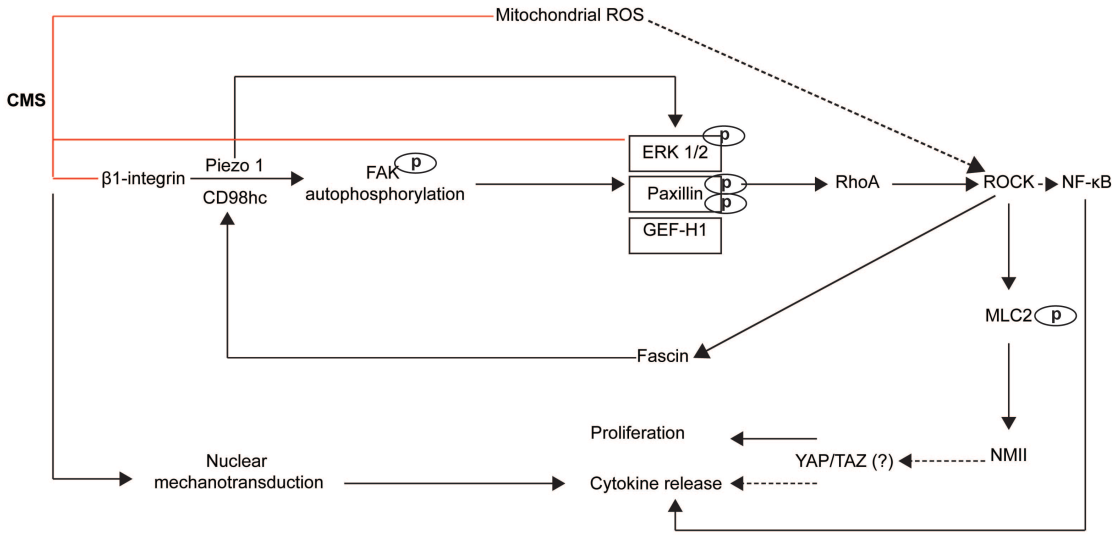


Figure 6-1 Proposed CMS-induced mechanotransduction pathway in alveolar epithelial cells

CMS induces β1-integrin activation (Guilluy et al. 2011), and both phosphorylation of focal adhesion kinase (FAK) at tyrosine 397, and of extracellular related kinase (ERK) p44/42 (1/2). FAK-dependent phosphorylation of paxillin leads to ERK-paxillin complex formation which recruits and activates guanine exchange factor H1, stimulating RhoA activity (Gawlak et al. 2014). I have shown that ROCK and NMII are necessary for CMS-induced cytokine release, and that CD98hc both mediates CMS-induced cytokine release and may affect RhoA activity, although whether this is through regulation of β1-integrin signalling remains to be seen. Mitochondrial ROS activated by CMS (Pinhu 2008) may directly induce ROCK signalling (Muliyil & Narasimha 2014) and ROCK may be a point of overlap between ERK and mitochondrial ROS pathways. CMS may also promote direct nuclear mechanotransduction of IL-8 signalling.

6.3 Targetting CD98hc-RhoA-NMII signalling in clinical practice

The work in this thesis demonstrates that both Rho-ROCK and CD98hc signalling are required for CMS-induced injurious signalling in alveolar epithelial cells *in vitro*. Although this is a small step in understanding the mechanobiology of the alveolar epithelium, an interesting aspect is that inhibitors of Rho-ROCK signalling are already in clinical use. Fasudil is a selective ROCK inhibitor in use in Japan for the prevention of cerebral

vasospasm (Veldeman et al. 2016), and is thought to reduce vasoconstriction through a combination of decreased MLC phosphatase activity (Takagi et al. 2011) and ERK nuclear translocation (Wang et al. 2011), and increased angiotensin-converting enzyme (ACE) activity (Ocaranza et al. 2011).

Another, more potent, ROCK inhibitor, Ripasudil hydrochloride hydrate (K-115) is also in use in Japan as a treatment for ocular hypertension and glaucoma (Kaneko et al. 2016). Rapasudil-induced cytoskeletal changes, including rounding and retraction of cells, reduced the compaction of trabecular meshwork tissue, reducing resistance to aqueous outflow (Koga et al. 2006). The overexpression of CD98 in solid and haematological malignancies has led to the generation of a CD98-specific mouse monoclonal antibody (IGN523), which has demonstrated inhibition of tumour growth in patient-derived cancer xenographs and tumour cell apoptosis (Hayes et al. 2015). This compound was found to be safe and associated with anti-leukaemic activity when administered in a phase I clinical trial for acute myeloid leukaemia (Bixby et al. 2015). Finally, CD98hc siRNA, complexed in nanoparticles and administered as an oral hydrogel, reduced inflammatory colitis in mice (Laroui et al. 2014). Therefore, two clinically approved inhibitors of ROCK, an anti-CD98hc monoclonal antibody, and a novel method to administer CD98hc siRNA to patients may be amenable to future testing in models of VALI, either using *ex vivo* lung perfusion or PCLS technology.

6.4 Future work

I have attempted to measure both RhoA activity and cellular tension using FRET probes before and after 1 minute of CMS (3.3.9 3.3.10).

However, responses to CMS are likely to be dynamic and cellular rheology may follow a biphasic pattern of initial softening followed by reinforcement (1.6.2). Therefore, my on-going work aims to measure cellular tension and RhoA activity over a range of time points after the onset of CMS, using frequency domain FLIM to increase the rate of data acquisition. Furthermore, preliminary imaging of stress fibres indicated potential 'breaks' following CMS with realignment of focal adhesions to damaged ends of stress fibres (3.3.2). My aims for future work include staining for the focal adhesion protein zyxin, to determine whether this protein is mobilised to stress fibres in a possible repair process. This work will also consolidate evidence of CMS-induced cellular 'hardening' with longer time courses of strain.

With regards to investigating CMS-induced RhoA activity, and the effect of CD98hc kd on this process, future work will aim to establish expression profiles of the RhoGEFs LARG and GEFH1, and phosphorylation of the myosin light chain MLC2 under these conditions. This will help establish the regulation of signalling upstream of RhoA and downstream of ROCK respectively. Furthermore, effects on downstream YAP/TAZ expression will be helpful to better characterise CMS and CD98hc-Rho mediated signalling. CD98 itself is composed of the integrin-associated component of the heavy chain, and light chains, which enable amino acid transport. Use of previously described mutations composed of only the cytoplasmic, transmembrane or extracellular domains (Feral et al. 2005) will help clarify the role of CD98hc in CMS-induced mechanotransduction.

The work in this thesis has been based on CMS-induced and β1-integrin-mediated cell signalling in a monolayer of epithelial cells, However, CMS induced gap formations between cells (3.3.1) and it is likely that cell-cell interactions play a major role in CMS-induced mechanoresponses. Therefore, future investigation of the expression and localisation of, for example, α and β catenin, would help improve understanding of the interplay between cell-cell and cell-matrix adhesions in response to CMS. This is particularly relevant given evidence that CMS-induced YAP/TAZ signalling is mediated via β-catenin, and that CD98hc silencing induced β-catenin degradation (Santiago-Gómez et al. 2013).

Finally, I attempted to develop a more physiologically relevant model of CMS-induced mechanotransduction in alveolar epithelial cells using PCLS. Further optimisation is needed to characterise cells involved in CMS-induced proliferation and cytokine release, and the dynamic interplay between cells over a time course of CMS. However, providing this can be achieved, the effect of ROCK and CD98hc inhibition on CMS-induced injurious signalling can be ascertained using clinically approved and validated inhibitors as discussed above.

6.5 Overall conclusions

ROCK-NMII activity and CD98hc expression are necessary for CMS-induced cytokine release in alveolar epithelial cells *in vitro*. However, it is likely that CMS-induced injury is a result of dynamic interplay between different cell types, cell-matrix and cell-cell interactions. The use of bridge platforms between *in vitro* and *in vivo* conditions, such as PCLS, will allow

further investigation of this important and exciting, but still poorly understood, discipline of alveolar epithelial biology.

7 References

Abiko, H. et al., 2015. Rho guanine nucleotide exchange factors involved in cyclic-stretch-induced reorientation of vascular endothelial cells. *Journal of cell science*, 128(9), pp.1683–95.

Alçada, J. et al., 2014. S98 A Novel Human Model To Study Alveolar Injury And Repair. *Thorax*, 69(Suppl 2), p.A53 LP-A53.

Alcaraz, J. et al., 2003. Microrheology of human lung epithelial cells measured by atomic force microscopy. *Biophysical journal*, 84(3), pp.2071–9.

Alexandrova, A.Y. et al., 2008. Comparative dynamics of retrograde actin flow and focal adhesions: Formation of nascent adhesions triggers transition from fast to slow flow. *PLoS ONE*, 3(9), p.e3234.

Amano, M. et al., 1996. Phosphorylation and activation of myosin by Rho-associated kinase (Rho-kinase). *The Journal of biological chemistry*, 271(34), pp.20246–9.

Andreeva, A. V, Kutuzov, M. a & Voyno-Yasenetskaya, T. a, 2007. Regulation of surfactant secretion in alveolar type II cells. *American journal of physiology. Lung cellular and molecular physiology*, 293(2), pp.L259-71.

Aragona, M. et al., 2013. A mechanical checkpoint controls multicellular growth through YAP/TAZ regulation by actin-processing factors. *Cell*, 154(5), pp.1047–59.

ARDS Network, 2000. Ventilation with lower tidal volumes as compared with traditional tidal volumes for acute lung injury and the acute respiratory distress syndrome. *New England Journal of Medicine*, 342(18), pp.1301–1308.

Arias-Salgado, E.G. et al., 2003. Src kinase activation by direct interaction with the integrin cytoplasmic domain. *Proceedings of the National Academy of Sciences*, 100(23), pp.13298–13302.

Arold, S.P., Bartolák-Suki, E. & Suki, B., 2009. Variable stretch pattern enhances surfactant secretion in alveolar type II cells in culture. *American journal of physiology. Lung cellular and molecular physiology*, 296(4), pp.L574-81.

Atabai, K. et al., 2002. Keratinocyte growth factor can enhance alveolar epithelial repair by nonmitogenic mechanisms. *American Journal of Physiology - Lung Cellular and Molecular Physiology*, 283(1), pp.L163–L169.

Atherton, P. et al., 2015. Vinculin controls talin engagement with the actomyosin machinery. *Nature Communications*, 6, p.10038.

Bagnato, G. & Harari, S., 2015. Cellular interactions in the pathogenesis of interstitial lung diseases. *European Respiratory Review*, 24(135).

Bajaj, J. et al., 2016. CD98-Mediated Adhesive Signaling Enables the Establishment and Propagation of Acute Myelogenous Leukemia. *Cancer Cell*, 30(5), pp.792–805.

Balcioglu, H.E. et al., 2015. The integrin expression profile modulates orientation and dynamics of force transmission at cell-matrix adhesions. *Journal of cell science*, 128(7), pp.1316–26.

Ballestrem, C. et al., 2006. Molecular mapping of tyrosine-phosphorylated proteins in focal adhesions using fluorescence resonance energy transfer. *J Cell Sci*, 119(Pt 5), pp.866–

875.

Banes, A.J. et al., 1985. A new vacuum-operated stress-providing instrument that applies static or variable duration cyclic tension or compression to cells in vitro. *Journal of cell science*, 75, pp.35–42.

Barber, P.. et al., 2009. Multiphoton time-domain fluorescence lifetime imaging microscopy: practical application to protein-protein interactions using global analysis. *Journal of The Royal Society Interface*, 6(Suppl_1), pp.S93–S105.

Barkauskas, C.E. et al., 2013. Type 2 alveolar cells are stem cells in adult lung. *The Journal of clinical investigation*, 123(7), pp.3025–36.

Bastin, A.J. et al., 2016. Systemic inflammation and oxidative stress post-lung resection: Effect of pretreatment with N-acetylcysteine. *Respirology*, 21(1), pp.180–187.

Belperio, J.A. et al., 2002. Critical role for CXCR2 and CXCR2 ligands during the pathogenesis of ventilator-induced lung injury. *Journal of Clinical Investigation*, 110(11), pp.1703–1716.

Belperio, J.A. et al., 2006. The role of cytokines during the pathogenesis of ventilator-associated and ventilator-induced lung injury. *Seminars in respiratory and critical care medicine*, 27(4), pp.350–64.

Benham-Pyle, B.W., Pruitt, B.L. & Nelson, W.J., 2015. Mechanical strain induces E-cadherin-dependent Yap1 and -catenin activation to drive cell cycle entry. *Science*, 348(6238), pp.1024–1027.

Bergner, A. & Sanderson, M.J., 2002. ATP stimulates Ca2+ oscillations and contraction in airway smooth muscle cells of mouse lung slices. *American journal of physiology. Lung cellular and molecular physiology*, 283(6), pp.L1271-9.

Bhuyan, Z.A. et al., 2014. CD98hc regulates the development of experimental colitis by controlling effector and regulatory CD4+ T cells. *Biochemical and Biophysical Research Communications*, 444(4), pp.628–633.

Bieler, F.H. et al., 2009. Biaxial cell stimulation: A mechanical validation. *Journal of Biomechanics*, 42(11), pp.1692–1696.

Birukova, A.A. et al., 2016. Selective Role of Vinculin in Contractile Mechanisms of Endothelial Permeability. *American Journal of Respiratory Cell and Molecular Biology*, 55(4), pp.476–486.

Birukova, A.A. et al., 2012. Stimulation of Rho signaling by pathologic mechanical stretch is a “second hit” to Rho-independent lung injury induced by IL-6. *American Journal of Physiology - Lung Cellular and Molecular Physiology*, 302(9), pp.L965–L975.

Bixby, D. et al., 2015. A Phase I Study of IGN523, a Novel Anti-CD98 Monoclonal Antibody in Patients with Relapsed or Refractory Acute Myeloid Leukemia (AML). *Blood*, 126, p.3809.

Bledzka, K. et al., 2016. Kindlin-2 directly binds actin and regulates integrin outside-in signaling. *The Journal of Cell Biology*, 213(1).

Borghi, N. et al., 2012. E-cadherin is under constitutive actomyosin-generated tension that is increased at cell-cell contacts upon externally applied stretch. *Proceedings of the National Academy of Sciences*, 109(31), pp.12568–12573.

Boulter, E. et al., 2013. CD98hc (SLC3A2) regulation of skin homeostasis wanes with age. *The Journal of experimental medicine*, 210(1), pp.173–90.

Brody, J.S., Burki, R. & Kaplan, N., 1978. Deoxyribonucleic acid synthesis in lung cells during compensatory lung growth after pneumonectomy. *The American review of respiratory disease*, 117(2), pp.307–16.

Buhain, W.J. & Brody, J.S., 1973. Compensatory growth of the lung following pneumonectomy. *Journal of applied physiology*, 35(6), pp.898–902.

Bulus, N. et al., 2012. CD98 Increases Renal Epithelial Cell Proliferation by Activating MAPKs. *PLoS ONE*, 7(6).

Burgstaller, G. et al., 2015. Multidimensional immunolabeling and 4D time-lapse imaging of vital ex vivo lung tissue. *American journal of physiology. Lung cellular and molecular physiology*, 309(4), pp.L323-32.

Burridge, K. & Guilluy, C., 2016. Focal adhesions, stress fibers and mechanical tension. *Experimental Cell Research*, 343(1), pp.14–20.

Butler, J.P. et al., 2012. Evidence for Adult Lung Growth in Humans. *New England Journal of Medicine*, 367(3), pp.244–247.

Byron, A. et al., 2009. Anti-integrin monoclonal antibodies. *Journal of cell science*, 122(Pt 22), pp.4009–11.

Cai, S. et al., 2005. CD98 modulates integrin beta1 function in polarized epithelial cells. *Journal of cell science*, 118(Pt 5), pp.889–99.

Calderwood, D., Campbell, I.D. & Critchley, D.R., 2013. Talins and kindlins: partners in integrin-mediated adhesion. *Nature reviews. Molecular cell biology*, 14(8), pp.503–17.

Campbell, I.D. & Humphries, M.J., 2011. Integrin Structure, Activation, and Interactions. *Cold Spring Harbor Perspectives in Biology*, 3(3), pp.a004994–a004994.

Cantor, J.M. & Ginsberg, M.H., 2012. CD98 at the crossroads of adaptive immunity and cancer. *J Cell Sci*, 125(Pt 6), pp.1373–1382.

Cantor, J.M., Ginsberg, M.H. & Rose, D.M., 2008. Integrin-associated proteins as potential therapeutic targets. *Immunological Reviews*, 223, pp.236–251.

Case, L.B. & Waterman, C.M., 2015. Integration of actin dynamics and cell adhesion by a three-dimensional, mechanosensitive molecular clutch. *Nature Cell Biology*, 17(8), p.955.

Chandrasekaran, S. et al., 1999. Pro-adhesive and chemotactic activities of thrombospondin-1 for breast carcinoma cells are mediated by alpha3beta1 integrin and regulated by insulin-like growth factor-1 and CD98. *The Journal of biological chemistry*, 274(16), pp.11408–16.

Chapman, H.A. et al., 2011. Integrin α6β4 identifies an adult distal lung epithelial population with regenerative potential in mice. *The Journal of clinical investigation*, 121(7), pp.2855–62.

Chapman, K.E. et al., 2005. Cyclic mechanical strain increases reactive oxygen species production in pulmonary epithelial cells. *Am J Physiol Lung Cell Mol Physiol*, 289(5), pp.L834-41.

Charras, G.T. & Horton, M.A., 2002. Single Cell Mechanotransduction and Its Modulation Analyzed by Atomic Force Microscope Indentation. *Biophysical Journal*, 82(6), pp.2970–2981.

Chaturvedi, L.S., Marsh, H.M. & Basson, M.D., 2006. Src and focal adhesion kinase mediate mechanical strain-induced proliferation and ERK1/2 phosphorylation in human H441 pulmonary epithelial cells. *AJP: Cell Physiology*, 292(5), pp.C1701–C1713.

Chen, B. et al., 2012. Cyclic Stretch Induces Cell Reorientation on Substrates by Destabilizing Catch Bonds in Focal Adhesions A. Pelling, ed. *PLoS ONE*, 7(11), p.e48346.

Chen, C. et al., 2010. Fluidization and resolidification of the human bladder smooth muscle cell in response to transient stretch. *PloS one*, 5(8), p.e12035.

Chess, P.R. et al., 2010. Murine mechanical ventilation stimulates alveolar epithelial cell proliferation. *Experimental lung research*, 36(6), pp.331–41.

Chignalia, A.Z. et al., 2015. p120-Catenin Expressed in Alveolar Type II Cells Is Essential for the Regulation of Lung Innate Immune Response. *The American Journal of Pathology*, 185(5), p.1251.

Chiumello, D., Pristine, G. & Slutsky, A.S., 1999. Mechanical ventilation affects local and systemic cytokines in an animal model of acute respiratory distress syndrome. *Am J Respir Crit Care Med*, 160(1), pp.109–116.

Choi, C.K. et al., 2008. Actin and α-actinin orchestrate the assembly and maturation of nascent adhesions in a myosin II motor-independent manner. *Nature Cell Biology*, 10(9), pp.1039–1050.

Chrzanowska-Wodnicka, M. & Burridge, K., 1996. Rho-stimulated Contractility Drives the Formation of Stress Fibers and Focal Adhesions. *The Journal of Cell Biology*, 133(6), pp.1403–1415.

Cinel, I. et al., 2012. Involvement of Rho kinase (ROCK) in sepsis-induced acute lung injury. *Journal of thoracic disease*, 4(1), pp.30–9.

Cirka, H. et al., 2016. Active Traction Force Response to Long-Term Cyclic Stretch Is Dependent on Cell Pre-stress. *Biophysical Journal*, 110(8), pp.1845–1857.

Colombelli, J. et al., 2009. Mechanosensing in actin stress fibers revealed by a close correlation between force and protein localization. *Journal of cell science*, 122(Pt 10), pp.1665–1679.

Conway, D.E. et al., 2013. Fluid Shear Stress on Endothelial Cells Modulates Mechanical Tension across VE-Cadherin and PECAM-1. *Current Biology*, 23(11), pp.1024–1030.

Cooke, C.R. et al., 2009. Cost-effectiveness of implementing low-tidal volume ventilation in patients with acute lung injury. *Chest*, 136(1), pp.79–88.

Cooper, J.R. et al., 2016. Long Term Culture of the A549 Cancer Cell Line Promotes Multilamellar Body Formation and Differentiation towards an Alveolar Type II Pneumocyte Phenotype F. Cappello, ed. *PLOS ONE*, 11(10), p.e0164438.

Copland, I.B. & Post, M., 2007. Stretch-activated signaling pathways responsible for early response gene expression in fetal lung epithelial cells. *Journal of Cellular Physiology*, 210(1), pp.133–143.

Correa-Meyer, E. et al., 2002. Cyclic stretch activates ERK1/2 via G proteins and EGFR in alveolar epithelial cells. *American journal of physiology. Lung cellular and molecular physiology*, 282(5), pp.L883-91.

Costello, M.L., Mathieu-Costello, O. & West, J.B., 1992. Stress Failure of Alveolar Epithelial Cells Studied by Scanning Electron Microscopy. *American Review of Respiratory*

Disease, 145(6), pp.1446–1455.

Craig, E.M. et al., 2012. Membrane Tension, Myosin Force, and Actin Turnover Maintain Actin Treadmill in the Nerve Growth Cone. *Biophysical Journal*, 102(7), pp.1503–1513.

Crosby, L.M. et al., 2011. Balance of life and death in alveolar epithelial type II cells: proliferation, apoptosis, and the effects of cyclic stretch on wound healing. *American journal of physiology. Lung cellular and molecular physiology*, 301(4), pp.L536-46.

Crosby, L.M. & Waters, C.M., 2010. Epithelial repair mechanisms in the lung. *American journal of physiology. Lung cellular and molecular physiology*, 298(6), pp.L715-31.

Cui, Y. et al., 2015. Cyclic stretching of soft substrates induces spreading and growth. *Nature communications*, 6, p.6333.

Cukierman, E. et al., 2001. Taking cell-matrix adhesions to the third dimension. *Science (New York, N.Y.)*, 294(5547), pp.1708–12.

Cypel, M. et al., 2011. Normothermic Ex Vivo Lung Perfusion in Clinical Lung Transplantation. *New England Journal of Medicine*, 364(15), pp.1431–1440.

Dassow, C. et al., 2010. Biaxial distension of precision-cut lung slices. *J Appl Physiol*, 108, pp.713–721.

Davidovich, N. et al., 2013. Cyclic Stretch–Induced Oxidative Stress Increases Pulmonary Alveolar Epithelial Permeability. *American Journal of Respiratory Cell and Molecular Biology*, 49(1), pp.156–164.

Davidovich, N., Huang, J. & Margulies, S.S., 2013. Reproducible uniform equibiaxial stretch of precision-cut lung slices. *American journal of physiology. Lung cellular and molecular physiology*, 304, pp.L210-20.

Davis, B.M. et al., 2016. Automatic quantitative analysis of experimental primary and secondary retinal neurodegeneration: implications for optic neuropathies. *Cell death discovery*, 2, p.16031.

Dembo, M. et al., 1988. The reaction-limited kinetics of membrane-to-surface adhesion and detachment. *Proceedings of the Royal Society of London. Series B, Biological sciences*, 234(1274), pp.55–83.

Desai, L.P. et al., 2007. High tidal volume mechanical ventilation with hyperoxia alters alveolar type II cell adhesion. *American journal of physiology. Lung cellular and molecular physiology*, 293(3), pp.L769-78.

Desai, L.P., Chapman, K.E. & Waters, C.M., 2008. Mechanical stretch decreases migration of alveolar epithelial cells through mechanisms involving Rac1 and Tiam1. *AJP: Lung Cellular and Molecular Physiology*, 295(5), pp.L958–L965.

Desai, L.P., White, S.R. & Waters, C.M., 2010. Cyclic mechanical stretch decreases cell migration by inhibiting phosphatidylinositol 3-kinase- and focal adhesion kinase-mediated JNK1 activation. *J Biol Chem*, 285(7), pp.4511–4519.

Desai, T.J., Brownfield, D.G. & Krasnow, M.A., 2014. Alveolar progenitor and stem cells in lung development, renewal and cancer. *Nature*, 507(7491), pp.190–4.

Devés, R. & Boyd, C.A., 2000. Surface antigen CD98(4F2): not a single membrane protein, but a family of proteins with multiple functions. *The Journal of membrane biology*, 173(3), pp.165–77.

Dipaolo, B.C. et al., 2013. Rac1 pathway mediates stretch response in pulmonary alveolar epithelial cells. *Am J Physiol Lung Cell Mol Physiol*, 305(2), pp.L141-53.

DiPaolo, B.C. et al., 2010. Stretch magnitude and frequency-dependent actin cytoskeleton remodeling in alveolar epithelia. *American journal of physiology. Cell physiology*, 299(2), pp.C345–C353.

DiPaolo, B.C. & Margulies, S.S., 2012. Rho kinase signaling pathways during stretch in primary alveolar epithelia. *AJP: Lung Cellular and Molecular Physiology*, 302(10), pp.L992–L1002.

Discher, D.E., Janmey, P. & Wang, Y., 2005. Tissue Cells Feel and Respond to the Stiffness of Their Substrate. *Science*, 310(5751).

Donnelly, S.C. et al., 1993. Interleukin-8 and development of adult respiratory distress syndrome in at-risk patient groups. *Lancet (London, England)*, 341(8846), pp.643–7.

Dreyfuss, D. et al., 1988. High inflation pressure pulmonary edema. Respective effects of high airway pressure, high tidal volume, and positive end-expiratory pressure. *Am Rev Respir Dis*, 137(5), pp.1159–1164.

Dreyfuss, D. & Saumon, G., 1998. Ventilator-induced lung injury: lessons from experimental studies. *American journal of respiratory and critical care medicine*, 157(1), pp.294–323.

Du, X. et al., 1991. Ligands “activate” integrin αIIbβ3 (platelet GPIIb-IIIa). *Cell*, 65(3), pp.409–416.

Dunsmore, S.E. & Rannels, D.E., 1996. Extracellular matrix biology in the lung. *The American journal of physiology*, 270(1 Pt 1), pp.L3-27.

Dupont, S. et al., 2011. Role of YAP/TAZ in mechanotransduction. *Nature*, 474(7350), pp.179–183.

Elbashir, S.M. et al., 2001. Duplexes of 21-nucleotide RNAs mediate RNA interference in cultured mammalian cells. *Nature*, 411(6836), pp.494–498.

Elosegui-Artola, A. et al., 2016. Mechanical regulation of a molecular clutch defines force transmission and transduction in response to matrix rigidity. *Nature cell biology*, 18(5), pp.540–8.

Elosegui-Artola, A. et al., 2014. Rigidity sensing and adaptation through regulation of integrin types. *Nature Materials*, 13(6), pp.631–7.

Engler, A.J. et al., 2006. Matrix Elasticity Directs Stem Cell Lineage Specification. *Cell*, 126(4), pp.677–689.

Estrach, S. et al., 2014. CD98hc (SLC3A2) loss protects against ras-driven tumorigenesis by modulating integrin-mediated mechanotransduction. *Cancer Research*, 74(23), pp.6878–6889.

Evans, M.J. et al., 1975. Transformation of alveolar Type 2 cells to Type 1 cells following exposure to NO2. *Experimental and Molecular Pathology*, 22(1), pp.142–150.

Even-Ram, S. et al., 2007. Myosin IIA regulates cell motility and actomyosin–microtubule crosstalk. *Nature Cell Biology*, 9(3), pp.299–309.

Faust, U. et al., 2011. Cyclic stress at mHz frequencies aligns fibroblasts in direction of zero strain. *PloS one*, 6(12), p.e28963.

Fenczik, C.A. et al., 1997. Complementation of dominant suppression implicates CD98 in integrin activation. *Nature*, 390(6655), pp.81–85.

Fenczik, C.A. et al., 2001. Distinct domains of CD98hc regulate integrins and amino acid transport. *J Biol Chem*, 276(12), pp.8746–8752.

Feral, C.C. et al., 2005. CD98hc (SLC3A2) mediates integrin signaling. *Proceedings of the National Academy of Sciences of the United States of America*, 102(2), pp.355–60.

Féral, C.C. et al., 2007. CD98hc (SLC3A2) participates in fibronectin matrix assembly by mediating integrin signaling. *The Journal of cell biology*, 178(4), pp.701–11.

Fernández-Pérez, E.R. et al., 2008. Ventilator settings and outcome of respiratory failure in chronic interstitial lung disease. *Chest*, 133(5), pp.1113–9.

Flecknoe, S. et al., 2000. Increased lung expansion alters the proportions of type I and type II alveolar epithelial cells in fetal sheep. *American Journal of Physiology - Lung Cellular and Molecular Physiology*, 278(6).

Flecknoe, S.J. et al., 2003. Changes in alveolar epithelial cell proportions during fetal and postnatal development in sheep. *American Journal of Physiology - Lung Cellular and Molecular Physiology*, 285(3), pp.L664–L670.

Flecknoe, S.J. et al., 2002. Determination of alveolar epithelial cell phenotypes in fetal sheep: evidence for the involvement of basal lung expansion. *The Journal of physiology*, 542(Pt 1), pp.245–53.

Fletcher, D.A. & Mullins, R.D., 2010. Cell mechanics and the cytoskeleton. *Nature*, 463(7280), pp.485–92.

Forrest, J.B., 1970. The effect of changes in lung volume on the size and shape of alveoli. *The Journal of physiology*, 210(3), pp.533–47.

Förster, T., 1948. Intermolecular energy transference and fluorescence. *Ann Physik*, 2, pp.55–75.

Fotiadis, D., Kanai, Y. & Palacín, M., 2013. The SLC3 and SLC7 families of amino acid transporters. *Molecular Aspects of Medicine*, 34(2–3), pp.139–158.

Frank, J.A. et al., 2002. Low tidal volume reduces epithelial and endothelial injury in acid-injured rat lungs. *American journal of respiratory and critical care medicine*, 165(2), pp.242–9.

Friedland, J.C., Lee, M.H. & Boettiger, D., 2009. Mechanically activated integrin switch controls alpha5beta1 function. *Science (New York, N.Y.)*, 323(5914), pp.642–4.

Fu, P. et al., 2011. Induction of cellular antioxidant defense by amifostine improves ventilator-induced lung injury*. *Critical Care Medicine*, 39(12), pp.2711–2721.

Fuchs, S. et al., 2003. Differentiation of human alveolar epithelial cells in primary culture: morphological characterization and synthesis of caveolin-1 and surfactant protein-C. *Cell and Tissue Research*, 311(1), pp.31–45.

Fujino, N. et al., 2010. Isolation of alveolar epithelial type II progenitor cells from adult human lungs. *Laboratory Investigation*, 91, pp.363–378.

Futier, E. et al., 2013. A Trial of Intraoperative Low-Tidal-Volume Ventilation in Abdominal Surgery. *New England Journal of Medicine*, 369(5), pp.428–437.

Futier, E. & Jaber, S., 2014. Lung-protective ventilation in abdominal surgery. *Current Opinion in Critical Care*, 20(4), pp.426–430.

Gajic, O. et al., 2003. Ventilator-induced cell wounding and repair in the intact lung. *Am J Respir Crit Care Med*, 167(8), pp.1057–1063.

Galiacy, S. et al., 2003. Keratinocyte growth factor promotes cell motility during alveolar epithelial repair in vitro. *Experimental cell research*, 283(2), pp.215–29.

Gallego Romero, I. et al., 2014. RNA-seq: impact of RNA degradation on transcript quantification. *BMC Biology*, 12(1), p.42.

García Cerdá, D. et al., 2015. Use of cyanoacrylate adhesives in general surgery. *Surgery Today*, 45(8), pp.939–956.

Gattinoni, L. et al., 1993. Regional effects and mechanism of positive end-expiratory pressure in early adult respiratory distress syndrome. *JAMA*, 269(16), pp.2122–7.

Gawlak, G. et al., 2014. Paxillin mediates stretch-induced Rho signaling and endothelial permeability via assembly of paxillin-p42/44MAPK-GEF-H1 complex. *FASEB journal : official publication of the Federation of American Societies for Experimental Biology*, 28(7), pp.3249–60.

Geiser, T. et al., 2000. Interleukin-1beta augments in vitro alveolar epithelial repair. *Am J Physiol Lung Cell Mol Physiol*, 279(6), pp.L1184-90.

Geiser, T. et al., 2001. Pulmonary edema fluid from patients with acute lung injury augments in vitro alveolar epithelial repair by an IL-1beta-dependent mechanism. *American journal of respiratory and critical care medicine*, 163(6), pp.1384–8.

Geiser, T.K. et al., 2001. Pseudomonas aeruginosa ExoT inhibits in vitro lung epithelial wound repair. *Cellular Microbiology*, 3(4), pp.223–236.

Gharib, S.A. et al., 2010. Of mice and men: comparative proteomics of bronchoalveolar fluid. *Eur Respir J*, 35(6), pp.1388–1395.

Ghazanfari, S., Tafazzoli-Shadpour, M. & Shokrgozar, M.A., 2009. *Effects of cyclic stretch on proliferation of mesenchymal stem cells and their differentiation to smooth muscle cells*,

Giannelli, G. et al., 2001. Human Hepatocellular Carcinoma (HCC) Cells Require Both α3β1 Integrin and Matrix Metalloproteinases Activity for Migration and Invasion. *Laboratory Investigation*, 81(4), pp.613–627.

Giard, D.J. et al., 1973. In vitro cultivation of human tumors: establishment of cell lines derived from a series of solid tumors. *Journal of the National Cancer Institute*, 51(5), pp.1417–23.

Gibbs, R.A., 1990. DNA amplification by the polymerase chain reaction. *Analytical chemistry*, 62(13), pp.1202–14.

Gil, J. et al., 1979. Alveolar volume-surface area relation in air- and saline-filled lungs fixed by vascular perfusion. *Journal of Applied Physiology*, 47(5).

Gilbert, J.A. et al., 1994. Strain profiles for circular cell culture plates containing flexible surfaces employed to mechanically deform cells in vitro. *Journal of biomechanics*, 27(9), pp.1169–77.

Ginsberg, M.H., Partridge, A. & Shattil, S.J., 2005. Integrin regulation. *Current Opinion in Cell Biology*, 17(5), pp.509–516.

Gjorevski, N. & Nelson, C.M., 2010. Endogenous patterns of mechanical stress are required for branching morphogenesis. *Integrative biology : quantitative biosciences from nano to macro*, 2(9), pp.424–34.

Godin, L.M. et al., 2011. Spatiotemporal dynamics of actin remodeling and endomembrane trafficking in alveolar epithelial type I cell wound healing. *American Journal of Physiology - Lung Cellular and Molecular Physiology*, 300(4).

Goldyn, A.M. et al., 2009. Force-induced cell polarisation is linked to RhoA-driven microtubule-independent focal-adhesion sliding. *Journal of cell science*, 122(Pt 20), pp.3644–51.

Goto, H. et al., 1999. Identification of a novel phosphorylation site on histone H3 coupled with mitotic chromosome condensation. *The Journal of biological chemistry*, 274(36), pp.25543–9.

Grashoff, C. et al., 2010. Measuring mechanical tension across vinculin reveals regulation of focal adhesion dynamics. *Nature*, 466(7303), pp.263–266.

Greiner, A.M. et al., 2013. Cyclic Tensile Strain Controls Cell Shape and Directs Actin Stress Fiber Formation and Focal Adhesion Alignment in Spreading Cells. *PLoS ONE*, 8(10).

Grembowicz, K.P., Sprague, D. & McNeil, P.L., 1999. Temporary disruption of the plasma membrane is required for c-fos expression in response to mechanical stress. *Mol Biol Cell*, 10(4), pp.1247–1257.

Griesenbach, U. et al., 2012. Assessment of F/HN-pseudotyped lentivirus as a clinically relevant vector for lung gene therapy. *American journal of respiratory and critical care medicine*, 186(9), pp.846–56.

Grochot-Przeczek, A. et al., 2009. Heme oxygenase-1 accelerates cutaneous wound healing in mice. *PloS one*, 4(6), p.e5803.

Guay, J. & Ochroch, E.A., 2015. Intraoperative use of low volume ventilation to decrease postoperative mortality, mechanical ventilation, lengths of stay and lung injury in patients without acute lung injury. J. Guay, ed. *The Cochrane database of systematic reviews*, 20(12), p.CD011151.

Gudipaty, S.A. et al., 2017. Mechanical stretch triggers rapid epithelial cell division through Piezo1. *Nature*, 543(7643), pp.118–121.

Guilluy, C. et al., 2014. Isolated nuclei adapt to force and reveal a mechanotransduction pathway in the nucleus. *Nature Cell Biology*, 16(4), pp.376–381.

Guilluy, C. et al., 2011. The Rho GEFs LARG and GEF-H1 regulate the mechanical response to force on integrins. *Nature cell biology*, 13(6), pp.722–727.

Güldner, A. et al., 2016. Comparative Effects of Volutrauma and Atelectrauma on Lung Inflammation in Experimental Acute Respiratory Distress Syndrome. *Critical Care Medicine*, 44(9), pp.e854–e865.

Guo, L. et al., 2016. Mechanical ventilation strategies for intensive care unit patients without acute lung injury or acute respiratory distress syndrome: a systematic review and network meta-analysis. *Critical Care*, 20(1), p.226.

Gupta, M. et al., 2015. Adaptive rheology and ordering of cell cytoskeleton govern matrix rigidity sensing. *Nature communications*, 6(May), p.7525.

Hamlington, K.L. et al., 2016. Modeling the Progression of Epithelial Leak Caused by Overdistension. *Cellular and Molecular Bioengineering*, 9(1), pp.151–161.

Hammerschmidt, S. et al., 2007. Stretch-induced alveolar type II cell apoptosis: role of endogenous bradykinin and PI3K-Akt signaling. *American journal of respiratory cell and molecular biology*, 37(6), pp.699–705.

Hamzeh, M.T., Sridhara, R. & Alexander, L.D., 2015. Cyclic stretch-induced TGF-β1 and fibronectin expression is mediated by β1-integrin through c-Src- and STAT3-dependent pathways in renal epithelial cells. *American journal of physiology. Renal physiology*, 308(5), pp.F425-36.

Hannus, M. et al., 2014. siPools: highly complex but accurately defined siRNA pools eliminate off-target effects. *Nucleic Acids Research*, 42(12), pp.8049–8061.

Hayakawa, K., Sato, N. & Obinata, T., 2001. Dynamic reorientation of cultured cells and stress fibers under mechanical stress from periodic stretching. *Experimental cell research*, 268(1), pp.104–14.

Hayakawa, K., Tatsumi, H. & Sokabe, M., 2008. Actin stress fibers transmit and focus force to activate mechanosensitive channels. *Journal of Cell Science*, 121(4).

Hayes, G.M. et al., 2015. Antitumor activity of an anti-CD98 antibody. *International Journal of Cancer*, 137(3), pp.710–720.

Haynes, B.F. et al., 1981. Characterization of a monoclonal antibody (4F2) that binds to human monocytes and to a subset of activated lymphocytes. *Journal of immunology (Baltimore, Md. : 1950)*, 126(4), pp.1409–14.

Heasman, S.J. et al., 2010. Coordinated RhoA signaling at the leading edge and uropod is required for T cell transendothelial migration. *The Journal of cell biology*, 190(4), pp.553–63.

Heijink, I.H. et al., 2010. Characterisation of cell adhesion in airway epithelial cell types using electric cell-substrate impedance sensing. *European Respiratory Journal*, 35(4), pp.894–903.

Henderson, N.C. et al., 2004. CD98hc (SLC3A2) interaction with β1 integrins is required for transformation. *Journal of Biological Chemistry*, 279(52), pp.54731–54741.

Hendzel, M.J. et al., 1997. Mitosis-specific phosphorylation of histone H3 initiates primarily within pericentromeric heterochromatin during G2 and spreads in an ordered fashion coincident with mitotic chromosome condensation. *Chromosoma*, 106(6), pp.348–60.

Henjakovic, M. et al., 2008. Ex Vivo Lung Function Measurements in Precision-Cut Lung Slices (PCLS) from Chemical Allergen–Sensitized Mice Represent a Suitable Alternative to In Vivo Studies. *Toxicological Sciences*, 106(2), pp.444–453.

Hernandez, L.A. et al., 1989. Chest wall restriction limits high airway pressure-induced lung injury in young rabbits. *Journal of applied physiology (Bethesda, Md.: 1985)*, 66(5), pp.2364–8.

Herrmann, H. et al., 2007. Intermediate filaments: from cell architecture to nanomechanics. *Nature Reviews Molecular Cell Biology*, 8(7), pp.562–573.

Herzog, E.L. et al., 2008. Knowns and unknowns of the alveolus. *Proceedings of the American Thoracic Society*, 5(7), pp.778–82.

Hirata, H. et al., 2015. Actomyosin bundles serve as a tension sensor and a platform for ERK activation. *EMBO Reports*, 16(2), pp.250–257.

Hittelman, W.N. et al., 2007. Proliferative changes in the bronchial epithelium of former smokers treated with retinoids. *Journal of the National Cancer Institute*, 99(21),

pp.1603–12.

Hoffman, A.M. et al., 2010. Matrix modulation of compensatory lung regrowth and progenitor cell proliferation in mice. *AJP: Lung Cellular and Molecular Physiology*, 298(2), pp.L158–L168.

Hoffman, B.D., Grashoff, C. & Schwartz, M.A., 2011. Dynamic molecular processes mediate cellular mechanotransduction. *Nature*, 475(7356), pp.316–323.

Hoffman, L.M. et al., 2012. Stretch-induced actin remodeling requires targeting of zyxin to stress fibers and recruitment of actin regulators. *Molecular Biology of the Cell*, 23(10), pp.1846–1859.

Hogan, B.M. et al., 2014. Repair and Regeneration of the Respiratory System: Complexity, Plasticity, and Mechanisms of Lung Stem Cell Function. *Cell Stem Cell*, 15(2), pp.123–138.

Hotulainen, P. & Lappalainen, P., 2006. Stress fibers are generated by two distinct actin assembly mechanisms in motile cells. *The Journal of cell biology*, 173(3), pp.383–94.

Hsia, C.C. et al., 1994. Compensatory lung growth occurs in adult dogs after right pneumonectomy. *The Journal of clinical investigation*, 94(1), pp.405–12.

Hsia, C.C. et al., 2001. Preventing mediastinal shift after pneumonectomy impairs regenerative alveolar tissue growth. *American journal of physiology. Lung cellular and molecular physiology*, 281(5), pp.L1279-87.

Hsia, C.C.W., 2004. Signals and mechanisms of compensatory lung growth. *J Appl Physiol*, 97(5), pp.1992–1998.

Hsu, H.-J. et al., 2010. Stretch-induced stress fiber remodeling and the activations of JNK and ERK depend on mechanical strain rate, but not FAK. M. Vooijs, ed. *PloS one*, 5(8), p.e12470.

Hu, P. & Luo, B.-H., 2013. Integrin bi-directional signaling across the plasma membrane. *Journal of Cellular Physiology*, 228(2), pp.306–312.

Hu, S. et al., 2017. Long-range self-organization of cytoskeletal myosin II filament stacks. *Nature Cell Biology*, 19(2), pp.133–141.

Hu, S. et al., 2005. Prestress mediates force propagation into the nucleus. *Biochemical and Biophysical Research Communications*, 329(2), pp.423–428.

Huang, J., Davidovich, N. & Margulies, S.S., 2012. Rat precision-cut lung slices as a model for deformation-induced lung injury studies. , pp.243–244.

Huang, X. et al., 2012. Matrix stiffness-induced myofibroblast differentiation is mediated by intrinsic mechanotransduction. *American journal of respiratory cell and molecular biology*, 47(3), pp.340–8.

Hubmayr, R.D., 2002. Perspective on Lung Injury and Recruitment. *American Journal of Respiratory and Critical Care Medicine*, 165(12), pp.1647–1653.

Huh, D. et al., 2010. Reconstituting organ-level lung functions on a chip. *Science*, 328(5986), pp.1662–1668.

Humphries, J.D., Byron, A. & Humphries, M.J., 2006. Integrin ligands at a glance. *Journal of Cell Science*, 119(19), pp.3901–3903.

Hung, C.T. & Williams, J.L., 1994. A method for inducing equi-biaxial and uniform strains in elastomeric membranes used as cell substrates. *Journal of biomechanics*, 27(2), pp.227–32.

Hwang, Y. & Barakat, A.I., 2012. Dynamics of mechanical signal transmission through prestressed stress fibers L. Kreplak, ed. *PLoS ONE*, 7(4), p.e35343.

Hynes, R.O., 2002. Integrins: Bidirectional, allosteric signaling machines. *Cell*, 110(6), pp.673–687.

Ingber, D.E. et al., 2014. Tensegrity, cellular biophysics, and the mechanics of living systems. *Reports on Progress in Physics*, 77(4), p.46603.

Jablonski, A., 1933. Efficiency of Anti-Stokes Fluorescence in Dyes. *Nature*, 131(3319), pp.839–840.

Jafari, B. et al., 2004. Intracellular glutathione in stretch-induced cytokine release from alveolar type-2 like cells. *Respirology*, 9(1), pp.43–53.

Jain, R. et al., 2015. Plasticity of Hopx(+) type I alveolar cells to regenerate type II cells in the lung. *Nature communications*, 6, p.6727.

Jayo, A., Parsons, M. & Adams, J.C., 2012. A novel Rho-dependent pathway that drives interaction of fascin-1 with p-Lin-11/Isl-1/Mec-3 kinase (LIMK) 1/2 to promote fascin-1/actin binding and filopodia stability. *BMC biology*, 10, p.72.

Johnson, S. & Rabinovitch, P., 2012. Ex vivo imaging of excised tissue using vital dyes and confocal microscopy. *Current protocols in cytometry*, Chapter 9, p.Unit 9.39.

Jokinen, J. et al., 2004. Integrin-mediated cell adhesion to type I collagen fibrils. *The Journal of biological chemistry*, 279(30), pp.31956–63.

Jungbauer, S. et al., 2008. Two characteristic regimes in frequency-dependent dynamic reorientation of fibroblasts on cyclically stretched substrates. *Biophysical journal*, 95(7), pp.3470–8.

Jurchenko, C. & Salaita, K.S., 2015. Lighting Up the Force: Investigating Mechanisms of Mechanotransduction Using Fluorescent Tension Probes. *Molecular and Cellular Biology*, 35(15), pp.2570–82.

Kallet, R.H. & Matthay, M.A., 2013. Hyperoxic acute lung injury. *Respiratory care*, 58(1), pp.123–41.

Kaneko, Y. et al., 2016. Effects of K-115 (Ripasudil), a novel ROCK inhibitor, on trabecular meshwork and Schlemm's canal endothelial cells. *Scientific reports*, 6(January), p.19640.

Kaplan, M. et al., 2004. Histopathological effects of ethyl 2-cyanoacrylate tissue adhesive following surgical application: an experimental study. *European journal of cardio-thoracic surgery : official journal of the European Association for Cardio-thoracic Surgery*, 25(2), pp.167–72.

Kassianidou, E. & Kumar, S., 2015. A biomechanical perspective on stress fiber structure and function. *Biochimica et Biophysica Acta (BBA) - Molecular Cell Research*, 1853(11), pp.3065–3074.

Kaunas, R. et al., 2005. Cooperative effects of Rho and mechanical stretch on stress fiber organization. *Proceedings of the National Academy of Sciences of the United States of America*, 102(44), pp.15895–15900.

Kawamoto, M. & Fukuda, Y., 1990. Cell proliferation during the process of bleomycin-induced pulmonary fibrosis in rats. *Acta pathologica japonica*, 40(4), pp.227–38.

Kawamura, S., Miyamoto, S. & Brown, J.H., 2003. Initiation and transduction of stretch-induced RhoA and Rac1 activation through caveolae: cytoskeletal regulation of ERK translocation. *The Journal of biological chemistry*, 278(33), pp.31111–7.

Kawano, Y. et al., 1999. Phosphorylation of myosin-binding subunit (MBS) of myosin phosphatase by Rho-kinase in vivo. *The Journal of cell biology*, 147(5), pp.1023–38.

Kho, A.T. et al., 2013. Identification of dedifferentiation and redevelopment phases during postpneumonectomy lung growth. *American Journal of Physiology - Lung Cellular and Molecular Physiology*, 305(8).

Kim, C.F.B. et al., 2005. Identification of bronchioalveolar stem cells in normal lung and lung cancer. *Cell*, 121(6), pp.823–35.

Kim, H.J. et al., 1997. Integrin mediation of alveolar epithelial cell migration on fibronectin and type I collagen. *American Journal of Physiology - Lung Cellular and Molecular Physiology*, 273(1).

Kimura, K. et al., 1996. Regulation of myosin phosphatase by Rho and Rho-associated kinase (Rho-kinase). *Science (New York, N.Y.)*, 273(5272), pp.245–8.

Knies, Y. et al., 2006. Mechanical stretch induces clustering of β1-integrins and facilitates adhesion. *Experimental Dermatology*, 15(5), pp.347–355.

Koga, T. et al., 2006. Rho-associated protein kinase inhibitor, Y-27632, induces alterations in adhesion, contraction and motility in cultured human trabecular meshwork cells. *Experimental Eye Research*, 82(3), pp.362–370.

Kong, F. et al., 2013. Cyclic Mechanical Reinforcement of Integrin–Ligand Interactions. *Molecular Cell*, 49(6), pp.1060–1068.

Kong, F. et al., 2009. Demonstration of catch bonds between an integrin and its ligand. *Journal of Cell Biology*, 185(7), pp.1275–1284.

Königshoff, M., 2014. Live and let die: Targeting alveolar epithelial cell proliferation in pulmonary fibrosis. *American Journal of Respiratory and Critical Care Medicine*, 190(12), pp.1339–1341.

Koukoulis, G.K. et al., 1997. Immunolocalization of integrins in the normal lung and in pulmonary carcinomas. *Human pathology*, 28(9), pp.1018–25.

Koushik, S. V & Vogel, S.S., 2008. Energy migration alters the fluorescence lifetime of Cerulean: implications for fluorescence lifetime imaging Forster resonance energy transfer measurements. *Journal of biomedical optics*, 13(3), p.31204.

Krishnan, R. et al., 2009. Reinforcement versus fluidization in cytoskeletal mechanoresponsiveness. *PloS one*, 4(5), p.e5486.

Kroon, A.A. et al., 2013. Mechanical ventilation-induced apoptosis in newborn rat lung is mediated via FasL/Fas pathway. *American Journal of Physiology - Lung Cellular and Molecular Physiology*, 305(11).

Kubista, M. et al., 2006. The real-time polymerase chain reaction. *Molecular Aspects of Medicine*, 27(2–3), pp.95–125.

Kuhn, H. et al., 2017. Stretch-induced apoptosis in rat alveolar epithelial cells is mediated by

the intrinsic mitochondrial pathway. *Experimental Lung Research*, 43(1), pp.49–56.

Kumar, S. et al., 2006. Viscoelastic Retraction of Single Living Stress Fibers and Its Impact on Cell Shape, Cytoskeletal Organization, and Extracellular Matrix Mechanics. *Biophysical Journal*, 90(10), pp.3762–3773.

de la Ballina, L.R. et al., 2016. Amino Acid Transport Associated to Cluster of Differentiation 98 Heavy Chain (CD98hc) Is at the Cross-road of Oxidative Stress and Amino Acid Availability. *The Journal of biological chemistry*, 291(18), pp.9700–11.

Lal, H. et al., 2007. Stretch-induced MAP kinase activation in cardiac myocytes: Differential regulation through β1-integrin and focal adhesion kinase. *Journal of Molecular and Cellular Cardiology*, 43(2), pp.137–147.

Lammerding, J. et al., 2004. Lamin A/C deficiency causes defective nuclear mechanics and mechanotransduction. *The Journal of clinical investigation*, 113(3), pp.370–8.

Laroui, H. et al., 2014. Targeting intestinal inflammation with CD98 siRNA/PEI-loaded nanoparticles. *Molecular therapy : the journal of the American Society of Gene Therapy*, 22(1), pp.69–80.

Lee, C.F. et al., 2010. Cyclic stretch-induced stress fiber dynamics - Dependence on strain rate, Rho-kinase and MLCK. *Biochemical and Biophysical Research Communications*, 401(3), pp.344–349.

Lee, J.-H. et al., 2013. Surfactant protein-C chromatin-bound green fluorescence protein reporter mice reveal heterogeneity of surfactant protein C-expressing lung cells. *American journal of respiratory cell and molecular biology*, 48(3), pp.288–98.

Lee, J.J. et al., 2001. Long-term impact of smoking on lung epithelial proliferation in current and former smokers. *Journal of the National Cancer Institute*, 93(14), pp.1081–8.

Lehoux, S. et al., 2005. Differential regulation of vascular focal adhesion kinase by steady stretch and pulsatility. *Circulation*, 111(5), pp.643–649.

Li, L.-F. et al., 2007. Hyperoxia increases ventilator-induced lung injury via mitogen-activated protein kinases: a prospective, controlled animal experiment. *Critical Care*, 11(1), p.R25.

Li, Z., Kong, F. & Zhu, C., 2016. A model for cyclic mechanical reinforcement. *Scientific Reports*, 6, p.35954.

Li, Z., Lee, H. & Zhu, C., 2016. Molecular mechanisms of mechanotransduction in integrin-mediated cell-matrix adhesion. *Experimental Cell Research*, 349(1), pp.85–94.

Liang, C.-C., Park, A.Y. & Guan, J.-L., 2007. In vitro scratch assay: a convenient and inexpensive method for analysis of cell migration in vitro. *Nature Protocols*, 2(2), pp.329–333.

Liberati, T.A., Randle, M.R. & Toth, L.A., 2010. In vitro lung slices: a powerful approach for assessment of lung pathophysiology. *Expert review of molecular diagnostics*, 10(4), pp.501–8.

Lieber, M. et al., 1976. A continuous tumor-cell line from a human lung carcinoma with properties of type II alveolar epithelial cells. *International journal of cancer*, 17(1), pp.62–70.

Lin, G.L. et al., 2013. Activation of beta 1 but not beta 3 integrin increases cell traction forces. *FEBS letters*, 587(6), pp.763–9.

Liu, F. et al., 2010. Feedback amplification of fibrosis through matrix stiffening and COX-2 suppression. *The Journal of cell biology*, 190(4), pp.693–706.

Liu, M. et al., 1995. Antisense oligonucleotides for PDGF-B and its receptor inhibit mechanical strain-induced fetal lung cell growth. *The American journal of physiology*, 269(2 Pt 1), pp.L178-84.

Liu, M. et al., 1994. Inhibition of mechanical strain-induced fetal rat lung cell proliferation by gadolinium, a stretch-activated channel blocker. *Journal of Cellular Physiology*, 161(3), pp.501–507.

Liu, S., Cimprich, J. & Varisco, B.M., 2014. Mouse Pneumonectomy Model of Compensatory Lung Growth. *Journal of Visualized Experiments*, (94).

Liu, X.Y. et al., 2011. Alveolar type II cells escape stress failure caused by tonic stretch through transient focal adhesion disassembly. *Int J Biol Sci*, 7(5), pp.588–599.

Livak, K.J. & Schmittgen, T.D., 2001. Analysis of Relative Gene Expression Data Using Real-Time Quantitative PCR and the 2−ΔΔCT Method. *Methods*, 25(4), pp.402–408.

Livne, A. & Geiger, B., 2016. The inner workings of stress fibers - from contractile machinery to focal adhesions and back. *Journal of Cell Science*, 129(7), pp.1293–1304.

Lo, C.-M. et al., 2000. Cell Movement Is Guided by the Rigidity of the Substrate. *Biophysical Journal*, 79(1), pp.144–152.

Lou, J. & Zhu, C., 2007. A Structure-Based Sliding-Rebinding Mechanism for Catch Bonds. *Biophysical Journal*, 92(5), pp.1471–1485.

Lukkarinen, H.P., Laine, J. & Kääpä, P.O., 2003. Lung Epithelial Cells Undergo Apoptosis in Neonatal Respiratory Distress Syndrome. *Pediatric Research*, 53(2), pp.254–259.

Luo, B.-H., Carman, C. V. & Springer, T.A., 2007. Structural Basis of Integrin Regulation and Signaling. *Annual Review of Immunology*, 25(1), pp.619–647.

Luo, B.-H. & Springer, T.A., 2006. Integrin structures and conformational signaling. *Current opinion in cell biology*, 18(5), pp.579–86.

Luo, B.-H., Springer, T.A. & Takagi, J., 2003. Stabilizing the open conformation of the integrin headpiece with a glycan wedge increases affinity for ligand. *Proceedings of the National Academy of Sciences*, 100(5), pp.2403–2408.

Luque, A. et al., 1996. Activated conformations of very late activation integrins detected by a group of antibodies (HUTS) specific for a novel regulatory region (355-425) of the common beta 1 chain. *The Journal of biological chemistry*, 271(19), pp.11067–75.

Machesky, L.M. & Hall, A., 1997. Role of actin polymerization and adhesion to extracellular matrix in Rac- and Rho-induced cytoskeletal reorganization. *The Journal of cell biology*, 138(4), pp.913–26.

Macklem, P.T., Macklem, D.M. & De Troyer, A., 1983. A model of inspiratory muscle mechanics. *Journal of applied physiology: respiratory, environmental and exercise physiology*, 55(2), pp.547–57.

Makena, P.S. et al., 2010. Preexposure to hyperoxia causes increased lung injury and epithelial apoptosis in mice ventilated with high tidal volumes. *AJP: Lung Cellular and Molecular Physiology*, 299(5), pp.L711–L719.

Makrogianneli, K. et al., 2009. Integrating receptor signal inputs that influence small Rho

GTPase activation dynamics at the immunological synapse. *Molecular and cellular biology*, 29(11), pp.2997–3006.

Mantella, L.E., Quan, A. & Verma, S., 2015. Variability in vascular smooth muscle cell stretch-induced responses in 2D culture. *Vasc Cell*, 7, p.7.

Mao, P. et al., 2015. Human alveolar epithelial type II cells in primary culture. *Physiological reports*, 3(2).

Marshall, B.T. et al., 2003. Direct observation of catch bonds involving cell-adhesion molecules. *Nature*, 423(6936), pp.190–193.

Martin, C., Uhlig, S. & Ullrich, V., 1996. Videomicroscopy of methacholine-induced contraction of individual airways in precision-cut lung slices. *The European respiratory journal*, 9(12), pp.2479–87.

Mason, R.J., 2006. Biology of alveolar type II cells. *Respirology (Carlton, Vic.)*, 11 Suppl, pp.S12-5.

Mason, R.J. et al., 1982. Transepithelial transport by pulmonary alveolar type II cells in primary culture. *Proceedings of the National Academy of Sciences of the United States of America*, 79(19), pp.6033–7.

Matthay, M.A., 2005. Alveolar Epithelium: Role in Lung Fluid Balance and Acute Lung Injury. *Proceedings of the American Thoracic Society*, 2(3), pp.206–213.

Matthay, M.A., Ware, L.B. & Zimmerman, G.A., 2012. The acute respiratory distress syndrome. *The Journal of clinical investigation*, 122(8), pp.2731–40.

Matthews, B.D. et al., 2006. Cellular adaptation to mechanical stress: role of integrins, Rho, cytoskeletal tension and mechanosensitive ion channels. *Journal of cell science*, 119(Pt 3), pp.508–18.

McBeath, R. et al., 2004. Cell shape, cytoskeletal tension, and RhoA regulate stem cell lineage commitment. *Developmental Cell*, 6(4), pp.483–495.

McCloy, R.A. et al., 2014. Partial inhibition of Cdk1 in G 2 phase overrides the SAC and decouples mitotic events. *Cell cycle (Georgetown, Tex.)*, 13(9), pp.1400–12.

McElroy, M.C. & Kasper, M., 2004. The use of alveolar epithelial type I cell-selective markers to investigate lung injury and repair. *European Respiratory Journal*, 24(4).

Mead, J., Takishima, T. & Leith, D., 1970. Stress distribution in lungs: a model of pulmonary elasticity. *Journal of applied physiology*, 28(5), pp.596–608.

Merkel, R. et al., 1999. Energy landscapes of receptor–ligand bonds explored with dynamic force spectroscopy. *Nature*, 397(6714), pp.50–53.

Mijailovich, S.M. et al., 2002. A finite element model of cell deformation during magnetic bead twisting. *Journal of Applied Physiology*, 93(4), pp.1429–1436.

Mills, G.B. & Moolenaar, W.H., 2003. The emerging role of lysophosphatidic acid in cancer. *Nature Reviews Cancer*, 3(8), pp.582–591.

Misumi, Y. et al., 1986. Novel blockade by brefeldin A of intracellular transport of secretory proteins in cultured rat hepatocytes. *The Journal of biological chemistry*, 261(24), pp.11398–403.

Mitchison, T. & Kirschner, M., 1988. Cytoskeletal dynamics and nerve growth. *Neuron*, 1(9),

pp.761–772.

Moessinger, A.C. et al., 1990. Role of lung fluid volume in growth and maturation of the fetal sheep lung. *Journal of Clinical Investigation*, 86(4), pp.1270–1277.

Mokres, L.M. et al., 2010. Prolonged mechanical ventilation with air induces apoptosis and causes failure of alveolar septation and angiogenesis in lungs of newborn mice. *AJP: Lung Cellular and Molecular Physiology*, 298(1), pp.L23–L35.

Moretti, M. et al., 2004. Endothelial cell alignment on cyclically-stretched silicone surfaces. *Journal of Materials Science: Materials in Medicine*, 15(10), pp.1159–1164.

Mortier, A., Van Damme, J. & Proost, P., 2008. Regulation of chemokine activity by posttranslational modification. *Pharmacology & Therapeutics*, 120(2), pp.197–217.

Muliyil, S. & Narasimha, M., 2014. Mitochondrial ROS regulates cytoskeletal and mitochondrial remodeling to tune cell and tissue dynamics in a model for wound healing. *Developmental cell*, 28(3), pp.239–52.

Nagre, N. et al., 2016. TRIM72 modulates caveolar endocytosis in repair of lung cells. *American Journal of Physiology - Lung Cellular and Molecular Physiology*, 310(5).

Nardo, L. et al., 2000. Changes in lung structure and cellular division induced by tracheal obstruction in fetal sheep. *Experimental lung research*, 26(2), pp.105–19.

Navajas, D., Maksym, G.N. & Bates, J.H., 1995. Dynamic viscoelastic nonlinearity of lung parenchymal tissue. *Journal of applied physiology (Bethesda, Md.: 1985)*, 79(1), pp.348–56.

Needham, D.M. et al., 2012. Lung protective mechanical ventilation and two year survival in patients with acute lung injury: prospective cohort study. *Bmj*, 344, p.e2124.

Ng-Blichfeldt, J.-P. et al., 2017. Deficient retinoid-driven angiogenesis may contribute to failure of adult human lung regeneration in emphysema. *Thorax*, 72(6), pp.510–521.

Ng-Blichfeldt, J.-P., 2014. *Retinoic Acid Signalling in Human Lung Disease and Repair*. Imperial College London.

Nordenfelt, P. et al., 2016. Coordinated integrin activation by actin-dependent force during T-cell migration. *Nature Communications*, 7, p.13119.

Oakes, P.W. et al., 2012. Tension is required but not sufficient for focal adhesion maturation without a stress fiber template. *The Journal of cell biology*, 196(3), pp.363–74.

Ocaranza, M.P. et al., 2011. Rho kinase inhibition activates the homologous angiotensin-converting enzyme-angiotensin-(1–9) axis in experimental hypertension. *Journal of Hypertension*, 29(4), pp.706–715.

Ochs, M. et al., 2004. The Number of Alveoli in the Human Lung. *American Journal of Respiratory and Critical Care Medicine*, 169(1), pp.120–124.

Paradise, R.K. et al., 2011. Acidic Extracellular pH Promotes Activation of Integrin αvβ3 J. Kanellopoulos, ed. *PLoS ONE*, 6(1), p.e15746.

Paszek, M.J. et al., 2009. Integrin clustering is driven by mechanical resistance from the glycocalyx and the substrate. *PLoS computational biology*, 5(12), p.e1000604.

Paszek, M.J. et al., 2005. Tensional homeostasis and the malignant phenotype. *Cancer cell*, 8(3), pp.241–54.

Pawley, J.B. & Masters, B.R., 2008. *Handbook of biological confocal microscopy*,

Perlman, C.E., Lederer, D.J. & Bhattacharya, J., 2011. Micromechanics of Alveolar Edema. *American Journal of Respiratory Cell and Molecular Biology*, 44(1), pp.34–39.

Pertz, O. et al., 2006. Spatiotemporal dynamics of RhoA activity in migrating cells. *Nature*, 440(7087), pp.1069–72.

Pietraszewska-Bogiel, A. & Gadella, T.W.J., 2011. FRET microscopy: From principle to routine technology in cell biology. *Journal of Microscopy*, 241(2), pp.111–118.

Pinheiro de Oliveira, R. et al., 2010. Mechanical ventilation with high tidal volume induces inflammation in patients without lung disease. *Critical care (London, England)*, 14(2), p.R39.

Pinhu, L., 2008. *Mechanotransduction in alveolar epithelial cells subjected to mechanical strain*. Imperial College London.

Pinhu, L. et al., 2008. Reference gene selection for real-time polymerase chain reaction in human lung cells subjected to cyclic mechanical strain. *Respirology*, 13(7), pp.990–999.

Pinhu, L. et al., 2003. Ventilator-associated lung injury. *The Lancet*, 361(9354), pp.332–340.

Pipparelli, A. et al., 2013. ROCK inhibitor enhances adhesion and wound healing of human corneal endothelial cells. C. J. Connon, ed. *PloS one*, 8(4), p.e62095.

Plosa, E.J. et al., 2014. Epithelial β1 integrin is required for lung branching morphogenesis and alveolarization. *Development (Cambridge, England)*, 5(24), pp.4751–4762.

Plotnikov, S.V. et al., 2012. Force Fluctuations within Focal Adhesions Mediate ECM-Rigidity Sensing to Guide Directed Cell Migration. *Cell*, 151(7), pp.1513–1527.

Poettler, M. et al., 2013. CD98hc (SLC3A2) drives integrin-dependent renal cancer cell behavior. *Molecular Cancer*, 12(1), pp.1–12.

Poland, S.P. et al., 2015. A high speed multifocal multiphoton fluorescence lifetime imaging microscope for live-cell FRET imaging. *Biomedical Optics Express*, 6(2), p.277.

Poobalasingam, T. et al., 2017. Imaging the lung: the old ways and the new. *Histology and histopathology*, 32(4), pp.325–337.

Pöttler, M. et al., 2011. Relationship of 4F2hc expression and grade of malignancy in renal cell cancer (RCC). *Journal of clinical oncology : official journal of the American Society of Clinical Oncology*, 29(15_suppl), p.e15129.

Prager, G.W. et al., 2009. CD98hc (SLC3A2), a novel marker in renal cell cancer. *European Journal of Clinical Investigation*, 39(4), pp.304–310.

Prager, G.W. et al., 2007. CD98hc (SLC3A2) interaction with the integrin beta subunit cytoplasmic domain mediates adhesive signaling. *J Biol Chem*, 282(33), pp.24477–24484.

de Prost, N. et al., 2011. Ventilator-induced lung injury: historical perspectives and clinical implications. *Ann Intensive Care*, 1(1), p.28.

Proudfoot, A.G., 2014. Differential tumour necrosis factor signalling in human models of acute lung injury. , pp.1–309.

Proudfoot, A.G. et al., 2011. Human models of acute lung injury. *Dis Model Mech*, 4(2),

pp.145–153.

Provenzano, P.P. et al., 2009. Matrix density-induced mechanoregulation of breast cell phenotype, signaling and gene expression through a FAK-ERK linkage. *Oncogene*, 28(49), pp.4326–43.

Provenzano, P.P. & Keely, P.J., 2011. Mechanical signaling through the cytoskeleton regulates cell proliferation by coordinated focal adhesion and Rho GTPase signaling. *Journal of cell science*, 124(Pt 8), pp.1195–1205.

Puklin-Faucher, E. & Sheetz, M.P., 2009. The mechanical integrin cycle. *Journal of cell science*, 122(Pt 2), pp.179–86.

Puliafito, A. et al., 2012. Collective and single cell behavior in epithelial contact inhibition. *Proceedings of the National Academy of Sciences of the United States of America*, 109(3), pp.739–44.

Qian, J. et al., 2010. Soft Matrices Suppress Cooperative Behaviors among Receptor-Ligand Bonds in Cell Adhesion M. J. Buehler, ed. *PLoS ONE*, 5(8), p.e12342.

Rahim, S. & Üren, A., 2011. A real-time electrical impedance based technique to measure invasion of endothelial cell monolayer by cancer cells. *Journal of visualized experiments : JoVE*, (50).

Ranieri, V.M. et al., 1999. Effect of mechanical ventilation on inflammatory mediators in patients with acute respiratory distress syndrome: a randomized controlled trial. *JAMA*, 282(1), pp.54–61.

Rannels, D.E., 1989. Role of physical forces in compensatory growth of the lung. *The American journal of physiology*, 257(4 Pt 1), pp.L179-89.

Rápalo, G. et al., 2015. Live Cell Imaging during Mechanical Stretch. *Journal of visualized experiments : JoVE*, (102), p.e52737.

Reffay, M. et al., 2014. Interplay of RhoA and mechanical forces in collective cell migration driven by leader cells. *Nature cell biology*, 16(3), pp.217–23.

Ressmeyer, A.R. et al., 2006. Characterisation of guinea pig precision-cut lung slices: comparison with human tissues. *European Respiratory Journal*, 28(3), pp.603–611.

Ricard, J.-D., Dreyfuss, D. & Saumon, G., 2003. Ventilator-induced lung injury. *European Respiratory Journal*, 22(Supplement 42), p.2s–9s.

Ridley, A.J. & Hall, A., 1992. The small GTP-binding protein rho regulates the assembly of focal adhesions and actin stress fibers in response to growth factors. *Cell*, 70(3), pp.389–399.

Rintoul, R.C. et al., 2002. Cross-linking CD98 promotes integrin-like signaling and anchorage-independent growth. *Molecular biology of the cell*, 13(8), pp.2841–52.

del Rio, A. et al., 2009. Stretching single talin rod molecules activates vinculin binding. *Science*, 323(5914), pp.638–641.

Riveline, D. et al., 2001. Focal contacts as mechanosensors: Externally applied local mechanical force induces growth of focal contacts by an mDia1-dependent and ROCK-independent mechanism. *Journal of Cell Biology*, 153(6), pp.1175–1185.

Roan, E. et al., 2012. Hyperoxia alters the mechanical properties of alveolar epithelial cells. *American journal of physiology. Lung cellular and molecular physiology*, 302(12),

pp.L1235-41.

Roan, E. & Waters, C.M., 2011. What do we know about mechanical strain in lung alveoli? *Am J Physiol Lung Cell Mol Physiol*, 301(5), pp.L625-35.

Roca-Cusachs, P. et al., 2009. Clustering of alpha(5)beta(1) integrins determines adhesion strength whereas alpha(v)beta(3) and talin enable mechanotransduction. *Proceedings of the National Academy of Sciences of the United States of America*, 106(38), pp.16245–50.

Rosner, S.R. et al., 2014. Airway contractility in the precision-cut lung slice after cryopreservation. *American Journal of Respiratory Cell and Molecular Biology*, 50(5), pp.876–881.

Rubenfeld, G.D. & Herridge, M.S., 2007. Epidemiology and outcomes of acute lung injury. *Chest*, 131(2), pp.554–562.

Saad, A. et al., 2016. Insights into a novel nuclear function for Fascin in the regulation of the amino-acid transporter SLC3A2. *Scientific Reports*, 6(1), p.36699.

Sabass, B. et al., 2008. High resolution traction force microscopy based on experimental and computational advances. *Biophysical journal*, 94(1), pp.207–20.

Saez, A. et al., 2007. Rigidity-driven growth and migration of epithelial cells on microstructured anisotropic substrates. *Proceedings of the National Academy of Sciences*, 104(20), pp.8281–8286.

Sakuma, T. et al., 1997. Beta-adrenergic agonist stimulated alveolar fluid clearance in ex vivo human and rat lungs. *American Journal of Respiratory and Critical Care Medicine*, 155(2), pp.506–512.

Salman, D., Finney, S.J. & Griffiths, M.J.D., 2013. Strategies to reduce ventilator-associated lung injury (VALI). *Burns*, 39(2), pp.200–211.

Sanchez-Esteban, J. et al., 2006. Integrins beta1, alpha6, and alpha3 contribute to mechanical strain-induced differentiation of fetal lung type II epithelial cells via distinct mechanisms. *American journal of physiology. Lung cellular and molecular physiology*, 290(2), pp.L343-50.

Sanchez-Esteban, J. et al., 2001. Mechanical stretch promotes alveolar epithelial type II cell differentiation. *Journal of applied physiology (Bethesda, Md. : 1985)*, 91(2), pp.589–95.

Sanderson, M.J., 2011. Exploring lung physiology in health and disease with lung slices. *Pulmonary Pharmacology & Therapeutics*, 24(5), pp.452–465.

Santiago-Gómez, A. et al., 2013. 4F2hc-silencing impairs tumorigenicity of HeLa cells via modulation of galectin-3 and β-catenin signaling, and MMP-2 expression. *Biochimica et Biophysica Acta (BBA) - Molecular Cell Research*, 1833(9), pp.2045–2056.

Savla, U., Olson, L.E. & Waters, C.M., 2004. Mathematical modeling of airway epithelial wound closure during cyclic mechanical strain. *Journal of Applied Physiology*, 96(2).

Savla, U. & Waters, C.M., 1998. Mechanical strain inhibits repair of airway epithelium in vitro. *The American journal of physiology*, 274(6 Pt 1), pp.883–892.

Saydain, G. et al., 2002. Outcome of Patients with Idiopathic Pulmonary Fibrosis Admitted to the Intensive Care Unit. *American Journal of Respiratory and Critical Care Medicine*, 166(6), pp.839–842.

Schaffer, J.L. et al., 1994. Device for the application of a dynamic biaxially uniform and isotropic strain to a flexible cell culture membrane. *Journal of Orthopaedic Research*, 12(5), pp.709–719.

Schaufler, V. et al., 2016. Selective binding and lateral clustering of α 5 β 1 and α v β 3 integrins: Unraveling the spatial requirements for cell spreading and focal adhesion assembly. *Cell Adhesion & Migration*, 10(5), pp.505–515.

Schiller, H.B. & Fässler, R., 2013. Mechanosensitivity and compositional dynamics of cell–matrix adhesions. *Nature Publishing Group*, 14(6), pp.509–519.

Schmittgen, T.D. & Livak, K.J., 2008. Analyzing real-time PCR data by the comparative CT method. *Nature Protocols*, 3(6), pp.1101–1108.

Schroeder, A. et al., 2006. The RIN: an RNA integrity number for assigning integrity values to RNA measurements. *BMC molecular biology*, 7(1), p.3.

Serpa Neto, A. et al., 2012. Association between use of lung-protective ventilation with lower tidal volumes and clinical outcomes among patients without acute respiratory distress syndrome: a meta-analysis. *JAMA*, 308(16), pp.1651–9.

Shapiro, S.D., 2006. Animal models of asthma - Pro: Allergic avoidance of animal (model[s]) is not an option. *American Journal of Respiratory and Critical Care Medicine*, 174(11), pp.1171–1173.

Shattil, S.J., Kim, C. & Ginsberg, M.H., 2010. The final steps of integrin activation: the end game. *Nature Reviews Molecular Cell Biology*, 11(4), pp.288–300.

Shen, B. et al., 2015. The interaction of Gα13 with integrin β1 mediates cell migration by dynamic regulation of RhoA. *Molecular biology of the cell*, 26(20), pp.3658–70.

Silbert, O. et al., 2008. Roles of RhoA and Rac1 on actin remodeling and cell alignment and differentiation in fetal type II epithelial cells exposed to cyclic mechanical stretch. *Experimental Lung Research*, 34(10), pp.663–680.

Slutsky, A.S., 2005. Ventilator-induced lung injury: from barotrauma to biotrauma. *Respir Care*, 50(5), pp.646–659.

Slutsky, A.S. & Ranieri, V.M., 2013. Ventilator-Induced Lung Injury. *New England Journal of Medicine*, 369(22), pp.2126–2136.

Smith, M.A. et al., 2010. A Zyxin-Mediated Mechanism for Actin Stress Fiber Maintenance and Repair. *Developmental Cell*, 19(3), pp.365–376.

Sniadecki, N.J. & Chen, C.S., 2007. Microfabricated Silicone Elastomeric Post Arrays for Measuring Traction Forces of Adherent Cells. *Methods in Cell Biology*, 83, pp.313–328.

Sonam, S. et al., 2016. Cell contractility arising from topography and shear flow determines human mesenchymal stem cell fate. *Scientific reports*, 6(February), p.20415.

Song, M.J. et al., 2016. Superoxide mediates tight junction complex dissociation in cyclically stretched lung slices. *Journal of Biomechanics*, 49(8), pp.1330–1335.

Springer, T.A. & Dustin, M.L., 2012. Integrin inside-out signaling and the immunological synapse. *Current opinion in cell biology*, 24(1), pp.107–15.

Sturton, R.G. et al., 2007. Pharmacological Characterization of Indacaterol, a Novel Once Daily Inhaled β2 Adrenoceptor Agonist, on Small Airways in Human and Rat Precision-Cut Lung Slices. *Journal of Pharmacology and Experimental Therapeutics*, 324(1).

Su, F. et al., 2013. Establishment and Evaluation of a Stable Cattle Type II Alveolar Epithelial Cell Line K. A. Brayton, ed. *PLoS ONE*, 8(9), p.e76036.

Suki, B. et al., 2005. Biomechanics of the lung parenchyma: critical roles of collagen and mechanical forces. *Journal of Applied Physiology*, 98(5), pp.1892–1899.

Sun, Z., Guo, S.S. & Fässler, R., 2016. Integrin-mediated mechanotransduction. *The Journal of cell biology*, 215(4), pp.445–456.

Sunyer, R. et al., 2009. The temperature dependence of cell mechanics measured by atomic force microscopy. *Physical Biology*, 6(2), p.25009.

Sutherasan, Y., Vargas, M. & Pelosi, P., 2014. Protective mechanical ventilation in the non-injured lung: review and meta-analysis. *Critical care (London, England)*, 18(2), p.211.

Sylvester, P.W., 2011. Optimization of the Tetrazolium Dye (MTT) Colorimetric Assay for Cellular Growth and Viability. In *Methods in molecular biology (Clifton, N.J.)*. pp. 157–168.

Szkudlarek, A.C. et al., 2011. Ethyl 2-cyanoacrylate tissue adhesive in partial lobectomy in rats. *Jornal brasileiro de pneumologia : publicacao oficial da Sociedade Brasileira de Pneumologia e Tisilogia*, 37(6), pp.729–34.

Takagi, J. et al., 2002. Global Conformational Rearrangements in Integrin Extracellular Domains in Outside-In and Inside-Out Signaling. *Cell*, 110(5), pp.599–611.

Takagi, T. et al., 2011. Intraradial administration of fasudil inhibits augmented Rho kinase activity to effectively dilate the spastic radial artery during coronary artery bypass grafting surgery. *The Journal of Thoracic and Cardiovascular Surgery*, 142(2), pp.e59–e65.

Tamkun, J.W. et al., 1986. Structure of integrin, a glycoprotein involved in the transmembrane linkage between fibronectin and actin. *Cell*, 46(2), pp.271–82.

Tane, S., Noda, K. & Shigemura, N., 2017. Ex Vivo Lung Perfusion: A Key Tool for Translational Science in the Lungs. *Chest*.

Terragni, P.P. et al., 2016. Ventilatory Management During Normothermic Ex Vivo Lung Perfusion. *Transplantation*, 100(5), pp.1128–1135.

The ARDS Definition Task Force, 2012. Acute respiratory distress syndrome: The berlin definition. *JAMA: The Journal of the American Medical Association*, 307(23), pp.2526–2533.

Theodosiou, M. et al., 2016. Kindlin-2 cooperates with talin to activate integrins and induces cell spreading by directly binding paxillin. *eLife*, 5, p.e10130.

Thomas, R.A. et al., 2006. Mechanical stretch has contrasting effects on mediator release from bronchial epithelial cells, with a rho-kinase-dependent component to the mechanotransduction pathway. *Respiratory Medicine*, 100(9), pp.1588–1597.

Thomas, W.E., Vogel, V. & Sokurenko, E., 2008. Biophysics of Catch Bonds. *Annual Review of Biophysics*, 37(1), pp.399–416.

Thurlbeck, W.M. & Langston, C., 1989. Long-term consequences of compensatory lung growth. *Journal of applied physiology (Bethesda, Md. : 1985)*, 66(6), pp.2891–4.

Tian, Y. et al., 2016. Modulation of Endothelial Inflammation by Low and High Magnitude Cyclic Stretch Y.-Y. Zhao, ed. *PLoS ONE*, 11(4), p.e0153387.

Tokuyama, E. et al., 2015. Mechanical Stretch on Human Skin Equivalents Increases the Epidermal Thickness and Develops the Basement Membrane. C. Egles, ed. *PloS one*, 10(11), p.e0141989.

Tomasek, J.J. et al., 1992. Fibroblast contraction occurs on release of tension in attached collagen lattices: Dependency on an organized actin cytoskeleton and serum. *The Anatomical Record*, 232(3), pp.359–368.

Torsoni, A.S. et al., 2005. RhoA/ROCK signaling is critical to FAK activation by cyclic stretch in cardiac myocytes. *American Journal of Physiology - Heart and Circulatory Physiology*, 289(4), pp.H1488–H1496.

Totsukawa, G. et al., 2000. Distinct Roles of ROCK (Rho-kinase) and MLCK in Spatial Regulation of MLC Phosphorylation for Assembly of Stress Fibers and Focal Adhesions in 3T3 Fibroblasts. *The Journal of Cell Biology*, 150(4), pp.797–806.

Tremblay, L.N. et al., 2002. Injurious ventilation induces widespread pulmonary epithelial expression of tumor necrosis factor-alpha and interleukin-6 messenger RNA. *Critical care medicine*, 30(8), pp.1693–700.

Trepat, X. et al., 2007. Universal physical responses to stretch in the living cell. *Nature*, 447(7144), pp.592–5.

Tschumperlin, D.J. & Margulies, S.S., 1999. Alveolar epithelial surface area-volume relationship in isolated rat lungs. *Journal of Applied Physiology*, 86(6).

Tschumperlin, D.J. & Margulies, S.S., 1998. Equibiaxial deformation-induced injury of alveolar epithelial cells in vitro. *Am J Physiol*, 275(6 Pt 1), pp.L1173-83.

Tsumura, H. et al., 2003. The targeted disruption of the CD98 gene results in embryonic lethality. *Biochem Biophys Res Commun*, 308(4), pp.847–851.

Tzima, E. et al., 2001. Activation of integrins in endothelial cells by fluid shear stress mediates Rho-dependent cytoskeletal alignment. *The EMBO journal*, 20(17), pp.4639–47.

Tzima, E., 2006. Role of Small GTPases in Endothelial Cytoskeletal Dynamics and the Shear Stress Response. *Circulation Research*, 98(2).

Uhl, F.E. et al., 2015. Preclinical validation and imaging of Wnt-induced repair in human 3D lung tissue cultures. *European Respiratory Journal*, 46(4), pp.1150–1166.

Ursekar, C.P. et al., 2014. Design and Construction of an Equibiaxial Cell Stretching System That Is Improved for Biochemical Analysis A. J. Kabla, ed. *PLoS ONE*, 9(3), p.e90665.

Uyeda, T.Q.P. et al., 2011. Stretching actin filaments within cells enhances their affinity for the myosin ii motor domain. *PLoS ONE*, 6(10).

Varner, V.D. et al., 2015. Mechanically patterning the embryonic airway epithelium. *Proceedings of the National Academy of Sciences of the United States of America*, 112(30), pp.9230–5.

Vaughan, A.E. et al., 2014. Lineage-negative progenitors mobilize to regenerate lung epithelium after major injury.

Veldeman, M. et al., 2016. Delayed cerebral ischaemia prevention and treatment after aneurysmal subarachnoid haemorrhage: a systematic review J. G. Hardman, ed. *British Journal of Anaesthesia*, 117(1), pp.17–40.

Verrey, F. et al., 1998. Amino-acid transport by heterodimers of 4F2hc/CD98 and members of

a permease family. *Nature*, 395(6699), pp.288–291.

Vinogradova, O. et al., 2002. A Structural Mechanism of Integrin αIIbβ3 “Inside-Out” Activation as Regulated by Its Cytoplasmic Face. *Cell*, 110(5), pp.587–597.

Vlahakis, N.E. et al., 2002. Role of deformation-induced lipid trafficking in the prevention of plasma membrane stress failure. *Am J Respir Crit Care Med*, 166(9), pp.1282–1289.

Vlahakis, N.E. et al., 1999. Stretch induces cytokine release by alveolar epithelial cells in vitro. *The American journal of physiology*, 277(1 Pt 1), pp.L167–L173.

Vlahakis, N.E. & Hubmayr, R.D., 2005. Cellular stress failure in ventilator-injured lungs. *Am J Respir Crit Care Med*, 171(12), pp.1328–1342.

Vlahakis, N.E. & Hubmayr, R.D., 2000. Invited Review: Plasma membrane stress failure in alveolar epithelial cells. *Journal of Applied Physiology*, 89(6).

Vogel, E.R. et al., 2017. Moderate hyperoxia induces extracellular matrix remodeling by human fetal airway smooth muscle cells. *Pediatric Research*, 81(2), pp.376–383.

Waite, J.H., 1983. Evidence for a repeating 3,4-dihydroxyphenylalanine- and hydroxyproline-containing decapeptide in the adhesive protein of the mussel, Mytilus edulis L. *The Journal of biological chemistry*, 258(5), pp.2911–5.

Wakabayashi, K. et al., 2014. Volutrauma, but not Atelectrauma, Induces Systemic Cytokine Production by Lung-Marginated Monocytes*. *Critical Care Medicine*, 42(1), pp.e49–e57.

Wall, M.E. et al., 2007. Comparison of cellular strain with applied substrate strain in vitro. *Journal of biomechanics*, 40(1), pp.173–81.

Wang, J.H.-C. et al., 2004. *Fibroblast responses to cyclic mechanical stretching depend on cell orientation to the stretching direction*,

Wang, J.H.-C. et al., 2001. Specificity of endothelial cell reorientation in response to cyclic mechanical stretching. *Journal of Biomechanics*, 34(12), pp.1563–1572.

Wang, N. et al., 2002. Cell prestress. I. Stiffness and prestress are closely associated in adherent contractile cells. *American journal of physiology. Cell physiology*, 282(3), pp.C606–C616.

Wang, N. et al., 2011. Fasudil hydrochloride hydrate, a Rho-kinase inhibitor, suppresses isoproterenol-induced heart failure in rats via JNK and ERK1/2 pathways. *Journal of Cellular Biochemistry*, 112(7), pp.1920–1929.

Wang, N. et al., 2001. Mechanical behavior in living cells consistent with the tensegrity model. *Proceedings of the National Academy of Sciences of the United States of America*, 98(14), pp.7765–70.

Wang, N. & Ingber, D.E., 1994. Control of cytoskeletal mechanics by extracellular matrix, cell shape, and mechanical tension. *Biophysical Journal*, 66(6), pp.2181–2189.

Watanabe-Nakayama, T. et al., 2011. Direct Detection of Cellular Adaptation to Local Cyclic Stretching at the Single Cell Level by Atomic Force Microscopy. *Biophysical Journal*, 100(3), pp.564–572.

Waters, C.M. et al., 2001. A system to impose prescribed homogenous strains on cultured cells. *Journal of applied physiology (Bethesda, Md. : 1985)*, 91(4), pp.1600–10.

Waters, C.M., Roan, E. & Navajas, D., 2012. Mechanobiology in lung epithelial cells:

measurements, perturbations, and responses. *Comprehensive Physiology*, 2(1), pp.1–29.

Waters, C.M. & Savla, U., 1999. Keratinocyte growth factor accelerates wound closure in airway epithelium during cyclic mechanical strain. *Journal of cellular physiology*, 181(3), pp.424–32.

Wayman, A.M. et al., 2010. Triphasic Force Dependence of E-Selectin/Ligand Dissociation Governs Cell Rolling under Flow. *Biophysical Journal*, 99(4), pp.1166–1174.

Welf, E.S., Naik, U.P. & Ogunnaike, B.A., 2012. A Spatial Model for Integrin Clustering as a Result of Feedback between Integrin Activation and Integrin Binding. *Biophysical Journal*, 103(6), pp.1379–1389.

Weng, T. et al., 2014. Hypoxia-induced Deoxycytidine Kinase Contributes to Epithelial Proliferation in Pulmonary Fibrosis. *American Journal of Respiratory and Critical Care Medicine*, 190(12), pp.1402–1412.

Wernig, F., Mayr, M. & Xu, Q., 2003. Mechanical Stretch-Induced Apoptosis in Smooth Muscle Cells Is Mediated by β1-Integrin Signaling Pathways. *Hypertension*, 41(4).

White, S.R. et al., 2008. Interleukin-1 mediates human airway epithelial cell migration via NF-B. *AJP: Lung Cellular and Molecular Physiology*, 295(6), pp.L1018–L1027.

White, S.R. et al., 1999. Role of Very Late Adhesion Integrins in Mediating Repair of Human Airway Epithelial Cell Monolayers after Mechanical Injury. *American Journal of Respiratory Cell and Molecular Biology*, 20(4), pp.787–796.

White, S.R., Tse, R. & Marroquin, B.A., 2005. Stress-activated protein kinases mediate cell migration in human airway epithelial cells. *American journal of respiratory cell and molecular biology*, 32(4), pp.301–10.

Wigglesworth, J.S. & Desai, R., 1979. Effect on lung growth of cervical cord section in the rabbit fetus. *Early human development*, 3(1), pp.51–65.

Wilhelm, K.R. et al., 2014. Hyperoxia increases the elastic modulus of alveolar epithelial cells through Rho kinase. *The FEBS journal*, 281(3), pp.957–69.

Williams, J.L., Chen, J.H. & Belloli, D.M., 1992. Strain fields on cell stressing devices employing clamped circular elastic diaphragms as substrates. *Journal of biomechanical engineering*, 114(3), pp.377–84.

Wilson, M.R. et al., 2003. High tidal volume upregulates intrapulmonary cytokines in an in vivo mouse model of ventilator-induced lung injury. *Journal of Applied Physiology*, 95(4), pp.1385–1393.

Winston, F.K. et al., 1989. A system to reproduce and quantify the biomechanical environment of the cell. *Journal of applied physiology (Bethesda, Md.: 1985)*, 67(1), pp.397–405.

Wirtz, H.R. & Dobbs, L.G., 1990. Calcium mobilization and exocytosis after one mechanical stretch of lung epithelial cells. *Science (New York, N.Y.)*, 250(4985), pp.1266–9.

Witherden, I.R. & Tetley, T.D., 2001. Isolation and Culture of Human Alveolar Type II Pneumocytes. In D. F. Rogers & L. E. Donnelly, eds. *Human Airway Inflammation: Sampling Techniques and Analytical Protocols*. Totowa, NJ: Humana Press, pp. 137–146.

Woods, S.J. et al., 2015. Kinetic profiling of in vivo lung cellular inflammatory responses to mechanical ventilation. *American Journal of Physiology - Lung Cellular and Molecular*

Physiology, 308(9), pp.L912–L921.

Wozniak, M. a et al., 2003. ROCK-generated contractility regulates breast epithelial cell differentiation in response to the physical properties of a three-dimensional collagen matrix. *The Journal of Cell Biology*, 163(3), pp.583–595.

Wu, B. et al., 2015. Basigin-mediated redistribution of CD98 promotes cell spreading and tumorigenicity in hepatocellular carcinoma. *Journal of experimental & clinical cancer research : CR*, 34, p.110.

Wu, B. et al., 2016. Dominant Suppression of β1 Integrin by Ectopic CD98-ICD Inhibits Hepatocellular Carcinoma Progression. *International journal of molecular sciences*, 17(11), p.1882.

Yalcin, H.C. et al., 2009. Influence of cytoskeletal structure and mechanics on epithelial cell injury during cyclic airway reopening. *Am J Physiol Lung Cell Mol Physiol*, 297(5), pp.L881-91.

Yang, J. et al., 2014. Conformational activation of talin by RIAM triggers integrin-mediated cell adhesion. *Nature Communications*, 5, p.5880.

Yao, H. et al., 2013. Nonmuscle myosin light-chain kinase mediates microglial migration induced by HIV Tat: involvement of β1 integrins. *FASEB journal : official publication of the Federation of American Societies for Experimental Biology*, 27(4), pp.1532–48.

Yao, M. et al., 2014. Mechanical activation of vinculin binding to talin locks talin in an unfolded conformation. *Scientific reports*, 4, p.4610.

Yao, M. et al., 2016. The mechanical response of talin. *Nature Communications*, 7, p.11966.

Ye, F., Snider, A.K. & Ginsberg, M.H., 2014. Talin and kindlin: The one-two punch in integrin activation. *Frontiers of Medicine in China*, 8(1), pp.6–16.

Yee, M. et al., 2017. Alternative progenitor lineages regenerate the adult lung depleted of alveolar epithelial type 2 cells. *American Journal of Respiratory Cell and Molecular Biology*, 56(4), pp.453–464.

Yoshigi, M. et al., 2005. JCB: REPORT Mechanical force mobilizes zyxin from focal adhesions to actin filaments and regulates cytoskeletal reinforcement. *The Journal of Cell Biology*, 171(2), pp.209–215.

Young, M.P. et al., 2004. Ventilation of patients with acute lung injury and acute respiratory distress syndrome: has new evidence changed clinical practice? *Crit Care Med*, 32(6), pp.1260–1265.

Zaidel-Bar, R. et al., 2006. A paxillin tyrosine phosphorylation switch regulates the assembly and form of cell-matrix adhesions. *Journal of Cell Science*, 120(1).

Zaidel-Bar, R. et al., 2003. Early molecular events in the assembly of matrix adhesions at the leading edge of migrating cells. *Journal of Cell Science*, 116(22).

Zemans, R.L. et al., 2015. Conceptual approaches to lung injury and repair. *Annals of the American Thoracic Society*, 12, pp.S9–S15.

Zeng, L. et al., 2016. The cellular kinetics of lung alveolar epithelial cells and its relationship with lung tissue repair after acute lung injury. *Respiratory Research*, 17(1), p.164.

Zent, R. et al., 2000. Class- and splice variant-specific association of CD98 with integrin beta cytoplasmic domains. *The Journal of biological chemistry*, 275(7), pp.5059–64.

Zhang, S., Garbutt, V. & McBride, J.T., 1996. Strain-induced growth of the immature lung. *Journal of applied physiology (Bethesda, Md. : 1985)*, 81(4), pp.1471–6.

Zheng, D. et al., 2017. Differentiation of Club Cells to Alveolar Epithelial Cells In Vitro. *Scientific Reports*, 7(December 2016), p.41661.

Zheng, W., Christensen, L.P. & Tomanek, R.J., 2008. Differential effects of cyclic and static stretch on coronary microvascular endothelial cell receptors and vasculogenic/angiogenic responses. *American journal of physiology. Heart and circulatory physiology*, 295(2), pp.H794-800.

Zhou, Y. et al., 2013. Inhibition of mechanosensitive signaling in myofibroblasts ameliorates experimental pulmonary fibrosis. *Journal of Clinical Investigation*, 123(3), pp.1096–1108.

Zhu, J. et al., 2008. Structure of a Complete Integrin Ectodomain in a Physiologic Resting State and Activation and Deactivation by Applied Forces. *Molecular Cell*, 32(6), pp.849–861.

Zuo, W. et al., 2014. p63+Krt5+ distal airway stem cells are essential for lung regeneration.

8 Appendix 1: Copyright and permissions

Page No.	Image	Source	Copyright holder and contact	Permission granted?	Permission note
29	Figure 1_1 Ventilator-associated lung injury (VALI)	(Slutsky & Ranieri 2013)	Massachusetts Medical Society	Yes for thesis and dissertations	Content (full-text or portions thereof) may be used in print and electronic versions of your dissertation or thesis without formal permission from the Massachusetts Medical Society, Publisher of the New England Journal of Medicine.
33	Figure 1_2	(McElroy & Kasper 2004)	European Respiratory Journal	Yes: for thesis and dissertations	Permission is granted for the material stated above to be reproduced for your thesis
46	Figure 1_5	(Cukierman et al. 2001)	American Society for the Advancement of Science	Yes for thesis and dissertations	If you are using figure(s)/table(s), permission is granted for use in print and electronic versions of your dissertation or thesis. Licence number: 4213180767787
51	Figure 1-6	(Springer & Dustin 2012)	Elsevier	Yes for thesis and dissertations	If your license is for use in a thesis/dissertation your thesis may be submitted to your institution in either print or electronic form. Licence number: 4213181504491
58	Figure 1-7	(Case & Waterman 2015)	Nature Publishing Group	Yes: thesis and dissertation	Licence number: 4241950493971
62	Figure 1-8	(Fort et al. 2007)	American Society for Biochemistry and Molecular Biology	Yes – no permissions needed	It is the policy of the American Society for Biochemistry and

					Molecular Biology to allow reuse of any material published in its journals (the Journal of Biological Chemistry, Molecular & Cellular Proteomics and the Journal of Lipid Research) in a thesis or dissertation at no cost and with no explicit permission needed. Please see our copyright permissions page on the journal site for more information.
123	Figure 2-10	(Grashoff et al. 2010)	Nature Publishing Group	Yes	Licence number: 4241971112520

Reuse of Content Within a Thesis or Dissertation

Content (full-text or portions thereof) may be used in print and electronic versions of a dissertation or thesis without formal permission from the Massachusetts Medical Society (MMS), Publisher of the *New England Journal of Medicine*.

The following credit line must be printed along with the copyrighted material:

> Reproduced with permission from (scientific reference citation), Copyright Massachusetts Medical Society.

RE: Permission to use a figure from ERJ in a PhD thesis

Kay Sharpe <Kay.Sharpe@ersj.org.uk> on behalf of permissions <permissions@ersj.org.uk>
Wed 25/10/2017 15:43

To:Salman, David <d.salman11@imperial.ac.uk>;

The use of alveolar epithelial type I cell---selec4ve markers to inves4gate lung injury and repair
M.C. McElroy, M. Kasper
European Respiratory Journal Oct 2004, 24 (4) 664---673; DOI: 10.1183/09031936.04.00096003
Material: 4

Acknowledgement Wording: Reproduced with permission of the © ERS 2004. *European Respiratory Journal Oct 2004, 24 (4) 664---673; DOI: 10.1183/09031936.04.00096003*

Permission is granted for the material stated above to be reproduced for your thesis in accordance with ERS copyright policy – see below

Notes, Terms & Condi4ons (where applicable)

"Green" Open Access and Author Archiving: Authors who do not wish to pay for the ERJ Open op4on will s4ll have their manuscripts made free to access via the ERJ online archive following the journal's 18---month embargo period; a[er this embargo period, authors also have licence to deposit their manuscripts in an ins4tu4onal (or other) repository for public archiving, provided the following requirements are met:

1) The final, peer---reviewed, author---submi^ed version that was accepted for publica4on is used (before copy---edi4ng and publica4on).

2) A permanent link is provided to the version of the ar4cle published in the ERJ, through the dx.doi.org pla`orm. For example, if your manuscript has the DOI 10.1183/09031936.00123412, then the link you provide must be dx.doi.org/10.1183/09031936.00123412

3) The repository on which the manuscript is deposited is not used for systema4c distribu4on or commercial sales purposes.

4) The following required archiving statement appears on the 4tle page of the archived manuscript: "This is an author---submi^ed, peer---reviewed version of a manuscript that has been accepted for publica4on in the European Respiratory Journal, prior to copy---edi4ng, forma**g**ng and typese**g**ng. This version of the manuscript may not be duplicated or reproduced without prior permission from the copyright owner, the European Respiratory Society. The publisher is not responsible or liable for any errors or omissions in this version of the manuscript or in any version derived from it by any other par4es. The final, copy---edited, published ar4cle, which is the version of record, is available without a subscrip4on 18 months a[er the date of issue publica4on."

Authors of ar4cles published under one of the Crea4ve Commons licences (this includes all ar4cles in ERJ Open Research, European Respiratory Review and Breathe) retain further rights to share, reuse or adapt their manuscript. The extent of these rights depends on the specific Crea4ve Commons licence used. Please consult the relevant sec4on of the online instruc4ons for authors. These publica4ons are copyrighted material and must not be copied, reproduced, transferred, distributed, leased, licensed, placed in a storage retrieval system or publicly performed or used in any way except as specifically permi^ed in wri4ng by the publishers (European Respiratory Society), as allowed under the terms and condi4ons of which it was purchased or as strictly permi^ed by applicable copyright law. Any unauthorised distribu4on or use of this text may be a direct infringement of the publisher's rights and those responsible may be liable in law accordingly. Copyright remains with ERS ©

Kind regards,

Kay

ERS
Kay Sharpe
European Respiratory Society Administration Coordinator
D +44 114 267 28 61
ERS 442 Glossop Road Sheffield S10 2PX United Kingdom
Central T +44 114 267 28 60 F +44 114 266 50 64 W ersnet.org



From: Salman, David [mailto:d.salman11@imperial.ac.uk]
Sent: 20 October 2017 18:26
To: permissions
Subject: Permission to use a figure from ERJ in a PhD thesis

Dear Permissions
Please see the a^ached permissions request form

Kind Regards
David Salman
Imperial College London

--
This message has been scanned for viruses and
dangerous content and is believed to be clean.

This message has been scanned for viruses and
dangerous content and is believed to be clean.

THE AMERICAN ASSOCIATION FOR THE ADVANCEMENT OF SCIENCE LICENSE TERMS AND CONDITIONS

Jan 31, 2018

This Agreement between David Salman ("You") and The American Association for the Advancement of Science ("The American Association for the Advancement of Science") consists of your license details and the terms and conditions provided by The American Association for the Advancement of Science and Copyright Clearance Center.

License Number	4213180767787
License date	Oct 20, 2017
Licensed Content Publisher	The American Association for the Advancement of Science
Licensed Content Publication	Science
Licensed Content Title	Taking Cell-Matrix Adhesions to the Third Dimension
Licensed Content Author	Edna Cukierman,Roumen Pankov,Daron R. Stevens,Kenneth M. Yamada
Licensed Content Date	Nov 23, 2001
Licensed Content Volume	294
Licensed Content Issue	5547
Volume number	294
Issue number	5547
Type of Use	Thesis / Dissertation
Requestor type	Scientist/individual at a research institution
Format	Print and electronic
Portion	Figure
Number of figures/tables	1
Order reference number	DS4911
Title of your thesis / dissertation	Cytoskeletal and integrin-mediated mechanobiology of the alveolar epithelium
Expected completion date	Nov 2017
Estimated size(pages)	304
Requestor Location	Dr. David Salman Imperial College London South Kensington Campus London, SW7 2AZ United Kingdom Attn: Dr. David Salman
Billing Type	Invoice
Billing Address	Dr. David Salman Imperial College London South Kensington Campus London, United Kingdom SW7 2AZ Attn: Dr. David Salman

Total 0.00 GBP

Terms and Conditions

American Association for the Advancement of Science TERMS AND CONDITIONS
Regarding your request, we are pleased to grant you non-exclusive, non-transferable permission, to republish the AAAS material identified above in your work identified above, subject to the terms and conditions herein. We must be contacted for permission for any uses other than those specifically identified in your request above.
The following credit line must be printed along with the AAAS material: "From [Full Reference Citation]. Reprinted with permission from AAAS."
All required credit lines and notices must be visible any time a user accesses any part of the AAAS material and must appear on any printed copies and authorized user might make.
This permission does not apply to figures / photos / artwork or any other content or materials included in your work that are credited to non-AAAS sources. If the requested material is sourced to or references non-AAAS sources, you must obtain authorization from that source as well before using that material. You agree to hold harmless and indemnify AAAS against any claims arising from your use of any content in your work that is credited to non-AAAS sources.
If the AAAS material covered by this permission was published in Science during the years 1974 - 1994, you must also obtain permission from the author, who may grant or withhold permission, and who may or may not charge a fee if permission is granted. See original article for author's address. This condition does not apply to news articles.
The AAAS material may not be modified or altered except that figures and tables may be modified with permission from the author. Author permission for any such changes must be secured prior to your use.
Whenever possible, we ask that electronic uses of the AAAS material permitted herein include a hyperlink to the original work on AAAS's website (hyperlink may be embedded in the reference citation).
AAAS material reproduced in your work identified herein must not account for more than 30% of the total contents of that work.
AAAS must publish the full paper prior to use of any text.
AAAS material must not imply any endorsement by the American Association for the Advancement of Science.
This permission is not valid for the use of the AAAS and/or Science logos.
AAAS makes no representations or warranties as to the accuracy of any information contained in the AAAS material covered by this permission, including any warranties of merchantability or fitness for a particular purpose.
If permission fees for this use are waived, please note that AAAS reserves the right to charge for reproduction of this material in the future.
Permission is not valid unless payment is received within sixty (60) days of the issuance of this permission. If payment is not received within this time period then all rights granted herein shall be revoked and this permission will be considered null and void.
In the event of breach of any of the terms and conditions herein or any of CCC's Billing and Payment terms and conditions, all rights granted herein shall be revoked and this permission will be considered null and void.
AAAS reserves the right to terminate this permission and all rights granted herein at its discretion, for any purpose, at any time. In the event that AAAS elects to terminate this permission, you will have no further right to publish, publicly perform, publicly display, distribute or otherwise use any matter in which the AAAS content had been included, and all fees paid hereunder shall be fully refunded to you. Notification of termination will be sent to the contact information as supplied by you during the request process and termination shall be immediate upon sending the notice. Neither AAAS nor CCC shall be liable for any costs,

expenses, or damages you may incur as a result of the termination of this permission, beyond the refund noted above.
This Permission may not be amended except by written document signed by both parties.
The terms above are applicable to all permissions granted for the use of AAAS material.
Below you will find additional conditions that apply to your particular type of use.

FOR A THESIS OR DISSERTATION

If you are using figure(s)/table(s), permission is granted for use in print and electronic versions of your dissertation or thesis. A full text article may be used in print versions only of a dissertation or thesis.
Permission covers the distribution of your dissertation or thesis on demand by ProQuest / UMI, provided the AAAS material covered by this permission remains in situ.
If you are an Original Author on the AAAS article being reproduced, please refer to your License to Publish for rules on reproducing your paper in a dissertation or thesis.

FOR JOURNALS:

Permission covers both print and electronic versions of your journal article, however the AAAS material may not be used in any manner other than within the context of your article.

FOR BOOKS/TEXTBOOKS:

If this license is to reuse figures/tables, then permission is granted for non-exclusive world rights in all languages in both print and electronic formats (electronic formats are defined below).
If this license is to reuse a text excerpt or a full text article, then permission is granted for non-exclusive world rights in English only. You have the option of securing either print or electronic rights or both, but electronic rights are not automatically granted and do garner additional fees. Permission for translations of text excerpts or full text articles into other languages must be obtained separately.
Licenses granted for use of AAAS material in electronic format books/textbooks are valid only in cases where the electronic version is equivalent to or substitutes for the print version of the book/textbook. The AAAS material reproduced as permitted herein must remain in situ and must not be exploited separately (for example, if permission covers the use of a full text article, the article may not be offered for access or for purchase as a stand-alone unit), except in the case of permitted textbook companions as noted below.
You must include the following notice in any electronic versions, either adjacent to the reprinted AAAS material or in the terms and conditions for use of your electronic products: "Readers may view, browse, and/or download material for temporary copying purposes only, provided these uses are for noncommercial personal purposes. Except as provided by law, this material may not be further reproduced, distributed, transmitted, modified, adapted, performed, displayed, published, or sold in whole or in part, without prior written permission from the publisher."
If your book is an academic textbook, permission covers the following companions to your textbook, provided such companions are distributed only in conjunction with your textbook at no additional cost to the user:

- Password-protected website
- Instructor's image CD/DVD and/or PowerPoint resource
- Student CD/DVD

All companions must contain instructions to users that the AAAS material may be used for non-commercial, classroom purposes only. Any other uses require the prior written permission from AAAS.
If your license is for the use of AAAS Figures/Tables, then the electronic rights granted herein permit use of the Licensed Material in any Custom Databases that you distribute the electronic versions of your textbook through, so long as the Licensed Material remains

within the context of a chapter of the title identified in your request and cannot be downloaded by a user as an independent image file.
Rights also extend to copies/files of your Work (as described above) that you are required to provide for use by the visually and/or print disabled in compliance with state and federal laws.
This permission only covers a single edition of your work as identified in your request.

FOR NEWSLETTERS:

Permission covers print and/or electronic versions, provided the AAAS material reproduced as permitted herein remains in situ and is not exploited separately (for example, if permission covers the use of a full text article, the article may not be offered for access or for purchase as a stand-alone unit)

FOR ANNUAL REPORTS:

Permission covers print and electronic versions provided the AAAS material reproduced as permitted herein remains in situ and is not exploited separately (for example, if permission covers the use of a full text article, the article may not be offered for access or for purchase as a stand-alone unit)

FOR PROMOTIONAL/MARKETING USES:

Permission covers the use of AAAS material in promotional or marketing pieces such as information packets, media kits, product slide kits, brochures, or flyers limited to a single print run. The AAAS Material may not be used in any manner which implies endorsement or promotion by the American Association for the Advancement of Science (AAAS) or Science of any product or service. AAAS does not permit the reproduction of its name, logo or text on promotional literature.
If permission to use a full text article is permitted, The Science article covered by this permission must not be altered in any way. No additional printing may be set onto an article copy other than the copyright credit line required above. Any alterations must be approved in advance and in writing by AAAS. This includes, but is not limited to, the placement of sponsorship identifiers, trademarks, logos, rubber stamping or self-adhesive stickers onto the article copies.
Additionally, article copies must be a freestanding part of any information package (i.e. media kit) into which they are inserted. They may not be physically attached to anything, such as an advertising insert, or have anything attached to them, such as a sample product. Article copies must be easily removable from any kits or informational packages in which they are used. The only exception is that article copies may be inserted into three-ring binders.

FOR CORPORATE INTERNAL USE:

The AAAS material covered by this permission may not be altered in any way. No additional printing may be set onto an article copy other than the required credit line. Any alterations must be approved in advance and in writing by AAAS. This includes, but is not limited to the placement of sponsorship identifiers, trademarks, logos, rubber stamping or self-adhesive stickers onto article copies.
If you are making article copies, copies are restricted to the number indicated in your request and must be distributed only to internal employees for internal use.
If you are using AAAS Material in Presentation Slides, the required credit line must be visible on the slide where the AAAS material will be reprinted
If you are using AAAS Material on a CD, DVD, Flash Drive, or the World Wide Web, you must include the following notice in any electronic versions, either adjacent to the reprinted AAAS material or in the terms and conditions for use of your electronic products: "Readers may view, browse, and/or download material for temporary copying purposes only, provided these uses are for noncommercial personal purposes. Except as provided by law, this material may not be further reproduced, distributed, transmitted, modified, adapted,

performed, displayed, published, or sold in whole or in part, without prior written permission from the publisher." Access to any such CD, DVD, Flash Drive or Web page must be restricted to your organization's employees only.

FOR CME COURSE and SCIENTIFIC SOCIETY MEETINGS:

Permission is restricted to the particular Course, Seminar, Conference, or Meeting indicated in your request. If this license covers a text excerpt or a Full Text Article, access to the reprinted AAAS material must be restricted to attendees of your event only (if you have been granted electronic rights for use of a full text article on your website, your website must be password protected, or access restricted so that only attendees can access the content on your site).

If you are using AAAS Material on a CD, DVD, Flash Drive, or the World Wide Web, you must include the following notice in any electronic versions, either adjacent to the reprinted AAAS material or in the terms and conditions for use of your electronic products: "Readers may view, browse, and/or download material for temporary copying purposes only, provided these uses are for noncommercial personal purposes. Except as provided by law, this material may not be further reproduced, distributed, transmitted, modified, adapted, performed, displayed, published, or sold in whole or in part, without prior written permission from the publisher."

FOR POLICY REPORTS:

These rights are granted only to non-profit organizations and/or government agencies. Permission covers print and electronic versions of a report, provided the required credit line appears in both versions and provided the AAAS material reproduced as permitted herein remains in situ and is not exploited separately.

FOR CLASSROOM PHOTOCOPIES:

Permission covers distribution in print copy format only. Article copies must be freestanding and not part of a course pack. They may not be physically attached to anything or have anything attached to them.

FOR COURSEPACKS OR COURSE WEBSITES:

These rights cover use of the AAAS material in one class at one institution. Permission is valid only for a single semester after which the AAAS material must be removed from the Electronic Course website, unless new permission is obtained for an additional semester. If the material is to be distributed online, access must be restricted to students and instructors enrolled in that particular course by some means of password or access control.

FOR WEBSITES:

You must include the following notice in any electronic versions, either adjacent to the reprinted AAAS material or in the terms and conditions for use of your electronic products: "Readers may view, browse, and/or download material for temporary copying purposes only, provided these uses are for noncommercial personal purposes. Except as provided by law, this material may not be further reproduced, distributed, transmitted, modified, adapted, performed, displayed, published, or sold in whole or in part, without prior written permission from the publisher."

Permissions for the use of Full Text articles on third party websites are granted on a case by case basis and only in cases where access to the AAAS Material is restricted by some means of password or access control. Alternately, an E-Print may be purchased through our reprints department (brocheleau@rockwaterinc.com).

REGARDING FULL TEXT ARTICLE USE ON THE WORLD WIDE WEB IF YOU ARE AN ‘ORIGINAL AUTHOR’ OF A SCIENCE PAPER

If you chose "Original Author" as the Requestor Type, you are warranting that you are one of authors listed on the License Agreement as a "Licensed content author" or that you are acting on that author's behalf to use the Licensed content in a new work that one of the authors listed on the License Agreement as a "Licensed content author" has written.

Original Authors may post the 'Accepted Version' of their full text article on their personal or on their University website and not on any other website. The 'Accepted Version' is the version of the paper accepted for publication by AAAS including changes resulting from peer review but prior to AAAS's copy editing and production (in other words not the AAAS published version).

FOR MOVIES / FILM / TELEVISION:

Permission is granted to use, record, film, photograph, and/or tape the AAAS material in connection with your program/film and in any medium your program/film may be shown or heard, including but not limited to broadcast and cable television, radio, print, world wide web, and videocassette.

The required credit line should run in the program/film's end credits.

FOR MUSEUM EXHIBITIONS:

Permission is granted to use the AAAS material as part of a single exhibition for the duration of that exhibit. Permission for use of the material in promotional materials for the exhibit must be cleared separately with AAAS (please contact us at permissions@aaas.org).

FOR TRANSLATIONS:

Translation rights apply only to the language identified in your request summary above.

The following disclaimer must appear with your translation, on the first page of the article, after the credit line: "This translation is not an official translation by AAAS staff, nor is it endorsed by AAAS as accurate. In crucial matters, please refer to the official English-language version originally published by AAAS."

FOR USE ON A COVER:

Permission is granted to use the AAAS material on the cover of a journal issue, newsletter issue, book, textbook, or annual report in print and electronic formats provided the AAAS material reproduced as permitted herein remains in situ and is not exploited separately

By using the AAAS Material identified in your request, you agree to abide by all the terms and conditions herein.

Questions about these terms can be directed to the AAAS Permissions department permissions@aaas.org.

Other Terms and Conditions:

v 2

Questions? customercare@copyright.com or +1-855-239-3415 (toll free in the US) or +1-978-646-2777.

ELSEVIER LICENSE
TERMS AND CONDITIONS

Jan 31, 2018

This Agreement between David Salman ("You") and Elsevier ("Elsevier") consists of your license details and the terms and conditions provided by Elsevier and Copyright Clearance Center.

License Number	4213181504491
License date	Oct 20, 2017
Licensed Content Publisher	Elsevier
Licensed Content Publication	Current Opinion in Cell Biology
Licensed Content Title	Integrin inside-out signaling and the immunological synapse
Licensed Content Author	Timothy A Springer,Michael L Dustin
Licensed Content Date	Feb 1, 2012
Licensed Content Volume	24
Licensed Content Issue	1
Licensed Content Pages	9
Start Page	107
End Page	115
Type of Use	reuse in a thesis/dissertation
Intended publisher of new work	other
Portion	figures/tables/illustrations
Number of figures/tables /illustrations	1
Format	both print and electronic
Are you the author of this Elsevier article?	No
Will you be translating?	No
Order reference number	DS4911
Original figure numbers	Figure 1
Title of your thesis/dissertation	Cytoskeletal and integrin-mediated mechanobiology of the alveolar epithelium
Expected completion date	Nov 2017
Estimated size (number of pages)	304
Requestor Location	Dr. David Salman Imperial College London South Kensington Campus London, SW7 2AZ United Kingdom Attn: Dr. David Salman

Publisher Tax ID	GB 494 6272 12
Total	0.00 USD

Terms and Conditions

INTRODUCTION

1. The publisher for this copyrighted material is Elsevier. By clicking "accept" in connection with completing this licensing transaction, you agree that the following terms and conditions apply to this transaction (along with the Billing and Payment terms and conditions established by Copyright Clearance Center, Inc. ("CCC"), at the time that you opened your Rightslink account and that are available at any time at http://myaccount.copyright.com).

GENERAL TERMS

2. Elsevier hereby grants you permission to reproduce the aforementioned material subject to the terms and conditions indicated.
3. Acknowledgement: If any part of the material to be used (for example, figures) has appeared in our publication with credit or acknowledgement to another source, permission must also be sought from that source. If such permission is not obtained then that material may not be included in your publication/copies. Suitable acknowledgement to the source must be made, either as a footnote or in a reference list at the end of your publication, as follows:
"Reprinted from Publication title, Vol /edition number, Author(s), Title of article / title of chapter, Pages No., Copyright (Year), with permission from Elsevier [OR APPLICABLE SOCIETY COPYRIGHT OWNER]." Also Lancet special credit - "Reprinted from The Lancet, Vol. number, Author(s), Title of article, Pages No., Copyright (Year), with permission from Elsevier."
4. Reproduction of this material is confined to the purpose and/or media for which permission is hereby given.
5. Altering/Modifying Material: Not Permitted. However figures and illustrations may be altered/adapted minimally to serve your work. Any other abbreviations, additions, deletions and/or any other alterations shall be made only with prior written authorization of Elsevier Ltd. (Please contact Elsevier at permissions@elsevier.com). No modifications can be made to any Lancet figures/tables and they must be reproduced in full.
6. If the permission fee for the requested use of our material is waived in this instance, please be advised that your future requests for Elsevier materials may attract a fee.
7. Reservation of Rights: Publisher reserves all rights not specifically granted in the combination of (i) the license details provided by you and accepted in the course of this licensing transaction, (ii) these terms and conditions and (iii) CCC's Billing and Payment terms and conditions.
8. License Contingent Upon Payment: While you may exercise the rights licensed immediately upon issuance of the license at the end of the licensing process for the transaction, provided that you have disclosed complete and accurate details of your proposed use, no license is finally effective unless and until full payment is received from you (either by publisher or by CCC) as provided in CCC's Billing and Payment terms and conditions. If full payment is not received on a timely basis, then any license preliminarily granted shall be deemed automatically revoked and shall be void as if never granted. Further, in the event that you breach any of these terms and conditions or any of CCC's Billing and Payment terms and conditions, the license is automatically revoked and shall be void as if never granted. Use of materials as described in a revoked license, as well as any use of the materials beyond the scope of an unrevoked license, may constitute copyright infringement and publisher reserves the right to take any and all action to protect its copyright in the materials.
9. Warranties: Publisher makes no representations or warranties with respect to the licensed material.

10. Indemnity: You hereby indemnify and agree to hold harmless publisher and CCC, and their respective officers, directors, employees and agents, from and against any and all claims arising out of your use of the licensed material other than as specifically authorized pursuant to this license.
11. No Transfer of License: This license is personal to you and may not be sublicensed, assigned, or transferred by you to any other person without publisher's written permission.
12. No Amendment Except in Writing: This license may not be amended except in a writing signed by both parties (or, in the case of publisher, by CCC on publisher's behalf).
13. Objection to Contrary Terms: Publisher hereby objects to any terms contained in any purchase order, acknowledgment, check endorsement or other writing prepared by you, which terms are inconsistent with these terms and conditions or CCC's Billing and Payment terms and conditions. These terms and conditions, together with CCC's Billing and Payment terms and conditions (which are incorporated herein), comprise the entire agreement between you and publisher (and CCC) concerning this licensing transaction. In the event of any conflict between your obligations established by these terms and conditions and those established by CCC's Billing and Payment terms and conditions, these terms and conditions shall control.
14. Revocation: Elsevier or Copyright Clearance Center may deny the permissions described in this License at their sole discretion, for any reason or no reason, with a full refund payable to you. Notice of such denial will be made using the contact information provided by you. Failure to receive such notice will not alter or invalidate the denial. In no event will Elsevier or Copyright Clearance Center be responsible or liable for any costs, expenses or damage incurred by you as a result of a denial of your permission request, other than a refund of the amount(s) paid by you to Elsevier and/or Copyright Clearance Center for denied permissions.

LIMITED LICENSE

The following terms and conditions apply only to specific license types:
15. **Translation**: This permission is granted for non-exclusive world **English** rights only unless your license was granted for translation rights. If you licensed translation rights you may only translate this content into the languages you requested. A professional translator must perform all translations and reproduce the content word for word preserving the integrity of the article.
16. **Posting licensed content on any Website**: The following terms and conditions apply as follows: Licensing material from an Elsevier journal: All content posted to the web site must maintain the copyright information line on the bottom of each image; A hyper-text must be included to the Homepage of the journal from which you are licensing at http://www.sciencedirect.com/science/journal/xxxxx or the Elsevier homepage for books at http://www.elsevier.com; Central Storage: This license does not include permission for a scanned version of the material to be stored in a central repository such as that provided by Heron/XanEdu.
Licensing material from an Elsevier book: A hyper-text link must be included to the Elsevier homepage at http://www.elsevier.com . All content posted to the web site must maintain the copyright information line on the bottom of each image.

Posting licensed content on Electronic reserve: In addition to the above the following clauses are applicable: The web site must be password-protected and made available only to bona fide students registered on a relevant course. This permission is granted for 1 year only. You may obtain a new license for future website posting.
17. **For journal authors:** the following clauses are applicable in addition to the above:
Preprints:
A preprint is an author's own write-up of research results and analysis, it has not been peer-

reviewed, nor has it had any other value added to it by a publisher (such as formatting, copyright, technical enhancement etc.).
Authors can share their preprints anywhere at any time. Preprints should not be added to or enhanced in any way in order to appear more like, or to substitute for, the final versions of articles however authors can update their preprints on arXiv or RePEc with their Accepted Author Manuscript (see below).
If accepted for publication, we encourage authors to link from the preprint to their formal publication via its DOI. Millions of researchers have access to the formal publications on ScienceDirect, and so links will help users to find, access, cite and use the best available version. Please note that Cell Press, The Lancet and some society-owned have different preprint policies. Information on these policies is available on the journal homepage.
Accepted Author Manuscripts: An accepted author manuscript is the manuscript of an article that has been accepted for publication and which typically includes author-incorporated changes suggested during submission, peer review and editor-author communications.
Authors can share their accepted author manuscript:

- immediately
  - via their non-commercial person homepage or blog
  - by updating a preprint in arXiv or RePEc with the accepted manuscript
  - via their research institute or institutional repository for internal institutional uses or as part of an invitation-only research collaboration work-group
  - directly by providing copies to their students or to research collaborators for their personal use
  - for private scholarly sharing as part of an invitation-only work group on commercial sites with which Elsevier has an agreement
- After the embargo period
  - via non-commercial hosting platforms such as their institutional repository
  - via commercial sites with which Elsevier has an agreement

In all cases accepted manuscripts should:

- link to the formal publication via its DOI
- bear a CC-BY-NC-ND license - this is easy to do
- if aggregated with other manuscripts, for example in a repository or other site, be shared in alignment with our hosting policy not be added to or enhanced in any way to appear more like, or to substitute for, the published journal article.

Published journal article (JPA): A published journal article (PJA) is the definitive final record of published research that appears or will appear in the journal and embodies all value-adding publishing activities including peer review co-ordination, copy-editing, formatting, (if relevant) pagination and online enrichment.
Policies for sharing publishing journal articles differ for subscription and gold open access articles:
Subscription Articles: If you are an author, please share a link to your article rather than the full-text. Millions of researchers have access to the formal publications on ScienceDirect, and so links will help your users to find, access, cite, and use the best available version.
Theses and dissertations which contain embedded PJAs as part of the formal submission can be posted publicly by the awarding institution with DOI links back to the formal publications on ScienceDirect.
If you are affiliated with a library that subscribes to ScienceDirect you have additional private sharing rights for others' research accessed under that agreement. This includes use

for classroom teaching and internal training at the institution (including use in course packs and courseware programs), and inclusion of the article for grant funding purposes.
Gold Open Access Articles: May be shared according to the author-selected end-user license and should contain a CrossMark logo, the end user license, and a DOI link to the formal publication on ScienceDirect.
Please refer to Elsevier's posting policy for further information.
18. **For book authors** the following clauses are applicable in addition to the above: Authors are permitted to place a brief summary of their work online only. You are not allowed to download and post the published electronic version of your chapter, nor may you scan the printed edition to create an electronic version. **Posting to a repository:** Authors are permitted to post a summary of their chapter only in their institution's repository.
19. **Thesis/Dissertation**: If your license is for use in a thesis/dissertation your thesis may be submitted to your institution in either print or electronic form. Should your thesis be published commercially, please reapply for permission. These requirements include permission for the Library and Archives of Canada to supply single copies, on demand, of the complete thesis and include permission for Proquest/UMI to supply single copies, on demand, of the complete thesis. Should your thesis be published commercially, please reapply for permission. Theses and dissertations which contain embedded PJAs as part of the formal submission can be posted publicly by the awarding institution with DOI links back to the formal publications on ScienceDirect.

Elsevier Open Access Terms and Conditions
You can publish open access with Elsevier in hundreds of open access journals or in nearly 2000 established subscription journals that support open access publishing. Permitted third party re-use of these open access articles is defined by the author's choice of Creative Commons user license. See our open access license policy for more information.
Terms & Conditions applicable to all Open Access articles published with Elsevier:
Any reuse of the article must not represent the author as endorsing the adaptation of the article nor should the article be modified in such a way as to damage the author's honour or reputation. If any changes have been made, such changes must be clearly indicated.
The author(s) must be appropriately credited and we ask that you include the end user license and a DOI link to the formal publication on ScienceDirect.
If any part of the material to be used (for example, figures) has appeared in our publication with credit or acknowledgement to another source it is the responsibility of the user to ensure their reuse complies with the terms and conditions determined by the rights holder.
Additional Terms & Conditions applicable to each Creative Commons user license:
CC BY: The CC-BY license allows users to copy, to create extracts, abstracts and new works from the Article, to alter and revise the Article and to make commercial use of the Article (including reuse and/or resale of the Article by commercial entities), provided the user gives appropriate credit (with a link to the formal publication through the relevant DOI), provides a link to the license, indicates if changes were made and the licensor is not represented as endorsing the use made of the work. The full details of the license are available at http://creativecommons.org/licenses/by/4.0.
CC BY NC SA: The CC BY-NC-SA license allows users to copy, to create extracts, abstracts and new works from the Article, to alter and revise the Article, provided this is not done for commercial purposes, and that the user gives appropriate credit (with a link to the formal publication through the relevant DOI), provides a link to the license, indicates if changes were made and the licensor is not represented as endorsing the use made of the work. Further, any new works must be made available on the same conditions. The full details of the license are available at http://creativecommons.org/licenses/by-nc-sa/4.0.
CC BY NC ND: The CC BY-NC-ND license allows users to copy and distribute the Article,

provided this is not done for commercial purposes and further does not permit distribution of the Article if it is changed or edited in any way, and provided the user gives appropriate credit (with a link to the formal publication through the relevant DOI), provides a link to the license, and that the licensor is not represented as endorsing the use made of the work. The full details of the license are available at http://creativecommons.org/licenses/by-nc-nd/4.0. Any commercial reuse of Open Access articles published with a CC BY NC SA or CC BY NC ND license requires permission from Elsevier and will be subject to a fee.
Commercial reuse includes:

- Associating advertising with the full text of the Article
- Charging fees for document delivery or access
- Article aggregation
- Systematic distribution via e-mail lists or share buttons

Posting or linking by commercial companies for use by customers of those companies.

20. **Other Conditions**:

v1.9

Questions? customercare@copyright.com or +1-855-239-3415 (toll free in the US) or +1-978-646-2777.

NATURE PUBLISHING GROUP LICENSE TERMS AND CONDITIONS

Jan 31, 2018

This Agreement between David Salman ("You") and Nature Publishing Group ("Nature Publishing Group") consists of your license details and the terms and conditions provided by Nature Publishing Group and Copyright Clearance Center.

License Number	4241950493971
License date	Dec 04, 2017
Licensed Content Publisher	Nature Publishing Group
Licensed Content Publication	Nature Cell Biology
Licensed Content Title	Integration of actin dynamics and cell adhesion by a three-dimensional, mechanosensitive molecular clutch
Licensed Content Author	Lindsay B. Case, Clare M. Waterman
Licensed Content Date	Jun 29, 2015
Licensed Content Volume	17
Licensed Content Issue	8
Type of Use	reuse in a dissertation / thesis
Requestor type	academic/educational
Format	print and electronic
Portion	figures/tables/illustrations
Number of figures/tables /illustrations	1
High-res required	no
Figures	Figure 1: the molecular clutch hypothesis
Author of this NPG article	no
Your reference number	
Title of your thesis / dissertation	Cytoskeletal and integrin-mediated mechanobiology of the alveolar epithelium
Expected completion date	Nov 2017
Estimated size (number of pages)	304
Requestor Location	Dr. David Salman Imperial College London South Kensington Campus London, SW7 2AZ United Kingdom Attn: Dr. David Salman
Billing Type	Invoice
Billing Address	Dr. David Salman Imperial College London South Kensington Campus

London, United Kingdom SW7 2AZ
Attn: Dr. David Salman

Total 0.00 GBP

Terms and Conditions

Terms and Conditions for Permissions

Nature Publishing Group hereby grants you a non-exclusive license to reproduce this material for this purpose, and for no other use,subject to the conditions below:

1. NPG warrants that it has, to the best of its knowledge, the rights to license reuse of this material. However, you should ensure that the material you are requesting is original to Nature Publishing Group and does not carry the copyright of another entity (as credited in the published version). If the credit line on any part of the material you have requested indicates that it was reprinted or adapted by NPG with permission from another source, then you should also seek permission from that source to reuse the material.

2. Permission granted free of charge for material in print is also usually granted for any electronic version of that work, provided that the material is incidental to the work as a whole and that the electronic version is essentially equivalent to, or substitutes for, the print version.Where print permission has been granted for a fee, separate permission must be obtained for any additional, electronic re-use (unless, as in the case of a full paper, this has already been accounted for during your initial request in the calculation of a print run).NB: In all cases, web-based use of full-text articles must be authorized separately through the 'Use on a Web Site' option when requesting permission.

3. Permission granted for a first edition does not apply to second and subsequent editions and for editions in other languages (except for signatories to the STM Permissions Guidelines, or where the first edition permission was granted for free).

4. Nature Publishing Group's permission must be acknowledged next to the figure, table or abstract in print. In electronic form, this acknowledgement must be visible at the same time as the figure/table/abstract, and must be hyperlinked to the journal's homepage.

5. The credit line should read:
   Reprinted by permission from Macmillan Publishers Ltd: [JOURNAL NAME] (reference citation), copyright (year of publication)
   For AOP papers, the credit line should read:
   Reprinted by permission from Macmillan Publishers Ltd: [JOURNAL NAME], advance online publication, day month year (doi: 10.1038/sj.[JOURNAL ACRONYM].XXXXX)

   Note: For republication from the *British Journal of Cancer,* the following credit lines apply.
   Reprinted by permission from Macmillan Publishers Ltd on behalf of Cancer Research UK: [JOURNAL NAME] (reference citation), copyright (year of publication)For AOP papers, the credit line should read:
   Reprinted by permission from Macmillan Publishers Ltd on behalf of Cancer Research UK: [JOURNAL NAME], advance online publication, day month year (doi: 10.1038/sj.[JOURNAL ACRONYM].XXXXX)

6. Adaptations of single figures do not require NPG approval. However, the adaptation should be credited as follows:

   Adapted by permission from Macmillan Publishers Ltd: [JOURNAL NAME] (reference citation), copyright (year of publication)

   Note: For adaptation from the *British Journal of Cancer,* the following credit line applies.
   Adapted by permission from Macmillan Publishers Ltd on behalf of Cancer Research UK: [JOURNAL NAME] (reference citation), copyright (year of publication)

7. Translations of 401 words up to a whole article require NPG approval. Please visit http://www.macmillanmedicalcommunications.com for more information.Translations of up to a 400 words do not require NPG approval. The translation should be credited as follows:

   Translated by permission from Macmillan Publishers Ltd: [JOURNAL NAME] (reference citation), copyright (year of publication).

   Note: For translation from the *British Journal of Cancer,* the following credit line applies.
   Translated by permission from Macmillan Publishers Ltd on behalf of Cancer Research UK: [JOURNAL NAME] (reference citation), copyright (year of publication)

We are certain that all parties will benefit from this agreement and wish you the best in the use of this material. Thank you.
Special Terms:
v1.1

Questions? customercare@copyright.com or +1-855-239-3415 (toll free in the US) or +1-978-646-2777.

11200 Rockville Pike
Suite 302
Rockville, Maryland 20852

August 19, 2011

American Society for Biochemistry and Molecular Biology

To whom it may concern,

It is the policy of the American Society for Biochemistry and Molecular Biology to allow reuse of any material published in its journals (the Journal of Biological Chemistry, Molecular & Cellular Proteomics and the Journal of Lipid Research) in a thesis or dissertation at no cost and with no explicit permission needed. Please see our copyright permissions page on the journal site for more information.

Best wishes,

Sarah Crespi

American Society for Biochemistry and Molecular Biology
11200 Rockville Pike, Rockville, MD
Suite 302
240-283-6616
JBC | MCP | JLR

NATURE PUBLISHING GROUP LICENSE TERMS AND CONDITIONS

Jan 31, 2018

This Agreement between David Salman ("You") and Nature Publishing Group ("Nature Publishing Group") consists of your license details and the terms and conditions provided by Nature Publishing Group and Copyright Clearance Center.

License Number	4241971112520
License date	Dec 04, 2017
Licensed Content Publisher	Nature Publishing Group
Licensed Content Publication	Nature
Licensed Content Title	Measuring mechanical tension across vinculin reveals regulation of focal adhesion dynamics
Licensed Content Author	Carsten Grashoff, Brenton D. Hoffman, Michael D. Brenner, Ruobo Zhou, Maddy Parsons et al.
Licensed Content Date	Jul 8, 2010
Licensed Content Volume	466
Licensed Content Issue	7303
Type of Use	reuse in a dissertation / thesis
Requestor type	academic/educational
Format	print and electronic
Portion	figures/tables/illustrations
Number of figures/tables /illustrations	1
High-res required	no
Figures	Figure 1: vinculin tension sensor construct
Author of this NPG article	no
Your reference number	
Title of your thesis / dissertation	Cytoskeletal and integrin-mediated mechanobiology of the alveolar epithelium
Expected completion date	Dec 2017
Estimated size (number of pages)	304
Requestor Location	David Salman Imperial College London South Kensington Campus London, SW7 2AZ United Kingdom Attn: Dr. David Salman
Billing Type	Invoice
Billing Address	Dr. David Salman Imperial College London South Kensington Campus

London, United Kingdom SW7 2AZ
Attn: Dr. David Salman

Total 0.00 GBP

Terms and Conditions

Terms and Conditions for Permissions

Nature Publishing Group hereby grants you a non-exclusive license to reproduce this material for this purpose, and for no other use,subject to the conditions below:

1. NPG warrants that it has, to the best of its knowledge, the rights to license reuse of this material. However, you should ensure that the material you are requesting is original to Nature Publishing Group and does not carry the copyright of another entity (as credited in the published version). If the credit line on any part of the material you have requested indicates that it was reprinted or adapted by NPG with permission from another source, then you should also seek permission from that source to reuse the material.

2. Permission granted free of charge for material in print is also usually granted for any electronic version of that work, provided that the material is incidental to the work as a whole and that the electronic version is essentially equivalent to, or substitutes for, the print version.Where print permission has been granted for a fee, separate permission must be obtained for any additional, electronic re-use (unless, as in the case of a full paper, this has already been accounted for during your initial request in the calculation of a print run).NB: In all cases, web-based use of full-text articles must be authorized separately through the 'Use on a Web Site' option when requesting permission.

3. Permission granted for a first edition does not apply to second and subsequent editions and for editions in other languages (except for signatories to the STM Permissions Guidelines, or where the first edition permission was granted for free).

4. Nature Publishing Group's permission must be acknowledged next to the figure, table or abstract in print. In electronic form, this acknowledgement must be visible at the same time as the figure/table/abstract, and must be hyperlinked to the journal's homepage.

5. The credit line should read:
   Reprinted by permission from Macmillan Publishers Ltd: [JOURNAL NAME] (reference citation), copyright (year of publication)
   For AOP papers, the credit line should read:
   Reprinted by permission from Macmillan Publishers Ltd: [JOURNAL NAME], advance online publication, day month year (doi: 10.1038/sj.[JOURNAL ACRONYM].XXXXX)

   Note: For republication from the *British Journal of Cancer,* the following credit lines apply.
   Reprinted by permission from Macmillan Publishers Ltd on behalf of Cancer Research UK: [JOURNAL NAME] (reference citation), copyright (year of publication)For AOP papers, the credit line should read:
   Reprinted by permission from Macmillan Publishers Ltd on behalf of Cancer Research UK: [JOURNAL NAME], advance online publication, day month year (doi: 10.1038/sj.[JOURNAL ACRONYM].XXXXX)

6. Adaptations of single figures do not require NPG approval. However, the adaptation should be credited as follows:

   Adapted by permission from Macmillan Publishers Ltd: [JOURNAL NAME] (reference citation), copyright (year of publication)

   Note: For adaptation from the *British Journal of Cancer,* the following credit line applies.
   Adapted by permission from Macmillan Publishers Ltd on behalf of Cancer Research UK:

[JOURNAL NAME] (reference citation), copyright (year of publication)

7. Translations of 401 words up to a whole article require NPG approval. Please visit http://www.macmillanmedicalcommunications.com for more information.Translations of up to a 400 words do not require NPG approval. The translation should be credited as follows:

   Translated by permission from Macmillan Publishers Ltd: [JOURNAL NAME] (reference citation), copyright (year of publication).

   Note: For translation from the *British Journal of Cancer,* the following credit line applies.
   Translated by permission from Macmillan Publishers Ltd on behalf of Cancer Research UK: [JOURNAL NAME] (reference citation), copyright (year of publication)

We are certain that all parties will benefit from this agreement and wish you the best in the use of this material. Thank you.
Special Terms:
v1.1

Questions? customercare@copyright.com or +1-855-239-3415 (toll free in the US) or +1-978-646-2777.